Analysis of the function of the IGF1R during the development and therapy of colorectal cancer

Doctoral thesis

In partial fulfillment of the requirements for the degree

"Doctor rerum naturalium (Dr. rer. nat.)"

in the Molecular Medicine Study Program

at the Georg-August University Göttingen

submitted by

Rabea Oberthür

born in

Duderstadt, Germany

Göttingen, 2016

Members of the Thesis Committee:

Supervisor:

Dr. rer. nat. Silke Kaulfuß

Department of Human Genetics, University Medical Center Göttingen

Official Supervisor:

Prof. Dr. rer. nat. Peter Burfeind

Department of Human Genetics, University Medical Center Göttingen

Second member of the Thesis Committee:

Prof. Dr. rer. nat. Matthias Dobbelstein

Institute of Molecular Oncology, University Medical Center Göttingen

Third member of the Thesis Committee:

Prof. Dr. med. Ralf Dressel

Institute for Cellular and Molecular Immunology, University Medical Center Göttingen

Date of Disputation:

AFFIDAVIT

Herewith I declare that my doctoral thesis entitled "Analysis of the function of the IGF1R during the development and therapy of colorectal cancer" has been written independently with no other sources and aids than quoted.

Göttingen, June 2016

Rabea Oberthür

Table of Contents

List of Abbreviations

α	Anti
AOM	Azoxymethane
AP	Alkaline phosphatase
APC	*Adenomatous polyposis coli*
approx.	Approximately
ATP	Adenosine triphosphate
BCIP	5-bromo, 4-chloro, 3-indolylphosphate
bp	Base pairs
BSA	Bovine serum albumin
°C	Degree Celsius
CA1	Carbonic anhydrase 1
CBCC	Crypt base columnar cells
Cdk	Cyclin-dependent kinase
cDNA	Complementary DNA
Co	Colon
CO_2	Carbon dioxide
CRC	Colorectal cancer
Ct	Threshold cycle
DAPI	4',6-Diamidino-2-phenylindole dihydrochloride
DCC	*Deleted in colorectal cancer*
ddH_2O	Bi-distilled water
DMAB	Dimethylaminoborane
DMF	Dimethylformamide
DMH	Dimethylhydrazine
DMSO	Dimethylsulfoxide
DNA	Deoxyribonucleic acid
dNTP	Deoxyribonucleotide phosphate
DPBS	Dulbecco’s phosphate buffered saline
DSS	Dextran sulfate sodium

DTT	1,4-Dithio-DL-threitol
ECL	Enhanced chemical luminescence
EDTA	Ethylenediamine tetraacetic acid
EEC	Enteroendocrine cell
e.g.	*exempli gratia* (for example)
EGF	Epidermal growth factor
EGFP	Enhanced green fluorescent protein
EGFR	Epidermal growth factor receptor
et al.	*et alteri* (and others)
EtOH	Ethanol
FAP	Familial adenomatous polyposis
Fabp	*Fatty acid-binding protein gene*
FBS	Fetal bovine serum
FGF	Fibroblast growth factor
FGFR	Fibroblast growth factor receptor
Fig.	Figure
Foxn1	*Forkhead box N1*
Fw	Forward
G	Gram
g	Gravity
GSK-3β	Glycogen synthase kinase 3β
Gy	Gray
H_2O_2	Hydrogen peroxide
H_3BO_3	Boric acid
HCA	Heterocyclic amine
HCl	Hydrochloric acid
HNPCC	Hereditary nonpolyposis colorectal cancer
Hprt	*Hypoxanthine-guanine phosphoribosyltransferase*
H-RAS	*Harvey rat sarcoma viral oncogene homolog*
HRP	Horseradish peroxidase

i.e.	*id es* (that is)
IGF-1, IGF-2	Insulin-like growth factor 1, insulin-like growth factor 2
IGF1R	Insulin-like growth factor 1 receptor
IHC	Immunohistochemistry
iNOS	Inducible nitric oxide synthase
IQ	2-amino-3-methylimidazo-[4,5-*f*]quinoline
IR	Insulin receptor
IRS-1, IRS-2	Insulin receptor substrate-1, insulin receptor substrate-2
ISC	Intestinal stem cells
kb	Kilobyte
kDa	Kilodalton
Kg	Kilogram
K-RAS	*Kirstein rat sarcoma viral oncogene homolog*
kV	Kilovoltage
Lgr5	Leucine-rich-repeat-containing G protein-coupled receptor 5
M	Molar (moles per liter)
m	Meter
mA	Milliampere
MALT	Mucosa-associated lymphoid tissue
MAM	Methylazoxymethanol
MAPK	Mitogen activated protein kinase
M cell	Microfold cell
MeOH	Methanol
MEM	Minimum essential media
$MgCl_2$	Magnesium chloride
min	Minute
Min	Multiple intestinal neoplasia
µg	Microgram
µl	Microliter

µm	Micrometer
µM	Micromolar
mg	Milligram
ml	Milliliter
mm	Millimeter
mM	Millimolar
MNNG	N-methyl-N-nitro-N-nitrosoguanidine
MNU	N-methyl-N-nitrosourea
mRNA	Messenger ribonucleic acid
mTOR	*Mechanistic target of rapamycin*
MUC2	Mucin 2
NaCl	Sodium chloride
NaOH	Sodium hydroxide
NBT	Nitroblue tetrazolium
NCBI	National Center for Biotechnology Information
NCT	Neoadjuvant chemotherapy
ng	Nanogram
nm	Nanometer
N-RAS	*Neuroblastoma RAS viral oncogene homolog*
P53	*Tumor-protein-53*
Pa	Pascal
PCR	Polymerase chain reaction
PDGFR	Platelet-derived growth factor receptor
pH	Preponderance of hydrogen ions
PhIP	2-amino-1-methyl-6-phenylimidazo[4,5-*b*]pyridine
PI3K	Phosphatidylinositol 3-kinase
pmol	Picomolar
PMSF	Phenylmethylsulfonyl fluoride
PVDF	Polyvinylidene fluoride
RAS	*Rat sarcoma*

RCT	Radiochemotherapy
Rev	Reverse
RNA	Ribonucleic acid
rpm	Rotations per minute
RPMI	Roswell Park Memorial Institute medium
RT	Room temperature
RTK	Receptor tyrosine kinase
SDS	Sodium dodecyl sulfate
SDS-PAGE	SDS-polyacrylamide gel electrophoresis
sec	Second
SHC	Src homology 2 domain containing
SI	Small intestine
siRNA	Small interfering RNA
SMAD4/2	SMAD family member 4/2
SV	Simian virus
Tab.	Table
TA cell	Transit-amplifying cell
Taq	*Thermus aquaticus*
Tbp	*TATA box binding protein*
TBS	Tris-buffered saline
TGF-β	Transforming growth factor-β
Tris	Trihydroxymethylaminomethane
U	Unit(s) (enzymatic activity)
UMG	University Medical Center Göttingen
V	Voltage
VEGF	Vascular endothelial growth factor
VEGFA	Vascular endothelial growth factor A
VEGFR	Vascular endothelial growth factor receptor
Vol.	Volume
5-FU	5-fluoruracil

∞	Infinite
±	Plus / Minus

List of Figures

List of Tables

1 Introduction

1.1 Definition and epidemiology of colorectal cancer (CRC)

Colorectal cancer (CRC) is a malignant epithelial tumor that originates in the colon or rectum (Bosman 2010). Worldwide, CRC is one of the most common cancer types with more than 1.3 million new cases in the year 2012 (Martel *et al.* 2012). In men, CRC is the fourth most frequent cancer after lung, prostate and stomach cancer. In women, CRC is the third most common cancer after cancers of the breast and uterine cervix (Bosman 2010). Several risk factors are known to be associated with the incidence of CRC. The incidence of CRC increases with age and more than 90% of CRC patients are aged 50 or older. Hereditary risk factors, such as familial adenomatous polyposis (FAP) and hereditary nonpolyposis colorectal cancer (HNPCC), account for 5 to 10% of CRCs. The geographic distribution of CRC varies largely and higher incidence rates of CRC occur in industrialized, high-resource countries, whereas developing countries account for lower rates. Interestingly, incidence rates among immigrants and their descendants converge to those of their adopted countries, indicating that diet, such as high-caloric food, obesity, meat and alcohol consumption, and lifestyle, are also important risk factors (Haggar and Boushey 2009; Bosman 2010). The survival rate of CRC is highly dependent upon the stage of disease at diagnosis. The earlier the stage at diagnosis, the higher is the chance of survival (Haggar and Boushey 2009). Regular screening is an option for the detection of early-stage adenocarcinomas and for the detection and removal of adenomatous polyps, the precursor lesions of CRC. Screening tests for the detection of CRC are e.g. fecal occult blood tests and colonoscopy (Shinya and Wolff 1979; Levin *et al.* 2008). Invasion of cancer cells through the muscularis mucosae into the submucosa is the defining feature of CRC. More than 90% of CRCs are adenocarcinomas developing from a non-malignant polyp (Bosman 2010).

1.2 Development of CRC

The development of CRC is a multistep process in which genetic alterations, involving the mutational activation of oncogenes coupled with the mutational inactivation of

tumor suppressor genes, accumulate (Fearon and Vogelstein 1990; Cho and Vogelstein 1992). The transition from normal colorectal epithelium to adenomas and furthermore their malignant transformation to adenocarcinomas requires years and possibly decades (Bedi *et al.* 1995; Gryfe *et al.* 1997). Fearon and Vogelstein (1990) developed a model to explain the genetic basis of colorectal tumorigenesis which includes several central features. First, colorectal tumors arise as a result of the mutational activation of oncogenes coupled with the mutational inactivation of tumor suppressor genes. Second, mutations in at least four to five genes are required to form a malignant tumor. Third, the total accumulation of genetic alterations, rather than their chronological order, is responsible for determining the biological properties of the tumor (Fearon and Vogelstein 1990). In correlation with the development of new methodical approaches, such as genome-wide sequencing, novel insights into the development of CRC could be gained. A recent study addressing the question how many “driver” gene mutations are required for a normal cell to become a cancer cell, proved, by combining conventional epidemiologic studies with genome-wide sequencing data, that only three sequential mutations are required for the development of CRC (Tomasetti *et al.* 2015).

1.2.1 Accumulation of genetic alterations in oncogenes and tumor suppressor genes

The tumor suppressor gene *Adenomatous polyposis coli (APC)* is mutated in more than 70% of sporadic cancers. Germline mutations in *APC* result in familial adenomatous polyposis (FAP) or in one of its variants (Kheirelseid *et al.* 2013). FAP is an autosomal dominant syndrome and accounts for approx. 0.5% of all CRCs (Haggar and Boushey 2009; Fearon 2011). The protein encoded by the *APC* gene is a member of the Wnt signaling pathway (Takayama *et al.* 2006) and has multiple functional domains that mediate oligomerization and binding to a variety of intracellular proteins, such as β-catenin, the glycogen synthase kinase (GSK)-3β and axin. One main tumor-promoting effect of the mutation in *APC* results in overactivation of the Wnt signaling pathway with subsequent expression of genes that promote cell growth (Kheirelseid *et al.* 2013). The majority of the mutations lead to a premature stop codon and thus to a truncated protein (Chung 2000; Takayama *et al.* 2006; Fearon 2011; Human Gene Mutation Database (HGMD® Professional 2016.1)). Powell *et al.* (1992) were able to

prove that mutations in *APC* occur as a very early event during colorectal tumorigenesis, and showed that the frequency of these mutations does not change between adenomas and carcinomas (Powell *et al.* 1992).

The *Kirstein rat sarcoma (K-RAS)* is among *H-RAS* (*Harvey rat sarcoma viral oncogene homolog*) and *N-RAS* (*neuroblastoma RAS viral oncogene homolog*) a member of the *RAS* family of genes (Forrester *et al.* 1987; Fearon 2011). RAS proteins function downstream of the receptor tyrosine kinase (RTK) epidermal growth factor receptor (EGFR) (Fearon 2011). *K-RAS* is mutated in approx. 50% of CRCs (Forrester *et al.* 1987; Fearon 2011). Alterations in this gene occur as activating point mutations mostly in codon 12 and 13 (Bos 1989; Fearon 2011; HGMD® Professional 2016.1), leading to continuous activation of downstream signaling pathways (Malumbres and Barbacid 2003). The percentage of mutations of intermediate-stage and late-stage adenomas is similar (Vogelstein *et al.* 1988), but in only 20% of small adenomas with *APC* mutations (Powell *et al.* 1992; Tsao and Shibata 1994). This leads to the suggestion that alterations of *K-RAS* follow *APC* mutations. Interestingly, mutations of *K-RAS* seem not to be necessary for the conversion of adenomas to malignant adenocarcinomas (Kheirelseid *et al.* 2013). Activated RAS regulates multiple cellular functions, such as cell proliferation, differentiation and survival (Shaukat *et al.* 2012).

The loss of chromosome 18q occurs in almost 50% of late adenomas and in more than 70% of CRCs (Vogelstein *et al.* 1988). The gene *Deleted in colorectal cancer (DCC)* is localized in the region 18q21. *DCC* is expressed in normal colonic mucosa, but its expression is reduced or even absent in the majority of CRCs (Fearon and Vogelstein 1990), leading to the idea of *DCC* being a tumor suppressor gene (Kheirelseid *et al.* 2013). Elimination of *DCC* is not believed to be a key genetic alteration in tumor formation, but one of a variety of changes that can promote growth of existing tumors (Kheirelseid *et al.* 2013). This hypothesis is supported by the observation of Krimpenfort *et al.* (2012). They showed, by using a mouse model of mammary carcinoma based on somatic inactivation of the *Tumor-protein-53* (*P53),* that the loss of *DCC* is irrelevant for primary tumor development, but in addition to inactivation of *P53* it promotes the formation of metastases (Krimpenfort *et al.* 2012). Importantly, this finding is contradictory to the model of Fearon and Vogelstein (1990), in which the *DCC* loss occurs before *P53* inactivation. Interestingly, other researchers even scrutinize the role of DCC during CRC development e.g. because of the absence of a cancer phenotype of *DCC*-deficient mice. They rather point to the tumor suppressor genes

SMAD4/2 as the candidate genes on 18q, because inactivation of SMAD4 has been shown to associate with the progression of cancer (Takayama *et al.* 2006). *SMAD4/2* encode proteins that are members of the TGF-β signaling pathway (Fearon 2011). Inactivating mutations in *SMAD4* were found in approx. 10 to 15% of CRCs, whereas mutations that inactivate *SMAD2* occur in approx. 5% of CRCs (Fearon 2011). Furthermore, *SMAD4* was shown to be one of the eight most frequent mutated genes in CRC among e.g. *APC*, *P53* and *K-RAS* (Muzny *et al.* 2012). These controversial data indicate that further research is needed.

The *Tumor-protein-53 (P53)* is a transcription factor with tumor suppressor activity. P53 recognizes DNA damage and controls cell cycle progression and cell survival and thus is called “guardian of the genome” (Kheirelseid *et al.* 2013). It is known to be mutated in 50% of primary human tumors (Somasundaram 2000; Kheirelseid *et al.* 2013). The vast majority of mutations in *P53* are missense mutations (Fearon 2011; HGMD® Professional 2016.1). Mutations and the loss of heterozygosity in the *P53* gene were detected at a low frequency in adenomas and at a high frequency in carcinomas, suggesting that alterations in *P53* mediate the conversion from adenoma to carcinoma (Vogelstein *et al.* 1988; Ohue *et al.* 1994; Fearon 2011). Furthermore, two or more of the described alterations (mutations in *K-RAS*, *APC*, *DCC* and *P53*) were found in more than 90% of CRCs, while only 7% of early adenomas had more than one of the four genetic alterations. The percentage of mutations gradually increases as the adenomas progress to intermediate and late stages. In addition, all late-stage adenomas contained all four genetic alterations. These facts support the idea that the alterations of the four genes were not sufficient for the progression to malignancy (Fearon and Vogelstein 1990).

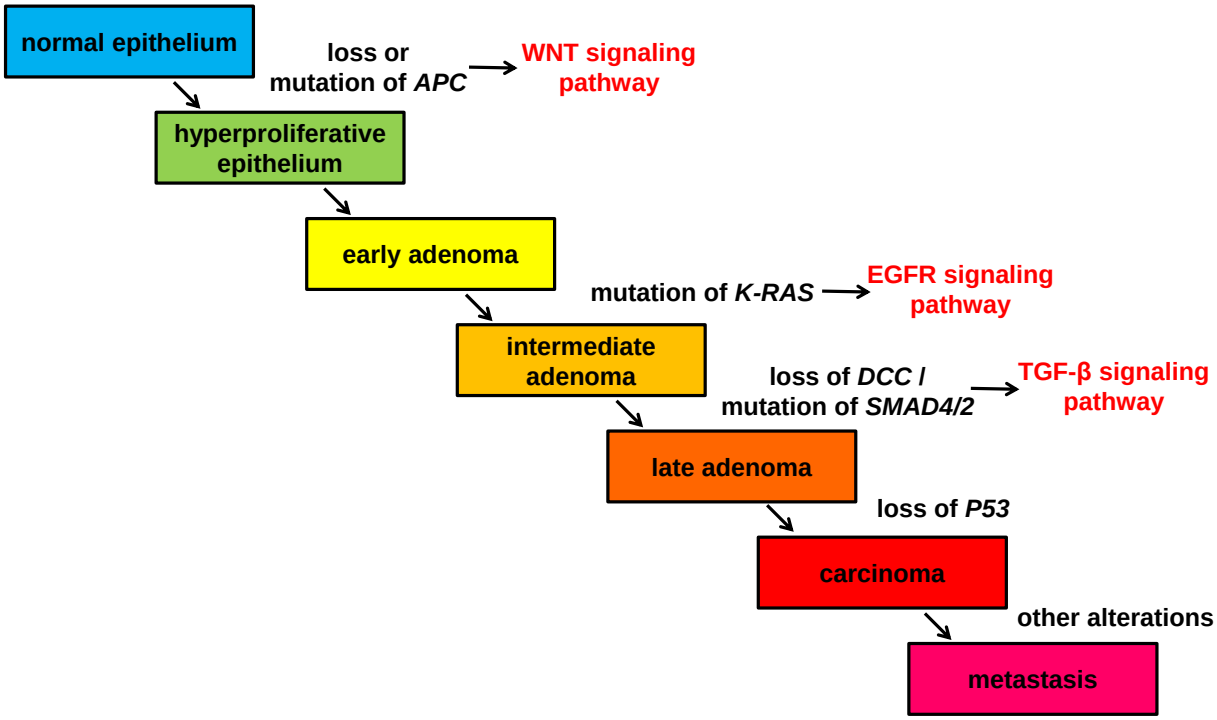

Fig. 1: Model for the multistep development of colorectal cancer.
Colorectal tumorigenesis proceeds through a series of genetic alterations involving oncogenes (*K-RAS*) and tumor suppressor genes (*APC*, *DCC* / *SMAD4/2*, *P53*). The loss or mutation of *APC* occurs at a relatively early stage of tumorigenesis and may be responsible for the hyperproliferative epithelium. Mutation of the *K-RAS* gene occurs in one cell of a pre-existing small adenoma and produces a larger and more dysplastic tumor through clonal expansion. Deletion of the *APC* gene occurs at a very early stage in tumorigenesis and deletions of *DCC* / *SMAD4/2* and *P53* usually appear at a later stage. Recent studies scrutinize the role of *DCC* during CRC development and rather *SMAD4/2* is currently a candidate gene. However, the order of these alterations differs, and accumulation of these alterations, rather than their order with respect to each other, is important. The signaling pathways, in which the proteins encoded by the mutated genes are involved in, are indicated in red (modified after Fearon and Vogelstein 1990; Fearon 2011).

1.2.2 Overexpression of the insulin-like growth factor 1 receptor (IGF1R)

It is well known that the *insulin-like growth factor 1 receptor (IGF1R)* is frequently overexpressed in a variety of human malignancies, such as breast (Jones *et al.* 2007), endometrial (Zhang *et al.* 2010) and colorectal cancer (Hakam *et al.* 1999; Reinmuth *et al.* 2002; Wu *et al.* 2014). The IGF1R is a transmembrane tyrosine kinase receptor and is composed of two covalently linked polypeptide chains (Sachdev and Yee 2007). Each chain consists of an extracellular α-subunit that contains ligand binding sites, and two transmembrane β-subunits that contain tyrosine kinase domains (Zhang *et al.* 2010). Binding of the ligands of the IGF1R, the insulin-like growth factor 1 (IGF-1) or

IGF-2, to the extracellular ligand binding site of the IGF1R leads to a conformational change that subsequently results in the transphosphorylation of one β-subunit by the other one. Adaptor proteins, such as the insulin receptor substrate-1 (IRS-1), IRS-2 or SHC, are recruited and phosphorylated by the IGF1R and thereby mediate downstream signaling, including the phosphatidylinositol 3-kinase (PI3K) and the mitogen-activated protein kinase (MAPK) pathways (Sachdev and Yee 2007; Ekyalongo *et al.* 2013).

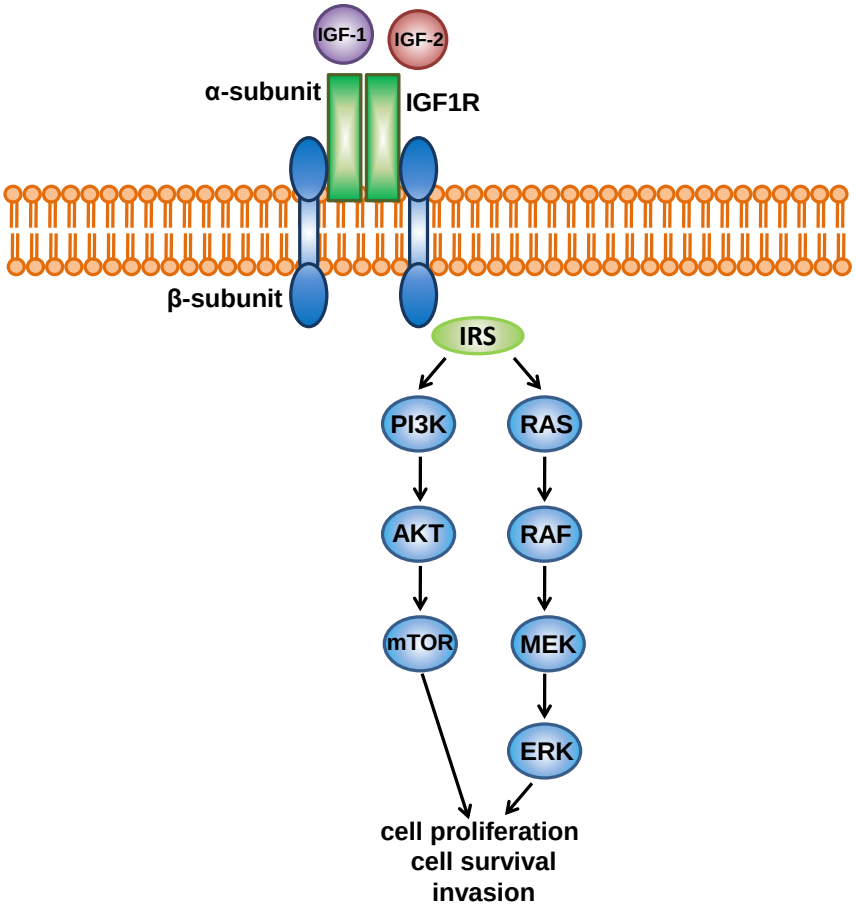

Fig. 2: The IGF1R signaling pathway.

Binding of the ligands IGF-1 or IGF-2 to the extracellular domain of the IGF1R leads to the activation of the tyrosine kinase domain of the IGF1R. The activation of the IGF1R subsequently results in the phosphorylation and thereby activation of the downstream signaling pathways, such as the PI3K (PI3K/AKT/mTOR) and MAPK (RAS/RAF/MEK/ERK) pathway, mediated through IRS, which promote cell proliferation, cell survival and even invasion (modified after Janku *et al.* 2010; Pillai and Ramalingam 2013).

Several studies analyzed the expression of the *IGF1R* in human colorectal carcinoma samples (Freier *et al.* 1999; Hakam *et al.* 1999; Weber *et al.* 2002; Zhang *et al.* 2013).

The majority of colorectal carcinomas reveal a strong overexpression of the *IGF1R* (Weber *et al.* 2002). Furthermore, *IGF1R* expression was found to progressively increase during the transition from normal to adenomatous to carcinomatous colonic mucosa, with the highest *IGF1R* expression in metastatic tumors (Hakam *et al.* 1999). Additionally, a correlation between IGF1R expression and the lymph node status was observed in 120 rectal tumor biopsies (unpublished data of the working group). Reinmuth *et al.* (2002) transfected the human colon cancer cell line KM12L4 with a truncated dominant-negative form of IGF1R (IGF1R dom-neg.) and demonstrated decreased expression of VEGF, a marker for angiogenesis. In addition, decreased tumor growth associated with decreased tumor cell proliferation, VEGF expression and increased tumor cell apoptosis was shown after injection of IGF1R dom-neg.-transfected cells in nude mice (Reinmuth *et al.* 2002). All these *in vitro* and in *vivo* studies support the hypothesis of an important role of the IGF1R in the pathogenesis of colorectal cancer. In other cancer entities, such as breast cancer, an oncogenic function of IGF1R could already be proven. Carboni *et al.* (2005) showed that transgenic mice that express a constitutively active IGF1R developed mammary adenocarcinomas (Carboni *et al.* 2005). Furthermore, it was shown that transgenic mice that overexpress wild type *IGF1R* under control of the mouse mammary tumor virus (MMTV) promoter developed mammary tumors. In addition, it could be proven that the overexpression of *IGF1R* is sufficient for mammary tumor formation *in vivo* (Jones *et al.* 2007). In contrast, comparable studies using transgenic mice that overexpress *IGF1R* in the intestine are not available to date. Therefore, it is of high interest to establish a mouse model with intestinal overexpression of the *IGF1R*, and also an intestine-specific *Igf1r* knockout mouse line in order to study the function of the IGF1R / Igf1r in intestinal tumor formation and progression *in vivo*.

1.3 Treatment of CRC

The current standard therapy of CRC is the complete excision of the affected tissue, including the associated lymphatic system (Kuhry *et al.* 2008). Furthermore, a combined radiochemotherapy (RCT) is recommended for advanced stages. Chemotherapy can be administered as a monotherapy or as a combination of different chemotherapeutics like 5-fluoruracil (5-FU) and Oxaliplatin. RCT can be applied in a neoadjuvant or adjuvant manner (McCarthy *et al.* 1996; Petersen *et al.* 1996;

Gustavsson *et al.* 2015). On purpose to prevent harm to healthy cells and to reduce side effects, targeted therapy is recently developed to specifically block cancer cells from growing and spreading (Tabernero *et al.* 2004; Hagan *et al.* 2013). Cancer cells often fail to regulate main cellular functions, such as proliferation and the induction of apoptosis, due to overexpression of receptors like receptor tyrosine kinases (RTKs) (Yano *et al.* 2003; Spano 2005a). RTKs are transmembrane receptors that regulate key cellular processes, such as proliferation and differentiation, cell survival and metabolism, cell migration and cell cycle control. All 58 known human RTKs have a similar molecular architecture with a ligand-binding region in the extracellular domain, a single transmembrane helix, and an intracellular tyrosine kinase domain (Lemmon and Schlessinger 2010). Dysregulation of the RTKs *insulin-like growth factor 1 receptor (IGF1R)* or *epidermal growth factor receptor (EGFR)* by overexpression was shown to be associated with an aggressive tumor phenotype, tumor progression and poor outcome in several malignancies, including ovarian-, prostate-, gastric-, bladder- and colorectal cancer (Hewish *et al.* 2009; Lurje and Lenz 2009). Several approaches have demonstrated the therapeutic efficacy of the interference with IGF1R or EGFR mediated signaling (Höpfner *et al.* 2006). These approaches include approved monoclonal antibodies, such as cetuximab or panitumumab (directed against the EGFR), which compete with the binding of activating ligands to the extracellular domain of the EGFR, and highly selective small molecule kinase inhibitors, such as erlotinib and gefitinib (directed against the EGFR), which competitively inhibit the binding of ATP to the tyrosine kinase domain of EGFR and thereby inhibit the autophosphorylation of EGFR (Christensen *et al.* 2001; Grünwald and Hidalgo 2003; Höpfner *et al.* 2006; Hewish *et al.* 2009). *De novo* resistance to cetuximab and erlotinib could be observed in the human metastatic CRC cell line DiFi and in lung cancer patients, respectively (Lin and Bivona 2012; Montagut *et al.* 2012; Tang *et al.* 2013; Suda *et al.* 2014). Suda *et al.* (2014) observed increased phosphorylation of the IGF1R in lung adenocarcinoma cells after the cells had acquired resistance to erlotinib, and suggested the IGF1R as an important molecular target to prevent or overcome acquired resistance to erlotinib in lung cancers (Suda *et al.* 2014). In 2009, Kaulfuß *et al.* (2009) showed that inhibition of the IGF1R transduction cascade elevates the antiproliferative and proapoptotic effects of EGFR inhibition in CRC cells (Kaulfuß *et al.* 2009). These results indicated that the combination therapy targeting both, the

EGFR and the IGF1R, could also be a promising therapeutic strategy in clinical applications.

1.4 Aims of the present study

In the present study the role of the receptor tyrosine kinase IGF1R during the development of the intestine and during the development and treatment of CRC is investigated.

Recent *in vitro* studies have shown that the simultaneous inhibition of the IGF1R and EGFR with or without the additional application of combined 5-FU-based RCT leads to a remarkably reduction of the cell survival fraction in CRC cells (Kaulfuß *et al.* 2009; Seemann 2013). The analysis if similar effects of the simultaneous RTK inhibition in addition to RCT can also be observed *in vivo* is one of the main subjects. The second focus is the basic research of the function of the IGF1R during the development of the intestine and during colonic tumor formation and progression.

- Establishment of the double transgenic Villin-TRE-IGF1R mouse line as a model for the inducible overexpression of human *IGF1R*
    - Establishment of the transgenic Villin-rtTA2-M2 mouse line
    - Establishment of the transgenic TRE-IGF1R mouse line
    - Breeding of the Villin-rtTA2-M2 mouse line with the TRE-IGF1R mouse line to establish the Villin-TRE-IGF1R mouse line

- Analysis of the role of the IGF1R during the development, maintenance and regulation of the intestine
    - Administration of doxycycline to Villin-TRE-IGF1R mice to induce the *IGF1R* overexpression
    - Staining of tissue sections of the small intestine and colon for goblet, enteroendocrine, Paneth and proliferating cells
    - Measurement of the villi length and crypt depth of the small intestine and colon

- Analysis if *IGF1R* overexpression *per se* induces intestinal tumor formation
    - Continuous administration of doxycycline to Villin-TRE-IGF1R mice for 1.5 years to induce *IGF1R* overexpression
    - Regular colonoscopy to screen for colonic tumor formation

- Analysis if the IGF1R plays a role during intestinal tumor progression
    - Administration of doxycycline to Villin-TRE-IGF1R mice to induce *IGF1R* overexpression
    - Treatment of the IGF1R-overexpressing and control Villin-TRE-IGF1R mice with the genotoxic agent azoxymethane (AOM) or the combination of AOM and the inflammatory agent dextran sulfate sodium (DSS) to induce colonic tumor formation and inflammation
    - Regular colonoscopy to screen for colonic tumor formation
    - Macroscopic and histopathological analyses of developed intestinal tumors
    - Immunohistochemical and immunofluorescence staining of intestinal tumor sections for IGF1R
    - Analysis of IGF1R expression as well as of the downstream PI3K and MAPK signaling pathways in developed intestinal tumors by western blot analysis

- Establishment of the double transgenic Villin-CreERT-Igf1r mouse line as a model for the inducible knockout of *Igf1r*
    - Establishment of the transgenic Villin-CreER^{T2} mouse line
    - Establishment of the transgenic Igf1r$^{(lox)}$ mouse line
    - Breeding of the Villin-CreER^{T2} mouse line with the Igf1r$^{(lox)}$ mouse line to establish the Villin-CreERT-Igf1r mouse line

- Analysis of the role of the Igf1r during the development, maintenance and regulation of the intestine
    - Intraperitoneal injection of Villin-CreERT-Igf1r mice with tamoxifen on five consecutive days to induce the knockout of *Igf1r*
    - Staining of tissue sections of the small intestine and colon for goblet, enteroendocrine, Paneth and proliferating cells

- Analysis if the Igf1r plays a role during intestinal tumor formation and progression
    - Injection of Villin-CreERT-Igf1r mice with tamoxifen to induce the knockout of *Igf1r*
    - Treatment of Villin-CreERT-Igf1r mice with the genotoxic agent azoxymethane (AOM) or the combination of AOM and the inflammatory agent dextran sulfate sodium (DSS) to induce colonic tumor formation and inflammation
    - Regular colonoscopy to screen for colonic tumor formation
    - Macroscopic and histopathological analyses of developed intestinal tumors
    - Immunohistochemical and immunofluorescence staining of tumor sections for Igf1r
    - Analysis of Igf1r expression as well as of the downstream PI3K and MAPK signaling pathways in developed intestinal tumors by western blot analysis

- Analysis of the effect of simultaneous inhibition of the IGF1R and EGFR in addition to combined 5-FU-based RCT on tumor progression *in vivo*
    - Subcutaneous implantation of the colorectal and rectal cancer cells DLD-1, CaCo-2 and SW837 into immune-deficient nude mice
    - Treatment of nude mice after tumor formation with RTK inhibitors and RCT
    - Macroscopic analysis of developed tumors
    - Analysis of IGF1R and EGFR expression as well as of the downstream PI3K and MAPK signaling pathways by western blot analysis

2 Materials and Methods

2.1 Chemicals and reagents

Chemicals	Manufacturer
AEW541	Novartis, Nürnberg, Germany
Agarose	Carl Roth GmbH, Karlsruhe, Germany
Ampuwa	Fresenius AG, Bad Homburg, Germany
Azoxymethane (AOM)	Sigma-Aldrich, Deisenhofen, Germany
Buffer (Mango *Taq* PCR) (5x)	Bioline, Luckenwalde, Germany
Cell culture media	PAN, Aidenbach, Germany; Life Technologies, Darmstadt, Germany
Citric acid monohydrate	AppliChem GmbH, Darmstadt, Germany
Dextran sulfate sodium (DSS) salt	MP Biomedicals, Illkirch, France
Dimethyl sulfoxide (DMSO)	Carl Roth GmbH, Karlsruhe, Germany
Dithiotreitol (DTT)	Bioline, Luckenwalde, Germany
DNA Stain G	Serva GmbH, Heidelberg, Germany
dNTPs (100 mM)	Life Technologies, Darmstadt, Germany
Doxycycline Hyclate	AppliChem GmbH, Darmstadt, Germany
DPBS	PAN, Aidenbach, Germany
Erlotinib	LC Laboratories, Woburn, USA
Ethanol	Walter CMP GmbH & Co. KG, Kiel, Germany
Ethylendiaminetetraacetic acid (EDTA)	ICN Biomedicals, Aurora, USA
5-fluouracil	Sigma-Aldrich, Deisenhofen, Germany
Formaldehyde (37%)	Carl Roth GmbH, Karlsruhe, Germany
Glycergel Mounting Medium	Dako, Carpinteria, USA
Glycine	Carl Roth GmbH, Karlsruhe, Germany
Hemalum solution	Carl Roth GmbH, Karlsruhe, Germany
Igepal CA-630 (NP-40)	Sigma-Aldrich, Deisenhofen, Germany
Isoflurane	Abbvie, Wiesbaden, Germany
Isopropanol	Carl Roth GmbH, Karlsruhe, Germany
Low fat dry milk	Carl Roth GmbH, Karlsruhe, Germany

Magnesium chloride ($MgCl_2$)	Bioline, Luckenwalde, Germany
Methanol	Carl Roth GmbH, Karlsruhe, Germany
NuPAGE™ LDS Sample buffer (4x)	Life Technologies, Darmstadt, Germany
NuPAGE™ MES Running buffer (20x)	Life Technologies, Darmstadt, Germany
NuPAGE™ See Blue Plus 2	Life Technologies, Darmstadt, Germany
Penicillin / Streptomycin	PAN, Aidenbach, Germany
Phenylmethylsulfonyl fluoride (PMSF)	Sigma-Aldrich, Deisenhofen, Germany
Potassium chloride	Carl Roth GmbH, Karlsruhe, Germany
Roti®Nanoquant	Carl Roth GmbH, Karlsruhe, Germany
Sodium chloride	AppliChem GmbH, Darmstadt, Germany
Sodium chloride, liquid	Braun, Melsungen, Germany
Sodium deoxycholate	Fluka, Deisenhofen, Germany
Sodium dihydrogen phosphate monohydrate	Fluka, Deisenhofen, Germany
Sodiumdodecylsulfate (SDS)	Serva GmbH, Heidelberg, Germany
Sodium phosphatase dibasic dihydrate	Sigma-Aldrich, Deisenhofen, Germany
Sunflower seed oil from Helianthus annuus	Sigma-Aldrich, Deisenhofen, Germany
Tamoxifen	Sigma-Aldrich, Deisenhofen, Germany
Temgesic®	RB Pharmaceuticals Limited, Berkshire, UK
Tris	AppliChem GmbH, Darmstadt, Germany
Tri- Sodium Citrate Dihydrate	Carl Roth GmbH, Karlsruhe, Germany
Triton X-100	Fluka, Deisenhofen, Germany
Trypan blue	Sarstedt, Nürnbrecht, Germany
Tween 20	Carl Roth GmbH, Karlsruhe, Germany
Vectashield with DAPI	VectorLab, Burlingame, USA

2.2 Biochemicals and enzymes

Biochemical	Manufacturer
Albumin fraction V (BSA)	Carl Roth GmbH, Karlsruhe, Germany
Complete Mini Protease Inhibitor Cocktail Tablets	Roche, Mannheim, Germany
Direct PCR Tail	Peqlab, Erlangen, Germany
ExtrAvidin®-Peroxidase	Sigma-Aldrich, Deisenhofen, Germany
Fetal bovine serum	PAN, Aidenbach, Germany
Mango*Taq*-DNA-Polymerase	Bioline, Luckenwalde, Germany
Matrigel™	BD Bioscience, San Jose, USA
MycoZAP™ Spray	Lonza, Cologne, Germany
Phosphatase Inhibitor Mix II, solution	Serva GmbH, Heidelberg, Germany
Platinum® SYBR® Green qPCRSuperMix-UDG with Rox	Life Technologie, Darmstadt, Germany
Proteinase K	Carl Roth GmbH, Karlsruhe, Germany
Trypsin / EDTA solution	PAN, Aidenbach, Germany

2.3 Usage ware

Usage ware	Manufacturer
5 ml, 10 ml Pipettes	Sarstedt, Nürnbrecht, Germany
13 ml Tubes	Sarstedt, Nürnbrecht, Germany
15 ml, 50 ml Cellstar® Tubes	Greiner-bio-one, Frickenhausen, Germany
384-well plates, white	ABgene, Hamburg, Germany
384-well plates, black	4titude® Ltd., Berlin, Germany
6-well cell culture plates	Greiner-bio-one, Frickenhausen, Germany
96-well cell culture plates	Thermo Scientific, Langenselbold, Germany
BD Discardit™ II (20 ml syringe)	BD, Heidelberg, Germany

BD Eclipse™ Needle (0.8 x 40 mm; 21 G x 1 ½ TW)	BD, Heidelberg, Germany
Blotting Paper GB 002, 003, 004	Schleicher & Schnüll, Dassel, Germany
Cell culture flasks	Sarstedt, Nürnbrecht, Germany
Combitips plus, 10 ml	Eppendorf, Hamburg, Germany
Coverglass 22x22 mm, 24x40 mm, 24x60 mm	Menzel Gläser, Braunschweig, Germany
Cryo.S™ cups with screw cap	Greiner-bio-one, Frickenhausen, Germany
Disposable insulin needle (0.45 x 12 mm; 26 G x ½")	Braun, Tuttlingen, Germany
Flat-bottomed Nuclon™ surface 96-well cell culture plates	Nunc A/S, Danmark
Microcentrifuge Tubes	Sarstedt, Nürnbrecht, Germany
Neubauer improved counting chamber	Hartenstein, Würzburg, Germany
NuPAGE™ 4-12% Bis-Tris Gels	Life Technologies, Darmstadt, Germany
Pasteur pipettes	Brand, Wertheim, Germany
Petri dishes	Sarstedt, Nürnbrecht, Germany
Pipet tips	Sarstedt, Nürnbrecht, Germany
PVDF transfer membrane	GE Healthcare, Munich, Germany
Quarz-Cuvette	Hellma, Mühlheim, Germany
Scissors (HSB-390-10 / HSB-006-10)	Hammacher, Solingen, Germany
Serological pipettes (5 ml, 10 ml)	Sarstedt, Nürnbrecht, Germany
Sterile Single-use filter Minisart	Sartorius, Göttingen, Germany
Syringe disposable filters, 0.45 µm / 20 µm	Sartorius, Göttingen, Germany

2.4 Technical equipment

Technical equipment	Manufacturer
Accu-jet® (Pipet-boy)	Brand, Wertheim, Germany
Balance	Sartorius, Göttingen, Germany
Bioruptor® Sonication System	Diagenode, Denville, USA
Centrifuges	Thermo Scientific, Langenselbold, Germany; Sigma-Aldrich, Deisenhofen, Germany
Circular rotor	Sprout, Vernon Hills, USA
CO_2 Incubator MCO-20AIC	Sanyo, Munich, Germany
Colonoscopy device	Karl Storz GmbH & Co. KG, Tuttlingen, Germany
Confocal Laser Scanning Microscope IX81	Olympus, Hamburg, Germany
C1000 Thermal Cycler	Bio-Rad Laboratories, Hercules, USA
Electro-blotter	Biometra, Göttingen, Germany
Electrophoresis power supply PS-304	Life technologies, Darmstadt, Germany
FluorChem® Q	Alpha Innotech, Logan, USA
Fluorescence microscope BX60	Olympus, Hamburg, Germany
Irradiation device 225A	Gulmaymedical, Camberley, UK
HT7900 Fast Real-Time PCR System	Applied Biosystems GmbH, Darmstadt, Germany
Nanodrop 2000c	Thermo Scientific, Langenselbold, Germany
pH-Meter 766	Knick, Berlin, Germany
SynergyMx	Bio Tek, Bad Friedrichshall, Germany
Tissue Lyser LT	Qiagen, Hilden, Germany
Vortexer	Schütt Labortechnik, Göttingen, Germany

2.5 Sterilization of solutions and equipment

Solutions and laboratory equipment were autoclaved at 121°C and 105 Pa for 60 minutes or sterilized at 220°C overnight.

2.6 Ready-to-use Reaction systems

Reaction system	Manufacturer
Dako REAL™ EnVision™ Detection System	Dako, Hamburg, Germany
Direct PCR tail reagent	Peqlab, Erlangen, Germany
ECL Prime	GE Healthcare, Munich, Germany
Myco Alert® Mycoplasma Detection Kit	Lonza, Cologne, Germany
PeqGold Total RNA Kit	Peqlab, Erlangen, Germany
PhosSTOP Phosphatase Inhibitor	Roche, Mannheim, Germany

2.7 Buffers and Solutions

Solutions for routine applications were prepared according to Mamiatis *et al.* (1985). Required chemicals were dissolved in ddH_2O and autoclaved or filtered under sterile conditions when necessary.

Solutions	Composition
AP Buffer	100 mM NaCl 50 mM $MgCl_2$ 100 mM Tris / HCl, pH 9.5
AP staining solution	45 µl NBT (75 mg / ml in DMF) 35 µl BCIP (50 mg / ml in DMF) in 10 ml AP Buffer
Blocking Buffer (IHC I)	1x DPBS 10% FBS
Blocking Buffer (IHC II)	1x DPBS 5% BSA

Blocking Buffer (IHC III)	1x DPBS 5% FBS 10% BSA
Blocking Buffer (Western Blot)	1x TBS-Tween 20 5% low-fat dry milk
Citrate Buffer (IHC I and III)	10 mM Citric acid monohydrate, pH 6
Formalin, buffered (4%)	1.66 g Sodium dihydrogen phosphate Monohydrate 9.79 g di-Sodiumhydrogen phosphate Dihydrate 100 ml Formaldehyde (37%)
Lysis Buffer for proteins (modified RIPA)	150 mM NaCl 1 mM EDTA 50 mM Tris-HCl, pH 7.4 1% Igepal CA-630 (NP-40) 0.25% Sodium deoxycholate 1% PMSF 1 tablet / 10 ml Complete Mini protease inhibitor 100 µl / 10 ml Phosphatase-Inhibitor-Mix II, solution
SE Buffer	75 mM NaCl 1 mM EDTA pH 8
Sodium Citrate Buffer (IHC II)	10 mM Tri- Sodium Citrate Dihydrate, pH 6 0.05% Tween 20
10x TBS	1.37 M NaCl 100 mM Tris / HCl, pH 7.6
1x TBS-Tween (TBS-T)	1x TBS 0.1% Tween 20
Transfer Buffer IIa (Western Blot)	25 mM Tris, pH 8.3 150 mM Glycine 20% Methanol

20x Turbo Buffer	0.2 M NaOH adjusted to pH 8 using solid H_3BO_3
Washing Buffer (Western Blot)	1x TBS-Tween 20 2.5% low-fat dry milk

2.8 Culture media for eukaryotic cell cultures

Media used for the cultivation of eukaryotic cell lines was purchased from PAN, Aidenbach, Germany and Life Technologies, Darmstadt, Germany. Before use, special processed fetal bovine serum (FBS) (PAN, Aidenbach, Germany) and antibiotics (PAN, Aidenbach, Germany) were added. Following media were used for eukaryotic cell culturing:

Medium for CaCo-2 cells:	MEM (Life Technologies, Darmstadt, Germany) 100 µg / ml Streptomycin 100 U / ml Penicillin 20% fetal bovine serum (FBS)
Medium for DLD-1 and SW837 cells:	RPMI 1640 (PAN, Aidenbach, Germany) 100 µg / ml Streptomycin 100 U / ml Penicillin 10% fetal bovine serum (FBS)

2.9 Biological material

2.9.1 Eukaryotic cell lines

CaCo-2 cells	Colorectal adenocarcinoma cells, adherent (ATCC®; Rockville, USA), aneuploid (Ghadimi *et al.* 2000), p53 wild type (ATCC®; Rockville, USA), intermediate RCT sensitive (Spitzner *et al.* 2010)

DLD-1 cells	Colorectal adenocarcinoma cells, adherent (ATCC®; Rockville, USA), pseudodiploid (Ghadimi *et al.* 2000), p53 deficient (ATCC®; Rockville, USA)
SW837 cells	Adenocarcinoma cells of the rectum, adherent (ATCC®; Rockville, USA), aneuploid (Ghadimi *et al.* 2000), p53 deficient (ATCC®; Rockville, USA), weakly sensitive to RCT (Spitzner *et al.* 2010)

2.9.2 Mouse strains

All experiments were conducted according to the European and German protection of animals act. The number of sacrificed animals and the stress and pain the mice were suffering was kept to the minimum. Euthanasia of mice was performed by CO_2-asphyxation. Mice were kept at a 12 hours light / dark cycle at 22°C and 55 ± 5% relative humidity. Animal food was purchased from ssniff (Soest, Germany).

2.9.2.1 RjOrl:NMRI-Foxn1^{nu}/Foxn1^{nu}

The mouse line RjOrl:NMRI-*Foxn1^{nu}/Foxn1^{nu}* carries an autosomal recessive mutation in the *Foxn1* (*forkhead box N1*) gene on chromosome 11. This mutation causes a thymic aplasia which results in an immunodeficiency. The mice lack T cells, B cells remain. The mutation also leads to a keratinization defect of the hair follicule and the epidermis. For this reason, mice appear nude. The RjOrl:NMRI-*Foxn1^{nu}/Foxn1^{nu}* mice were purchased from Janvier Labs (Le Genest-Saint-Isle, France).

2.9.2.2 Villin-rtTA2-M2

The mouse line Villin-rtTA2-M2 is a transgenic mouse line expressing the reverse tetracycline transactivator rtTA2-M2 under the control of the 12.4 kb murine villin promoter. By administration of doxycycline, the Villin-rtTA2-M2 system drives transgene expression in a dosage-dependent manner (Roth *et al.*, 2008). The Villin-rtTA2-M2 mouse line was a kind gift of Ron Smits (Department of Gastroenterology and Hepatology, Erasmus MC, Rotterdam, The Netherlands).

2.9.2.3 TRE-IGF1R

The TRE-IGF1R mouse line is a transgenic mouse line expressing the full-length human *IGF1R* cDNA under the control of the doxycycline inducible pTRE2 promoter (Jones *et al.* 2007). The TRE-IGF1R mouse line was kindly provided by Dr. Moorehead (Department of Biomedical Sciences, Ontario Veterinary College, University of Guelph, Guelph, Canada).

2.9.2.4 Villin-TRE-IGF1R

The Villin-TRE-IGF1R mouse line is a double transgenic mouse line expressing the reverse tetracycline transactivator rtTA2-M2 under the villin promoter (see chapter 2.9.2.2) as well as the human *IGF1R* cDNA under the control of the doxycycline inducible pTRE2 promoter (see chapter 2.9.2.3). Villin is broadly expressed in every cell of the intestinal epithelium on both the vertical axis (crypt to villus tip) and the horizontal axis (duodenum through colon) of the intestine (Madison 2002). The transactivator protein rtTA2-M2 is able to bind the pTRE2 promoter of the TRE-IGF1R mouse line when the antibiotic doxycycline is present (Jones *et al.* 2007). Thus, the overexpression of human *IGF1R* in the intestine can be induced by the administration of doxycycline.

2.9.2.5 Villin-CreER^{T2}

The Villin-CreER^{T2} mouse line is a transgenic mouse line expressing the tamoxifen-dependent cre recombinase under the control of a 9 kb regulatory region of the murine villin promoter (vil-Cre-ER^{T2}) (El Marjou *et al.* 2004). The vil-Cre-ER^{T2} construct is based on a fusion of the cre recombinase with a mutated ligand-binding domain of the human estrogen receptor, which results in a tamoxifen-dependent cre recombinase (Feil *et al.* 1996; El Marjou *et al.* 2004). The Villin-CreER^{T2} mouse line was kindly provided by Sylvie Robine (Institut Curie, Paris, France).

2.9.2.6 B6;129-Igf1r^{tm2Arge}/J

The *B6;129-Igf1r^{tm2Arge}/J* mouse line is also known as Igf1r$^{(lox)}$ mouse line and is called Igf1r$^{(lox)}$ mouse line in the further study. The Igf1r$^{(lox)}$ mouse line is a cre-responder mouse line carrying *loxP*-modified alleles of the gene encoding the *Igf1r*. The floxed segment of the reporter loci is exon 3 of the *Igf1r.* A third *loxP* site is localized next to the 3‘end of the neomycin selection cassette (Dietrich *et al.* 2000). Igf1r$^{(lox)}$ mice were purchased from The Jackson Laboratory (Sulzfeld, Germany).

2.9.2.7 Villin-CreERT-Igf1r

The Villin-CreERT-Igf1r mouse line is a model for the inducible knockout of the *Igf1r* specifically in epithelial cells of the murine intestine. This mouse model is generated by crossing the Villin-CreER^{T2} mouse line (see chapter 2.9.2.5) with the mouse line *Igf1r$^{(lox)}$* (see chapter 2.9.2.6). Administration of tamoxifen to the Villin-CreERT-Igf1r mouse line leads to the deletion of exon 3 of the *Igf1r* gene specifically in the intestine of the mouse at a desired time point.

2.9.3 Synthetic DNA-oligonucleotides

Synthetic DNA-oligonucleotides for the generation of PCR products were purchased from Eurofins MWG Operon (Ebersberg, Germany).

Mouse-specific primers for genotyping:

Primer name	Sequence
Villin-rtTA2-For 2	5‘-CAA GAC TTT CTG CGG AAC AAC-3‘
Villin-rtTA2-Rev 3	5‘-GTG TCT CTC TTT CCT CTT TTG-3‘
IGF-IR-F2	5‘-CAT CCA CGC TGT TTT GAC CTC C-3‘
IGF-IR-R3	5‘-GAT CAC CGT GCA GTT CTC CAG G-3‘
Villin-2kbseqS	5‘- CAA GCC TGG CTC GAC GGC C-3‘
Villin-Cre198	5‘-CGC GAA CAT CTT CAG GTT CT-3‘
IGF-IR-Floxed-Fw	5‘-CTT CCC AGC TTG CTA CTC TAG G-3‘
IGF-IR-Floxed-Re	5‘-CAG GCT TGC AAT GAG ACA TGG G-3‘

Mouse-specific primers for the confirmation of the *Igf1r* knockout:

Primer name	Sequence
P1	5‘-CTT CCC AGC TTG CTA CTC TAG G-3‘
P2	5‘-CAG GCT TGC AAT GAG ACA TGG G-3‘
P3	5‘-TGA GAC GTA GCG AGA TTG CTG TA-3‘

2.9.4 Antibodies

2.9.4.1 Primary antibodies

Primary antibody	Manufacturer
α-AKT, monoclonal antibody, rabbit	Cell Signaling Technology Inc., Danvers, USA
α-Chr. A, polyclonal antibody, rabbit	Santa Cruz Biotechnology, Heidelberg, Germany
α-HSC-70, monoclonal antibody, mouse	Santa Cruz Biotechnology, Heidelberg, Germany
α-IGF1R, polyclonal antibody, goat	R&D Systems, Minneapolis, USA
α-IGF1Rα, polyclonal antibody, rabbit	Santa Cruz Biotechnology, Heidelberg, Germany
α-IGF1Rβ, monoclonal antibody, mouse	Merck Millipore, Darmstadt, Germany
α-IGF1Rβ, polyclonal antibody, rabbit	Santa Cruz Biotechnology, Heidelberg, Germany
α-Ki 67, monoclonal antibody, mouse	BD, Heidelberg, Germany
α-Lysozyme, monoclonal antibody, rabbit	Abcam, Cambridge, UK
α-Mucin 2, polyclonal antibody, rabbit	Santa Cruz Biotechnology, Heidelberg, Germany
α-p44/42 MAPK (ERK1/2), polyclonal antibody, rabbit	Cell Signaling Technology Inc., Danvers, USA

α-Phospho-AKT (Ser473), monoclonal antibody, rabbit	Cell Signaling Technology Inc., Danvers, USA
α-Phospho-AKT (Thr308), monoclonal antibody, rabbit	Cell Signaling Technology Inc., Danvers, USA
α-Phospho-IGF1R, polyclonal antibody, rabbit	Abcam, Cambridge, UK
α-Phospho-p44/42 MAPK (ERK1/2) (Thr202/Tyr204), monoclonal antibody, rabbit	Cell Signaling Technology Inc., Danvers, USA
α-Tubulin, monoclonal antibody, mouse	Sigma-Aldrich, Deisenhofen, Germany
α-Villin, monoclonal antibody, rabbit	Abcam, Cambridge, UK

2.9.4.2 Secondary antibodies

Secondary antibody	Manufacturer
α-goat IgG, Cy3-conjugated	Sigma-Aldrich, Deisenhofen, Germany
α-mouse IgG, Cy3-conjugated (C2181)	Sigma-Aldrich, Deisenhofen, Germany
α-mouse IgG, FITC-Phalloidin-conjugated	Sigma-Aldrich, Deisenhofen, Germany
α-mouse IgG (H+L), HRP-conjugated, rabbit	Dianova Jackson ImmunoResearch, Hamburg, Germany
α-rabbit IgG, biotinylated species-specific whole antibody	GE Healthcare, Braunschweig, Germany
α-rabbit IgG, Cy3-conjugated (C2306)	Sigma-Aldrich, Deisenhofen, Germany
α-rabbit IgG, FITC-Phalloidin-conjugated	Sigma-Aldrich, Deisenhofen, Germany
α-rabbit IgG (H+L), HRP-conjugated, goat	Dianova Jackson ImmunoResearch, Hamburg, Germany
Peroxidase / DAB+, rabbit / mouse	Dako, Hamburg, Germany

2.10 Databases

Application	Database
Analysis of DNA- and protein sequences	BLAST-program (Altschul *et al.*, 1990) (http://ncbi.nlm.nih.gov)
Analysis of statistical significance	GraphPad Prism, (http://graphpad.com/quickcalcs/ttest1.cfm)
Bioinformatics	Ensembl v32 (http://www.ensembl.org) Nation Center for Biotechnology Information (http://ncbi.nlm.nih.goc)
Collection of published human inherited disease mutations	Human Gene Mutation Database (HGMD® Professional 2016.1)
Primer design	Primer3 (http://frofo.wi.mit.edu/chi-bin/primer3/primer3_www.cgi)

2.11 Isolation and purification of nucleic acids

2.11.1 Isolation of genomic DNA from the small intestine and colon

For the confirmation of the *Igf1r* knockout in the small intestine and colon of Villin-CreERT-Igf1r mice, genomic DNA was isolated. Therefore, small intestinal and colonic tissue was solved in 2.5 ml SE buffer by vortexing. Afterwards, 125 µl proteinase K as well as 250 µl 10% SDS were added. Tubes were swung and incubated at 56°C overnight. The next day, 750 µl 6M NaCl were added and the suspension was vortexed for 15 seconds. The suspension was centrifuged at 5200 rpm at 25°C for 15 minutes and the supernatant was added to 2.5 vol. 100% EtOH. The accumulated DNA was purified with 70% EtOH and centrifuged at 1400 rpm for 5 minutes. Afterwards, the extracted DNA was dried and resuspended in ddH_2O.

2.11.2 Precipitation of genomic DNA for genotyping by quantitative *real time* PCR

For the preparation of the genomic DNA that was extracted from tail biopsies (see chapter 2.13.1) for genotyping by quantitative *real time* PCR, the DNA, which was

before lysed using 200 µl PCR direct (Peqlab, Erlangen, Germany) and 1 µl proteinase K (Carl Roth GmbH, Karlsruhe, Germany) was precipitated. Therefore, 144.2 µl isopropanol and 26 µl 2 M NaCl were added to each DNA sample. The suspension was inverted and incubated at -20°C overnight. The next day, the DNA was precipitated by centrifugation at 13.000 rpm at 4°C for 30 minutes. The samples were washed with 70% EtOH and centrifuged at 13.000 rpm at 4°C for 5 minutes. Afterwards, the EtOH evaporated at 50°C and the DNA pellet was dissolved in 10 mM Tris-HCl, pH 8.0 by using the thermomixer at 50°C for 10 minutes. The DNA was stored at -20°C.

2.12 Gel electrophoresis

2.12.1 Agarose gel electrophoresis of DNA

Gel electrophoresis is a technique for the separation of nucleic acid molecules. Depending on the fragment size, agarose gels with a concentration of 0.5 to 2% (w / v) were prepared. The agarose was dissolved by boiling it in 30 ml 1x Turbo buffer. DNA Stain G was used to stain the DNA and added according to the manufacturer's instructions. The gel was poured into the gel chamber. After the agarose gel was completely solidified, electrophoresis was performed at 150 mA and 150 V.

2.12.2 Length standard

For the determination of the DNA fragment length, the 1 Kb Plus DNA Ladder was used.

2.13 Polymerase Chain Reaction (PCR)

(Saiki *et al.* 1985)

The polymerase chain reaction is an *in vitro* method for the amplification of specific DNA fragments. This method uses high temperatures to denature double strand

template DNA (denaturation), so that short oligonucleotides (primers) are able to bind to the DNA (annealing). Once bound to the single stranded DNA, these oligonucleotides are elongated by a polymerase (elongation). The multiple repetition of these three steps of denaturation, annealing and elongation results in an exponential increase of specific DNA fragments. The success of the DNA amplification can be checked by agarose gel electrophoresis (see chapter 2.12).

2.13.1 Mango *Taq*-PCR for genotyping

For the genotyping of newborn pubs, DNA was extracted from tail biopsies. Therefore, tails were incubated with 200 µl PCR direct (Peqlab, Erlangen, Germany) and 1 µl proteinase K (Carl Roth GmbH, Karlsruhe, Germany) at 55°C overnight. The reaction was terminated by heating the solution at 85°C for 45 min.
Afterwards, a Mango *Taq*-PCR was performed using the genotyping primers specific for each mouse line (see chapter 2.9.2).

The following PCR reaction mixture was prepared:

1 µl DNA

0.75 µl $MgCl_2$ (50 mM)

0.7 µl Mango *Taq* DNA polymerase (1 U / µl)

5 µl 5x buffer

2.5 µl dNTP’s (2 mM)

0.5 µl Primer 1 (10 pmol / µl, sequence-specific)

0.5 µl Primer 2 (10 pmol / µl, sequence-specific)

14.05 µl ddH_2O

Following conditions were used:

Cycle step	Temperature	Times	Cycles
Initial denaturation	95°C	5 min	1
Denaturation	95°C	30 sec	30
Annealing	62°C	1 min	
Elongation	72°C	1 min	
Final elongation	72°C	10 min	1
Pause	12°C	∞	

After completion of the run, Stop mix was added to 1 µl of the reaction mixture and loaded on a 1% agarose gel.

2.13.2 Quantitative *real time* PCR for genotyping

The quantitative *real time* PCR is a PCR method that relies on the convential PCR principle, but additionally enables the quantification of the amount of the synthesized PCR product in real time after each cycle. The increase of the PCR product is quantified using a fluorescent dye that binds unspecifically double strand DNA. In the present study, the PCR Mastermix Platinum® SYBR® Green qPCRSuperMix-UDG with Rox (Life technologies, Darmstadt, Germany) was used. This dye binds the minor groove of double strand DNA and then fluoresce 1000 x stronger than its unbound state. SYBR® Green is excited by a wavelength of 480 nm and shows an emission spectrum with a maximum at 520 nm. The Rox reference dye serves for normalization of non-PCR-related fluctuations in fluorescence. The fluorescent intensity was quantified using the ABI Prism 7900T Sequence Detection System. During the exponential phase of the PCR reaction, in which the conditions are optimal, which means optimal polymerase activity and a sufficient amount of reaction materials (primers, $MgCl_2$), the threshold value is determined. The threshold value defines the PCR cycle with the optimal conditions and is further used for the calculation of the quantification (Ct value). The generated data was analyzed using the Sequence Detection System software (SDS Version 2.1, PE Applied Biosystems).
In the present study, quantitative *real time* PCR was performed to be able to distinguish between the heterozygous and homozygous state of the Villin-rtTA2-M2 mice (see

chapter 2.9.2.2) during genotyping. Therefore, the DNA of the mice, which were positive for the Villin-rtTA2-M2 transgene after Mango-*Taq*-PCR (see chapter 2.13.1) was purified overnight (see chapter 2.11.2). Afterwards, quantitative *real time* PCR was performed. The reaction consisted of the following components:

2.5 µl purified DNA

2.5 µl Primer (fw + rev 100 pmol / µl)

5.0 µl SYBR® Green

The following programme on the ABI Prism 7900T Sequence Detection System was used:

Cycle step	Temperature	Times	Cycles
	50°C	2 min	
Taq activation	95°C	3 min	
Denaturation	94°C	15 sec	40
Annealing	60°C	30 sec	
Elongation	72°C	30 sec	
	95°C	15 sec	
	60°C	15 sec	
Melting curve	60°C–95°C	2°C / min	

After completion of the measurement, data was transferred to MS Excel (Microsoft). The relative expression was determined by the ΔΔ-Ct-method using the following formulas:

ΔCt = Ct (gene of interest) – Ct (housekeeping gene)

$\Delta\Delta Ct = \Delta Ct$ (control) – ΔCt (sample of interest)

Relative expression = $2^{\Delta\Delta Ct}$

For normalization, the mRNA expression of the two housekeeping genes *Hprt* (hypoxanthine-guanine phosphoribosyltransferase) and *Tbp* (TATA box binding protein) was used.

2.14 Protein chemical techniques

2.14.1 Isolation of total protein from tumors derived in xenograft mice and from colonic tumors induced by AOM / DSS, respectively

For the isolation of total protein from tumors derived in xenograft mice and from colonic tumors induced in Villin-TRE-IGF1R and Villin-CreERT-Igf1r mice by AOM / DSS, respectively, the tumors were excised from the mice, transferred into a screw cap cup and quick-frozen in liquid nitrogen. A small piece of the quick-frozen sample was administered to approx. 50 µl modified RIPA buffer and lysed using the Tissue Lyser LT (Qiagen, Hilden, Germany) at an oscillation of 50 / s for 5 min. Afterwards, the samples were sonicated for 5 cycles á 20 sec and centrifuged at 13.000 rpm at 4°C for 10 min. The supernatant was transferred into a new reaction tube and stored at -20°C.

2.14.2 Isolation of total protein from intestinal tissue

For the isolation of total protein from intestinal tissue, the small intestine and colon were excised from the mice and cut longitudinally. The epithelial cells of the small intestine and colon were scraped using a 22 x 22 mm coverglass, transferred into a screw cap cup and quick-frozen in liquid nitrogen. A small piece of the quick-frozen sample was administered to approx. 50 µl modified RIPA buffer and lysed using the Tissue Lyser LT (Qiagen, Hilden, Germany) at an oscillation of 50 / s for 5 min. Afterwards, the samples were sonicated for 5 cycles á 20 sec and centrifuged at 13.000 rpm at 4°C for 10 min. The supernatant was transferred into a new reaction tube and stored at -20°C.

2.14.3 Determination of protein concentration

(Bradford 1976)

Protein concentration was determined using the Roti®Nanoquant reagent (Carl Roth GmbH, Karlsruhe, Germany) according to the method of Bradford. The principle of this method is based on the change of the absorption after binding of the Coomassie

Brilliant Blue dye to cationic and hydrophobic side chains of proteins. Upon binding, the absorption maximum increases from 495 nm to 595 nm, which is proportional to the concentration of the proteins. For measurement, proteins from cell cultures were diluted 1:100, while proteins from tissue samples were diluted 1:200, and triplicates of 50 µl of each solution were appended into a 96-well plate. 200 µl 1x Roti®Nanoquant was added to each sample and incubated for 5 min at RT. The measurement was performed using the Synergy Mx plate reader (BioTek, Friedrichshall, Germany). For western blot analysis, 5 µg to 25 µg protein was used.

2.14.4 Sodium Dodecyl Sulfate Polyacrylamide Gel Electrophoresis (SDS-PAGE)

For the separation of proteins, the NuPAGE® Pre-Cast Gel System (Life Technologies, Darmstadt, Germany) was used. This is a polyacrylamide gel system for high performance gel electrophoresis and is based on SDS-PAGE gel chemistry (Laemmli 1970). The system consists of NuPAGE® Bis-Tris pre-cast gels and specifically optimized buffers with a pH of 7.0. This neutral pH increases the stability of proteins and gels, providing increased confidence in electrophoresis.
Five to 25 µg protein was mixed with 0.4 vol NuPAGE® LDS Sample Buffer (4x) (Life Technologies, Darmstadt, Germany) and 10% of the reducing agent DTT. The proteins were denatured at 70°C for 10 minutes, centrifuged and loaded onto the NuPAGE™ 4-12% Bis-Tris gel (Life Technologies, Darmstadt, Germany). Gel electrophoresis was performed at 160 V for approx. 30 min to 2 hours depending on the molecular weight of the target proteins using 1x MES buffer (Life technologies, Darmstadt, Germany). For the determination of the size of the proteins, the NuPAGE™ See Blue Plus2 (Life Technologies, Darmstadt, Germany) was used.

2.14.5 Transfer of proteins from Polyacrylamide gels to PVDF membranes

(Gershoni and Palade 1982, 1983)

To detect proteins by western blot analysis, separated proteins were transferred on a PVDF membrane by semi-dry blotting. Therefore, a PVDF membrane (GE Healthcare, Freiburg, Germany) was activated in 100% methanol for 5–10 sec and equilibrated in transfer buffer IIa for approx. 10 min together with six Whatman filter papers

(Schleicher & Schull, Dassel, Germany). For blotting, three Whatman filter papers, the activated and equilibrated PVDF membrane, the polyacrylamide gel and again three Whatman filter papers were placed on the anode. The electro-blotter (Biometra, Göttingen, Germany) was closed placing the cathode on top. The transfer was performed at 25 V and 220 mA for approx. 30 min to 1 hour depending on the molecular weight of the proteins.

2.14.6 Incubation of protein-bound membranes with antibodies

To block unspecific binding sites, the membrane was incubated in 1x TBS-T with 5% low-fat dry milk (blocking buffer) for 1 hour. The membrane was washed with 1x TBS-T and incubated with the primary antibody specific against the protein of interest in TBS-T at 4°C overnight. Subsequently, the membrane was washed twice with 1x TBS-T with 2.5% low-fat dry milk (washing buffer) and incubated with the appropriate horseradish peroxidase conjugated secondary antibody diluted in blocking buffer for 2 hours at RT. After incubation, the membrane was washed three times for 15 min with washing buffer and 5 min with TBS-T. For the detection of chemiluminescent signals, the ECL Prime Kit (GE Healthcare, Freiburg, Germany) was used. The solution was appended on the membrane, incubated and the signal was digitally developed using the western blot detection system FlourChem® Q Alpha with the appropriate AlphaView software (Innotech, Logan, USA). Following antibodies and dilutions were used:

Primary antibody	Dilution of primary antibody	Dilution of secondary antibody
α-AKT	1:2000	1:20000
α-HSC-70	1:20000	1:40000
α-IGF1Rα	1:1000	1:10000
α-IGF1Rβ	1:2000	1:20000
α-p44/42 MAPK (ERK1/2)	1:2000	1:20000
α-Phospho-AKT (Ser473)	1:2000	1:20000
α-Phospho-AKT (Thr308)	1:2000	1:20000
α-Phospho-IGF1R	1:1000	1:10000
α-Phospho-p44/42 MAPK (ERK1/2)	1:2000	1:20000
α-Tubulin	1:10000	1:20000
α-Villin	1:1000	1:10000

2.15 Cell biological methods

2.15.1 Cell culture of eukaryotic cells

The adherent growing human colorectal cancer cell lines CaCo-2, DLD-1 and the rectal cancer cell line SW837 were used for the xenograft experiments (see chapter 2.17.10). DLD-1 and SW837 cells were cultured in commercially purchased RPMI 1640 medium (PAN, Aidenbach, Germany), the CaCo-2 cells were grown in MEM medium (Life Technologies, Darmstadt, Germany). The cells were cultured at 37°C in a humified atmosphere with 5% CO_2. Depending on the proliferation rate, cells were splitted one to two times per week. For splitting, the cells were incubated with a minimal amount of Trypsin / EDTA (PAN, Aidenbach, Germany) at 37°C until cells detached from the bottom of the culture flask, which was controlled using the AE2000 inverted microscope (Ted Pella, Inc., Redding, USA). After cells have detached, the proteolytic activity of Trypsin / EDTA was terminated by the addition of growth medium. Then, cells were diluted in fresh growth medium. For the xenograft experiments, a distinct number of cells was used. Therefore, cells were counted with a Neubauer improved counting chamber (Hartenstein, Würzburg, Germany).

2.15.2 Cryo-preservation and revitalization of eukaryotic cells

For the cryo-preservation, cells were grown to a confluence higher than 80%, washed with DPBS (PAN, Aidenbach, Germany) and trypsinized. After detachment, cells were centrifuged at 500 g for 5 min to remove remaining Trypsin / EDTA and resuspended in an appropriate amount of culture medium containing 10% DMSO. Subsequently, the cells were slowly cooled to -80°C (1°C / min) in a freezer using the Mr. Frosty system (Thermo Scientific, Langenselbold, Germany). Frozen cells were transferred to liquid nitrogen for long term storage.
For the revitalization of eukaryotic cells, frozen cells were quickly thawed within a water bath at 37°C, centrifuged at 200 g for 5 min and the supernatant was discarded. The cells were gently resuspended in fresh culture medium, transferred into a culture flask and incubated at 37°C in a humified atmosphere with 5% CO_2.

2.15.3 Test for Mycoplasma contamination

The test for mycoplasma contamination was routinely performed using the MycoAlert® Mycoplasma Detection Kit (Lonza, Cologne, Germany) according to the manufacturer's instructions. Importantly, only half of the recommended amounts of the reagent and substrate were used.
Mycoplasma are small prokaryotes that compete with the cultured cells for the nutrients in the growth media and therefore change cellular functions, such as proliferation and gene expression. The MycoAlert® Mycoplasma Detection Kit is based on the measurement of the activity of mycoplasma-specific enzymes before and after application of specific substrates.
Weakly contaminated cells were treated with Mycokill AB (Lonza, Cologne, Germany) diluted 1:50 in growth medium for 2 to 3 passages, while highly contaminated cells were discarded.

2.16 Immunostainings

2.16.1 Immunohistochemistry on paraffin-embedded tissue sections

Immunohistochemistry was performed on paraffin-embedded murine tissue sections (2 to 4 µm) of the small intestine and colon. For the different staining experiments different protocols were used. At first, tissue sections were depariffinized in xylene for 15 to 20 min and rehydrated through graded ethanol series at RT. For antigen retrieval, tissue sections were boiled in citrate buffer or sodium citrate buffer, respectively, for 15 to 20 min. Afterwards, the endogenous peroxidase was blocked using 1% or 3% H_2O_2, respectively, for 15 to 45 min at RT. For the blocking of unspecific binding sites, the small intestinal and colonic tissue sections were blocked with either 10% FBS in DPBS, 5% BSA in DPBS or 5% FBS and 10% BSA in DPBS for 20 min to 1 hour, depending on the protocol. Subsequently, tissue sections were incubated with the primary antibody at 4°C overnight. The next day, the sections were washed and incubated with the secondary antibody depending on the protocol. The staining was developed using DAB Chromogen (Dako, Hamburg, Germany), counterstained using hemalum solution (Carl Roth GmbH, Karlsruhe, Germany) and covered with Glycergel Mounting Medium (Dako, Carpinteria, USA).

Primary antibody	Dilution of primary antibody	Secondary Antibody	Dilution of secondary antibody
Chromogranin A	1 : 200	α-rabbit biotinylated antibody	1 : 1000
IGF1R	1 : 100	α-goat biotin conjugated antibody	1 : 1000
Ki 67	1 : 50	α-rabbit / mouse HRP conjugated antibody	1 : 1 in TBS
Lysozyme	1 : 200	α-rabbit biotinylated antibody	1 : 1000
Mucin 2	1 : 200	α-rabbit biotinylated antibody	1 : 1000

2.16.2 Alkaline phosphatase (AP) staining of enterocytes

The small intestinal and colonic tissue sections (2 to 4 µm) were depariffinized in xylene for 10 min and rehydrated through graded ethanol series at RT. Then, 200 µl AP buffer was added and incubated for 5 to 10 min at RT. The AP buffer was removed and approx. 120 µl AP staining solution was added and incubated for approx. 25 min at RT until sufficient staining was visible. The sections were washed, counterstained with hemalum solution (Carl Roth GmbH, Karlsruhe, Germany) and covered using Glycergel Mounting Medium (Dako, Carpinteria, USA).

2.16.3 Immunofluorescence double staining on paraffin-embedded tissue sections

Immunofluorescence double staining was performed on paraffin-embedded murine tissue sections (2 to 4 µm) of the small intestine and colon. At first, tissue sections were depariffinized in xylene for 20 min and rehydrated through graded ethanol series at RT. For antigen retrieval, tissue sections were boiled in 10 mM citrate buffer for 3 x 5 min. For the blocking of unspecific binding sites, the small intestinal and colonic

tissue sections were blocked with 10% FBS in DPBS for 1 hour. Subsequently, tissue sections were incubated with the primary antibodies at 4°C overnight. The next day, sections were incubated with the Cy3-conjugated and FITC-Phalloidin-conjugated secondary antibodies diluted in DPBS for 2 hous at RT. Afterwards, sections were washed 3 x 10 min in DPBS and 1 x 10 min in ddH_2O. Tissue sections were covered using Vectashield with DAPI (VectorLab, Burlingame, USA).

1st primary antibody + dilution	2nd primary antibody + dilution	1st secondary antibody + dilution	2nd secondary antibody + dilution
IGF1R 1 : 100	Mucin 2 1 : 200	α-goat IgG, Cy3-conjugated 1 : 1000	α-rabbit IgG, FITC-Phalloidin-conjugated 1 : 1000
IGF1R 1 : 100	Chromogranin A 1 : 200	α-goat IgG, Cy3-conjugated 1 : 1000	α-rabbit IgG, FITC-Phalloidin-conjugated 1 : 1000
IGF1R 1 : 100	Lysozyme 1 : 200	α-goat IgG, Cy3-conjugated 1 : 1000	α-rabbit IgG, FITC-Phalloidin-conjugated 1 : 1000

2.17 *In vivo* studies

2.17.1 Induction of the *IGF1R* overexpression in epithelial cells of the intestine of Villin-TRE-IGF1R mice by doxycycline administration

For the induction of the overexpression of human *IGF1R* in epithelial cells of the intestine, 4 week old Villin-TRE-IGF1R mice were administered to 0.2 mg / ml and 2 mg / ml doxycycline hyclate (AppliChem GmbH, Darmstadt, Germany), respectively,

over the drinking water. Common household sweetener “Das gesunde PLUS” (dm-drogerie markt GmbH + Co. KG, Karlsruhe, Germany) was additionally added to the drinking water (1 tablet per 150 ml drinking water). Mice in the control group received only drinking water with sweetener. Villin-TRE-IGF1R mice received doxycycline over the drinking water until they were sacrificed.

2.17.2 Induction of the *Igf1r* knockout in epithelial cells of the intestine of Villin-CreERT-Igf1r mice by tamoxifen injection

For the induction of the *Igf1r* knockout in epithelial cells of the intestine, 4 week old Villin-CreERT-Igf1r mice were intraperitoneally injected with 1 mg tamoxifen (Sigma-Aldrich, Deisenhofen, Germany) per day on five consecutive days. Therefore, 200 mg tamoxifen was dissolved in 800 µl EtOH and 19.2 ml sunflower seed oil from Helianthus annuus (Sigma-Aldrich, Deisenhofen, Germany).

2.17.3 Induction of colonic tumor formation by AOM or AOM / DSS

For the induction of tumor formation in the colon of Villin-TRE-IGF1R or Villin-CreERT-Igf1r mice, respectively, the mutagenic agent azoxymethane (AOM) (Neufert *et al.* 2007) or the combination of azoxymethane and the inflammatory agent dextran sulfate sodium (DSS) (Neufert *et al.* 2007; Thaker *et al.* 2012) were used.

2.17.3.1 AOM treatment

To induce tumor formation in the colon of Villin-TRE-IGF1R and Villin-CreERT-Igf1r mice by AOM, mice were injected intraperitoneally with 10 mg / ml AOM in NaCl once per week on four consecutive weeks.

2.17.3.2 AOM / DSS treatment

For the induction of colonic tumor formation and inflammation in Villin-TRE-IGF1R and Villin-CreERT-Igf1r mice by AOM / DSS, mice were once intraperitoneally injected with 10 mg / ml AOM to induce colonic tumor formation followed by two cycles of 2% DSS

over the drinking water to induce intestinal inflammation. Common household sweetener “Das gesunde PLUS” (dm-drogerie markt GmbH + Co. KG, Karlsruhe, Germany) was additionally added to the drinking water (1 tablet per 150 ml drinking water). The first DSS cycle started one week after the AOM injection and lasted four days. The second cycle started one week after the end of cycle one and lasted three days. Between the DSS cycles and for 21 days after completion of the second DSS cycle, mice were fed with cereal mush to prevent dehydration of the mice. DSS administration often led to rapid loss of weight, diarrhea or bloody feces. To minimize the pain, mice were subcutaneously injected with 0.1 mg / kg body weight of the analgesic Buprenorphin (Temgesic®, RB Pharmaceuticals Limited, Berkshire, UK) diluted in NaCl.

2.17.4 Colonoscopy

Colonoscopy was performed to check for tumor formation in the colon of Villin-TRE-IGF1R and Villin-CreERT-Igf1r mice. In cooperation with Dr. Ramona Schulz (Department of Molecular Oncology, University Medical Center Göttingen, Germany) the colonoscopy device (Karl Storz GmbH & Co. KG, Tuttlingen, Germany) was used according to the manufacturer’s instructions. To minimize the stress during the process of colonoscopy, a special, very thin endoscope was used. The mice were anesthetized using the inhalant isoflurane (Abbvie, Wiesbaden, Germany). To estimate tumor size, grading of tumors was done related to Becker *et al.* (2007). The scores 1 to 5 indicate the tumor size relative to the circumference of the colon. Is the tumor just detectable, it has a score of 1. If the tumor surrounds 12.5% of the circumference of the colon, it has a score of 2. A score of 3 is at 25%, a score of 4 at 50% tumor size relative to the circumference of the colon. If the tumor comprises more than 50% of the circumference of the colon, it has a score of 5.

2.17.5 Macroscopic analysis of the tumors

For macroscopic analysis of the developed tumors induced by AOM or AOM / DSS treatment, the Villin-TRE-IGF1R and Villin-CreERT-Igf1r mice were sacrificed and the small intestine and colon were excised from the animals. The intestinal tissue was cut

longitudinally and the number of colonic tumors was counted. Furthermore, the part of the colon, where the tumors have developed, was determined. Therefore, the colon was divided into three parts: distal, middle and proximal part from the anus to the stomach (Fig. 3). Afterwards, the length and width of all tumors was measured using a caliper. Subsequently, the intestinal samples were fixed in formalin and paraffin-embedded for histopathological analysis.

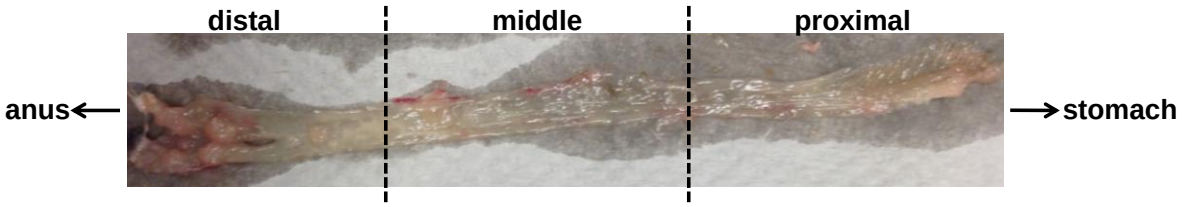

Fig. 3: Preparation of the murine colon for analysis.

The colon was excised from the sacrificed mice and cut longitudinally. For the determination of the tumor location in the colon, the colon was divided into three parts: distal, middle and proximal part from the anus to the stomach. The number of tumors per part was counted.

2.17.6 Histopathological analysis of tumors

For the histopathological analysis of the colonic tumors after AOM or AOM / DSS administration, the fixed colon samples were paraffin-embedded and hematoxylin and eosin staining was prepared in the Institute of Pathology, University Medical Center Göttingen, Germany. Importantly, the colonic tissue samples with tumors induced by AOM / DSS were cut stepwise as follows: the first section was taken and the following ten sections were discarded. This process was repeated until three tissue sections were prepared. This process was done to increase the probability to detect as many tumors as possible along the axis from distal to proximal for histopathological analysis. Afterwards, the tumor stage and tumor size were determined together with Dr. med. Felix Bremmer (Institute of Pathology, University Medical Center Göttingen, Germany) using the Axio Scope.A1 microscope and the appropriate ZEN lite 2012 software (Zeiss, Oberkochen, Germany).

2.17.7 Histopathological analysis of liver tissue and lymph nodes in regional colonic fat tissue

In order to screen for metastatic cells in the liver tissue and lymph nodes in regional colonic fat tissue, liver tissue and lymph nodes in the regional colonic fat tissue were excised from the mice, fixed in 4% formalin and paraffin-embedded. Ten sections were each cut and stained with hematoxylin and eosin. Afterwards, Dr. med. Felix Bremmer (Institute of Pathology, University Medical Center Göttingen, Germany) screened the ten sections of the livers and lymph nodes for metastases, respectively.

2.17.8 Quantification of goblet cells, Paneth cells, enteroendocrine cells and proliferating cells

For the quantification of goblet cells, Paneth cells, enteroendocrine cells and proliferating cells, Villin-TRE-IGF1R mice were administered to doxycycline to induce the *IGF1R* overexpression (see chapter 2.17.1) and Villin-CreERT-Igf1r mice were intraperitoneally injected with tamoxifen to induce the knockout of the *Igf1r* (see chapter 2.17.2), respectively. Four weeks, three months and 1.5 years after the induction of the *IGF1R* overexpression and the *Igf1r* knockout, respectively, mice were sacrificed, the small intestinal and colonic tissue were dissected from the mice, cut longitudinally, rolled and fixed in 4% formalin. The fixed tissue samples were paraffin-embedded and cut in the Institute of Pathology, University Medical Center Göttingen, Germany. Ten sections (2 to 4µm) were each cut. Immunohistochemistry was performed (see chapter 2.16.1). For the quantification of the different cell types, stained cells of 50 crypts and 50 villi, respectively, per mouse were manually counted using the AlphaView software (Innotech, Logan, USA).

2.17.9 Determination of the villi length and crypt depth of Villin-TRE-IGF1R mice

For the determination of the villi length and crypt depth, Villin-TRE-IGF1R mice were continuously treated with 0 mg / ml or 2 mg / ml doxycycline for three months to induce the *IGF1R* overexpression (see chapter 2.17.1). Subsequently, the animals were sacrificed, the small intestinal and colonic tissues were excised from the mice and divided into small pieces without cutting them longitudinally. Thus, the villi and crypts

were kept in their “natural” appearance without squeezing. The tissue samples were fixed in 4% formalin, paraffin-embedded and cut. Hematoxylin and eosin staining was performed on 10 tissue sections (Institute of Pathology, University Medical Center Göttingen, Germany). Afterwards, the length of 50 villi and the depth of 50 crypts of each mouse were measured using the cellSens Dimension software appropriate to the microscope BX60 (Olympus, Hamburg, Germany).

2.17.10 Xenograft experiments

For the xenograft experiments, a distinct number of DLD-1, CaCo-2 and SW837 cells, respectively (see chapter 2.15.1) in the logarithmic phase of growth were added to 0.5 mg / ml matrigel (BD Bioscience, San Jose, USA) and subcutaneously injected into each flank of 6 to 8 week old female immune-deficient RjOrl:NMRI-*Foxn1*^{nu}/*Foxn1*^{nu} mice (see chapter 2.9.2.1). Tumor volume was determined regularly using a caliper and calculated using the formula “V = width^2 x length x 0.5”. When the tumors reached a volume of approx. 300 mm^3, mice were randomized into either a treatment group of AEW541 (40 mg / kg; dissolved in 25 mM L(+)-Tartaric acid (Sigma-Aldrich, Deisenhofen, Germany)), erlotinib (100 mg / kg; dissolved in 0.2% (w / v) Carboxymethylcellulose with 0.1% Tween 80), the combination of AEW541 and erlotinib or a control group. Mice were treated with combined 5-FU-based RCT (50 mg / kg, dissolved in PBS followed by 1.8 Gy irradiation per day (Department of Radiotherapy and Radio Oncology, University Medical Center Göttingen, Germany) in addition to inhibitor treatment. Mice in the control group received combined RCT like the treatment groups in combination with the same amount of the solvent. Combined 5-FU-based RCT was applied on five consecutive days. In addition, inhibitors were administered on eight consecutive days. Since the mice did not tolerate the treatment, the treatment scheme was changed in cooperation with Dr. rer. nat. Melanie Spitzner (Department of General, Visceral and Pediatric Surgery, University Medical Center Göttingen, Germany). Thus, mice were administered to combined 5-FU-based RCT on the first three days of treatment as well as on the days ten and eleven. Inhibitors were applied in two cycles. The first cycle started on day one of treatment and lasted for four days, whereas the second cycle started on day seven and lasted for five days. Tumor volume was measured daily using a caliper. When the tumors reached a volume of approx. 1500 mm^3, the tumors were dissected from the mice, weighed and measured.

Here, tumor volume was calculated using the formula “V = width x length x height x π / 6”.

2.18 Statistical analysis

To test for statistical significance, the unpaired student’s *t* test was performed. The program GraphPad Prism was used to calculate the P value. The P value indicates the probability that the results are not different. A P value smaller than * $p < 0.05$ means statistically significant; ** $p < 0.01$ means very significant; *** $p < 0.001$ means extremely significant.

3 Results

3.1 Establishment of a mouse line used to induce overexpression of the *IGF1R* in the intestine

To study the role of the IGF1R during the development of the intestine and during intestinal tumor formation and progression, respectively, a mouse model for the inducible overexpression of the *IGF1R* was established, called thereafter Villin-TRE-IGF1R. The Villin-TRE-IGF1R mouse line is a double transgenic mouse line and was generated by the breeding of the Villin-rtTA2-M2 mouse line (chapter 2.9.2.2) with the TRE-IGF1R mouse line (chapter 2.9.2.3).

3.1.1 Genotyping of the Villin-rtTA2-M2 mouse line

The Villin-rtTA2-M2 mouse line is a transgenic mouse line that expresses the doxycycline-dependent reverse tetracycline transactivator rtTA2-M2 under the intestine specific villin promoter (Roth *et al.* 2009).

To check the newborn pubs for the presence of the Villin-rtTA2-M2 transgene, DNA of the tail was isolated and analyzed by PCR. Therefore, transgene-specific primers were used (Roth *et al.* 2009). In Fig. 4a the result of a genotyping PCR is shown. T/+ is a positive control meaning that the transgene is present. H_2O was used as a negative control. Mice #236 and #237 are negative for Villin-rtTA2-M2. However, mice #238 to #246 show a band for T/+, which means that those mice are carriers of the Villin-rtTA2-M2 transgene. To be able to distinguish between the heterozygous and homozygous state for Villin-rtTA2-M2, the expression of the transgene was analyzed by quantitative *real time* PCR. Therefore, the DNA of the mice, which were positive for Villin-rtTA2-M2 (#238 to #246) was purified overnight and quantitative *real time* PCR was performed. The relative expression of the transgene of the heterozygous mice was half the relative expression of homozygous mice (Fig. 4b).

For further breedings only the homozygous mice for Villin-rtTA2-M2 (T/T) were used, so that genotyping was not necessary for each breeding experiment. Nevertheless, genotyping PCRs were performed on a regular basis to check for the correct genotype.

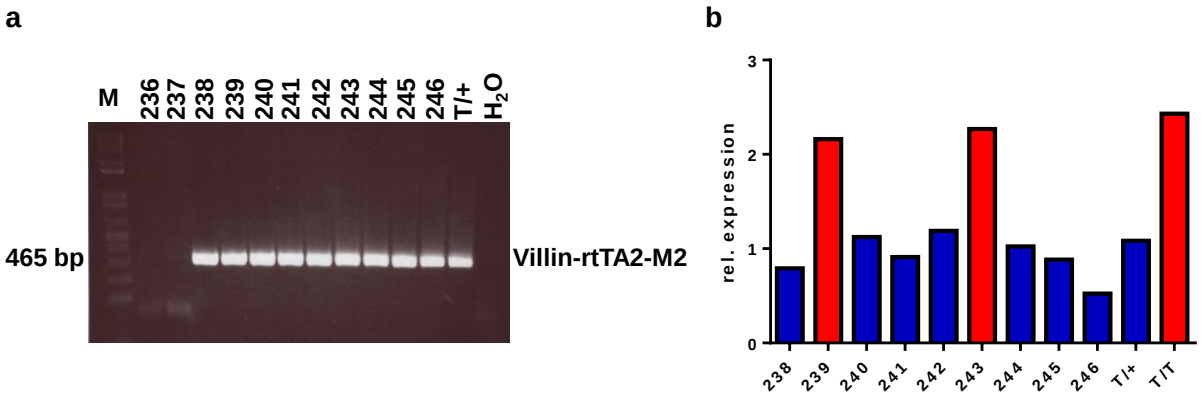

Fig. 4: Genotyping of the Villin-rtTA2-M2 mouse line.

For genotyping, tail DNA was extracted and used in the PCR together with transgene-specific primers. **(a)** Mice #238 to #246 carried the Villin-rtTA2-M2 transgene. **(b)** For the discrimination between mice heterozygous or homozygous for the transgene, the expression of the Villin-rtTA2-M2 transgene was analyzed by quantitative *real time* PCR. Mice #239 and #243 were homozygous for the transgene, whereas mice #238, #240 to #242 and #244 to #246 were heterozygous for the Villin-rtTA2-M2 transgene. M=1 Kb Plus DNA Ladder, T/+=positive control of a heterozygous Villin-rtTA2-M2 mouse, T/T=positive control of a homozygous Villin-rtTA2-M2 mouse, H_2O=negative control without DNA.

3.1.2 Genotyping of the TRE-IGF1R mouse line

The TRE-IGF1R mouse line is a transgenic mouse line expressing the human *IGF1R* under the control of the doxycycline-inducible pTRE2 promoter (Jones *et al.* 2007). To analyze the genotype of the pubs, PCR amplification of tail DNA was performed using specific primers for the TRE-IGF1R transgene. The product length is 450 bp. Mice #340 and #342 to #344 showed a band for the TRE-IGF1R transgene. Only mouse #341 was a wild type mouse (Fig. 5). This mouse line was kept as a heterozygous mouse line. Therefore, heterozygous animals (T/+) were crossed with wild type mice (+/+).

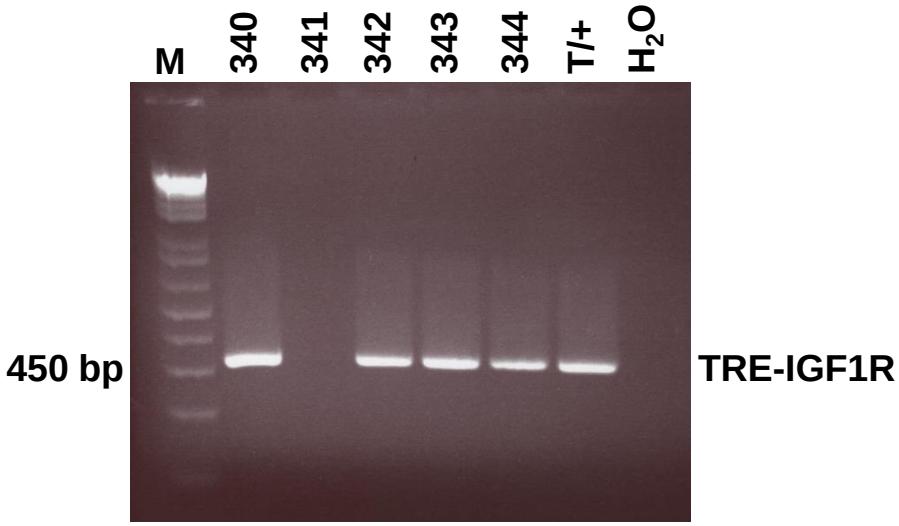

Fig. 5: Genotyping of the TRE-IGF1R mouse line.

Tail DNA was extracted and used as template in the PCR. Agarose gel electrophoresis was performed. The transgene-specific PCR-product has a size of 450 bp. Mice #340 and #342 to #344 showed a band of 450 bp and were therefore carriers of the TRE-IGF1R transgene. M=1 Kb Plus DNA Ladder, T/+=positive control of a heterozygous TRE-IGF1R mouse, H_2O=negative control without DNA.

3.1.3 Genotyping of the Villin-TRE-IGF1R mouse line

For the generation of the double transgenic Villin-TRE-IGF1R mouse line, the transgenic Villin-rtTA2-M2 mouse line was crossed with the transgenic TRE-IGF1R mouse line. For the genotyping of the pubs, tail DNA was amplified by one PCR with specific primers for the Villin-rtTA2-M2 transgene (Fig. 6a) and by another PCR with specific primers for the TRE-IGF1R transgene (Fig. 6b). The Villin-rtTA2-M2 mouse line was kept as a homozygous mouse line, while the TRE-IGF1R mouse line was kept as a heterozygous mouse line. Therefore, the offspring could either be heterozygous for Villin-rtTA2-M2 and heterozygous for TRE-IGF1R (T/+; T/+) or heterozygous for Villin-rtTA2-M2 and wild type for TRE-IGF1R (T/+; +/+).

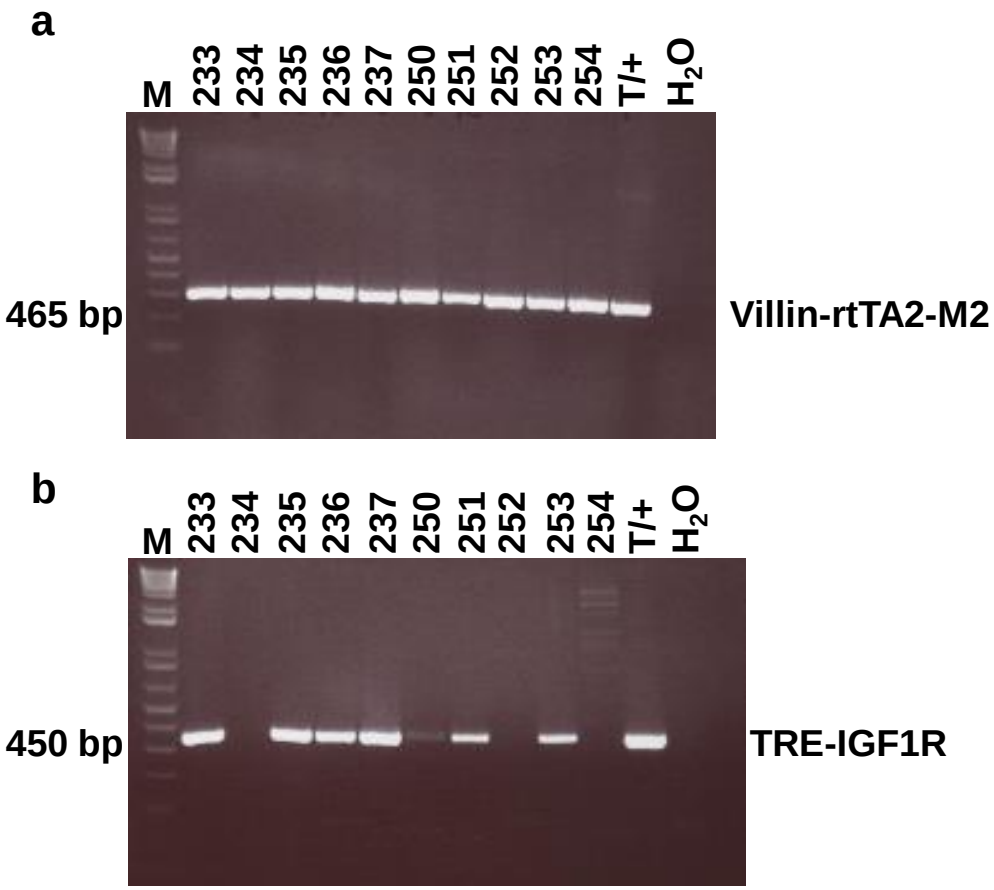

Fig. 6: Genotyping of the Villin-TRE-IGF1R mouse line used for the induction of the *IGF1R* overexpression.

For the genotyping of the newborn pubs of the Villin-TRE-IGF1R mouse line, DNA extracted from tail biopsies was amplified by PCR. Here, two PCR experiments were performed. **(a)** PCR using specific primers for the Villin-rtTA2-M2 transgene. **(b)** PCR with specific primers for the TRE-IGF1R transgene. All pubs were carriers of the Villin-rtTA2-M2 transgene, while only mice #204, #206 to #207, #210 and #212 to #215 carried the TRE-IGF1R transgene. M=1 Kb Plus DNA Ladder, T/+=positive control of either a heterozygous Villin-rtTA2-M2 mouse or a heterozygous TRE-IGF1R mouse, H_2O=negative control without DNA.

3.2 Induction of *IGF1R* overexpression in Villin-TRE-IGF1R mice

To study the effect of *IGF1R* overexpression during the development of the intestine and during intestinal tumor formation and progression, the Villin-TRE-IGF1R mouse line was used. As described in chapter 3.1.3, Villin-TRE-IGF1R mice could either be heterozygous for Villin-rtTA2-M2 and heterozygous for TRE-IGF1R (T/+; T/+; double transgenic) or heterozygous for Villin-rtTA2-M2 and wild type for TRE-IGF1R (T/+; +/+). Importantly, the overexpression of *IGF1R* can only be induced in the double transgenic Villin-TRE-IGF1R mice. The double transgenic Villin-TRE-IGF1R mice

express the reverse tetracycline transactivator rtTA2-M2 under the intestine-specific villin promoter, and the human *IGF1R* under the doxycycline inducible pTRE2 promoter. In the presence of doxycycline, the reverse tetracycline transactivator is able to bind to the pTRE2 promoter and therefore induces the overexpression of human *IGF1R* in the intestine.

For the following experiments, double transgenic Villin-TRE-IGF1R mice were administered to 0.2 mg / ml or 2 mg / ml doxycycline over the drinking water to induce *IGF1R* overexpression. This group of mice was named thereafter IGF1R-oe (for IGF1R-overexpressing mice). As control, double transgenic Villin-TRE-IGF1R mice were administered to H_2O instead of doxycycline (0 mg / ml doxycycline), and, in addition, Villin-TRE-IGF1R mice, which only carried the Villin-rtTA2-M2 transgene but not the TRE-IGF1R transgene, were administered to 0.2 mg / ml or 2 mg / ml doxycycline over the drinking water. These two latter groups of mice were summarized as control group. The drinking water was exchanged twice a week. For the experiments, doxycycline was continuously administered until the mice were sacrificed (Fig. 7).

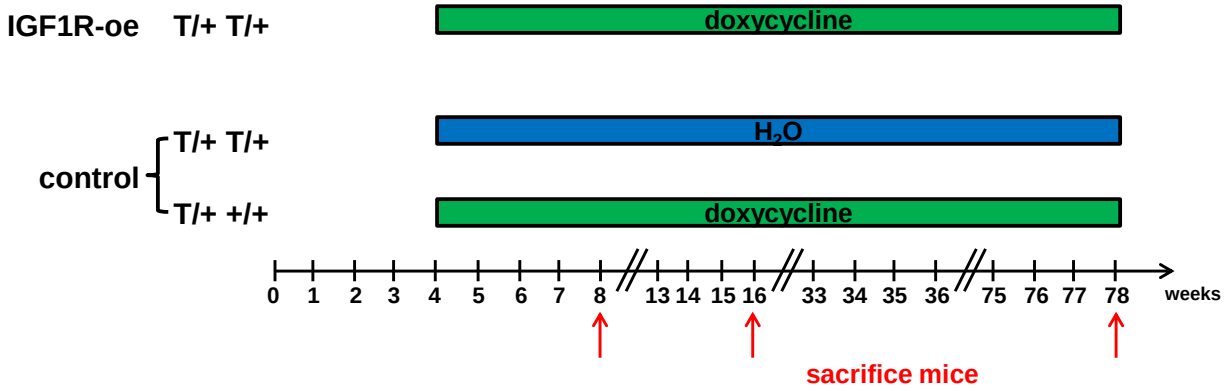

Fig. 7: Treatment scheme for the induction of *IGF1R* overexpression in the intestine of Villin-TRE-IGF1R mice.

To develop *IGF1R* overexpressing mice (IGF1R-oe), Villin-TRE-IGF1R mice that carried both, the Villin-rtTA2-M2 and the TRE-IGF1R transgene (T/+ T/+), were continuously administered to doxycycline over the drinking water. As control mice, double transgenic Villin-TRE-IGF1R mice (T/+ T/+), which were administered to H_2O, and Villin-TRE-IGF1R mice, which carried only the Villin-rtTA2-M2 transgene (T/+ +/+), but which were continuously administered to doxycycline over the drinking water, were used. The drinking water was exchanged twice a week. The red arrows mark time points when the mice were sacrificed for subsequent experiments.

3.3 Confirmation of villin expression in epithelial cells of the intestine of Villin-TRE-IGF1R mice *via* immunohistochemistry

Villin is known to be broadly expressed in every cell of the intestinal epithelium on both the vertical axis (crypt to villus tip) and the horizontal axis (duodenum through colon) of the intestine (Madison 2002). To confirm the expression of villin in epithelial cells of the small intestine (SI) and colon of Villin-TRE-IGF1R mice, intestinal tissue sections were stained with an antibody specific for villin. In Fig. 8 representative pictures of the staining are shown. Villin was highly expressed in epithelial cells of the villi of the small intestine. A gradient from strong villin expression in the villi to weak villin expression in the crypts of the small intestine was visible. In colonic epithelial cells, villin was highly expressed at the top of the crypts, whereas the expression of villin at the bottom of the crypts was weak.

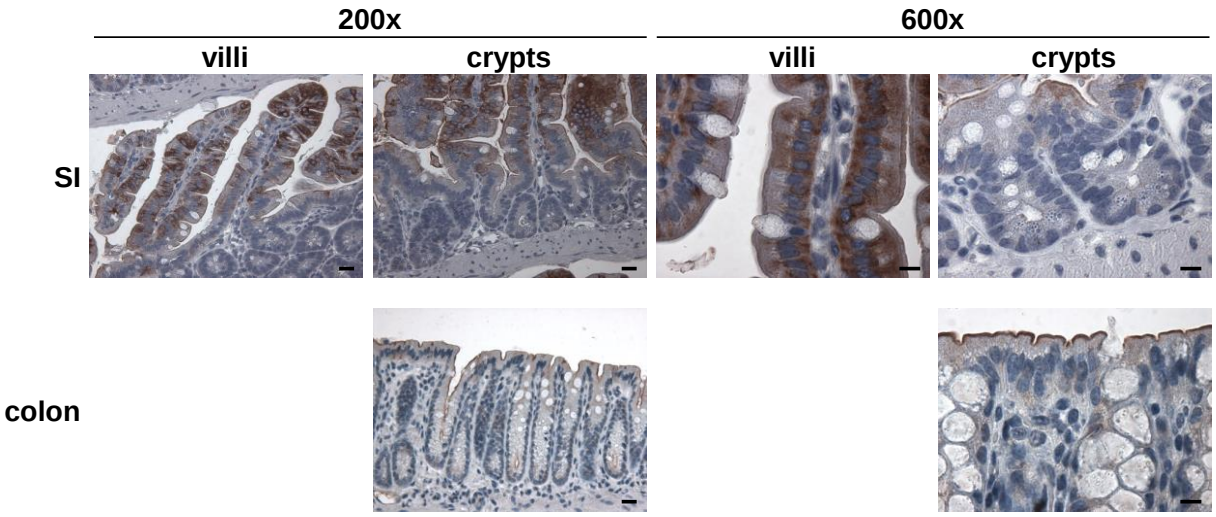

Fig. 8: Villin is expressed in epithelial cells of the murine intestine.

For the confirmation of villin expression in epithelial cells of the murine intestine, tissue sections of the small intestine (SI) (n=5) and colon (n=5) were stained for villin (brown). Cell nuclei were stained with hemalum solution (blue). Expression was visible in epithelial cells of the intestine. A gradient of villin expression could be observed from strong expression in the villi to weak expression in the crypts of the small intestine as well as strong expression at the top of the crypts to weak expression at the bottom of the crypts of the colon.

3.4 Confirmation of *IGF1R* overexpression in epithelial cells of the intestine *via* immunohistochemistry

The overexpression of human *IGF1R* in IGF1R-oe mice was confirmed by immunohistochemistry. Therefore, Villin-TRE-IGF1R mice were continuously treated with 0 mg / ml, 0.2 mg / ml and 2 mg / ml doxycycline over the drinking water for four weeks. The mice were sacrificed, the small intestine and colon were excised from the animals, fixed in formalin and paraffin-embedded. Afterwards, tissue sections were stained with a specific antibody for human IGF1R. IGF1R-oe mice revealed strong expression of human IGF1R in epithelial cells of the small intestine (Fig. 9a) and colon (Fig. 9b) compared to control mice, which showed no staining for human IGF1R.

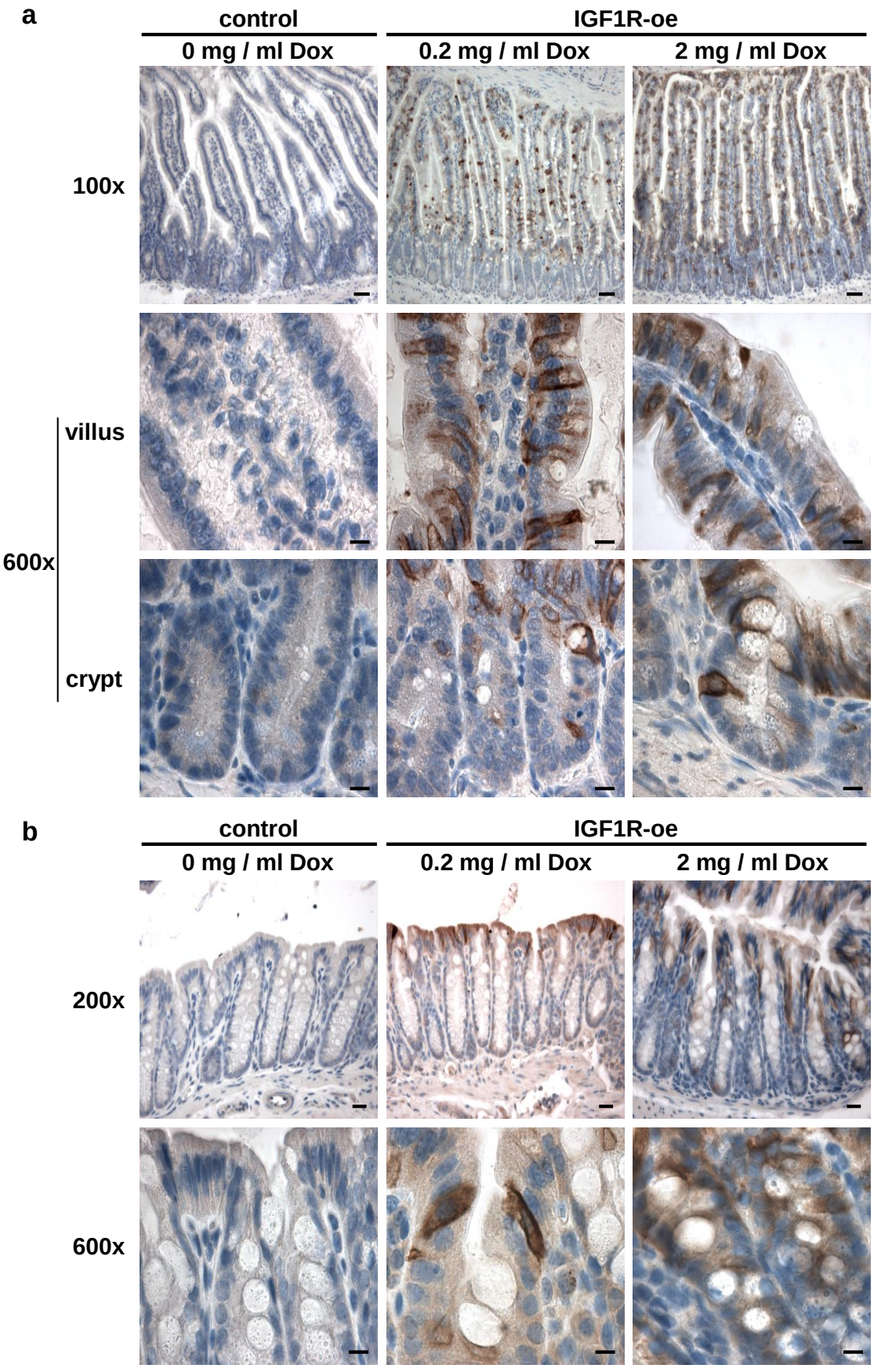
a
control
IGF1R-oe
0 mg / ml Dox
0.2 mg / ml Dox
2 mg / ml Dox
100x
600x
villus
crypt
b
control
IGF1R-oe
0 mg / ml Dox
0.2 mg / ml Dox
2 mg / ml Dox
200x
600x

Fig. 9: The IGF1R is overexpressed in epithelial cells of the villi and crypts in the small intestine and in epithelial cells of the crypts of the colon of IGF1R-oe Villin-TRE-IGF1R mice.
For the confirmation of the overexpression of *IGF1R*, Villin-TRE-IGF1R mice were continuously treated with doxycycline or H_2O for four weeks. The mice were sacrificed and tissue sections of the small intestine (n=5) and colon (n=5) were stained with an antibody specific for human IGF1R (brown). Cell nuclei were stained with hemalum solution (blue). IGF1R-oe mice highly expressed human IGF1R in the small intestine and colon in comparison to control mice.

3.5 Confirmation of *IGF1R* overexpression in the intestine and analysis of its downstream PI3K and MAPK signaling pathways

For the confirmation of the overexpression of *IGF1R* in epithelial cells of the mouse intestine, western blot analysis was performed (Fig. 10). Therefore, Villin-TRE-IGF1R mice were continuously treated with 0 mg / ml, 0.2 mg / ml or 2 mg / ml doxycycline for four weeks. After sacrificing the mice, the small intestine and colon were excised from the animals, cut longitudinally and proteins of epithelial cells were extracted separately. Western blot analysis revealed strong expression of IGF1Rα and IGF1Rβ in epithelial cells of the small intestine and colon of IGF1R-oe mice compared to control mice. Interestingly, in IGF1R-oe mice, the expression level of IGF1Rα and IGF1Rβ was extremely elevated in epithelial cells of the small intestine compared to the colon. Furthermore, the expression level of IGF1R depended on the doxycycline concentration. Thus, the expression of IGF1Rα and IGF1Rβ was highly increased in IGF1R-oe mice treated with 2 mg / ml doxycycline compared to IGF1R-oe mice treated with only 0.2 mg / ml doxycycline or control mice. To analyze if overexpression of the *IGF1R* results in the activation of its downstream PI3K and MAPK signaling pathways, western blot analysis was performed with specific antibodies for the phosphorylated forms of AKT (pAKT) and ERK (pERK). Notably, IGF1R-oe mice showed strong activation of AKT, whereas control mice revealed only a low AKT phosphorylation level. Of note, one control mouse also displayed AKT phosphorylation in the colon. The activation level of AKT depended on the doxycycline concentration with an increase of activated AKT in IGF1R-oe mice treated with 2 mg / ml doxycycline. This fact is of high interest when comparing the expression level of IGF1Rα and IGF1Rβ with the activation level of AKT. As already described, cells of the small intestine revealed an extremely high expression level of IGF1Rα and IGF1Rβ compared to cells of the colon, while in contrast the activation level of the downstream AKT was higher in cells of the

colon compared to the small intestine. Strong ERK activation was visible in the small intestine of the IGF1R-oe mice administered to 0.2 mg / ml doxycycline, whereas the two IGF1R-oe mice administered to 2 mg / ml doxycycline showed lower or even no activation of ERK in the small intestine. In the colon, a high phosphorylation level of ERK was visible in one control mouse, whereas IGF1R-oe mice showed lower ERK activation.

Taken together, western blot analyses demonstrated that the human IGF1R was overexpressed in the small intestine and colon of IGF1R-oe mice. Additionally, the downstream PI3K signaling pathway was activated in IGF1R-oe mice, whereas IGF1R overexpression seemed to have no influence on the activation of the downstream MAPK signaling pathway.

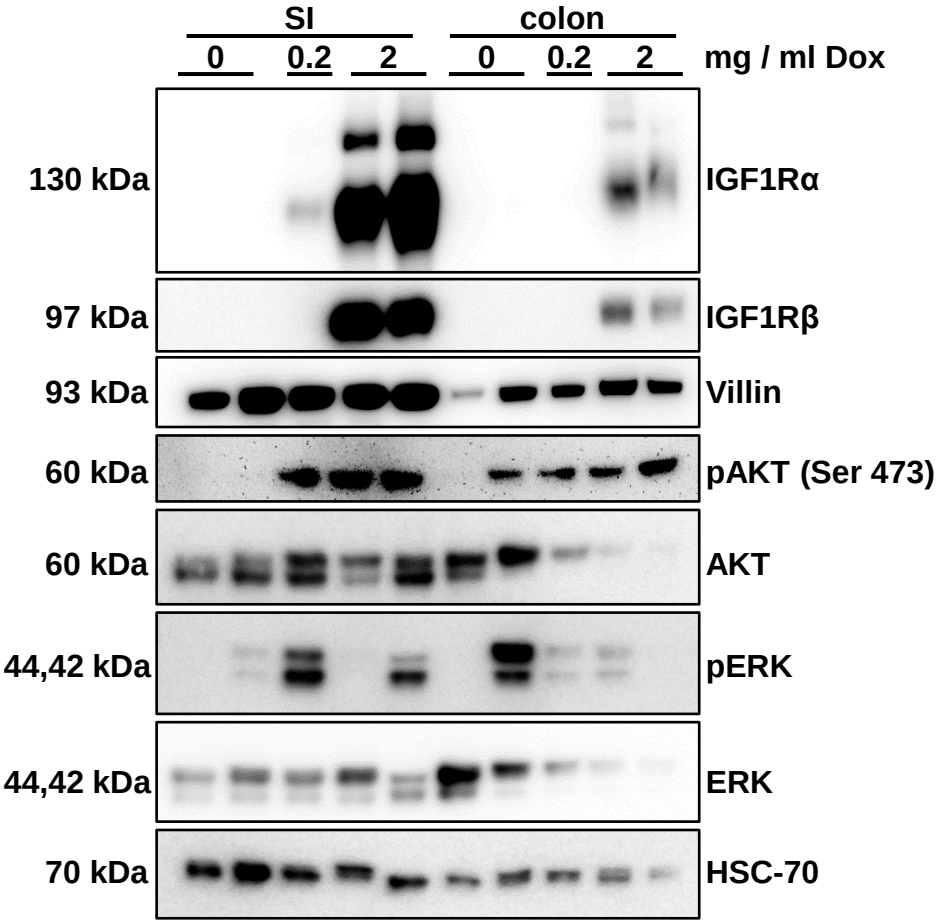

Fig. 10: Confirmation of IGF1R overexpression and the induction of downstream signaling pathways in IGF1R-oe mice.

Proteins were extracted from epithelial cells of the small intestine (SI) and colon of Villin-TRE-IGF1R mice administered to 0 mg / ml doxycycline (n=2), 0.2 mg / ml doxycycline (n=1) and 2 mg / ml doxycycline (n=2), respectively. Western blot analysis was performed. IGF1R-oe mice highly expressed IGF1Rα and IGF1Rβ in a doxycycline concentration-dependent manner. The phosphorylation level of AKT (pAKT) increased in IGF1R-oe mice dependent on doxycycline concentration. ERK activation

(pERK) was visible in the small intestine of the IGF1R-oe mouse administered to 0.2 mg / ml doxycycline as well as in the colon of one control mouse.

3.6 Identification of the intestinal cell type overexpressing the IGF1R

The overexpression of the IGF1R in the small intestine and colon of IGF1R-oe Villin-TRE-IGF1R mice could be verified by both immunohistochemistry (chapter 3.4) and western blot analysis (chapter 3.5). Immunofluorescence staining also revealed intense overexpression of IGF1R in cells of the small intestine (representative picture shown in Fig. 11). The expression pattern of IGF1R was evenly distributed over the villi, but, importantly, not all cells of the small intestine displayed IGF1R overexpression. This observation was in contrast to findings published by El Marjou *et al.* (2004) who generated a transgenic mouse line expressing a tamoxifen-dependent cre recombinase under the villin promoter. The authors proved that the villin-guided cre recombinase is homogenously expressed in epithelial cells all along the crypt-villus axis. Furthermore, they showed that also the undifferentiated progenitor cells in the intestine express the villin-guided cre recombinase, and observed stronger expression in the differentiated cells compared to the cells in the crypts, which was similar to the expression gradient of endogenous villin (El Marjou *et al.* 2004). In addition, Madison (2002) proved that villin is broadly expressed in every cell of the intestinal epithelium (Madison 2002). This led to the assumption that, despite the villin-guided *IGF1R* overexpression, only a special intestinal cell type overexpresses the *IGF1R* upon doxycycline treatment. For this reason, it was of high interest to identify the cell type in the small intestine and colon overexpressing the IGF1R.

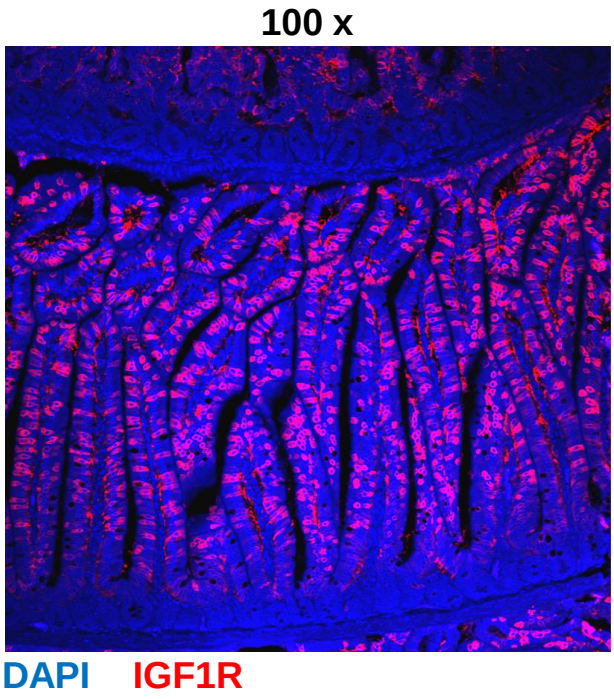

Fig. 11: Overexpression of the IGF1R in cells of the small intestine of IGF1R-oe mice.
Villin-TRE-IGF1R mice (n=10) were administered continuously to 2 mg / ml doxycycline for four weeks to induce *IGF1R* overexpression. The mice were sacrificed and tissue samples were fixed and paraffin-embedded. Immunofluorescence staining was performed using an antibody specific for the human IGF1R (red). DAPI visualized cell nuclei (blue). Intense expression of IGF1R was visible in the villi, but not all cells revealed IGF1R expression.

Therefore, IGF1R-oe mice were continuously treated with 2 mg / ml doxycycline for four weeks to induce *IGF1R* overexpression. The mice were sacrificed, the small intestine and colon were excised from the animals, fixed and paraffin-embedded. Afterwards, double stainings with an antibody specific for a distinct intestinal cell type together with an antibody specific for human IGF1R were performed on the tissue sections. In this context, mucin 2 was used as a marker for goblet cells, Chromogranin A (CHGA) as a marker for enteroendocrine cells and lysozyme was used to stain Paneth cells. In Fig. 12 representative pictures of the double stainings of mucin 2, CHGA and lysozyme, respectively, together with IGF1R in the small intestine and colon of IGF1R-oe mice are shown. All three double stainings revealed both, expression of the distinct cell type and intense IGF1R overexpression. A gradient of IGF1R overexpression from high expression in the villi of the small intestine and at the top of the crypts of the colon to low expression in the crypts of the small intestine and at the bottom of the crypts of the colon was visible. Interestingly, a concordant

expression of IGF1R together with mucin 2, IGF1R together with CHGA or IGF1R together with lysozyme, respectively, could not be observed in the small intestine and colon, showing that neither goblet cells nor enteroendocrine cells nor Paneth cells overexpressed the IGF1R.

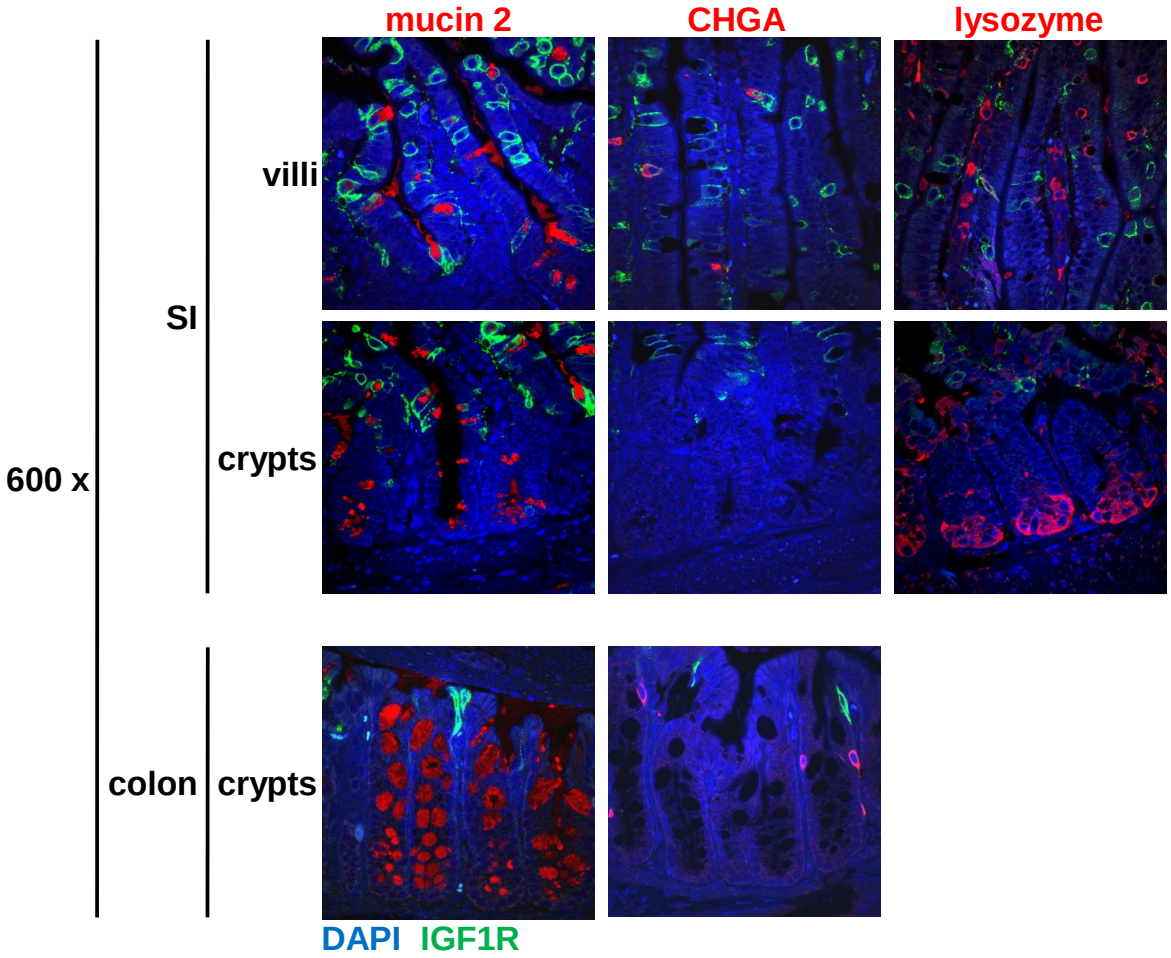

Fig. 12: Identification of the intestinal cell type overexpressing the IGF1R upon doxycycline treatment.

For the identification of the cell type overexpressing the IGF1R, epithelial cells of the small intestine and colon were doublestained for mucin 2 as a marker for goblet cells (red), CHGA as a marker for enteroendocrine cells (red) and lysozyme as a marker for Paneth cells (red), respectively, together with human IGF1R (green). The expression of all three cell types as well as intense IGF1R overexpression was visible. A concordant expression pattern of IGF1R together with mucin 2, IGF1R together with CHGA and IGF1R together with lysozyme, respectively, in the small intestine and colon could not be observed, showing that neither goblet cells nor enteroendocrine cells nor Paneth cells overexpressed the IGF1R. Doublestainings were each performed five times. DAPI visualized cell nuclei (blue).

3.7 *IGF1R* overexpression does not induce intestinal tumor formation *per se*

Jones *et al.* (2007) demonstrated that *IGF1R* overexpression is sufficient to induce mammary tumor formation *in vivo* by using a transgenic mouse model containing the human *IGF1R* under the doxycycline-inducible MMTV (mouse mammary tumor virus) promoter. To investigate if *IGF1R* overexpression *per se* also induces intestinal tumor formation, overexpression of *IGF1R* was induced in Villin-TRE-IGF1R mice. Therefore, the mice were continuously treated with 0 mg / ml, 0.2 mg / ml or 2 mg / ml doxycycline for 1.5 years. As described in chapter 3.2, *IGF1R* overexpression can only be induced in double transgenic mice that receive doxycycline (IGF1R-oe mice). Mice which were administered to 0 mg / ml doxycycline, and mice which carried only the Villin-rtTA2-M2 transgene but were administered to doxycycline, were used as controls. To check for intestinal tumor formation, colonoscopies were regularly performed (Fig. 13).

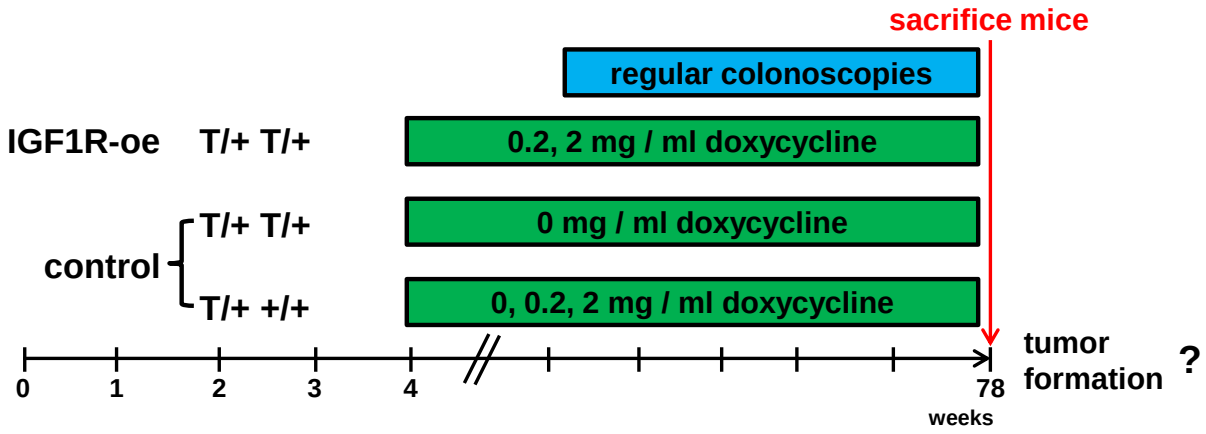

Fig. 13: Treatment scheme for the long-term experiment to analyze if *IGF1R* overexpression induces intestinal tumor formation.

Villin-TRE-IGF1R mice were continuously administered to 0 mg / ml (n=4), 0.2 mg / ml (n=7) or 2 mg / ml doxycycline (n=10) for 78 weeks to induce *IGF1R* overexpression. To check for tumor formation, colonoscopy was regularly performed. After 78 weeks, the mice were sacrificed and the small intestine and colon were excised from the mice, fixed and paraffin-embedded for immunohistochemical examination.

As can be seen in Fig. 14, colonoscopy one year and 1.5 years after the start of doxycycline administration did not reveal colonic tumor formation in IGF1R-oe and control mice.

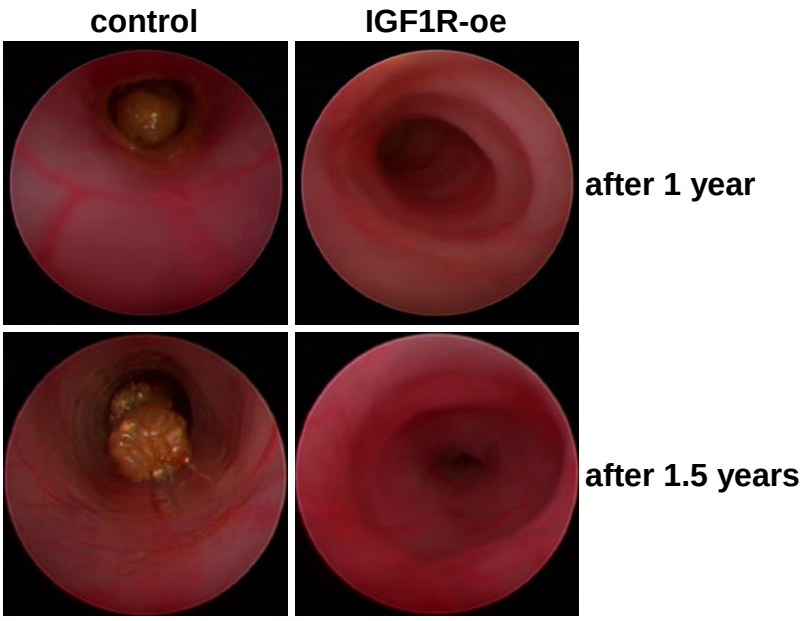

Fig. 14: Colonoscopy of IGF1R-oe and control Villin-TRE-IGF1R mice.

To examine if tumors have formed in the colon of Villin-TRE-IGF1R mice upon doxycycline treatment, colonoscopy was regularly performed. Therefore, the mice were anesthetized using isoflurane and the endoscope was rectally penetrated. Tumor development could not be observed in IGF1R-oe (n=6) or control mice (n=15) 1 year and 1.5 years after the start of doxycycline administration, respectively.

To prove that the *IGF1R* was still overexpressed in the colon and small intestine of IGF1R-oe mice that were continuously treated with doxycycline after 1.5 years, immunohistochemical staining was performed on intestinal tissue sections. In Fig. 15 representative pictures of the stainings are shown. One and a half year after the start of doxycycline administration, IGF1R overexpression was still detectable in the small intestine and colon of the IGF1R-oe mice. Control mice showed no IGF1R overexpression in the small intestine and colon.

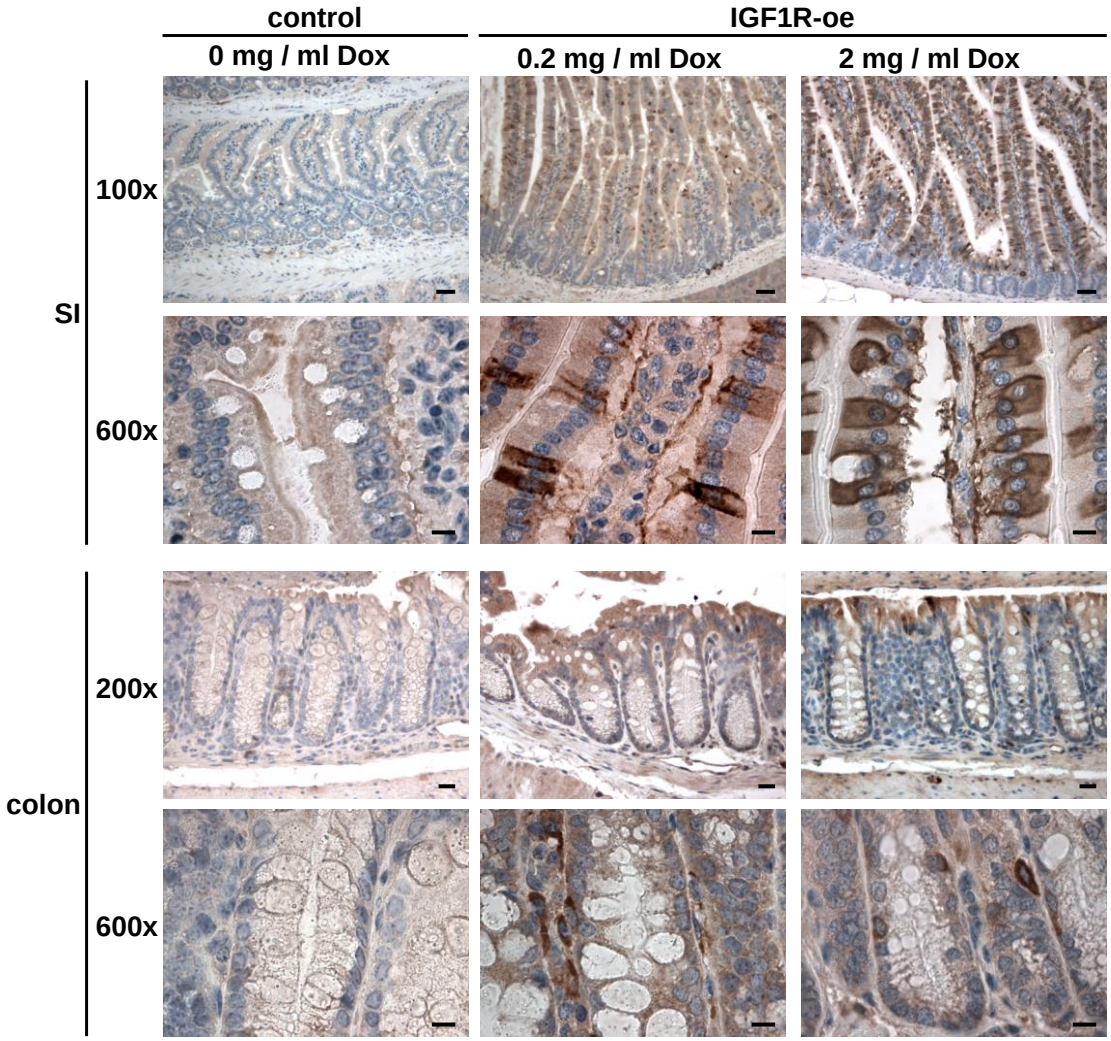

Fig. 15: IGF1R overexpression in epithelial cells of the small intestine and colon of IGF1R-oe and control Villin-TRE-IGF1R mice after 1.5 years.

For the confirmation that IGF1R was still overexpressed in cells of the small intestine (SI) and colon of IGF1R-oe mice after 1.5 years, immunohistochemical staining was performed using an antibody specific for the human IGF1R (brown). Cell nuclei were stained with hemalum solution (blue). IGF1R-oe (n=6: n=3 (0.2 mg / ml doxycycline) + n=3 (2 mg / ml doxycycline)) mice showed intense expression of human IGF1R, while IGF1R expression could not be observed in the small intestine and colon of control mice (n=15).

3.8 Analyses of the morphology of the small intestinal and colonic villi and crypts of Villin-TRE-IGF1R mice

To analyze if *IGF1R* overexpression altered the morphology of the intestine, hematoxylin and eosin stainings of small intestinal and colonic tissue sections were compared between IGF1R-oe and control Villin-TRE-IGF1R mice. Therefore,

IGF1R-oe and control mice with five mice per group were continuously treated with 0 mg / ml, 0.2 mg / ml or 2 mg / ml doxycycline to induce the overexpression of the *IGF1R*. The mice were sacrificed after four weeks, three months and 1.5 years, respectively. Together with Dr. med. Felix Bremmer (Institute of Pathology, University Medical Center Göttingen, Germany) the morphology of the villi and crypts was examined. In Fig. 16 representative pictures of the villi and crypts of the small intestine and colon after the three time points are shown. A difference in the morphology of the small intestinal and colonic villi and crypts between IGF1R-oe and control animals was not visible. Furthermore, a time-dependent difference in the morphology was also not observed.

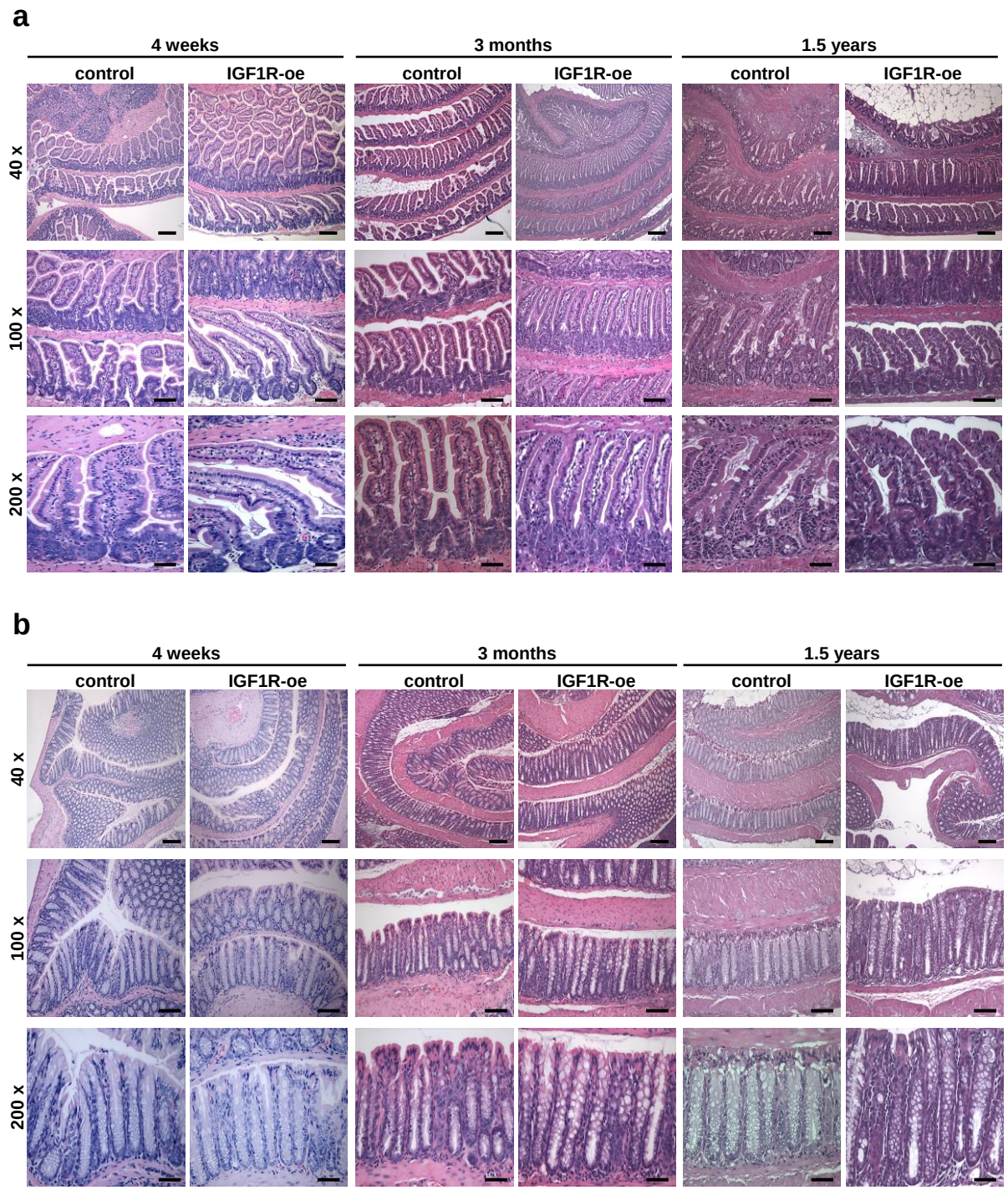

Fig. 16: Hematoxylin and eosin stainings of the small intestine and colon of IGF1R-oe and control Villin-TRE-IGF1R mice after four weeks, three months and 1.5 years of *IGF1R* overexpression.
IGF1R-oe (n=5) and control (n=5) Villin-TRE-IGF1R mice were continuously administered to 0 mg / ml, 0.2 mg / ml or 2 mg / ml doxycycline to induce *IGF1R* overexpression. After four weeks, three months and 1.5 years, mice were sacrificed, the small intestine and colon were dissected from the mice, fixed, paraffin-embedded and cut. Hematoxylin and eosin stainings were performed on the sections in the Institute of Pathology (University Medical Center Göttingen, Germany). Together with Dr. med. Felix Bremmer (Institute of Pathology, University Medical Center Göttingen, Germany) the morphology of both the villi and crypts were analyzed. **(a)** A difference in the morphology of the small intestine and **(b)** colon between IGF1R-oe and control animals was not observed.

Also a difference in the morphology of the villi and crypts of the small intestine and colon could not be observed, further analysis with regard to the villus length and crypt depth was performed. Therefore, ten IGF1R-oe and control mice each were continuously treated with 0 mg / ml, 0.2 mg / ml or 2 mg / ml doxycycline for three months. Subsequently, the animals were sacrificed, the small intestinal and colonic tissues were excised from the mice and divided into small pieces without cutting them longitudinally. Thus, the villi and crypts were kept in their “natural” appearance without squeezing, and the length of the villi and the depth of the crypts could be measured. For measurement, the samples were fixed and paraffin-embedded, hematoxylin and eosin stainings were performed and the length of 50 villi and the depth of 50 crypts of each mouse were measured using the cellSens Dimension software appropriate to the microscope BX60 (Olympus, Hamburg, Germany). In Fig. 17a a representative image of how the measurement was performed is shown.

In the small intestine, IGF1R-oe mice showed a significantly extended depth of the crypts (Fig. 17b), whereas the length of the villi revealed no alterations compared to the control mice (Fig. 17c). In the colon, *IGF1R* overexpression did not result in a difference in crypt depth between IGF1R-oe and control animals (Fig. 17d).

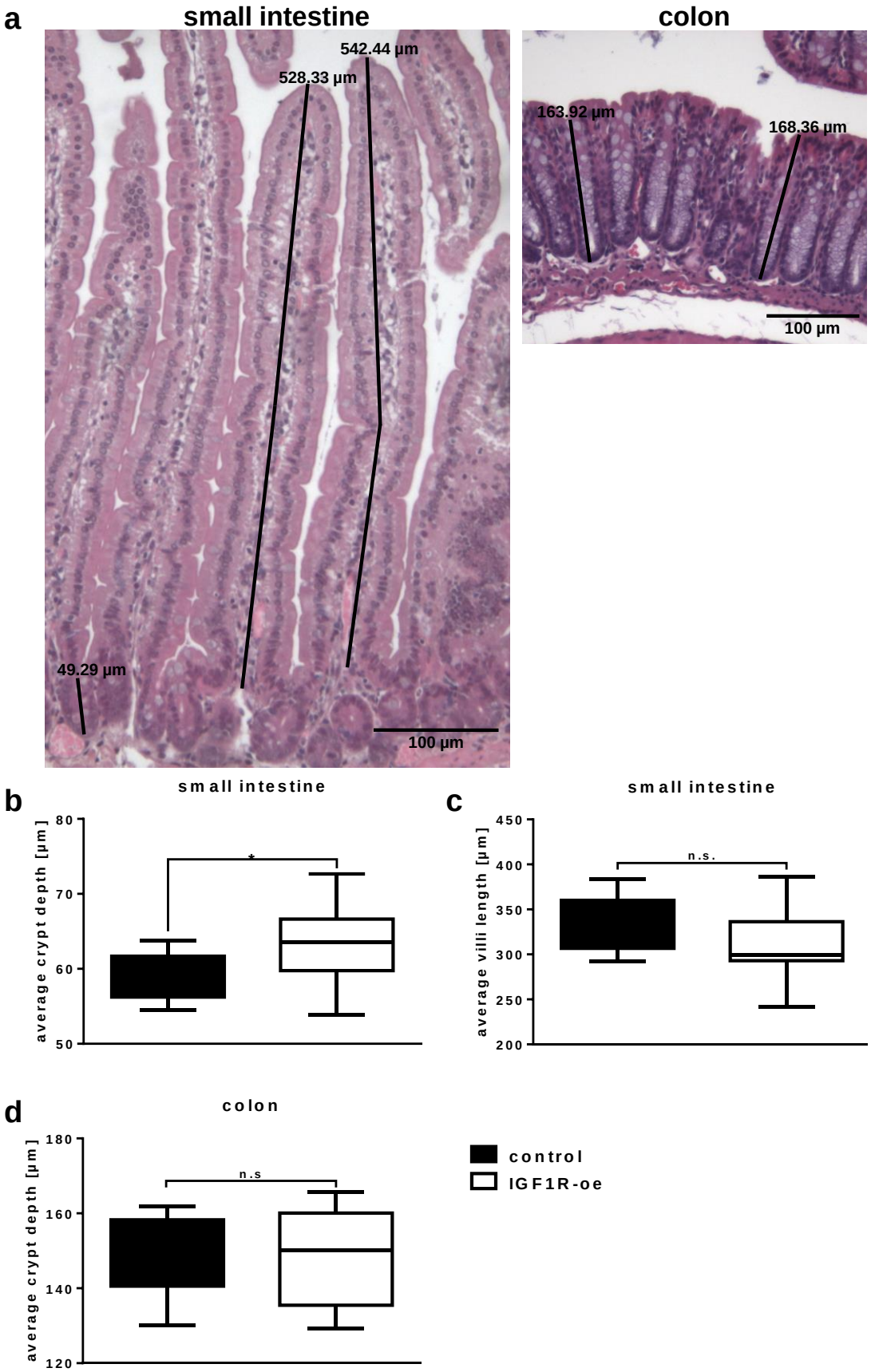

Fig. 17: *IGF1R* overexpression significantly altered the crypt depth in the small intestine of IGF1R-oe mice compared to control mice.

(a) For the analysis of the villus length and the crypt depth, hematoxylin and eosin stainings were performed on tissue sections of the small intestine and colon of IGF1R-oe (n=10) and control (n=10)

Villin-TRE-IGF1R mice, respectively. Pictures were taken and the villus length and the depth of the crypts were determined using the cellSens Dimension software (Olympus, Hamburg, Germany). **(b)** IGF1R-oe mice revealed a significant increase in the average crypt depth of the small intestine compared to control mice. **(c, d)** The average villi length of the small intestine as well as the average crypt depth of the colon was not altered after *IGF1R* overexpression. * $P < 0.05$ (student's *t* test).

3.9 Quantification of the different intestinal cell types of Villin-TRE-IGF1R mice after four weeks, three months and 1.5 years of doxycycline treatment

To analyze the maintenance and regeneration of the intestine, the number of the different intestinal cell types was quantified. Therefore, IGF1R-oe and control Villin-TRE-IGF1R mice with five mice per group were continuously treated with 0 mg / ml, 0.2 mg / ml or 2 mg / ml doxycycline for four weeks, three months and 1.5 years to induce *IGF1R* overexpression. The mice were sacrificed, intestinal tissues were fixed and paraffin-embedded and tissue sections were stained for the different cell types. In Fig. 18 representative pictures of the stainings for Villin-TRE-IGF1R mice are shown. Hereby, mucin 2 was used as a marker for goblet cells, Chromogranin A (CHGA) as a marker for enteroendocrine cells, lysozyme was used to stain Paneth cells and Ki 67 staining was used to detect proliferating cells. For the quantification of the number of the different cell types, pictures of the stainings were taken using the microscope BX60 (Olympus, Hamburg, Germany). Importantly, the stained cells of 50 villi and 50 crypts per mouse, respectively, were counted manually.

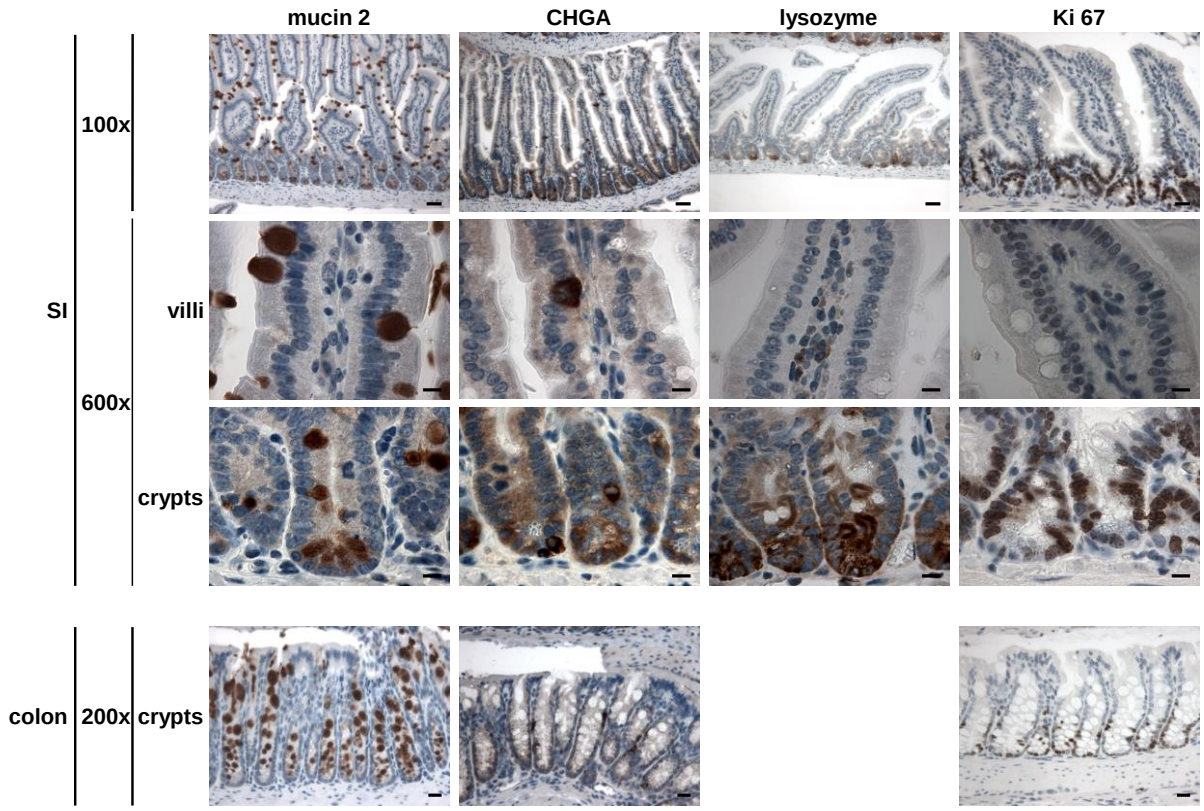

Fig. 18: Stainings of goblet cells (mucin 2), enteroendocrine cells (CHGA), Paneth cells (lysozyme) and proliferating cells (Ki 67) for the quantification of the different cell types in the small intestine and colon of Villin-TRE-IGF1R mice.

To analyze if *IGF1R* overexpression has any influence on the maintenance and regeneration of the intestine, the number of the different intestinal cell types was quantified and compared to control mice. Therefore, immunohistochemical stainings were performed on tissue sections of the small intestine (SI) and colon of IGF1R-oe (n=5) and control (n=5) Villin-TRE-IGF1R mice using antibodies specific for the different cell types (brown) as indicated. Cell nuclei were stained with hemalum solution (blue).

3.9.1 *IGF1R* overexpression results in a significant reduction of goblet cells

For the quantification of goblet cells in the small intestine and colon, mucin 2-positive cells of 50 villi and 50 crypts per mouse were counted. In IGF1R-oe mice, the number of goblet cells was significantly reduced in the crypts and villi of the small intestine as well as in the crypts of the colon compared to control mice. However, the number of goblet cells of the IGF1R-oe mice decreased after three months, but showed no change after 1.5 years. Interestingly, a significant decrease of goblet cells with time in the crypts of the small intestine and colon was observed in control mice, whereas a significant increase from four weeks to 1.5 years was observed in the villi of control mice (Fig. 19).

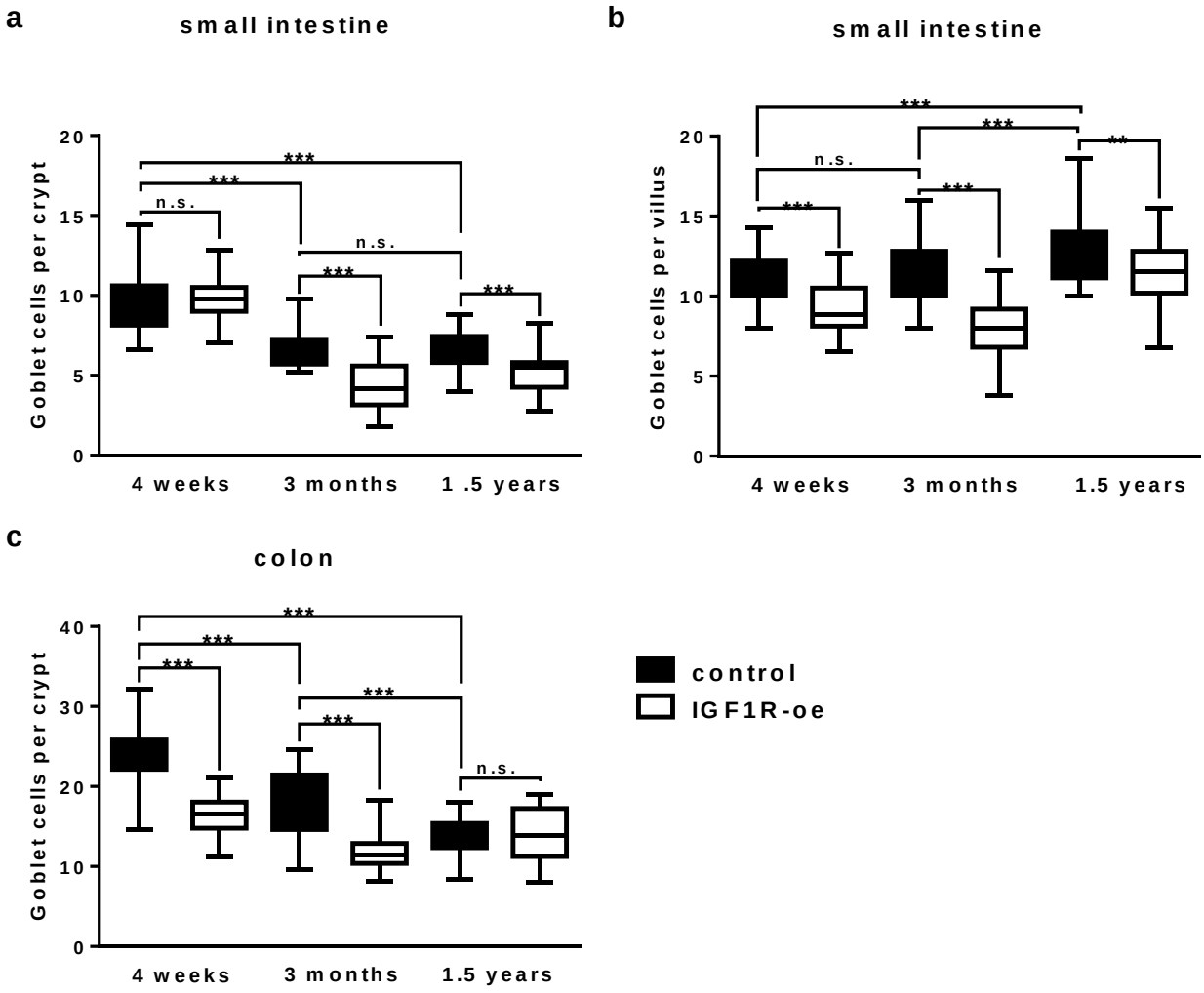

Fig. 19: *IGF1R* overexpression resulted in a significant reduction of goblet cells.

Cells of the small intestine **(a, b)** and colon **(c)** were stained for mucin 2, a marker for goblet cells. The number of goblet cells per crypt and villus with 50 crypts and villi per mouse was counted. The number of goblet cells per crypt and villus of the small intestine and per crypt of the colon significantly decreased in IGF1R-oe mice (n=5) compared to control mice (n=5). ** $P < 0.01$, *** $P < 0.0001$ (student's *t* test).

3.9.2 The number of enteroendocrine cells increases with time after *IGF1R* overexpression

To quantify the number of enteroendocrine cells, chromogranin A-positive cells of 50 villi of the small intestine and of 50 crypts of the colon per mouse were counted. Enteroendocrine cells are known to be not localized in the crypts of the small intestine (Medema and Vermeulen, 2011). In the small intestine and colon, the number of enteroendocrine cells increased significantly with time. After three months, IGF1R-oe mice showed a significantly higher number of chromogranin A-positive cells in the small intestine, but revealed a significantly lower number after 1.5 years compared to control

mice. In the colon, the IGF1R-oe mice revealed a significantly higher number of enteroendocrine cells than control mice after four weeks, but after three months and 1.5 years no difference in the number of chromogranin A-positive cells was visible (Fig. 20).

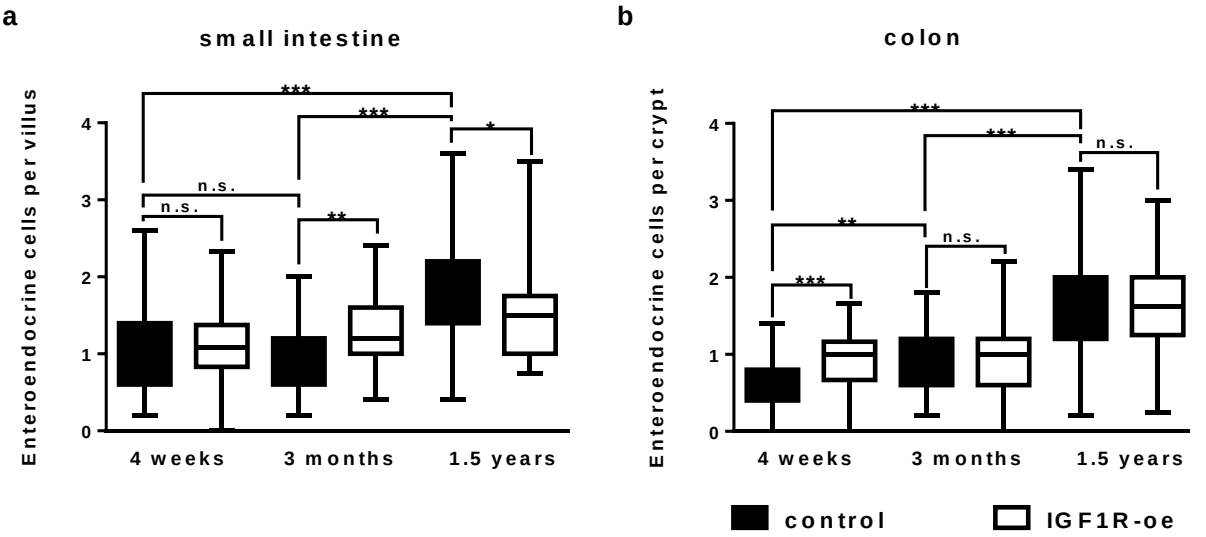

Fig. 20: The number of enteroendocrine cells increased with time after *IGF1R* overexpression. For the quantification of enteroendocrine cells, cells of the small intestine **(a)** and colon **(b)** were stained for chromogranin A (CHGA) as a marker for enteroendocrine cells. The number of enteroendocrine cells per villus or crypt, respectively, significantly increased over time in IGF1R-oe (n=5) and control mice (n=5). * P <0.05, ** P < 0.01, *** P < 0.0001 (student's t test).

3.9.3 The number of Paneth cells decreases over time in IGF1R-oe and control mice

Paneth cells are localized in the crypts of the small intestine, but are not detected in the colon (Medema and Vermeulen, 2011). Paneth cells are characterized by the expression of lysozyme, and lysozyme-positive cells per crypt were counted. The number of Paneth cells decreased significantly over time in IGF1R-oe and control mice. After four weeks and three months of doxycycline treatment, the number of lysozyme-positve cells was significantly lower in IGF1R-oe mice compared to control mice. Interestingly, the number of Paneth cells was significantly increased in IGF1R-oe mice after 1.5 years compared to control mice (Fig. 21).

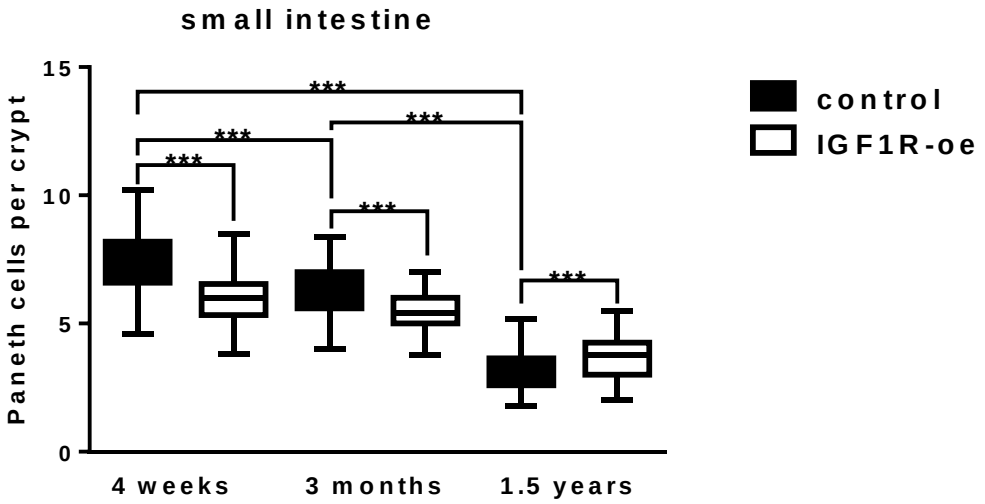

Fig. 21: The number of Paneth cells decreased over time in IGF1R-oe and control mice.
Tissue sections of the small intestine were stained for lysozyme, a marker for Paneth cells. Lysozyme-positive cells per villus of 50 villi per mouse were manually counted. The number of Paneth cells significantly decreased over time in IGF1R-oe (n=5) and control mice (n=5). *** $P < 0.0001$ (student's *t* test).

3.9.4 The number of proliferating cells is decreased in the colon of IGF1R-oe mice

Ki 67 is a marker for proliferating cells. The process of proliferation is known to occur at the bottom of the crypts. At the top of the crypts, proliferation halts and cells differentiate into goblet cells, Paneth cells or enteroendocrine cells or into enterocytes (Medema and Vermeulen 2011).

In the small intestine, the number of proliferating cells significantly increased after three months, but significantly decreased after 1.5 years in both IGF1R-oe and control mice. In the small intestine, the number of Ki 67-positive cells was significantly higher in IGF1R-oe animals compared to control mice four weeks after the start of doxycycline treatment. After three months and 1.5 years, no difference in the number of proliferating cells between IGF1R-oe and control mice was visible. In the crypts of the colon, the number of proliferating cells slightly decreased over time in IGF1R-oe and control mice. Comparison of the number of Ki 67-positive cells between IGF1R-oe and control mice revealed a significant reduction after four weeks, three months and 1.5 years (Fig. 22).

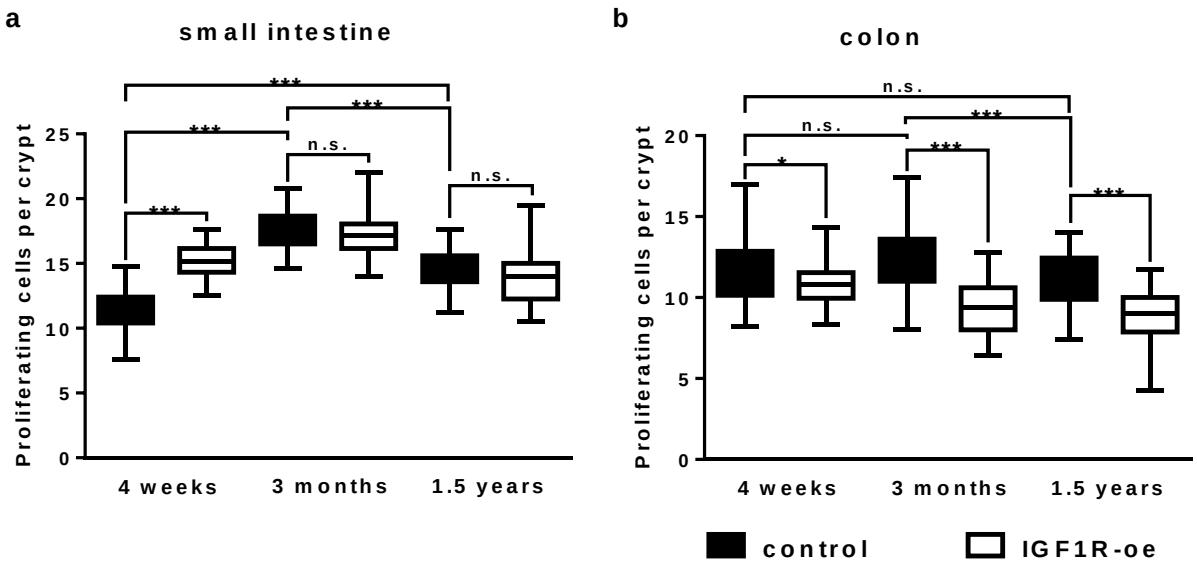

Fig. 22: The number of proliferating cells was decreased in the colon of IGF1R-oe mice.
Sections of the small intestine **(a)** and colon **(b)** of IGF1R-oe (n=5) and control mice (n=5) were stained for Ki 67 as a marker for proliferating cells. The Ki 67-positve cells per crypt were manually counted. In the small intestine, the number of Ki 67-positive cells increased in IGF1R-oe mice compared to control mice after four weeks of doxycycline administration, but decreased after three months and 1.5 years of doxycycline administration. The number of proliferating cells per crypt in the colon of IGF1R-oe mice was significantly decreased compared to control mice after four weeks, three months and 1.5 years. * P <0.05, *** P < 0.0001 (student's t test).

3.9.5 *IGF1R* overexpression does not alter the presence of enterocytes

Enterocytes are absorptive cells in the intestinal epithelium. Enterocytes originate from the intestinal stem cells in the crypts and differentiate and migrate from the crypt to the villus tip in the small intestine and from the bottom of the crypt to the top of the crypt in the colon, respectively (Overeem *et al.* 2016). To analyze if *IGF1R* overexpression altered the presence of enterocytes in the intestine, five tissue sections of the small intestine and colon of IGF1R-oe and control Villin-TRE-IGF1R mice each were stained for enterocytes by alkaline phosphatase staining. In Fig. 23 representative pictures of the stainings are shown. A difference in the presence of enterocytes in the intestinal epithelium between the IGF1R-oe and control mice was not visible.

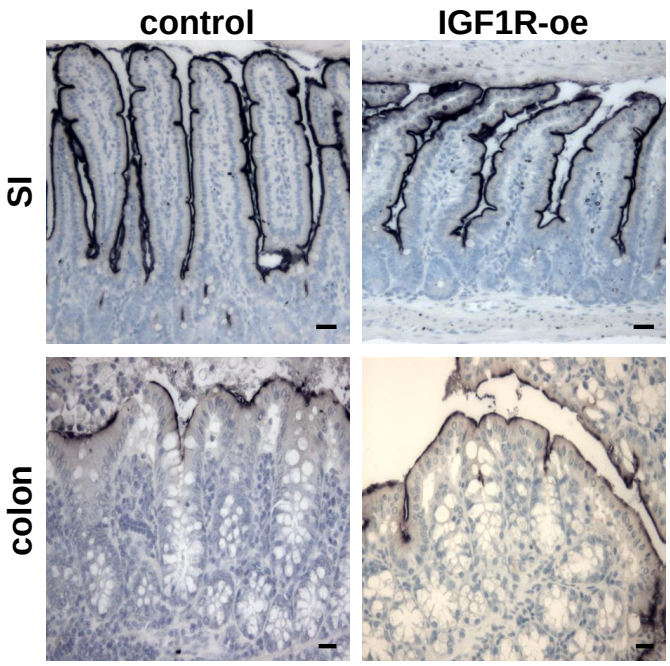

Fig. 23: The presence of enterocytes in the small intestine and colon of Villin-TRE-IGF1R mice. IGF1R-oe (n=5) and control mice (n=5) were each treated with doxycycline to induce the overexpression of *IGF1R*. The mice were sacrificed and tissue sections of the small intestine and colon were stained for enterocytes by alkaline phosphatase (brown). Cell nuclei were stained with hemalum solution (blue). A difference in the presence of enterocytes between IGF1R-oe and control Villin-TRE-IGF1R mice could not be observed.

3.10 The *IGF1R* overexpression in the intestine promotes intestinal tumor formation and progression (AOM model)

As already shown, *IGF1R* overexpression did not induce intestinal tumor formation *per se* (chapter 3.7). To analyze if *IGF1R* overexpression plays a role during intestinal tumor progression, intestinal tumor formation was induced in Villin-TRE-IGF1R mice using the mutagenic agent azoxymethane (AOM). AOM is known to initiate cancer by alkylation of DNA and thereby facilitation of base mispairings (Neufert *et al.* 2007). Therefore, IGF1R-oe and control Villin-TRE-IGF1R mice were administered to doxycycline. In the following experiments mice that carried only the Villin-rtTA2-M2 transgene (T/+ +/+) treated with doxycycline were used as control. In addition, IGF1R-oe and control mice were only administered to 2 mg / ml doxycycline. Furthermore, all mice were intraperitoneally injected with four weekly repeated injections of 10 mg / ml AOM to induce colonic tumor formation (Fig. 24).

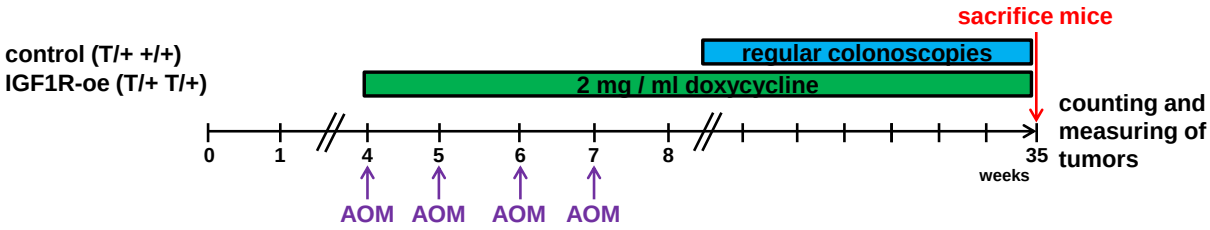

Fig. 24: Treatment scheme for the analysis if *IGF1R* overexpression has any influence on colonic tumor progression (AOM model).

IGF1R-oe (T/+ T/+) (n=11) and control (T/+ +/+) (n=11) Villin-TRE-IGF1R mice were administered to 2 mg / ml doxycycline to induce *IGF1R* overexpression and injected four times with azoxymethane (AOM) to induce colonic tumor formation. To check if tumors have developed, colonoscopy was regularly performed. Thirty-five weeks after the first AOM injection, the mice were sacrificed and the tumors were counted and measured.

To screen for intestinal tumor formation, regular colonoscopies were performed. For the estimation of the tumor size, tumors were scored relating to Becker *et al.* (2007).

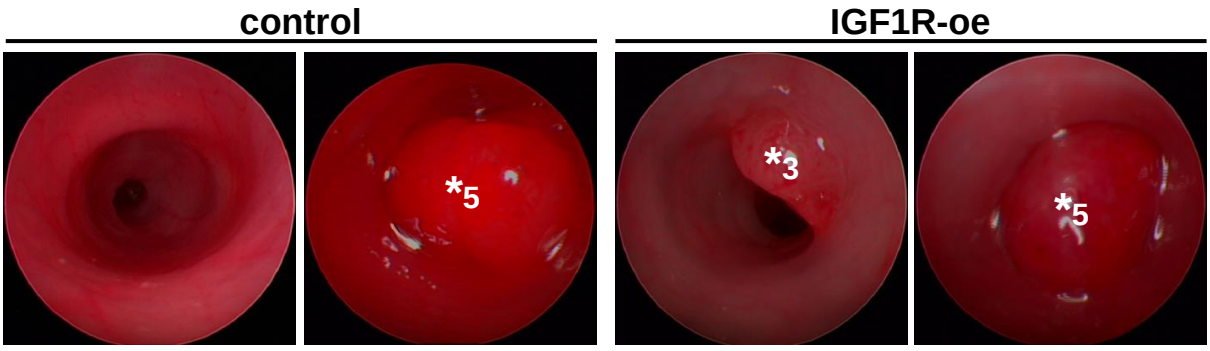

Fig. 25: Colonoscopy of IGF1R-oe and control Villin-TRE-IGF1R mice treated with AOM to induce colonic tumor formation.

To examine if tumors have formed in the colon of Villin-TRE-IGF1R mice, colonoscopy was regularly performed. IGF1R-oe (n=11) and control mice (n=11) developed tumors in the colon. Stars mark the formed tumors. The numbers indicate the score of the tumor (after Becker *et al.* 2007).

Thirty-five weeks after the first AOM injection, the mice were sacrificed, the colon length of the mice that have developed tumors was measured using a caliper (Fig. 27) and the developed tumors were macroscopically counted and measured. Therefore, the colon was divided into three parts (distal, middle and proximal part of the colon from anus to stomach) to determine tumor localization (Fig. 26).

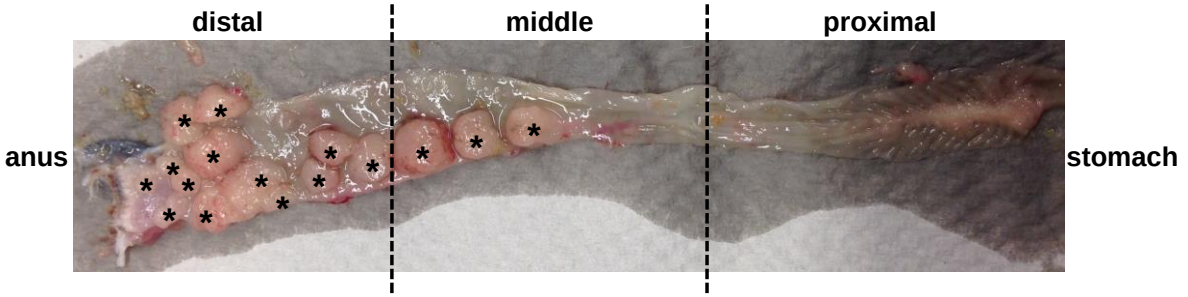

Fig. 26: Example of the macroscopic analysis of tumors developed in an IGF1R-oe Villin-TRE-IGF1R mouse.

The colon was determined into three parts: distal, middle and proximal part from the anus to the stomach. The number of tumors per colonic part was counted and the tumors were measured using a caliper. Stars indicate tumors.

Shortening of the colon is a typical sign of acute intestinal inflammation (Ito *et al.* 2006). For this reason, the average colon length of IGF1R-oe and control mice that have developed tumors was compared (Fig. 27). There was no significant difference in the average colon length.

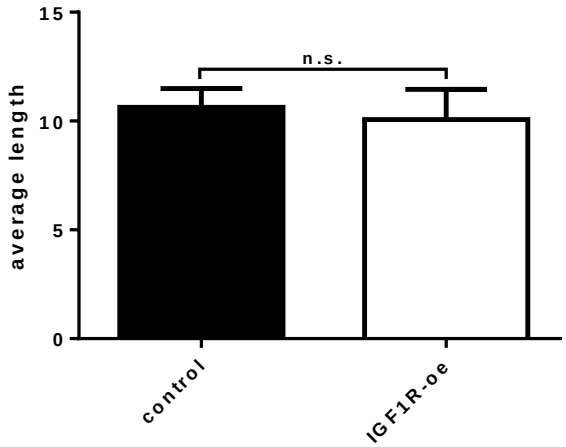

Fig. 27: Average colon length of IGF1R-oe and control Villin-TRE-IGF1R mice after tumor induction by AOM.

No significant difference in the average colon length between IGF1R-oe (n=11) and control mice (n=11) was observed (student's *t* test).

In Fig. 28a a comparison of the total number of IGF1R-oe and control mice with or without tumor formation after the four AOM injections is shown. Interestingly, only three out of eleven (27.3%) control mice developed tumors, whereas six out of eleven (54.6%) IGF1R-oe mice revealed tumor formation. For further analysis the IGF1R-oe

and control mice were splitted regarding their sex (Fig. 28b, c). While half (50%) of the female control mice showed tumor formation, not one male control mouse out of five (0%) developed a tumor (Fig. 28b). In IGF1R-oe mice, six out of ten (60%) female mice formed a tumor, whereas the only male IGF1R-oe mouse did not develop a tumor (0%) (Fig. 28c). These results indicated that female mice could be more sensitive to AOM treatment than male mice. In Fig. 28d the average number of tumors of IGF1R-oe and control mice is shown. In Fig. 28e the localization and in Fig. 28f the size of the tumors was compared between IGF1R-oe and control mice. Here, only those mice which developed a tumor were included for analyses. Control mice developed on average 1.67 tumors, whereas IGF1R-oe even developed on average 2.5 tumors. Regarding the localization of developed tumors, IGF1R-oe mice showed twice the number of distal tumors than control mice. The development of tumors in the middle part of the colon differed only weakly between IGF1R-oe and control mice. Neither IGF1R-oe nor control mice formed tumors in the proximal part of the colon. Regarding the size of the tumors, IGF1R-oe mice revealed a higher number of tumors larger than 2 mm in size than control mice.

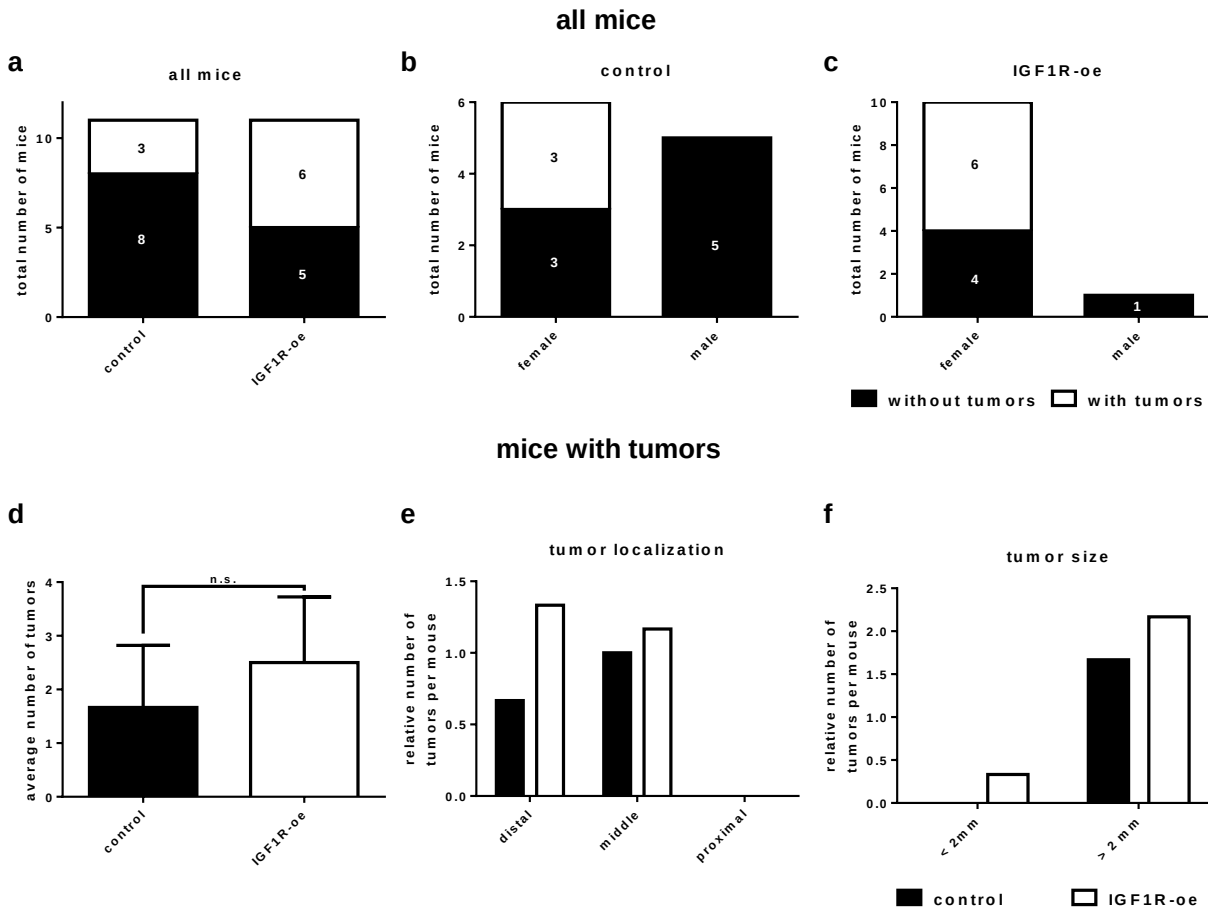

Fig. 28: Macroscopic analyses of the tumors developed in the colon of Villin-TRE-IGF1R mice after induction of tumor formation by AOM.

IGF1R-oe (n=11) and control (n=11) mice were treated according to the treatment scheme (Fig. 24). Mice were sacrificed and the tumors were macroscopically analyzed. Therefore, the number of the tumors was counted, the size of the tumors was measured and the localization was determined. **(a)** IGF1R-oe mice developed a higher number of tumors compared to control mice. **(b, c)** Male mice did not form any tumors, only female mice revealed tumor development. **(d)** Analyzing only those mice which developed tumors, IGF1R-oe mice (n=6) developed on average more tumors compared to control mice (n=3). **(e)** IGF1R-oe mice showed a higher number of tumors in the distal and middle part of the colon compared to control mice. Neither control nor IGF1R-oe mice formed tumors in the proximal part of the colon. **(f)** Regarding the tumor size, IGF1R-oe mice formed a higher number of tumors bigger than 2 mm compared to control mice. (student's *t* test).

For histopathological analyses of the tumors the colonic tissues were fixed, paraffin-embedded and hematoxylin and eosin stainings were prepared. In Fig. 29a a representative picture of the hematoxylin and eosin staining is shown. Together with Dr. med. Felix Bremmer (Institute of Pathology, University Medical Center Göttingen, Germany) the stage and size of the tumors were determined. To check for invasion and metastasis of tumor cells, hematoxylin and eosin stainings of the liver and lymph nodes in regional colonic fat tissue were also histopathologically analyzed. Regarding the stage of the tumors, IGF1R-oe mice revealed twice the number of low grade intraepithelial neoplasias per mouse than control mice. In fact, control mice showed a higher number of high grade neoplasias per mouse than IGF1R-oe mice. But, interestingly, one IGF1R-oe mouse even developed an intramucosal as well as an invasive adenocarcinoma (Fig. 29b). The determination of the average tumor size per mouse showed an increase of the tumor size of about 22.5% in IGF1R-oe mice (average tumor size: 2771.52 μm^2) compared to control mice (average tumor size: 2148.26 μm^2) (Fig. 29c).

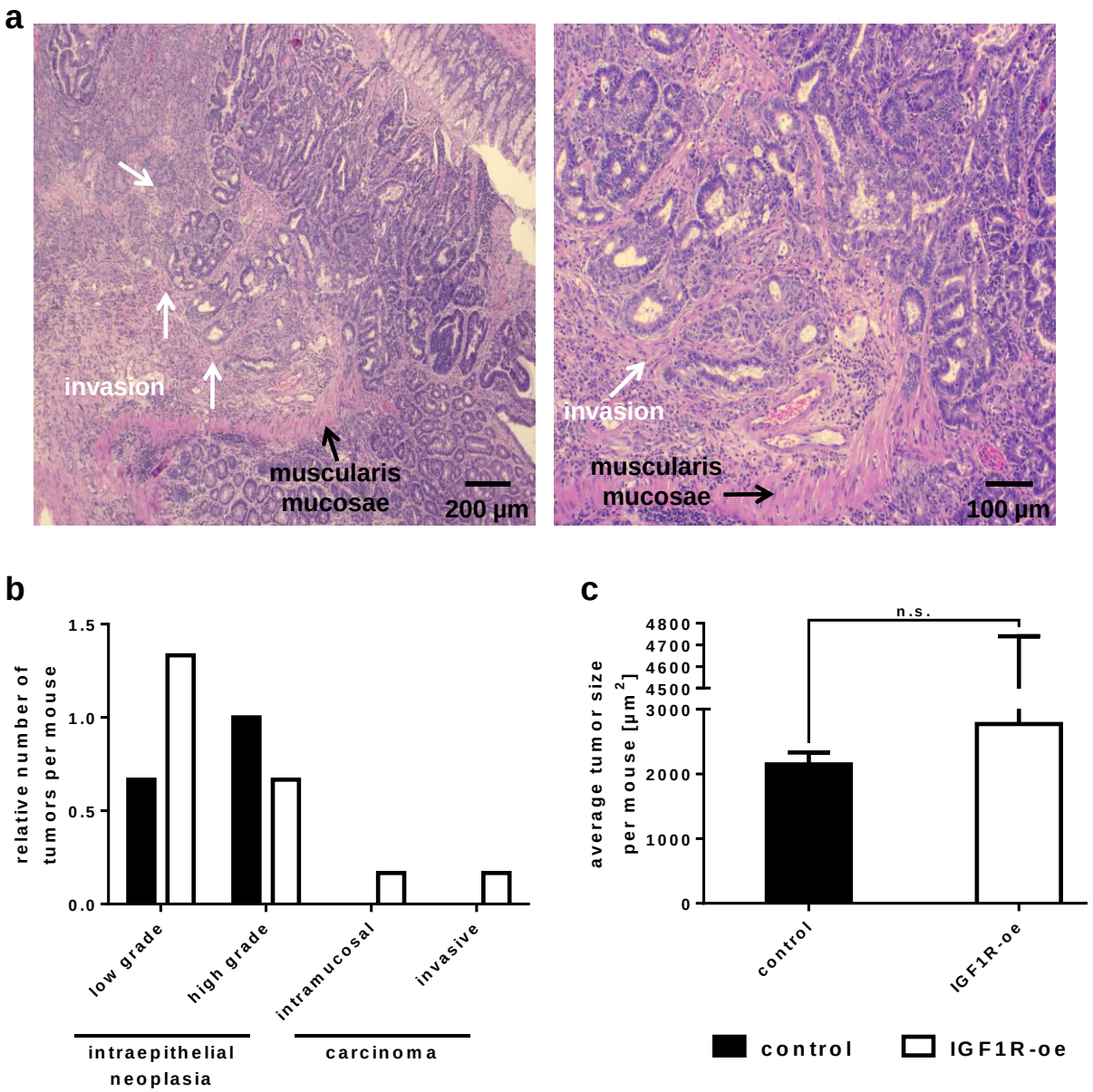

Fig. 29: Histopathological analyses of the colonic tumors developed in IGF1R-oe and control Villin-TRE-IGF1R mice after AOM treatment.

IGF1R-oe (n=11) and control mice (n=11) were administered to doxycycline to induce *IGF1R* overexpression and injected with AOM to induce intestinal tumor formation. Sections of paraffin-embedded tissue samples of IGF1R-oe (n=6) and control mice (n=3) with tumors were stained with hematoxylin and eosin and the tumors were histopathologically analyzed together with Dr. med. Felix Bremmer (Institute of Pathology, University Medical Center Göttingen, Germany). **(a)** Hematoxylin and eosin stainings of an invasive tumor developed in the colon of an IGF1R-oe Villin-TRE-IGF1R mouse. The white arrows mark the zone of invasion. The black arrow indicates the muscularis mucosae. **(b)** IGF1R-oe mice developed a higher number of low grade intraepithelial neoplasias, but a lower number of high grade intraepithelial neoplasias compared to control mice. Even one IGF1R-oe mouse formed an intramucosal as well as an invasive carcinoma. **(c)** The average tumor size per mouse was 22.5% higher in IGF1R-oe mice compared to control mice (student's *t* test).

In addition, lymph nodes in the regional colonic fat tissue and liver tissue were excised from the mice to analyze both the lymph node status and to check for metastatic cells in the liver. It is known that colonic tumor cells predominantly metastasize to these organs (Hess *et al.* 2006). The tissue samples were fixed, paraffin-embedded, approx. 10 sections per mouse were cut and hematoxylin and eosin stainings were prepared. The tissue sections were then examined for the lymph node status and screened for metastatic cells in the liver. However, metastases in the lymph nodes and livers could not be detected, neither in tissue sections from IGF1R-oe mice nor in lymph nodes and livers from control mice.

3.11 *IGF1R* overexpression promotes intestinal tumor formation and progression (AOM / DSS model)

Another model for the analysis of intestinal tumor formation and progression is the azoxymethane / dextran sulfate sodium (AOM / DSS) model. Dextran sulfate sodium (DSS) is an agent that has direct toxic effects on the colonic epithelium and thus creates a chronic inflammatory state. To induce tumor development, mice are treated with a combination of the genotoxic agent AOM and the inflammatory agent DSS (Thaker *et al.* 2012). For the combinational treatment of mice with AOM / DSS several different protocols exist (Neufert *et al.* 2007; Thaker *et al.* 2012). For the experiment of the present study, Villin-TRE-IGF1R mice were once intraperitoneally injected with 10 mg / ml AOM and were afterwards administered to two cycles of 2% DSS over the drinking water. In addition, control (T/+ +/+) and IGF1R-oe (T/+ T/+) mice were treated with 2 mg / ml doxycycline (Fig. 30).

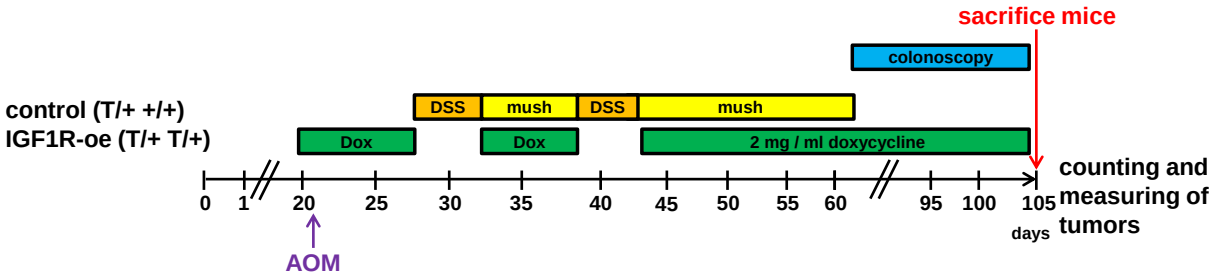

Fig. 30: Treatment scheme for the induction of colonic tumors in Villin-TRE-IGF1R mice.

IGF1R-oe (n=20) and control (n=22) Villin-TRE-IGF1R mice were administered to 2 mg / ml doxycycline to induce *IGF1R* overexpression. Furthermore, mice were once injected with AOM to induce colonic tumor formation and administered to two cycles of 2% DSS over the drinking water to induce intestinal inflammation. Cereal mush was given between and after DSS treatment to avoid dehydration of the

mice. To screen for tumor development, colonoscopy was performed regularly. The mice were sacrificed and the formed tumors were counted and measured.

To screen for intestinal tumor development, colonoscopy was performed regularly.

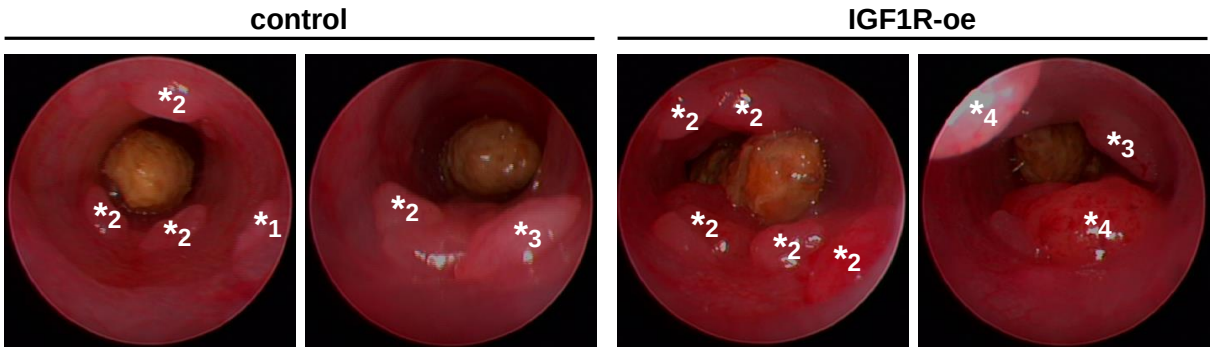

Fig. 31: Colonoscopy of Villin-TRE-IGF1R mice treated with AOM / DSS to induce colonic tumor formation and inflammation.

To examine if tumors have formed in the colon of IGF1R-oe (n=20) and control (n=22) Villin-TRE-IGF1R mice, colonoscopy was regularly performed. IGF1R-oe and control mice developed tumors in the colon. Stars mark the developed tumors. The numbers indicate the score of the tumor (after Becker *et al.* 2007).

Twelve weeks after the AOM injection, many tumors revealed a score of 4 to 5 (after Becker *et al.*, 2007) and the Villin-TRE-IGF1R mice had to be sacrificed. The colon length of mice that have developed tumors was measured using a caliper (Fig. 32). IGF1R-oe mice revealed a significant reduction in the average colon length compared to control mice, which is a typical sign of acute intestinal inflammation (Ito *et al.* 2006).

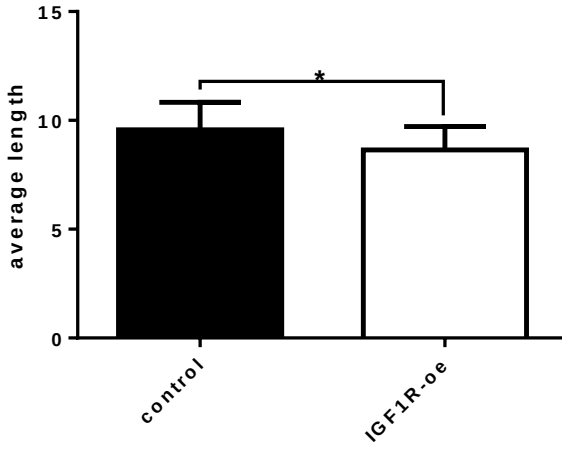

Fig. 32: Average colon length of IGF1R-oe and control Villin-TRE-IGF1R mice after colonic tumor induction by AOM / DSS.

The average colon length was significantly reduced in IGF1R-oe mice (n=17) compared to control mice (n=20). * *P* <0.05 (student's *t* test).

Furthermore, the developed tumors were counted and measured macroscopically. Twenty out of 22 (91%) control mice developed colonic tumors, whereas 17 out of 20 (85%) IGF1R-oe mice formed a tumor (Fig. 33a). Regarding their sex, eight female (80%) and twelve male (100%) control mice revealed tumor formation (Fig. 33b). In IGF1R-oe mice, seven female (78%) and ten male (91%) mice formed a tumor (Fig. 33c). These results showed that the sex of the mice did not significantly influence tumor development induced by AOM / DSS. In Fig. 33d the average number of tumors of IGF1R-oe and control mice that developed tumors is shown. On average, control mice developed 3.3 tumors, whereas IGF1R-oe even developed on average 4.3 tumors. In Fig. 33e and Fig. 33f tumor localization and tumor size are shown. Control mice displayed tumor development predominantly in the distal part of the colon, only a small number of tumors developed in the middle part of the colon. However, IGF1R-oe mice formed tumors only in the distal part of the colon (Fig. 33e). Regarding the size of the tumors, IGF1R-oe mice presented 50% more tumors smaller than 2 mm than control mice. The number of tumors bigger than 2 mm did not differ between IGF1R-oe and control mice (Fig. 33f).

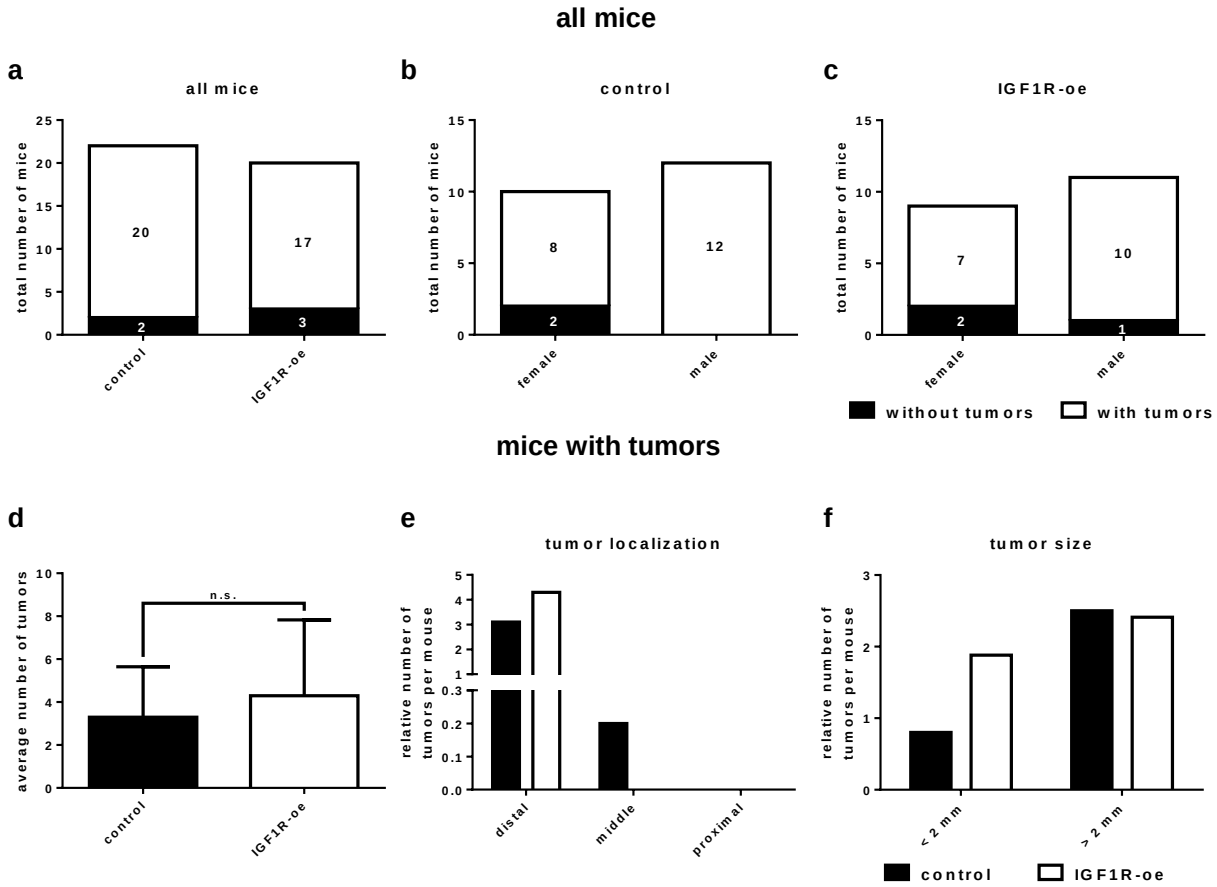

Fig. 33: Macroscopic analyses of the colonic tumors induced in Villin-TRE-IGF1R mice by AOM / DSS.

IGF1R-oe (n=20) and control mice (n=22) were treated with 2 mg / ml doxycycline to induce the overexpression of *IGF1R* and administered to AOM / DSS to induce intestinal tumor formation and inflammation. Mice were sacrificed when the tumors exhibited a score of 4 to 5 (after (Becker *et al.* 2007), and the tumors were macroscopically analyzed. **(a- c)** No difference regarding the number of mice that have developed tumors between IGF1R-oe and control mice as well as between female and male mice was observed. **(d)** IGF1R-oe mice (n=17) formed on average 4.3 tumors, whereas control mice (n=20) developed an average number of 3.3 tumors. **(e)** IGF1R mice formed a higher number of distal tumors, but did not develop any tumors in the middle part of the colon as control mice. **(f)** IGF1R-oe mice formed a higher number of tumors smaller than 2 mm in size, whereas the number of tumors bigger than 2 mm was nearly identical between IGF1R-oe and control mice. (student's *t* test).

Furthermore, intestinal tissue was fixed, paraffin-embedded and cut stepwise. Here, the first section was taken and the following ten sections were discarded. This process was repeated until three tissue sections were available. This process was performed to increase the probability to detect as many tumors as possible along the axis from distal to proximal for histopathological analyses. The three hematoxylin and eosin stainings were analyzed together with Dr. med. Felix Bremmer (Institute of Pathology,

University Medical Center Göttingen, Germany). Tumors were classified in low grade and high grade intraepithelial neoplasia, and intramucosal and invasive carcinoma, respectively. In Fig. 34a representative pictures of the different tumor stages are shown. As depicted in Fig. 34b, control mice displayed a reduced number of tumors with increasing tumor stage, whereas IGF1R-oe mice showed an increased number of intramucosal and even invasive carcinomas. In addition, the average tumor size per mouse was examined. Control mice developed tumors with an average size of 953 μm^2 per mouse. However, IGF1R-oe mice revealed a 66.2% increased average tumor size (1440 μm^2) compared to control mice (Fig. 34c).

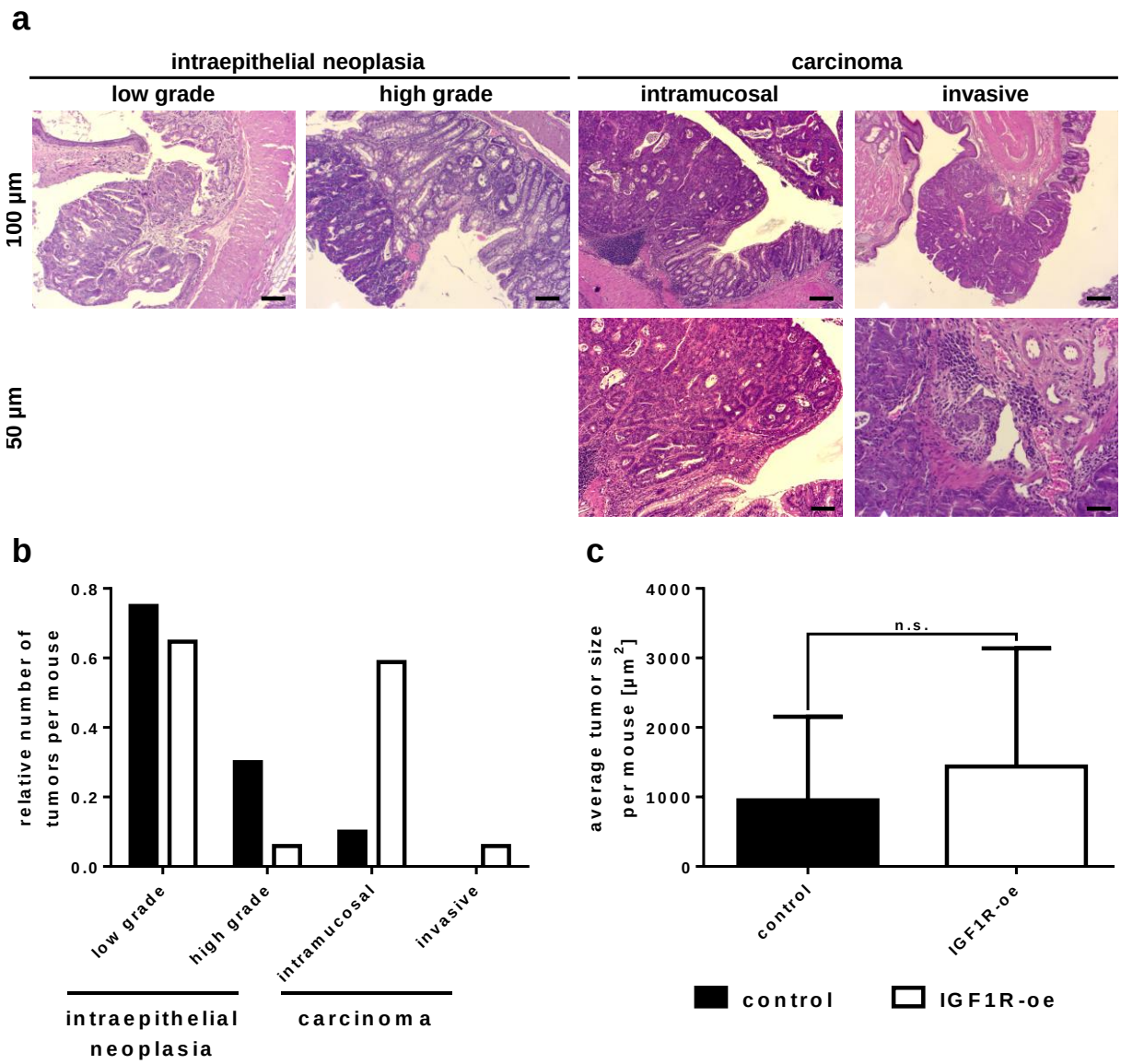

Fig. 34: Histopathological analyses of the AOM / DSS-induced tumors developed in IGF1R-oe and control Villin-TRE-IGF1R mice.

(a) Representative pictures of low and high grade neoplasia, and intramucosal and invasive carcinomas of Villin-TRE-IGF1R mice. Therefore, colonic tissue was fixed, paraffin-embedded and cut stepwise. Hematoxylin and eosin stainings of the tissue sections were performed (n=37).

(b) IGF1R-oe mice (n=17) developed a lower number of low grade and high grade intraepithelial neoplasias than control mice (n=20), but formed nearly six-fold more intramucosal carcinomas compared to control mice. One IGF1R-oe mouse even developed one invasive carcinoma, which was not present in control mice. **(c)** The average tumor size per mouse was approx. 500 µm^2 (66.2%) increased in IGF1R-oe mice compared to control mice (student's *t* test).

In addition, lymph nodes in the regional colonic fat tissue and liver tissue were excised from the mice to analyze the lymph node status and to screen for metastatic cells in the liver. The tissue samples were fixed and paraffin-embedded, cut as described in chapter 3.10 and hematoxylin and eosin stainings were prepared. Representative pictures of the hematoxylin and eosin stainings are shown in Fig. 35. Analyses of the lymph nodes and livers of IGF1R-oe and control mice performed by Dr. med. Felix Bremmer (Institute of Pathology, UMG, Germany) revealed no metastatic cells.

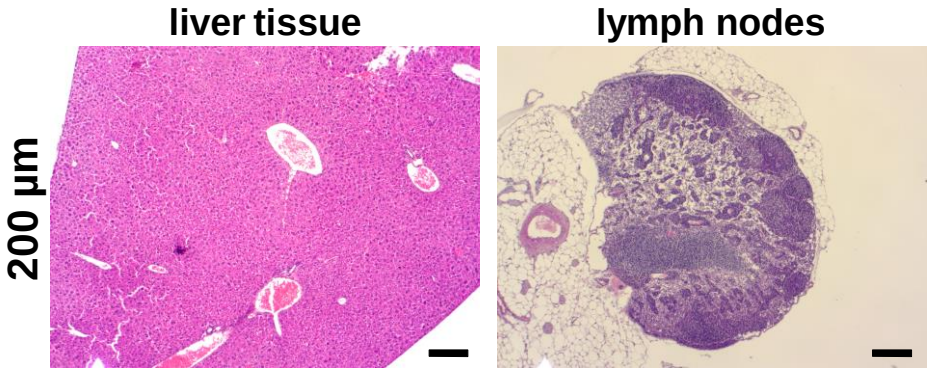

Fig. 35: Representative hematoxylin and eosin staining of liver tissue and lymph nodes in regional colonic fat tissue of Villin-TRE-IGF1R mice.
IGF1R-oe (n=20) and control mice (n=22) were administered to doxycycline to induce *IGF1R* overexpression and to AOM / DSS to induce colonic tumor formation and inflammation. After colonic tumors have developed, mice were sacrificed and the liver tissue and lymph nodes in regional colonic fat tissue were excised from the animals. Hematoxylin and eosin stainings of the tissue sections of IGF1R-oe (n=17) and control mice (n=20) were prepared and microscopically analyzed for metastatic cells. Metastatic cells could not be detected in liver tissues or lymph nodes of IGF1R-oe and control Villin-TRE-IGF1R mice.

3.12 Confirmation of *IGF1R* overexpression in tumor tissue

To check if the tumors of IGF1R-oe mice, which were induced by AOM / DSS, show *IGF1R* overexpression, colonic tissue sections were stained with an antibody specific for human IGF1R. Immunohistochemical (Fig. 36a) as well as immunofluorescence

stainings (Fig. 36b) revealed that the IGF1R is overexpressed in normal colonic as well as in colonic tumor tissue.

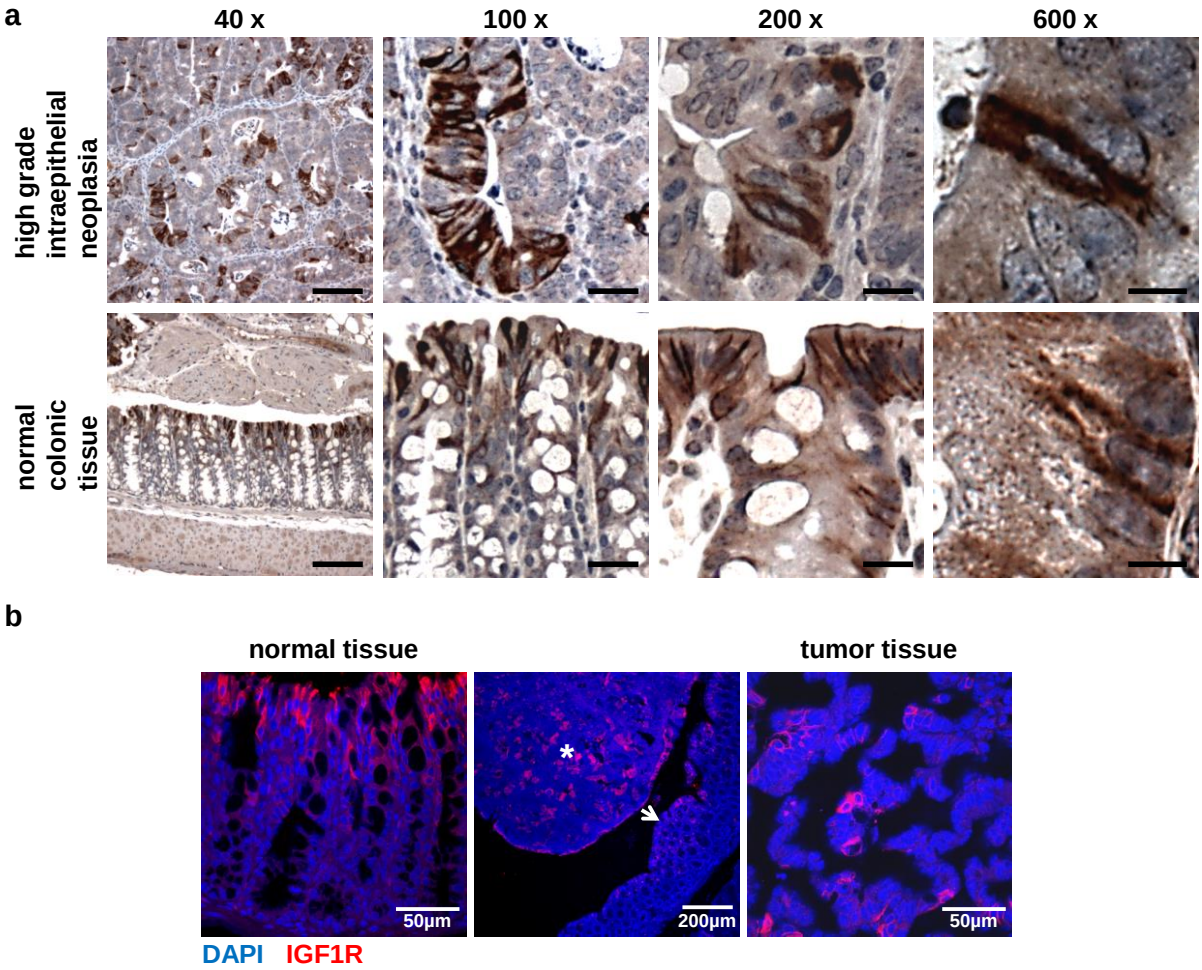

Fig. 36: IGF1R overexpression in AOM / DSS-induced tumors developed in IGF1R-oe Villin-TRE-IGF1R mice.

(a) Immunohistochemical stainings (brown) of normal colonic and colonic tumor tissue of IGF1R-oe (n=10) and control mice (n=10). Cell nuclei were stained with hemalum solution (blue). **(b)** Immunofluorescence stainings of normal colonic tissue and colonic tumor tissue of IGF1R-oe (n=5) and control mice (n=5). The arrow marks normal colonic tissue, the star indicates intestinal tumor tissue. DAPI visualized cell nuclei (blue). Immunohistochemical and immunofluorescence stainings revealed IGF1R overexpression in normal colonic tissue as well as in colonic tumor tissue.

3.13 Confirmation of villin expression in tumor tissue

It is known from the literature that expression of villin is commonly lost in poorly differentiated colon cancer (Arango *et al.*, 2012). To confirm that villin is expressed in the colonic tumor tissue of IGF1R-oe and control mice induced by AOM / DSS treatment, immunofluorescence staining using an antibody specific for villin was

performed. In Fig. 37 representative pictures of the fluorescence stainings are shown. Villin was expressed in normal colonic as well as in colonic tumor tissue.

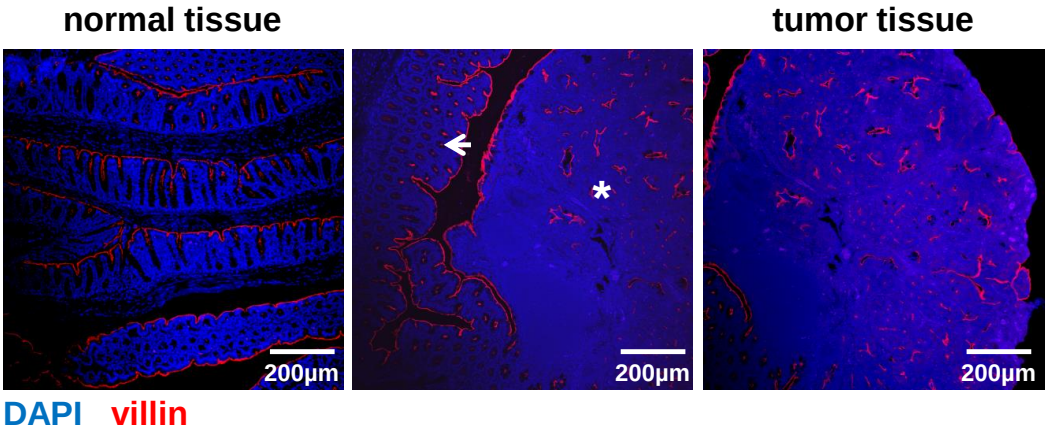

Fig. 37: Villin was expressed in AOM / DSS-induced tumors of Villin-TRE-IGF1R mice. Immunofluorescence staining showed villin expression (red) in normal colonic tissue as well as in colonic tumor tissue of IGF1R-oe (n=5) and control mice (n=5). The arrow marks normal colonic tissue, the star indicates intestinal tumor tissue. DAPI visualized cell nuclei (blue).

3.14 *IGF1R* overexpression results in the activation of the downstream PI3K signaling pathway in colonic tumors

To analyze if the downstream PI3K and MAPK signaling pathways are activated in the colonic tumors which developed in IGF1R-oe and control mice after AOM / DSS administration, proteins of the tumors were extracted and western blot (Fig. 38a) and subsequent densitometrical analyses (Fig. 38b- g) were performed. Additionally, proteins of epithelial cells derived from either the small intestine (SI) or from the colon were extracted and analyzed.

IGF1Rα and IGF1Rβ expression was weakly increased in tumors developed in IGF1R-oe mice compared to control mice (Fig. 38a- c). Interestingly, AKT was highly activated in tumors developed in IGF1R-oe mice compared to tumors from control mice when phosphorylated at the serine 473 (Ser 473) residue (pAKT), but the activity of AKT was decreased in tumors from IGF1R-oe mice compared to tumors from control mice when phosphorylated at the threonine 308 (Thr 308) residue (pAKT) (Fig. 38a, d, e). The activation level of ERK (pERK) was reduced in tumors from IGF1R-oe mice compared to tumors from control mice (Fig. 38a, f). These results demonstrated that the downstream PI3K and MAPK signaling pathways were activated in colonic tumors

induced by AOM / DSS. Tumors of IGF1R-oe mice displayed a 2-fold higher expression level of villin compared to tumors from control mice (Fig. 38a, g).

Furthermore, IGF1Rα expression was approx. 10-fold increased in epithelial cells of the small intestine (SI) and colon of IGF1R-oe mice compared to control mice, whereas IGF1Rβ expression was evenly up to 30-fold elevated in the small intestine and colon of IGF1R-oe mice. Again, these data confirmed the inducible overexpression of *IGF1R* upon doxycycline administration (Fig. 38a- c). Interestingly, the phosphorylation level of AKT (pAKT) was only weakly increased in the small intestine and colon of IGF1R-oe mice when phosphorylated at the Ser 473 residue, whereas the activity of AKT was up to 6-fold increased in the small intestine and colon of IGF1R-oe mice when phosphorylated at the Thr 308 residue compared to control mice (Fig. 38a, d, e). The activity of ERK (pERK) was weakly elevated in the small intestine of IGF1R-oe mice, whereas the phosphorylation level was reduced in the colon of IGF1R-oe mice compared to control mice (Fig. 38a, f). Villin was evenly expressed in the small intestine and colon in IGF1R-oe and control mice (Fig. 38a, g).

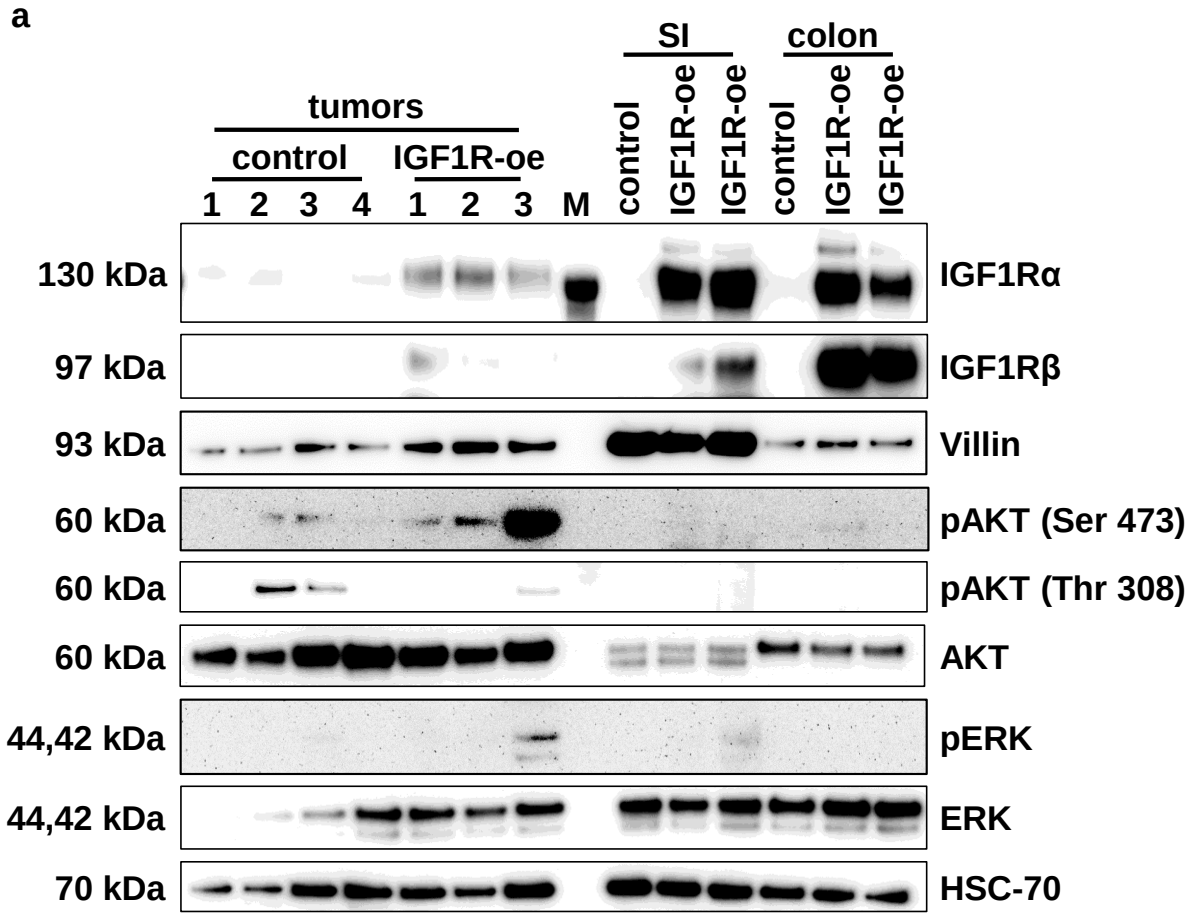

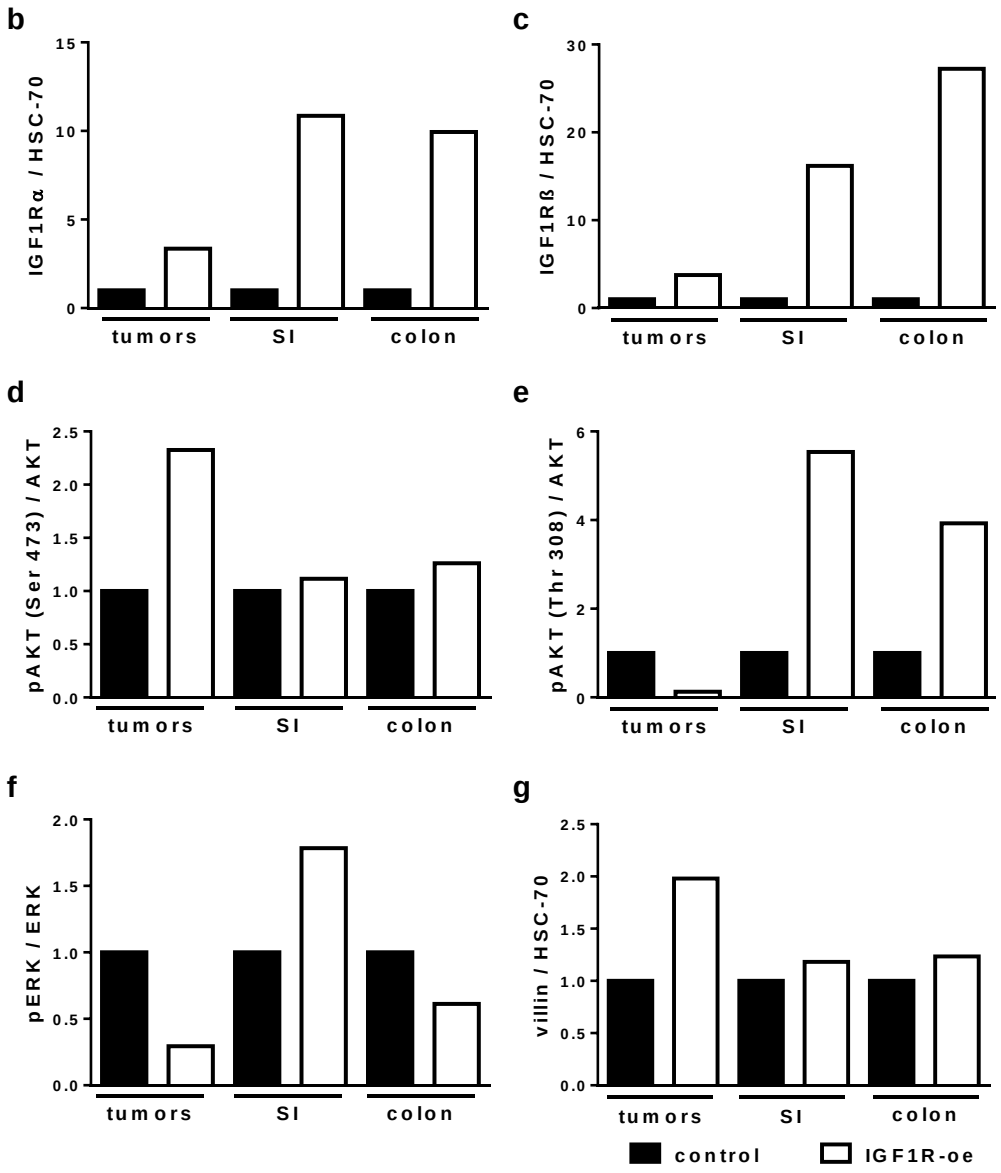

Fig. 38: Western blot and subsequent densitometrical analyses of colonic tumors induced by AOM / DSS as well as of epithelial cells of the small intestine (SI) and colon of Villin-TRE-IGF1R mice.

Both IGF1R-oe (n=20) and control (n=22) Villin-TRE-IGF1R mice were administered to 2 mg / ml doxycycline. Additionally, mice were administered to AOM / DSS to induce colonic tumor formation and inflammation. After intestinal tumors have developed, mice were sacrificed and proteins of tumors as well as of epithelial cells of the small intestine and colon of one IGF1R-oe and one control mouse were extracted. Western blot **(a)** and subsequent densitometrical analyses **(b- g)** were performed on three tumors developed in IGF1R-oe mice and on four tumors formed in control mice. **(a- c)** Elevated levels of IGF1R expression could be observed in tumors developed in IGF1R-oe mice as well as in epithelial cells of the small intestine and colon of IGF1R-oe mice compared to control mice. **(a, d, e)** The phosphorylation level of AKT (pAKT Ser473) was highly increased in the tumors and epithelial cells of the small intestine and colon of IGF1R-oe mice compared to control mice. **(a, f)** The phosphorylation level of ERK (pERK) was decreased in tumors developed in IGF1R-oe mice compared to control mice, whereas ERK was highly activated in epithelial cells of the small intestine of IGF1R-oe mice compared

to control mice. **(a, g)** Villin was expressed in tumors and in epithelial cells of the small intestine and colon of IGF1R-oe and control mice. M=SeeBlue® Plus2 Pre-Stained Standard.

3.15 Tumors induced in Villin-TRE-IGF1R mice by AOM / DSS do not metastasize to the liver and nearby lymph nodes

To analyze if tumors induced by AOM / DSS are able to grow invasive and metastasize to nearby lymph nodes and to the liver, IGF1R-oe and control Villin-TRE-IGF1R mice were administered to AOM / DSS. Tumor formation was regularly examined by colonoscopy (Fig. 39).

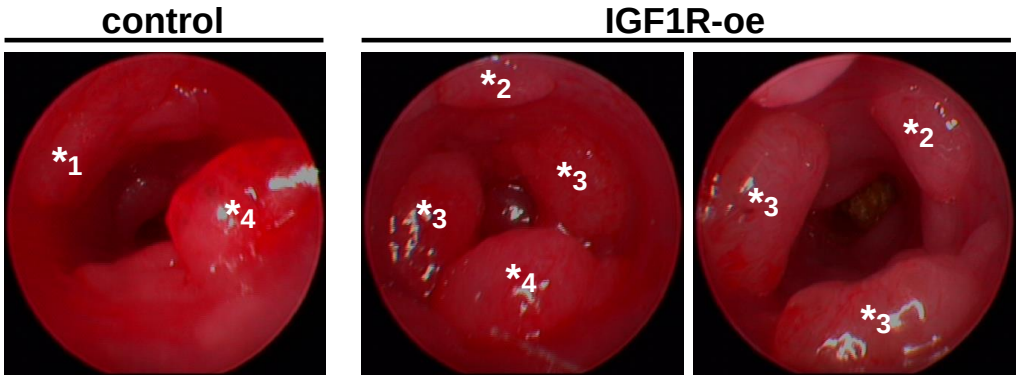

Fig. 39: Colonoscopy of IGF1R-oe and control Villin-TRE-IGF1R mice administered to AOM / DSS. For colonoscopy, mice were anesthetized using isoflurane. The number of tumors was counted and tumor localization was determined. Both IGF1R-oe (n=16) and control mice (n=11) revealed a high number of tumors of score 3 to 4 or even 5 (after Becker *et al.* 2007).

Twenty weeks after the AOM injection, the majority of tumors developed in IGF1R-oe and control mice had a score of 3 to 4 or even 5 related to Becker *et al.* (2007) and mice were sacrificed. The colon length of those mice that have developed tumors was measured using a caliper. Comparison of the average colon length revealed no significant difference between IGF1R-oe and control mice (Fig. 40).

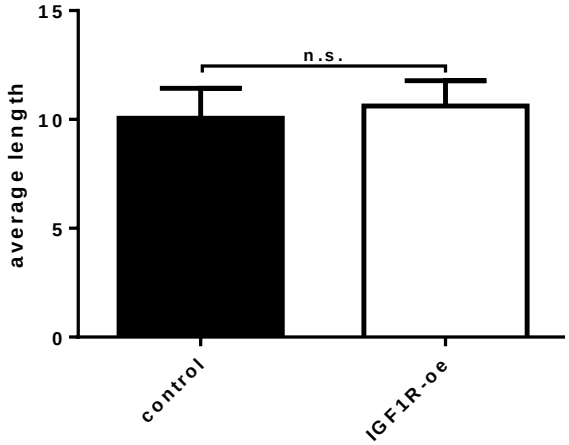

Fig. 40: Average colon length of IGF1R-oe and control Villin-TRE-IGF1R mice after tumor induction by AOM / DSS.

No significant difference in the average colon length between IGF1R-oe (n=14) and control mice (n=7) could be observed (student's *t* test).

Macroscopic analyses of the colons revealed that seven out of eleven (63.6%) control mice and 14 out of 16 (87.5%) IGF1R-oe mice developed tumors (Fig. 41a). The differentiation between the sexes showed that five out of seven (71.4%) female control mice and two out of four (50%) male control mice formed tumors (Fig. 41b). In IGF1R-oe mice, four out of six (66.7%) female mice and all ten (100%) male mice displayed tumor formation (Fig. 41c). These results indicated that both sexes had the same susceptibility to AOM / DSS administration. On average, control mice developed 2.6 tumors, whereas IGF1R-oe mice formed on average 6.1 tumors (Fig. 41d). Regarding the localization of the tumors in the colon, the majority of mice developed tumors in the distal part. Here, IGF1R-oe mice formed more than twice as many tumors than control mice. A few IGF1R-oe and control mice formed tumors in the middle part of the colon, whereas two IGF1R-oe mice developed tumors in the proximal part of the colon (Fig. 41e). Furthermore, the number of tumors smaller than 2 mm as well as bigger than 2 mm was increased in IGF1R-oe mice compared to control mice. Both, control and IGF1R-oe mice, revealed an increased number of tumors bigger than 2 mm (Fig. 41f).

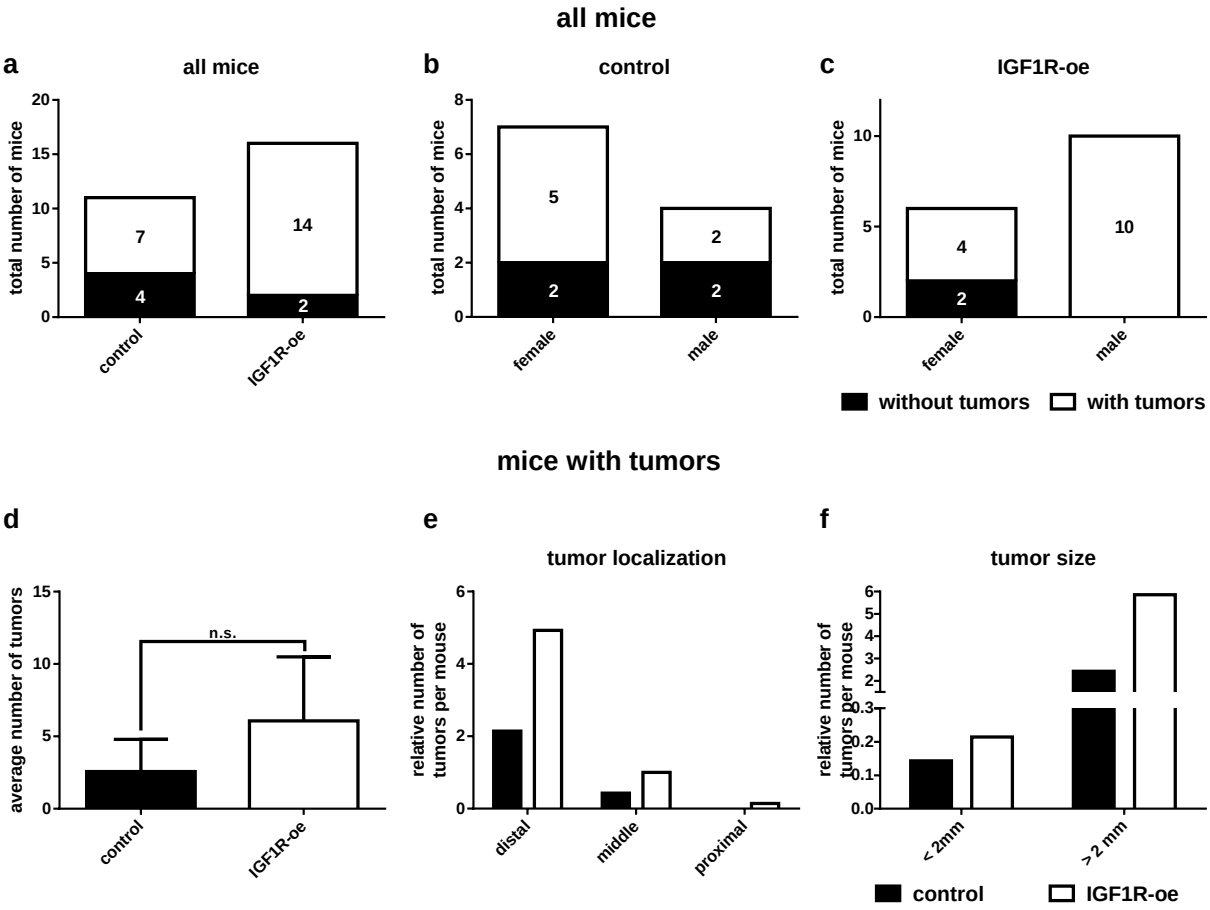

Fig. 41: Macroscopic analyses of the colonic tumors of Villin-TRE-IGF1R mice induced by AOM / DSS.

(a) Approx. 88% IGF1R-oe mice (n=16) developed a tumor in the colon, whereas only 64% of control mice (n=11) formed a tumor. **(b, c)** One hundred percent of male and 67% of female IGF1R-oe mice showed tumor formation in the colon, whereas only in 50% of male and in 71% of female control mice tumor development could be observed. **(d)** IGF1R-oe mice (n=14) developed on average 6.1 tumors, control mice (n =7) formed only 2.6 tumors on average. **(e)** IGF1R-oe mice showed a 2-fold higher number of tumors in the distal part of the colon than control mice and an increased number of tumors in the middle and proximal part of the colon. **(f)** IGF1R-oe mice developed a higher number of tumors smaller than 2 mm as well as bigger than 2 mm compared to control mice.

In addition, histopathological analyses were performed. Therefore, colonic tissue sections were cut and stained with hematoxylin and eosin. Of note, paraffin-embedded colonic tissue of the three IGF1R-oe mice #545, #546 and #557 was cut stepwise, because the first analyzed section revealed many intramucosal tumors. IGF1R-oe mice developed a higher number of tumors with increasing stage and even invasive carcinomas compared to control mice (Fig. 42a). Control mice formed tumors with an

average tumor size of 189 µm^2. In IGF1R-oe mice, the average tumor size was increased for 90.3% to 1948 µm^2 (Fig. 42b).

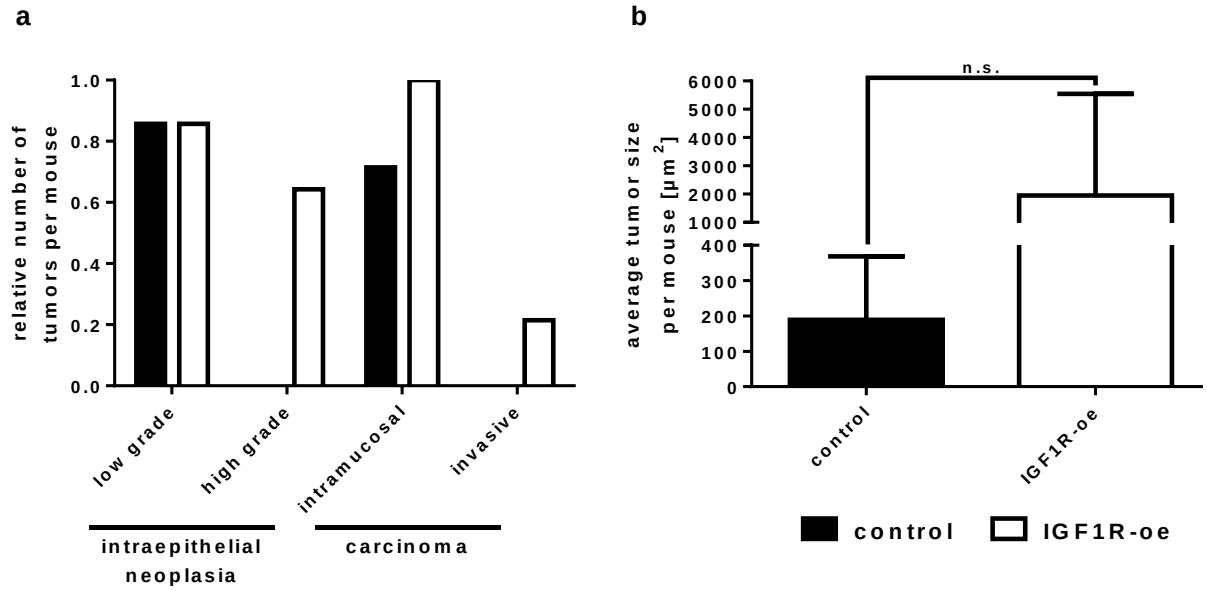

Fig. 42: Histopathological analyses of the AOM / DSS-induced tumors developed in IGF1R-oe and control Villin-TRE-IGF1R mice.

(a) IGF1R-oe mice (n=14) developed a higher number of tumors with increasing stage and even invasive carcinomas compared to control mice (n=7). **(b)** Control mice formed tumors with an average tumor size of 189 µm^2. The average tumor size of IGF1R-oe mice is increased for approx. 90% to 1948 µm^2.

To investigate if tumors that were induced by AOM / DSS are able to grow invasive and metastasize, liver tissue and lymph nodes in the regional colonic fat tissue were histopathologically analyzed together with Dr. med. Felix Bremmer (Institute of Pathology, University Medical Center Göttingen, Germany). Therefore, liver tissue and lymph nodes in the regional colonic fat tissue were fixed, paraffin-embedded, cut and hematoxylin and eosin staining was performed on the sections. Neither control nor IGF1R-oe mice revealed metastatic cells in the liver or lymph nodes, indicating that tumors induced by AOM / DSS did not develop metastases.

3.16 Establishment of a mouse line used to induce the knockout of the murine *Igf1r* in the intestine

In order to analyze if the Igf1r plays a role during the development of the intestine as well as during intestinal tumor formation and progression, respectively, a mouse model

for an inducible knockout of the murine *Igf1r* was established, called Villin-CreERT-Igf1r. The Villin-CreERT-Igf1r mouse represents a double transgenic mouse line and was generated by crossing the Villin-CreER^{T2} mouse line with the Igf1r$^{(lox)}$ mouse line.

3.16.1 Genotyping of the Villin-CreER^{T2} mouse line

The Villin-CreER^{T2} mouse line is a transgenic mouse expressing the tamoxifen-dependent cre recombinase under the control of the murine villin promoter (chapter 2.9.2.5). To analyze if the newborn pubs expressed the Villin-CreER^{T2} transgene, DNA of the tail was amplified by PCR using specific primers which were complementary to the villin promoter and the cre coding sequence, respectively (El Marjou *et al.* 2004). In Fig. 43 the result of a representative genotyping-PCR is shown. While mouse #193 carried the transgene, mice #190 to #192 did not contain the Villin-CreER^{T2} transgene in their genome. To maintain the population of Villin-CreER^{T2} mice, Villin-CreER^{T2}-positive mice were crossed with Villin-CreER^{T2}-negative mice. Therefore, the Villin-CreER^{T2} mice were kept in a heterozygous stage.

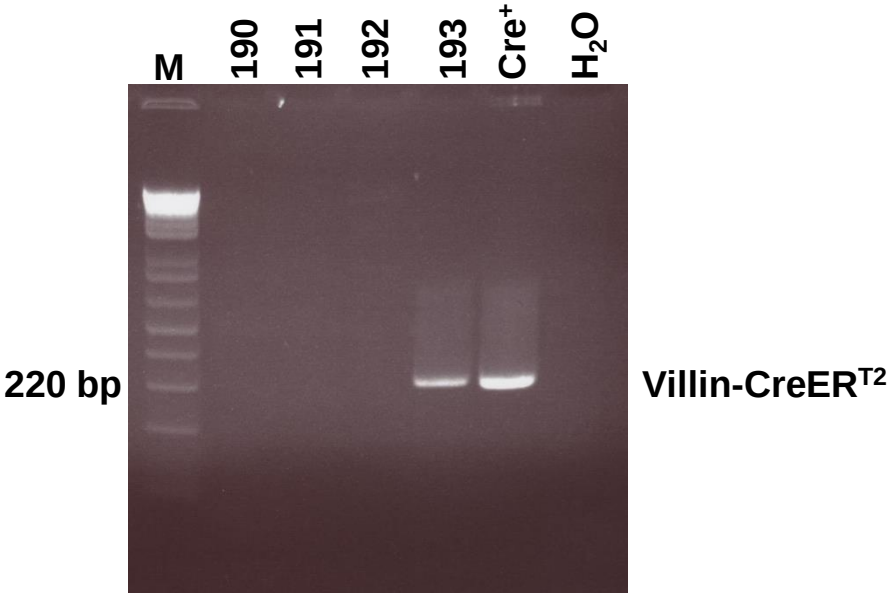

Fig. 43: Result of a representative genotyping-PCR of the Villin-CreER^{T2} mouse line.
Tail DNA was extracted and used as a template in the PCR. Mouse #193 showed a band of 220 bp in size and thus carried the cre recombinase. Mice #190 to #192 did not carry the cre recombinase in their genome and were thus negative for the cre recombinase. M=1 Kb Plus DNA Ladder, Cre^{+}=positive control of a mouse carrying the cre recombinase, H_2O=negative control without DNA.

3.16.2 Genotyping of the Igf1r$^{(lox)}$ mouse line

The Igf1r$^{(lox)}$ mouse line is a cre-responder mouse line that carries *loxP*-modified alleles of the *Igf1r* gene (chapter 2.9.2.6). To check if the offspring of the Igf1r$^{(lox)}$ mice carried the *loxP*-modified alleles of the *Igf1r* in their genome, tail DNA was amplified by PCR. In Fig. 44 the result of a representative PCR amplification is shown. Mice #10 to #18 and #20 carried the *loxP*-modified alleles of the *Igf1r* gene, whereas mouse #19 did not carry the *loxP*-modified allele of the *Igf1r* in its genome. For maintaining the mouse population, homozygous Igf1r$^{(lox)}$ mice were crossed with each other.

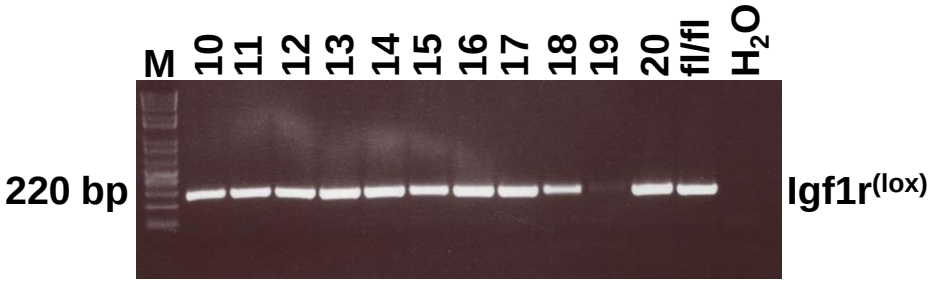

Fig. 44: Result of a representative genotyping-PCR of the Igf1r$^{(lox)}$ mouse line.
Tail DNA was extracted and amplified by PCR using primers specific for the Igf1r$^{(lox)}$ transgene. All mice except mouse #19 showed a band of 220 bp in size and therefore carried two *loxP*-modified alleles of the *Igf1r.* M=1 Kb Plus DNA Ladder, fl / fl=positive control of a mouse carrying two *loxP*-modified alleles of the *Igf1r,* H_2O=negative control without DNA.

3.16.3 Genotyping of the Villin-CreERT-Igf1r mouse line

The Villin-CreERT-Igf1r mouse line is a model for the inducible knockout of the *Igf1r* specifically in epithelial cells of the murine intestine (chapter 2.9.2.7). For the generation of the tamoxifen-inducible *Igf1r* knockout mouse line, the transgenic Villin-CreER^{T2} mouse line was crossed with the transgenic Igf1r$^{(lox)}$ mouse line. To determine the genotype of the offspring, tail DNA was extracted and analyzed by PCR using specific primers for the Villin-CreER^{T2} transgene as well as specific primers used for the genotyping of the Igf1r$^{(lox)}$ mouse line. In Fig. 45 the result of a representative genotyping-PCR is shown. Mice #488, #490 and #493 carried the cre recombinase, whereas mice #485 to #487, #489, #491 to #492 and #494 were negative for the cre recombinase. Furthermore, mice #486, #487, #489, #492, #493 and #494 carried the wild type and one *loxP*-modified allele of the *Igf1r* and were therefore heterozygous, whereas mouse #488 carried two *loxP*-modified alleles of the *Igf1r* and was therefore homozygous. Two *Igf1r* wild type alleles were detected in mice #485, #490 and #491.

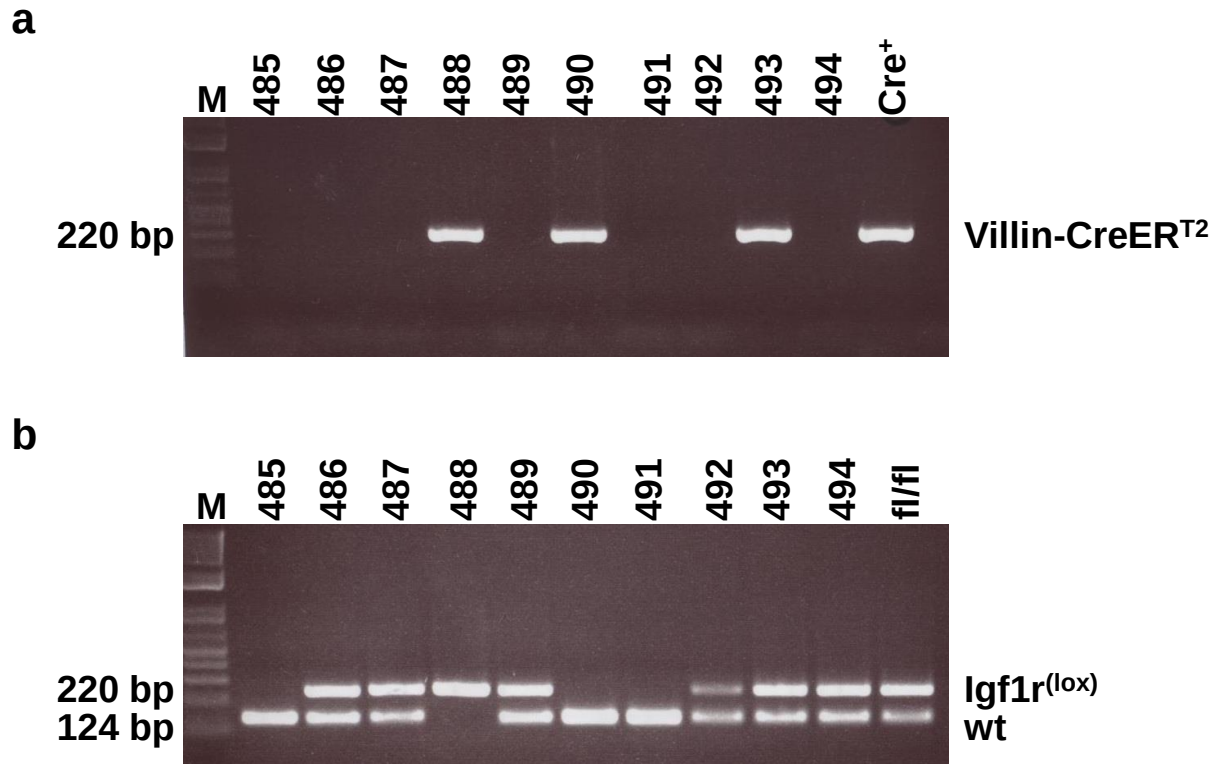

Fig. 45: Result of a representative genotyping-PCR of the Villin-CreERT-Igf1r mouse line.
For the genotyping of the newborn pubs, DNA of tail biopsies was extracted and PCR-amplified using a primer pair specific for the Villin-CreER^{T2} transgene and primers specific for the Igf1r$^{(lox)}$ transgene. Mice #486, #487, #489, #492, #493 and #494 carried the cre recombinase in their genome, whereas mice #485, #486, #487, #489, #491, #492 and #494 were negative for the cre recombinase. Mice #486, #487, #489, #492, #493 and #494 carried a wild type (wt) and a *loxP*-modified allele of the *Igf1r,* and were therefore heterozygous mice, whereas mouse #488 carried two *loxP*-modified alleles of the *Igf1r* and was therefore a homozygous mouse. Two *Igf1r* wild type alleles were detected in mice #485, #490 and #491. M=1 Kb Plus DNA Ladder, Cre^{+}=positive control of a mouse carrying the cre recombinase, fl / fl=positive control of a mouse carrying two *loxP*-modified alleles of the *Igf1r.*

3.17 Induction of the knockout of *Igf1r* in the Villin-CreERT-Igf1r mice

To study the influence of the Igf1r during the development of the intestine and during intestinal tumor formation and progression, the Villin-CreERT-Igf1r mouse line was used. As described in chapter 3.16.3, Villin-CreERT-Igf1r can have the following genotypes: Cre^{+}/*Igf1r*$^{fl/fl}$ (homozygous *Igf1r* knockout mice), Cre^{+}/*Igf1r*$^{fl/+}$ (heterozygous *Igf1r* knockout mice) as well as Cre^{-}/*Igf1r*$^{fl/fl}$ or Cre^{-}/*Igf1r*$^{fl/+}$ (control mice). The complete knockout of the *Igf1r* in epithelial cells of the intestine can only be induced in homozygous Cre^{+}/*Igf1r*$^{fl/fl}$ mice, because only these mice express the cre recombinase

and additionally carry the two *loxP*-modified alleles of the *Igf1r* gene. In contrast, Cre^{+}/*Igf1r*$^{fl/+}$ mice are in fact positive for the cre recombinase, but carry only one *loxP*-modified allele of the *Igf1r.* Therefore, these mice are heterozygous and still express the *Igf1r* in the intestine. As control, both Cre^{-}/*Igf1r*$^{fl/fl}$ and Cre^{-}/*Igf1r*$^{fl/+}$ mice were used for the following experiments. Indeed, these mice carry one or even two modified alleles of the *Igf1r,* but these mice do not express the cre recombinase. Therefore, the *Igf1r* cannot be deleted by the cre recombinase and is still expressed in these control mice.

To induce the knockout of the *Igf1r* in the Villin-CreERT-Igf1r mice, Cre^{+}/*Igf1r*$^{fl/fl}$, Cre^{+}/*Igf1r*$^{fl/+}$ as well as Cre^{-}/*Igf1r*$^{fl/fl}$ and Cre^{-}/*Igf1r*$^{fl/+}$ mice as control were injected with 1 mg / day tamoxifen on five consecutive days (Fig. 46). The Villin-CreER^{T2} is a fusion construct of the cre recombinase with a mutated ligand-binding domain of the human estrogen receptor, resulting in a tamoxifen-dependent cre recombinase. Furthermore, the expression of this construct is under the control of the villin promoter leading to stable and homogenous expression of the cre recombinase in the small intestine and colon along the crypt-villus axis (El Marjou *et al.*, 2004). Thus, administration of tamoxifen to the Villin-CreERT-Igf1r mouse line led to the deletion of exon 3 of the *Igf1r* gene specifically in the intestine of the mouse at a desired time point in Cre^{+}/*Igf1r*$^{fl/fl}$ mice.

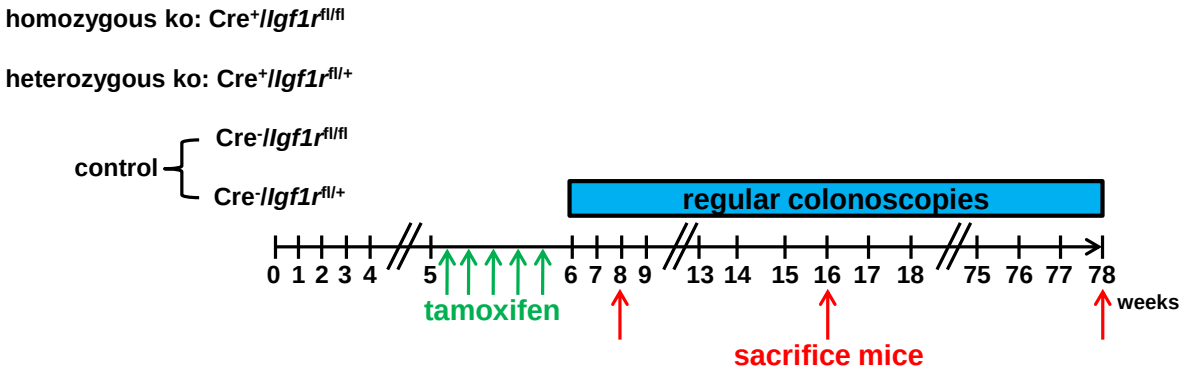

Fig. 46: Treatment scheme for the induction of the *Igf1r* knockout in the intestine of Villin-CreERT-Igf1r mice.

To develop *Igf1r* knockout mice, Villin-CreERT-Igf1r mice were injected with tamoxifen on five consecutive days. Cre^{+}/*Igf1r*$^{fl/fl}$ were homozygous knockout (ko) mice, Cre^{+}/*Igf1r*$^{fl/+}$ were heterozygous knockout (ko) mice. As control mice, both Cre^{-}/*Igf1r*$^{fl/fl}$ and Cre^{-}/*Igf1r*$^{fl/+}$ mice were used. The green arrows mark the five tamoxifen injections. The red arrows mark time points when the mice were sacrificed.

3.18 Confirmation of villin expression in epithelial cells of the Villin-CreERT-Igf1r mouse line *via* immunohistochemistry

To confirm the expression of villin in all epithelial cells of the small intestine and colon of Cre^{+}/*Igf1r*$^{fl/fl}$, Cre^{+}/*Igf1r*$^{fl/+}$ and control Villin-CreERT-Igf1r mice injected with tamoxifen, tissue sections of the small intestine and colon were stained for villin expression. In Fig. 47 representative pictures of the villin stainings are shown. An intense staining for villin in the villi of the small intestine could be observed. In the crypt of the small intestine, villin expression was weak. In the colon, epithelial cells at the top of the crypts highly expressed villin, while cells at the bottom of the crypts showed only slight villin expression. These stainings led to the assumption that there was a gradient of villin expression from high expression in the villi of the small intestine as well as at the top of the crypts of the colon to low expression of villin in the crypts of the small intestine and at the bottom of the crypts of the colon. These results were similar to the results of the villin staining of Villin-TRE-IGF1R mice (chapter 3.3). Furthermore, an increasing gradient of villin expression from crypt to tip was also shown by other authors (Braunstein *et al.* 2002; Madison 2002).

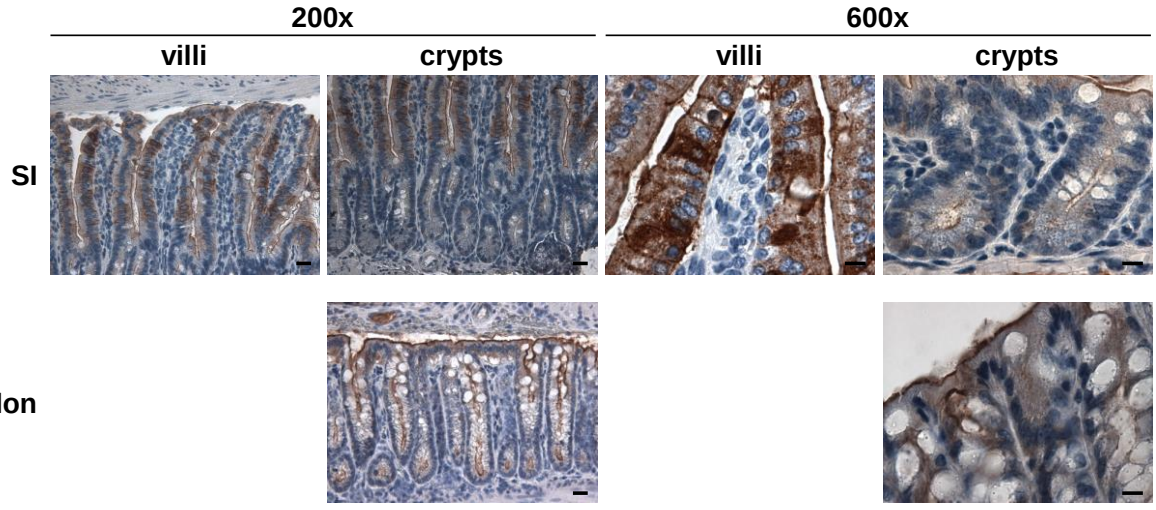

Fig. 47: Villin was expressed in epithelial cells of the small intestine (SI) and colon of the Villin-CreERT-Igf1r mouse.

Tissue sections of the small intestine and colon of Cre^{+}/*Igf1r*$^{fl/fl}$ (n=5), Cre^{+}/*Igf1r*$^{fl/+}$ (n=5) and control mice (n=5) injected with tamoxifen were stained for villin expression (brown). Cell nuclei were stained with hemalum solution (blue). Representative pictures of the villin stainings in control mice are shown. Villin was highly expressed in epithelial cells of the small intestine and colon. An increasing gradient of villin expression from the crypt to the villus and from the bottom of the crypt to the top of the crypt, respectively, was visible.

3.19 Confirmation of the *Igf1r* knockout in Villin-CreERT-Igf1r mice by PCR on genomic DNA from the small intestine and colon

To confirm the knockout of the *Igf1r* in Villin-CreERT-Igf1r mice, three mice with different genetic backgrounds ($Cre^{+}/Igf1r^{fl/fl}$, $Cre^{+}/Igf1r^{fl/+}$ and $Cre^{-}/Igf1r^{fl/+}$) were injected once with tamoxifen on five consecutive days and genomic DNA from epithelial cells of the small intestine and colon was extracted nine days after the first tamoxifen injection, respectively. A PCR was performed using the three specific primers P1, P2 and P3 to discriminate the wild type, $Igf1r^{lox}$ and $Igf1r^{\Delta lox}$ allele. The wild type and $Igf1r^{lox}$ alleles were detected using the forward primer P1, which is localized upstream of the second *lox*P site, and the reverse primer P2, which is localized downstream of the same *lox*P site. The $Igf1r^{\Delta lox}$ allele was detected using the forward primer P3 localized 5' of the *lox*P site in intron 2 and the reverse primer P2 (Xuan *et al.* 2002) (Fig. 48a). In Fig. 48b the result of the performed PCR analysis is shown. Only a single band of 320 bp was visible for the small intestine and colon of the $Cre^{+}/Igf1r^{fl/fl}$ mouse, confirming a complete knockout of both *Igf1r* alleles. The $Cre^{+}/Igf1r^{fl/+}$ mouse revealed the wild type band (120 bp) using the primers P1 and P2 as well as the band for the $Igf1r^{\Delta lox}$ allele (320 bp) using the primers P3 and P2. The mouse being negative for the cre recombinase (Cre^{-}), but carrying one *loxP*-modified allele of *Igf1r* showed the band of 120 bp for the wild type allele as well as the band of 220 bp for the *loxP*-modified allele of *Igf1r,* confirming that the knockout was only induced if the cre recombinase is present.

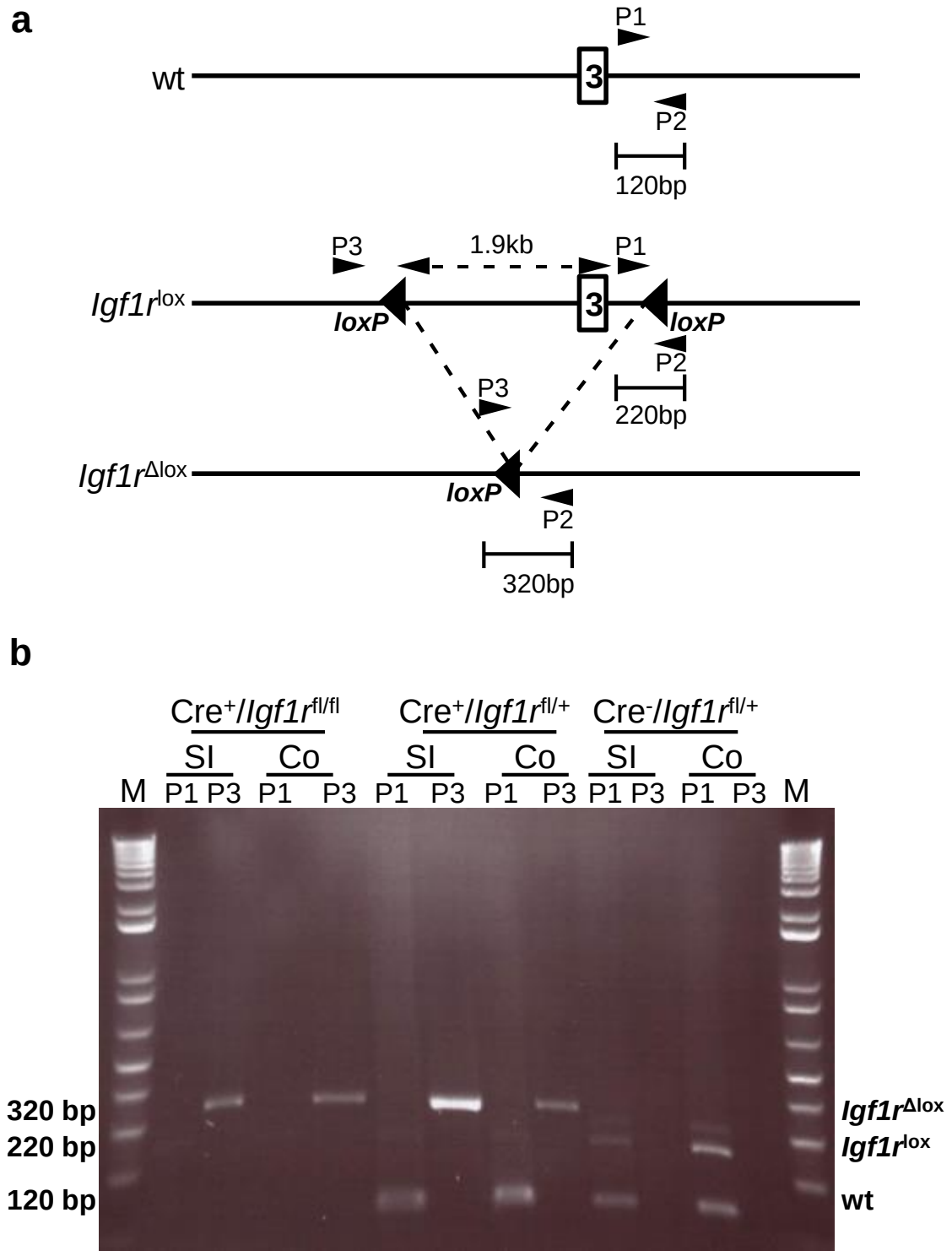

Fig. 48: Confirmation of the *Igf1r* knockout in the intestine of Villin-CreERT-Igf1r mice injected with tamoxifen.

Three mice with the indicated genotypes were injected with tamoxifen on five consecutive days and genomic DNA was isolated from the small intestine (SI) and colon (Co). A PCR using two different primer pairs specific for the wild type (wt), *Igf1r*^{lox} and the *Igf1r*$^{\Delta lox}$ alleles was performed. **(a)** Diagrams of the *Igf1r* locus around exon 3 (square), the floxed (*Igf1r*^{lox}) and the recombined floxed *Igf1r*$^{\Delta lox}$ alleles are shown. The primers P1, P2 and P3, the *loxP* sites and the length of the PCR products are indicated. **(b)**

The Cre$^+$/*Igf1r*$^{fl/fl}$ mouse (n=1) only showed a 320 bp band for the *Igf1r*$^{\Delta lox}$ allele. The Cre$^+$/*Igf1r*$^{fl/+}$ mouse (n=1) revealed a 120 bp band for the wild type allele as well as a 320 bp band for the *Igf1r*$^{\Delta lox}$ allele. In the Cre$^-$/*Igf1r*$^{fl/+}$mouse (n=1) a 120 bp band for the wild type allele and a 220 bp band for the *Igf1r*^{lox} allele were detectable. M=1 Kb Plus DNA Ladder. P1=Primer P1 and P2 were used to detect the *Igf1r* wild type and *Igf1r*^{lox} alleles. P3=Primer P2 and P3 were used to detect the *Igf1r*$^{\Delta lox}$ allele.

3.20 Confirmation of the *Igf1r* knockout in the intestine of Villin-CreERT-Igf1r mice *via* western blot analysis

To confirm the knockout of the *Igf1r* in the small intestine (SI) and colon (Co) of Villin-CreERT-Igf1r mice, three Cre$^+$/*Igf1r*$^{fl/fl}$ and two control Villin-CreERT-Igf1r mice were intraperitoneally injected with tamoxifen on five consecutive days and proteins of epithelial cells of the small intestine and colon were extracted, respectively. Western blot analysis revealed expression of the IGF1Rα in epithelial cells of the small intestine and colon of control mice, whereas IGF1Rα expression was not detectable in the small intestine and colon of Cre$^+$/*Igf1r*$^{fl/fl}$ mice, confirming the knockout of the *Igf1r* in epithelial cells of the small intestine and colon of Cre$^+$/*Igf1r*$^{fl/fl}$ mice. Of note, control mice showed a higher expression of the IGF1Rα in the colon compared to the small intestine (Fig. 49).

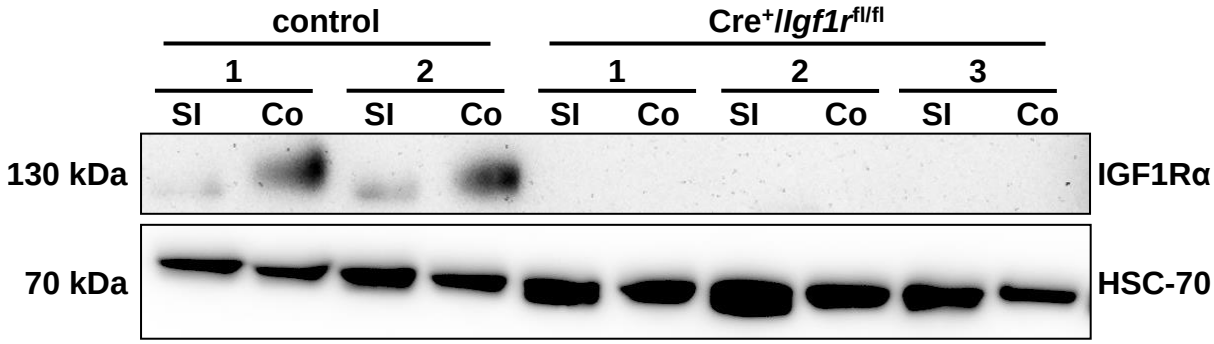

Fig. 49: Confirmation of the *Igf1r* knockout in epithelial cells of the small intestine (SI) and colon (Co) of Cre$^+$/*Igf1r*$^{fl/fl}$ Villin-CreERT-Igf1r mice.

Protein was extracted from epithelial cells of the small intestine (SI) and colon of Cre$^+$/*Igf1r*$^{fl/fl}$ and control Villin-CreERT-Igf1r mice, respectively, and western blot analysis using a specific antibody against the IGF1Rα was performed. Control mice (n=2) showed high expression of the IGF1Rα, whereas IGF1Rα expression was not visible in the small intestine and colon of Cre$^+$/*Igf1r*$^{fl/fl}$ mice (n=3).

3.21 Morphological analyses of small intestinal and colonic villi and crypts of Villin-CreERT-Igf1r mice

To examine if the *Igf1r* knockout has any influence on the morphology of the villi and crypts of the small intestine and colon, Cre^{+}/*Igf1r*$^{fl/fl}$, Cre^{+}/*Igf1r*$^{fl/+}$ and control mice were injected with tamoxifen to induce the *Igf1* knockout (for treatment scheme see Fig. 46). To check for changes in the intestinal epithelium, colonoscopy was performed regularly. Changes in the colonic morphology were not observed by colonoscopy (Fig. 50).

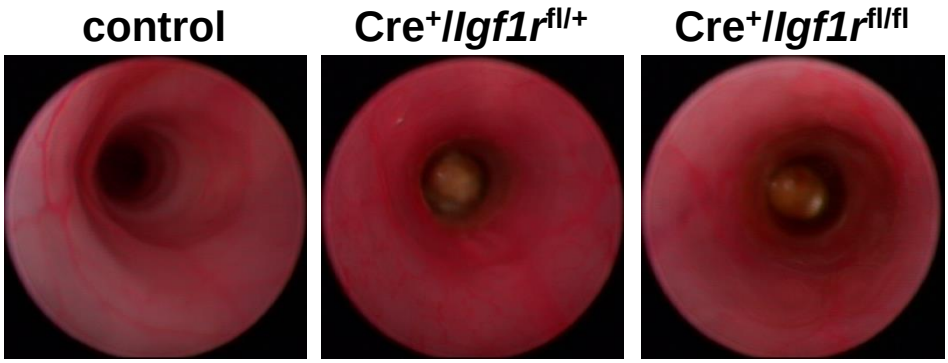

Fig. 50: Colonoscopy of Villin-CreERT-Igf1r mice 1.5 years after tamoxifen injections.
Cre^{+}/*Igf1r*$^{fl/fl}$ (n=6), Cre^{+}/*Igf1r*$^{fl/+}$ (n=5) and control mice (n=5) were injected with tamoxifen. To check for morphological changes in the colon, colonoscopy was regularly performed. After 1.5 years, the animals were sacrificed. Changes in the colonic morphology were not observed by colonoscopy.

Four weeks, three months and 1.5 years after tamoxifen injection, mice were sacrificed, the small intestine and colon were excised from the animals, fixed, paraffin-embedded and hematoxylin and eosin staining was performed. Together with Dr. med. Felix Bremmer (Institute of Pathology, University Medical Center Göttingen, Germany) the morphology of the villi and crypts was examined. Unfortunately, hematoxylin and eosin stainings after 1.5 years after tamoxifen injection were not prepared and analyzed to date. In Fig. 51 representative pictures of the hematoxylin and eosin stainings of the intestinal tissues after 4 weeks and 3 months are shown. A difference in the morphology of the villi and crypts between Cre^{+}/*Igf1r*$^{fl/fl}$, Cre^{+}/*Igf1r*$^{fl/+}$ and control mice and between the two different time points was not observed. Thus, the stainings revealed that the *Igf1r* knockout did not alter the appearance of the villi and crypts of the small intestine and colon.

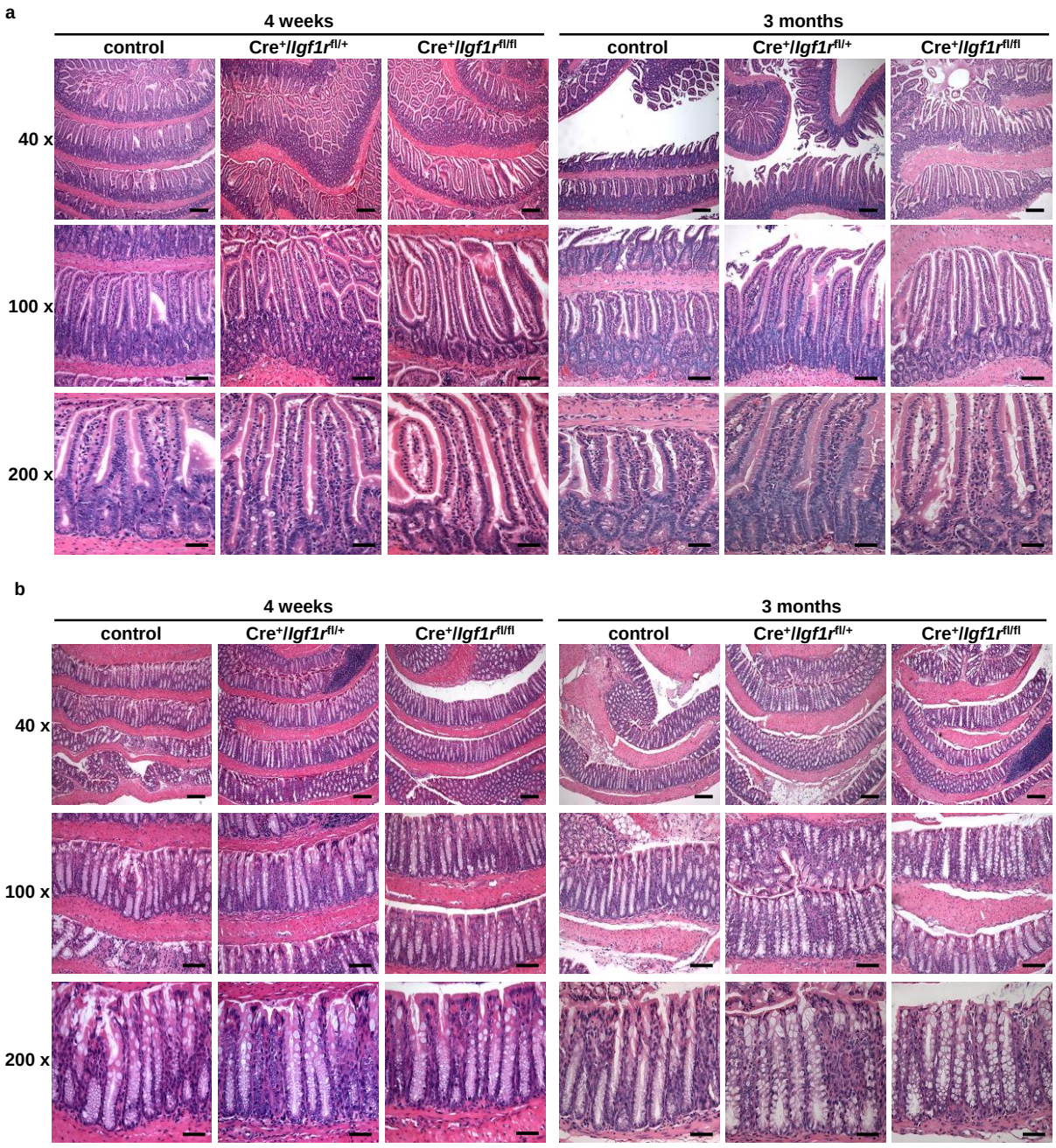

Fig. 51: Hematoxylin and eosin stainings of the small intestine and colon of Cre$^+$/*Igf1r*$^{fl/fl}$, Cre$^+$/*Igf1r*$^{fl/+}$ and control Villin-CreERT-Igf1r mice four weeks and three months after tamoxifen injection.

Cre$^+$/*Igf1r*$^{fl/fl}$ (n=5), Cre$^+$/*Igf1r*$^{fl/+}$ (n=5) and control mice (n=5) were injected with tamoxifen. After four weeks and 3 months, mice were sacrificed and hematoxylin and eosin stainings of the **(a)** small intestine and **(b)** colon were performed. Together with Dr. med. Felix Bremmer (Institute of Pathology, University Medical Center Göttingen, Germany) the morphology of the villi and crypts was examined. A difference in the morphology of the small intestine and colon between Cre$^+$/*Igf1r*$^{fl/fl}$, Cre$^+$/*Igf1r*$^{fl/+}$ and control animals was not observed.

Additionally, the mice that were sacrificed 1.5 years after the tamoxifen injections were macroscopically analyzed. Four mice (two Cre$^+$/*Igf1r*$^{fl/fl}$ mice, one Cre$^+$/*Igf1r*$^{fl/+}$ mouse and one control mouse) showed enlarged seminal vesicles. Furthermore, the length of the small intestine and colon of these mice was measured and compared between Cre$^+$/*Igf1r*$^{fl/fl}$, Cre$^+$/*Igf1r*$^{fl/+}$ and control mice. A difference in the average length of the small intestine and colon could not be observed (Fig. 52).

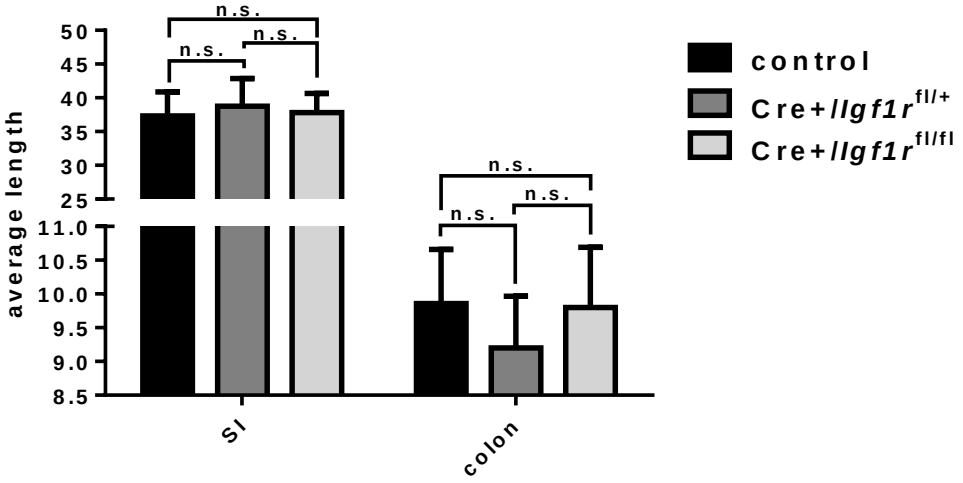

Fig. 52: The *Igf1r* knockout did not influence the average length of the small intestine (SI) and colon.

Cre$^+$/*Igf1r*$^{fl/fl}$ (n=6), Cre$^+$/*Igf1r*$^{fl/+}$ (n=5) and control mice (n=5) were injected with tamoxifen. After 1.5 years, mice were sacrificed and the small intestine and colon were excised from the animals. The comparison of the average length of the small intestine and colon, respectively, revealed no difference between Cre$^+$/*Igf1r*$^{fl/fl}$, Cre$^+$/*Igf1r*$^{fl/+}$ and control mice (student's *t* test).

3.22 Quantification of the different intestinal cell types of Villin-CreERT-Igf1r mice after four weeks, three months and 1.5 years

For the determination of the number of the different cell types in the villi and crypts of the small intestine and in the crypts of the colon, small intestinal and colonic tissue sections were stained using antibodies specific for goblet cells (mucin 2), enteroendocrine cells (Chromogranin A), Paneth cells (lysozyme) and proliferating cells (Ki 67). Therefore, Cre$^+$/*Igf1r*$^{fl/fl}$, Cre$^+$/*Igf1r*$^{fl/+}$ and control Villin-CreERT-Igf1r mice were injected with tamoxifen on five consecutive days to induce the knockout of the *Igf1r*. After four weeks, three months and 1.5 years, mice were sacrificed, intestinal tissues were fixed, paraffin-embedded and sections were stained for the different cell

types. The positive cells of 50 villi and 50 crypts per mouse of five mice per group were manually counted.

3.22.1 The *Igf1r* knockout results in a significant increase in goblet cells in the small intestine

To quantify the number of goblet cells in the small intestine and colon, tissue sections were stained for mucin 2. In the crypts of the small intestine the number of goblet cells was significantly increased in both $Cre^{+}/Igf1r^{fl/fl}$ and $Cre^{+}/Igf1r^{fl/+}$ mice after three months and 1.5 years compared to control mice (Fig. 53a). However, in the villi of the small intestine, the number of goblet cells was significantly elevated only in $Cre^{+}/Igf1r^{fl/fl}$ mice after three months and 1.5 years (Fig. 53b). In contrast, the number of goblet cells in the crypts of the colon was significantly reduced in both $Cre^{+}/Igf1r^{fl/fl}$ and $Cre^{+}/Igf1r^{fl/+}$ mice after four weeks, whereas after three months the number was significantly increased in $Cre^{+}/Igf1r^{fl/+}$ mice. After 1.5 years, the number of goblet cells was again significantly decreased in $Cre^{+}/Igf1r^{fl/+}$ mice but there was no change for $Cre^{+}/Igf1r^{fl/fl}$ mice (Fig. 53c). The number of goblet cells significantly decreased over time in the villi and crypts of the small intestine and colon of control mice.

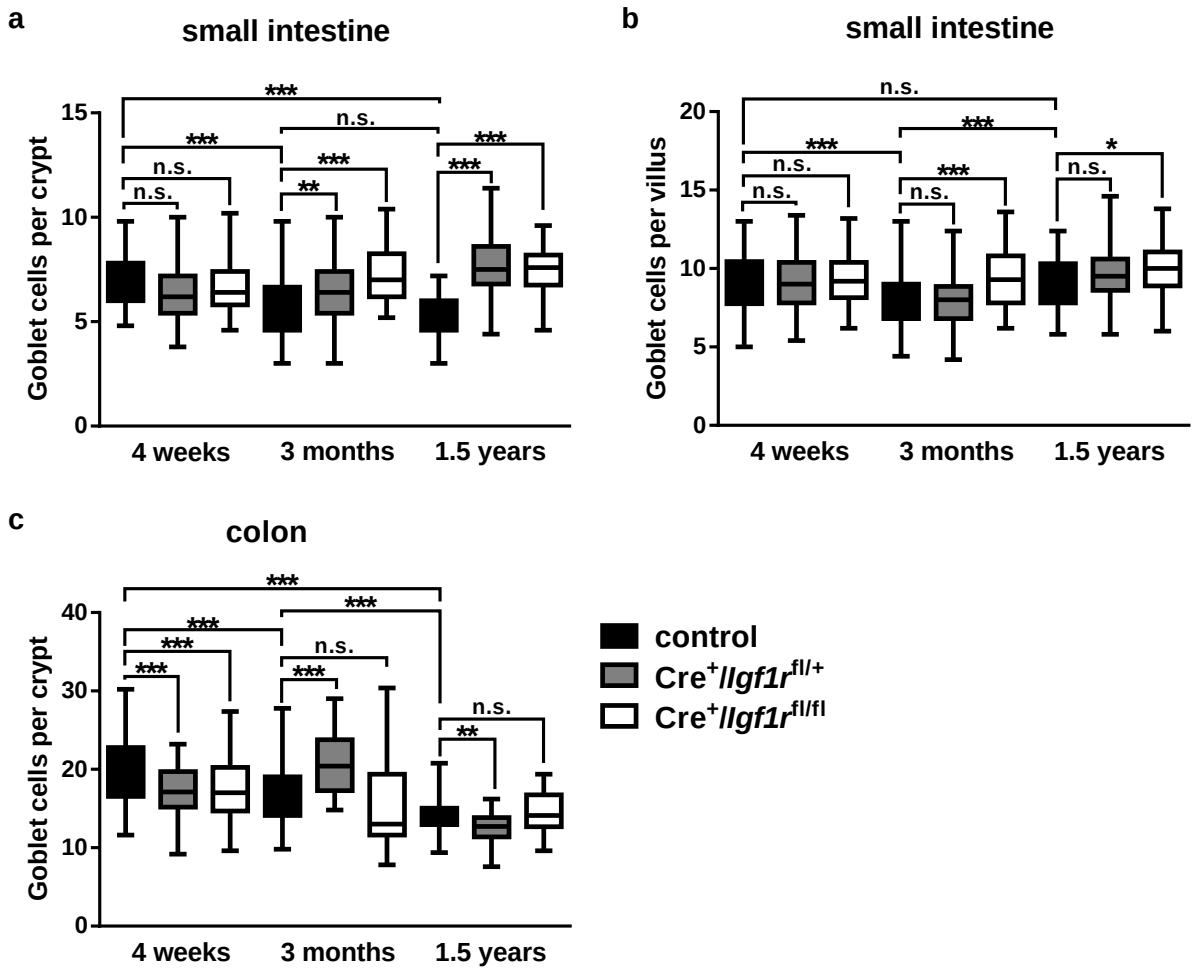

Fig. 53: The *Igf1r* knockout led to a significant increase of the goblet cell number.

For the quantification of goblet cells, Cre$^+$/*Igf1r*$^{fl/fl}$ (n=5), Cre$^+$/*Igf1r*$^{fl/+}$ (n=5) and control mice (n=5) per time point were each injected with tamoxifen. After four weeks, three months and 1.5 years the mice were sacrificed and tissue sections of the small intestine and colon were stained with mucin 2. Mucin 2-positive cells of 50 villi and 50 crypts per mouse were manually counted. **(a)** In the small intestine, the number of goblet cells per crypt significantly increased in Cre$^+$/*Igf1r*$^{fl/fl}$ and Cre$^+$/*Igf1r*$^{fl/+}$ mice after three months and 1.5 years compared to control mice. **(b)** The number of goblet cells per villus in the small intestine was significantly elevated in the Cre$^+$/*Igf1r*$^{fl/fl}$ mice compared to control mice. **(c)** In the colon, Cre$^+$/*Igf1r*$^{fl/fl}$ mice showed a significant reduction of the number of goblet cells per crypt after four weeks. * P <0.05, ** P < 0.01, *** P < 0.0001 (student's t test).

3.22.2 The *Igf1r* knockout results in a significant increase of enteroendocrine cells in the small intestine and a significant decrease in the colon

For the quantification of the number of enteroendocrine cells, small intestinal and colonic tissue sections were stained for Chromogranin A (CHGA) and positive cells were counted per villus and crypt, respectively. In the small intestine, the number of enteroendocrine cells changed not before 1.5 years between Cre$^+$/*Igf1r*$^{fl/fl}$ and

Cre+/*Igf1r*fl/+ and control mice. After 1.5 years, the number of enteroendocrine cells significantly increased in Cre+/*Igf1r*fl/fl and Cre+/*Igf1r*fl/+ mice compared to control mice (Fig. 54a). The number of CHGA-positive cells in the colon significantly decreased in Cre+/*Igf1r*fl/fl mice after four weeks and three months compared to Cre+/*Igf1r*fl/+ and control mice. After 1.5 years, a difference in the number of enteroendocrine cells was not observed (Fig. 54b). In the colon, a significant increase in the number of CHGA-positive cells over time was detected (Fig. 54b).

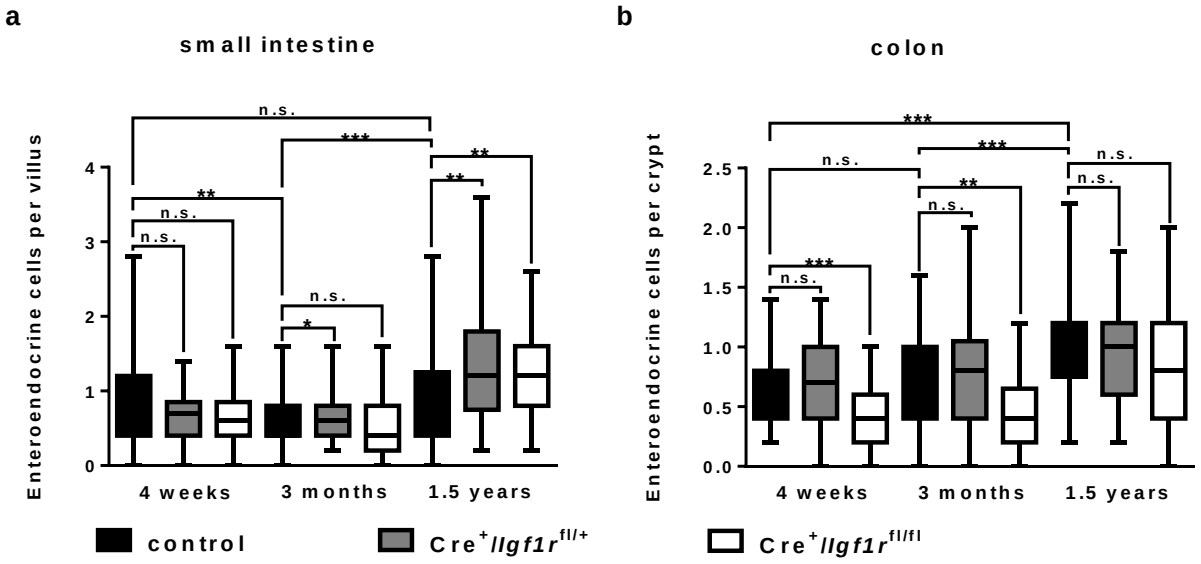

Fig. 54: The number of enteroendocrine cells increased in the small intestine, but decreased in the colon of Cre+/*Igf1r*fl/fl mice.

(a) The number of enteroendocrine cells per villus significantly increased in Cre+/*Igf1r*fl/fl (n=5) and Cre+/*Igf1r*fl/+ mice (n=5) after 1.5 years compared to control mice (n=5). **(b)** In the colon, the number of enteroendocrine cells per crypt significantly decreased in Cre+/*Igf1r*fl/fl mice after four weeks and three months. * P <0.05, ** P < 0.01, *** P < 0.0001 (student's *t* test).

3.22.3 The *Igf1r* knockout results in a significant reduction of Paneth cells in the small intestine

The number of Paneth cells was quantified by staining sections of the small intestine for lysozyme. After three months, the number of Paneth cells decreased significantly in Cre+/*Igf1r*fl/fl and Cre+/*Igf1r*fl/+ mice compared to control mice. After 1.5 years, a significant reduction of Paneth cells was observed in Cre+/*Igf1r*fl/fl mice. A significant increase of Paneth cells over time was detected in control mice (Fig. 55).

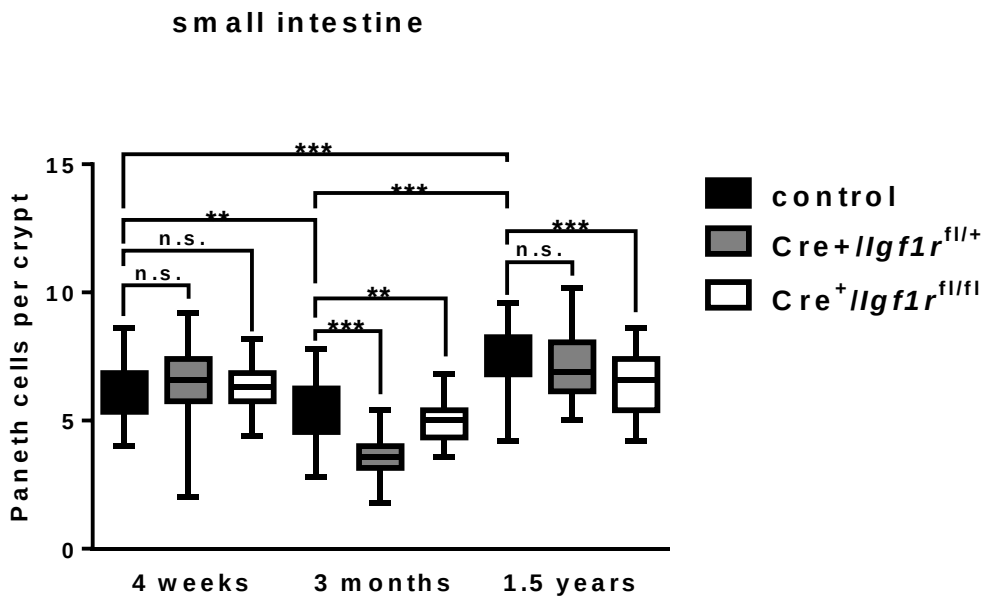

Fig. 55: The *Igf1r* knockout resulted in a significant reduction of Paneth cells in the small intestine.

The number of Paneth cells significantly decreased in the crypts of the small intestine of Cre^{+}/*Igf1r*$^{fl/fl}$ (n=5) and Cre^{+}/*Igf1r*$^{fl/+}$ mice (n=5) after three months and 1.5 years compared to control mice (n=5). * P <0.05, ** P < 0.01, *** P < 0.0001 (student's *t* test).

3.22.4 The effect of the *Igf1r* knockout regarding the number of proliferating cells per crypt is time-dependent

For the quantification of proliferating cells, tissue sections of the small intestine and colon were stained for Ki 67 and positive cells per crypt were counted. The number of proliferating cells per crypt in the small intestine significantly decreased after four weeks, but increased after three months and 1.5 years in Cre^{+}/*Igf1r*$^{fl/fl}$ mice compared to control mice. Altogether, the number of Ki 67-positve cells per crypt in the small intestine significantly decreased over time in Cre^{+}/*Igf1r*$^{fl/fl}$, Cre^{+}/*Igf1r*$^{fl/+}$ and control mice (Fig. 56a). In the colon, the number of proliferating cells per crypt significantly decreased after four weeks, but increased after three months and 1.5 years in Cre^{+}/*Igf1r*$^{fl/fl}$ mice compared to control mice. Altogether, the number of proliferating cells significantly decreased over time in Cre^{+}/*Igf1r*$^{fl/fl}$, Cre^{+}/*Igf1r*$^{fl/+}$ and control mice (Fig. 56b).

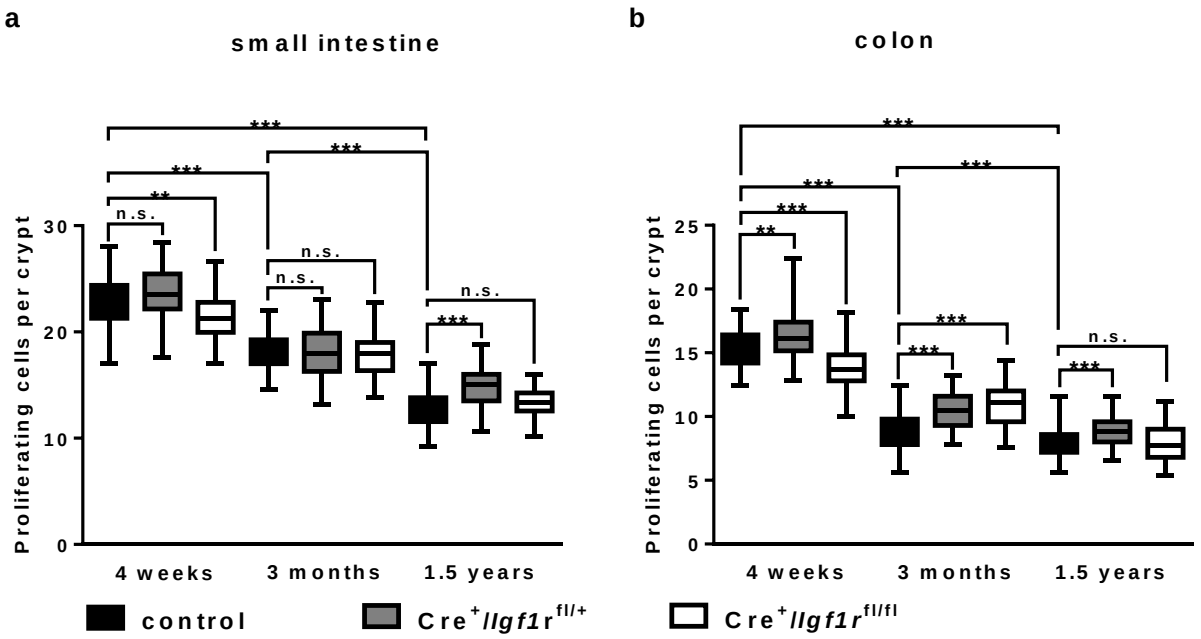

Fig. 56: The number of proliferating cells per crypt differed over time.

To quantify the number of proliferating cells, small intestinal and colonic tissue sections were stained for Ki 67 and positive cells of 50 crypts per mouse were counted. **(a, b)** In the crypts of the small intestine and colon, the number of proliferating cells significantly decreased over time in Cre^{+}/*Igf1r*$^{fl/fl}$ (n=5), Cre^{+}/*Igf1r*$^{fl/+}$ (n=5) and control mice (n=5). **(b)** In the colon, Cre^{+}/*Igf1r*$^{fl/fl}$ mice showed a significant reduction of Ki 67-positive cells after four weeks, whereas after three months the number of proliferating cells significantly increased. ** $P < 0.01$, *** $P < 0.0001$ (student's *t* test).

3.22.5 The knockout of the *Igf1r* does not influence the presence of enterocytes

To analyze if the *Igf1r* has any influence on the presence of enterocytes in the intestinal epithelium of Cre^{+}/*Igf1r*$^{fl/fl}$, Cre^{+}/*Igf1r*$^{fl/+}$ and control Villin-CreERT-Igf1r mice, alkaline phosphatase stainings (AP-staining) to detect enterocytes were performed on tissue sections of the small intestine and colon. In Fig. 57 representative pictures of the AP-stainings are shown. A difference in the presence of enterocytes between Cre^{+}/*Igf1r*$^{fl/fl}$, Cre^{+}/*Igf1r*$^{fl/+}$ and control mice was not observed.

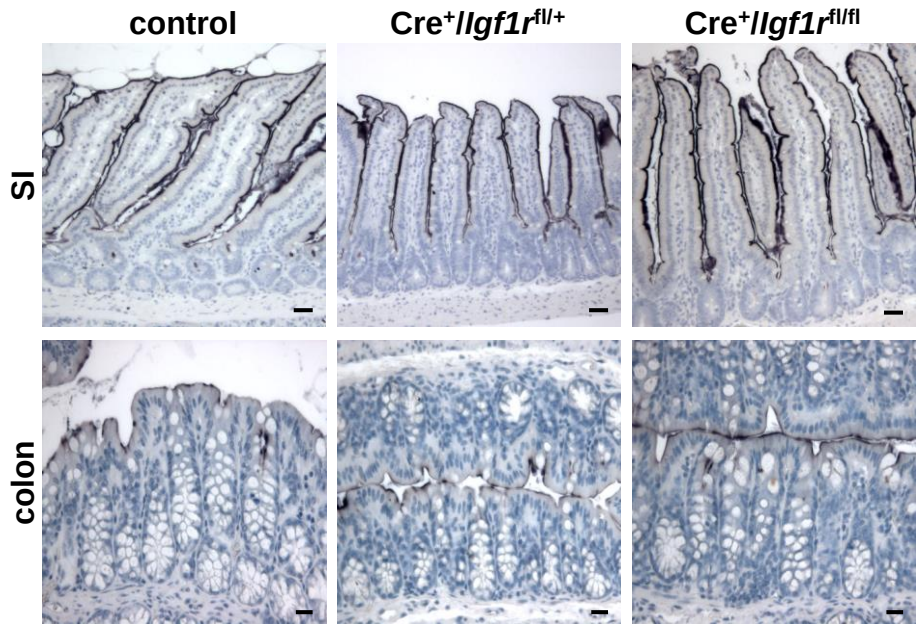

Fig. 57: The presence of enterocytes in the epithelium of the small intestine and colon of Villin-CreERT-Igf1r mice.

To detect enterocytes, alkaline phosphatase stainings on tissue sections of the small intestine and colon of Cre$^+$/*Igf1r*$^{fl/fl}$ (n=5), Cre$^+$/*Igf1r*$^{fl/+}$ (n=5) and control mice (n=5) were performed. Enterocytes were stained brown, cell nuclei were stained with hemalum solution (blue). A difference in the presence of enterocytes between Cre$^+$/*Igf1r*$^{fl/fl}$, Cre$^+$/*Igf1r*$^{fl/+}$ and control mice was not observed.

3.23 The *Igf1r* knockout inhibits intestinal tumor formation and progression (AOM model)

To analyze the effect of the *Igf1r* knockout on tumor formation and progression, Cre$^+$/*Igf1r*$^{fl/fl}$, Cre$^+$/*Igf1r*$^{fl/+}$ and control Villin-CreERT-Igf1r mice were injected with tamoxifen on five consecutive days. In addition, the mice were intraperitoneally injected with four weekly repeated injections of 10 mg / ml AOM to induce colonic tumor formation (Fig. 58). To screen for the development of tumors, colonoscopy was regularly performed (Fig. 59). Importantly, this experiment was merely a preliminary study. For this reason, the experiment was performed only with a small number of mice.

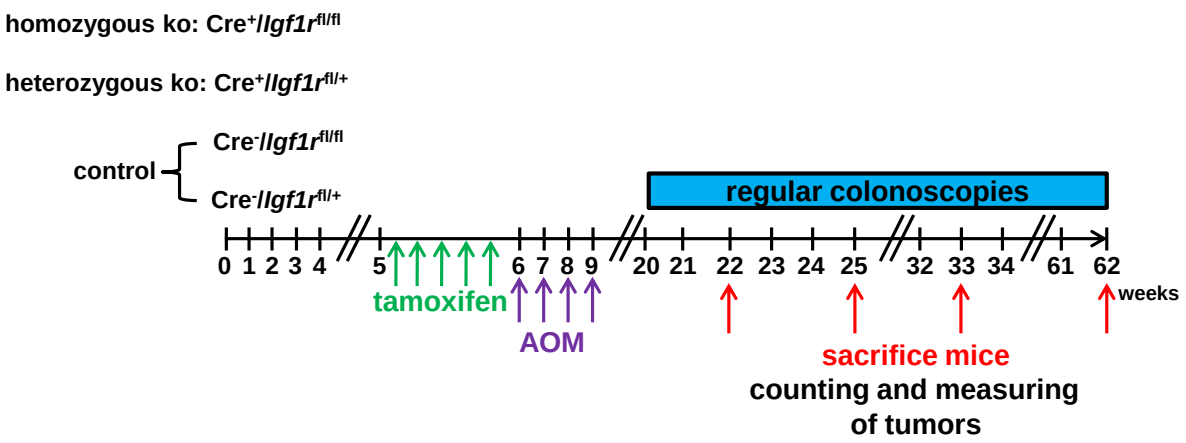

Fig. 58: Treatment scheme for the analysis if the *Igf1r* has any influence on colonic tumor progression (AOM model).

Cre+/*Igf1r*fl/fl (n=3), Cre+/*Igf1r*fl/+ (n=4) and control (n=4) Villin-CreERT-Igf1r mice were injected with tamoxifen to induce the knockout of the *Igf1r* in the intestine. In addition, the mice were injected four times with azoxymethane (AOM) to induce colonic tumor formation. To check if tumors had developed, colonoscopy was regularly performed. Between the period of 22 and 62 weeks after the first AOM injection, mice were sacrificed and the tumors were counted and measured.

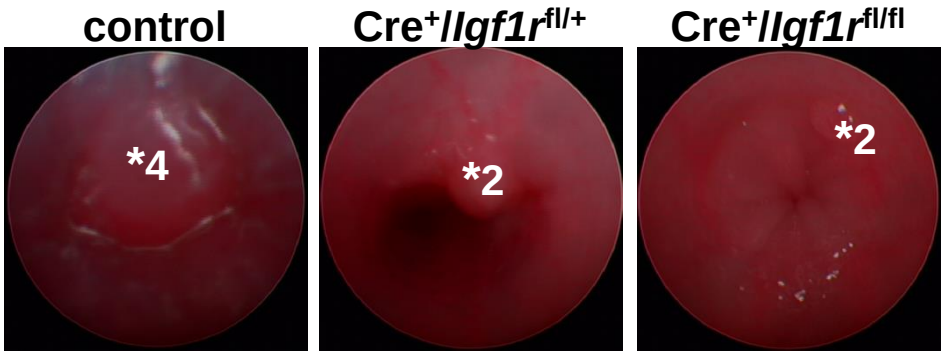

Fig. 59: Colonoscopy of Villin-CreERT-Igf1r mice after AOM injection.

To induce the *Igf1r* knockout, Cre+/*Igf1r*fl/fl (n=3), Cre+/*Igf1r*fl/+ (n=4) and control (n=4) Villin-CreERT-Igf1r mice were injected with tamoxifen. For the induction of tumor formation, the mice were afterwards injected with AOM. Regular colonoscopies were performed to check for intestinal tumor formation. Cre+/*Igf1r*fl/fl, Cre+/*Igf1r*fl/+ and control mice revealed colonic tumor formation. Stars mark the tumors. The numbers indicate the score of the tumor (after Becker *et al.* 2007).

When the mice had developed tumors, they were sacrificed, the small intestinal and colonic tissues were excised from the mice and the tumors were macroscopically analyzed. Interestingly, tumor progression differed strongly between the mice. Therefore, the mice were sacrificed as soon as the tumors reached the maximum

allowed tumor size (score 5). For this reason, a survival curve of the different mouse groups could be determined. Fifty percent of the control mice had to be sacrificed after approx. 20 weeks, whereas the other 50% were sacrificed after 62 weeks. Fifty percent of Cre^{+}/*Igf1r*$^{fl/+}$ mice had to be sacrificed between week 22 and 25, whereas the other 50% of the Cre^{+}/*Igf1r*$^{fl/+}$ mice were sacrificed after 62 weeks. One Cre^{+}/*Igf1r*$^{fl/fl}$ mouse was sacrificed in week 22, the second mouse was sacrificed in week 33 and the third Cre^{+}/*Igf1r*$^{fl/fl}$ mouse was sacrificed in week 62. All mice sacrificed in week 62 showed no tumor formation. These data led to the assumption that the *Igf1r* did not influence the time point of colonic tumor formation (Fig. 60a). Regarding the number of mice with and without tumors, respectively, 50% of control mice formed tumors. Only one out of four (25%) Cre^{+}/*Igf1r*$^{fl/+}$ mice developed any tumors, while two out of three (66.7%) Cre^{+}/*Igf1r*$^{fl/fl}$ mice showed tumor formation (Fig. 60b). Discrimination between the sexes showed that 50% of female as well as 50% of male control mice revealed tumor development (Fig. 60c). In Cre^{+}/*Igf1r*$^{fl/+}$ mice, 50% of the female and no male mouse formed any tumors (Fig. 60d). The one female mouse (100%) and 50% of the male Cre^{+}/*Igf1r*$^{fl/fl}$ mice showed tumor formation (Fig. 60e). The results indicated that both sexes were similarly sensitive to AOM. For further analyses only those mice which had developed tumors were included. Control mice developed on average 1.5 tumors, the Cre^{+}/*Igf1r*$^{fl/+}$ mouse formed one tumor and Cre^{+}/*Igf1r*$^{fl/fl}$ mice developed on average one tumor (Fig. 60f). Regarding tumor localization, control mice developed 3-fold more tumors than Cre^{+}/*Igf1r*$^{fl/fl}$ mice and 2-fold more tumors than Cre^{+}/*Igf1r*$^{fl/+}$ mice in the distal part of the colon. However, only Cre^{+}/*Igf1r*$^{fl/fl}$ mice formed tumors in the middle part of the colon (Fig. 60g). Analyzing both the tumor size and tumor number demonstrated that Cre^{+}/*Igf1r*$^{fl/fl}$ mice developed only half the number of tumors smaller than 2 mm in diameter than control mice. The number of tumors bigger than 2 mm was identical between Cre^{+}/*Igf1r*$^{fl/fl}$ and control mice. Cre^{+}/*Igf1r*$^{fl/+}$ mice revealed the same number of tumors smaller than 2 mm compared to control mice, but displayed no development of tumors bigger than 2 mm (Fig. 60h).

Taken together, these results indicated that the *Igf1r* knockout in the intestine led to decreased tumor formation (< 2 mm) in the distal part of the colon after AOM administration. However, because only a small number of mice was used for the experiments described above, the data is still preliminary and has to be verified in future experiments with an increased number of mice.

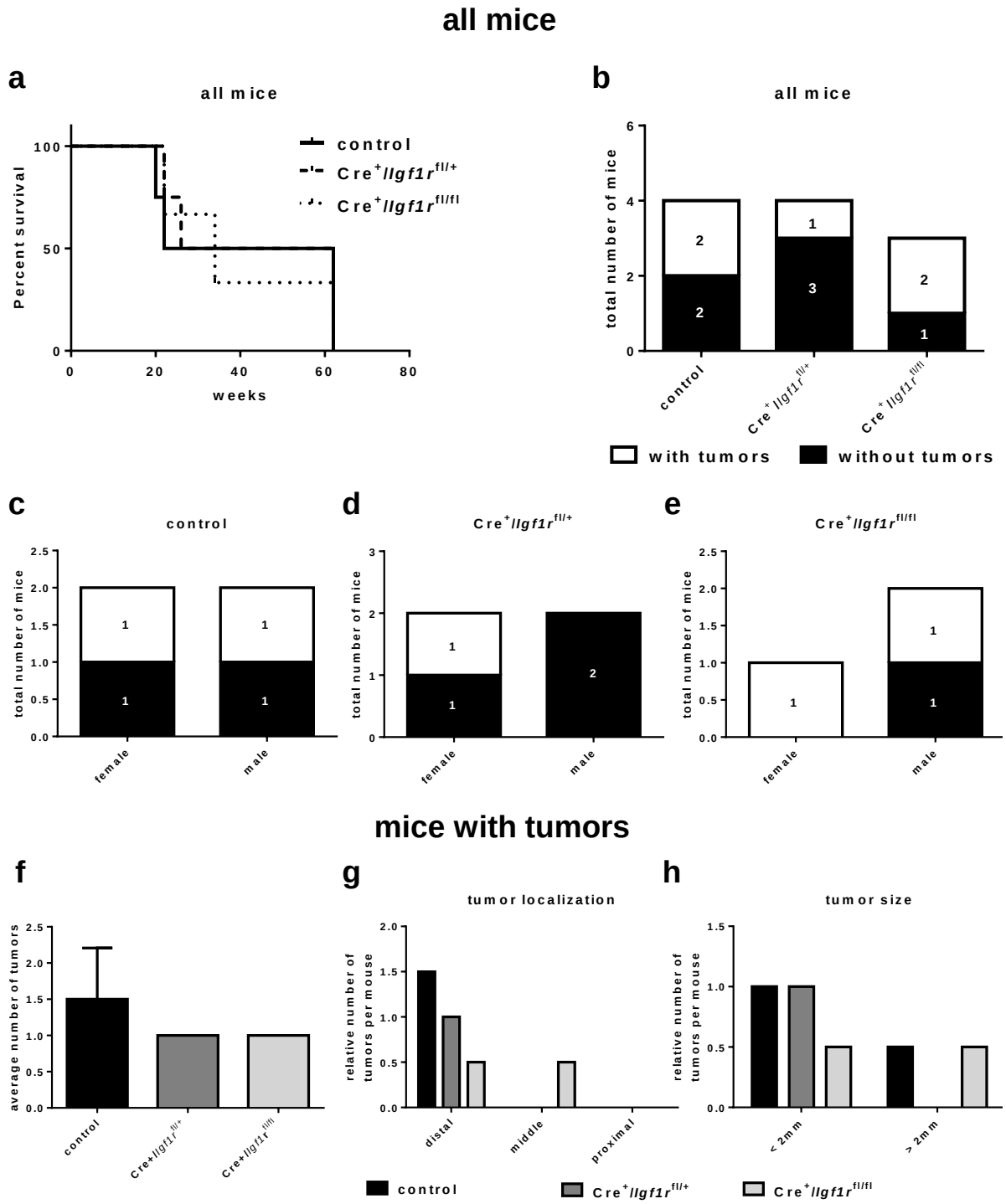

Fig. 60: Macroscopic analyses of intestinal tumors induced in Villin-CreERT-Igf1r mice by AOM injection.

(a) Survival curve of Cre$^+$/*Igf1r*$^{fl/fl}$ (n=3), Cre$^+$/*Igf1r*$^{fl/+}$ (n=4) and control mice (n=4) after induction of tumor formation by AOM. Tumor progression differed strongly between the mice. For this reason, the mice were sacrificed gradually. **(b)** Fifty percent of control mice, 25% of Cre$^+$/*Igf1r*$^{fl/+}$ mice and 50% of Cre$^+$/*Igf1r*$^{fl/fl}$ mice formed tumors in the colon. **(c)** Fifty percent of female and 50% of male control mice formed tumors. **(d)** Fifty percent of female and no male Cre$^+$/*Igf1r*$^{fl/+}$ mouse showed intestinal tumor formation. **(e)** The one female mouse and 50% of male Cre$^+$/*Igf1r*$^{fl/fl}$ mice developed tumors. **(f)** Control mice (n=2) developed on average 1.5 tumors, the Cre$^+$/*Igf1r*$^{fl/+}$ mouse (n=1) formed 1 tumor and Cre$^+$/*Igf1r*$^{fl/fl}$ mice (n=2) developed on average 1 tumor. **(g)** Control mice developed 3-fold more tumors

than Cre+/*Igf1r*fl/fl mice and 2-fold more tumors than Cre+/*Igf1r*fl/+ mice in the distal part of the colon. Only Cre+/*Igf1r*fl/fl mice formed tumors in the middle part of the colon. **(h)** Cre+/*Igf1r*fl/fl mice developed half the number of tumors smaller than 2 mm than control mice. The number of tumors bigger than 2 mm was identical between Cre+/*Igf1r*fl/fl and control mice. Cre+/*Igf1r*fl/+ mice revealed the same number of tumors smaller than 2 mm compared to control mice, but showed no development of tumors bigger than 2 mm.

3.24 The *Igf1r* knockout does not influence intestinal tumor formation but inhibits tumor progression (AOM / DSS model)

In order to analyze if the knockout of the *Igf1r* in the intestine influences tumor formation and progression, Cre+/*Igf1r*fl/fl and control Villin-CreERT-Igf1r mice were injected with tamoxifen and treated with AOM / DSS to induce colonic tumor formation and inflammation. Importantly, Cre+/*Igf1r*fl/+ mice were not involved in the following experiment.

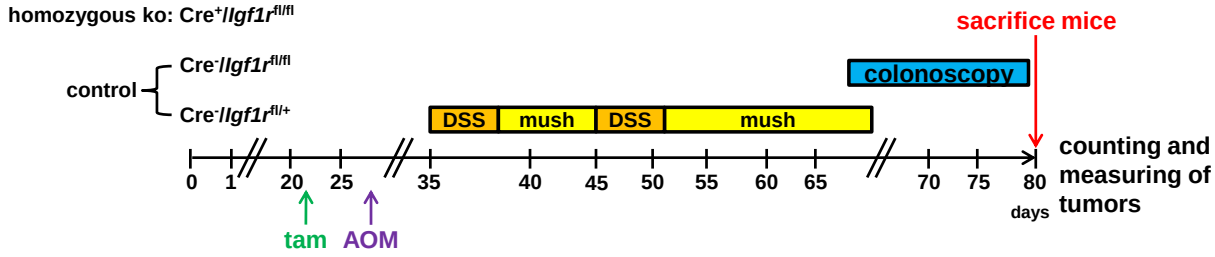

Fig. 61: Treatment scheme for the analysis if the *Igf1r* knockout in the intestine has any influence on colonic tumor progression (AOM / DSS model).

Cre+/*Igf1r*fl/fl (n=11) and control (n=13) Villin-CreERT-Igf1r mice were injected with tamoxifen (tam). Furthermore, mice were once injected with AOM to induce colonic tumor formation and administered to two cycles of 2% DSS over the drinking water to induce intestinal inflammation. Cereal mush was given between and after DSS treatment to avoid dehydration of the mice. To screen for tumor development, colonoscopy was performed regularly. Mice were sacrificed and the formed tumors were counted and measured.

Regular colonoscopies were performed to check for tumor formation in the colon of the Cre^{+}/*Igf1r*$^{fl/fl}$ and control mice (Fig. 62).

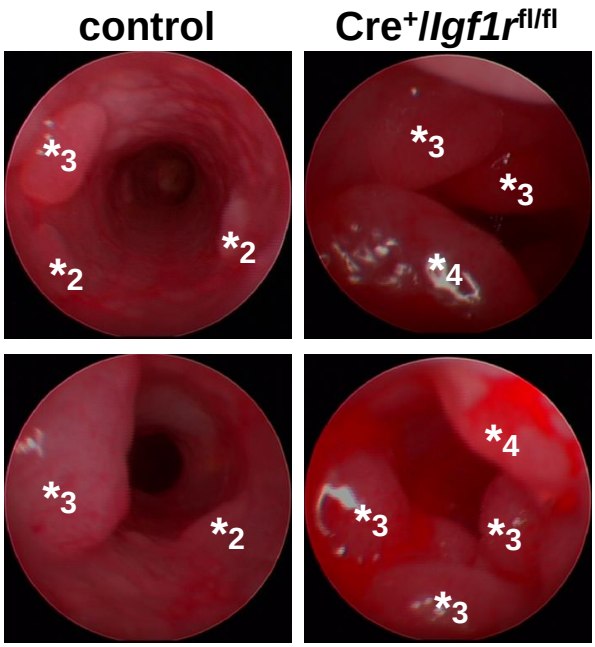

Fig. 62: Colonoscopy of Cre^{+}/*Igf1r*$^{fl/fl}$ and control Villin-CreERT-Igf1r mice administered to AOM / DSS.

Cre^{+}/*Igf1r*$^{fl/fl}$ (n=11) and control (n=13) Villin-CreERT-Igf1r mice were injected with tamoxifen. Afterwards, mice were administered to AOM / DSS to induce colonic tumor formation and inflammation. To examine if tumors have developed in the colon of the mice, colonoscopy was performed regularly. Cre^{+}/*Igf1r*$^{fl/fl}$ and control mice showed colonic tumor formation after AOM / DSS treatment. Stars mark the tumors. The numbers indicate the score of the tumor (after Becker *et al.* 2007).

Seven weeks after the AOM injection, some tumors had reached the maximum size (score 4 to 5) and the mice were sacrificed. Intestinal tissue was excised from the animals, the colon length of the mice that have developed tumors was measured and the tumors were macroscopically and histopathologically analyzed. The average colon length of Cre^{+}/*Igf1r*$^{fl/fl}$ and control mice revealed no significant difference (Fig. 63).

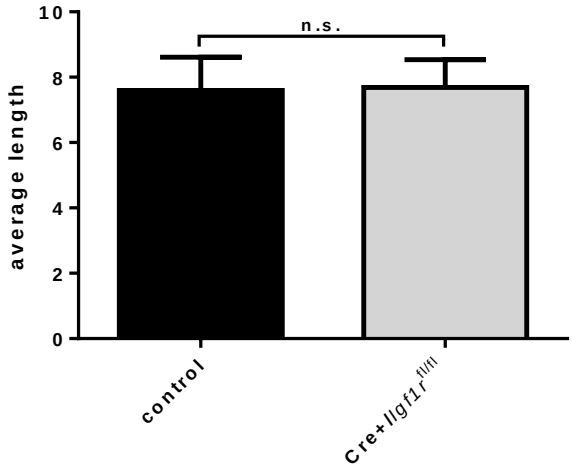

Fig. 63: Average colon length of Cre$^+$/*Igf1r*$^{fl/fl}$ and control Villin-CreERT-Igf1r mice after development of tumors induced by AOM / DSS.

Cre$^+$/*Igf1r*$^{fl/fl}$ (n=11) and control mice (n=13) were injected with tamoxifen and additionally administered to AOM / DSS to induce colonic tumor formation and inflammation. Mice were sacrificed and the colon was excised from the animals and measured. The comparison of the average length of the colon between Cre$^+$/*Igf1r*$^{fl/fl}$ and control mice showed no significant difference (student's *t* test).

Macroscopic analyses revealed tumor formation in twelve out of 13 (92.3%) control mice and in nine out of eleven (81.8%) Cre$^+$/*Igf1r*$^{fl/fl}$ mice (Fig. 64a). Distinguishing between the sexes, all eight (100%) female control and four out of five (80%) male control mice developed intestinal tumors (Fig. 64b). Furthermore, tumors were observed in all five (100%) female and in four out of six (66.7%) male Cre$^+$/*Igf1r*$^{fl/fl}$ mice (Fig. 64c), leading to the assumption that female mice could be more sensitive to AOM / DSS administration. Regarding the average tumor number, the tumor localization and tumor size, only mice which had developed colonic tumors were included. Here, control mice developed on average 5.25 tumors, whereas Cre$^+$/*Igf1r*$^{fl/fl}$ mice formed on average 6 tumors (Fig. 64f). Cre$^+$/*Igf1r*$^{fl/fl}$ mice showed a higher number of distal tumors per mouse, but a decreased number of tumors in the middle and proximal part of the colon compared to control mice (Fig. 64e). Regarding the size of the tumors analyzed, Cre$^+$/*Igf1r*$^{fl/fl}$ mice developed a higher number of tumors smaller than 2 mm as well as bigger than 2 mm compared to control mice (Fig. 64f). In summary, a difference in the number of developed tumors induced by AOM / DSS between Cre$^+$/*Igf1r*$^{fl/fl}$ and control mice could not be observed, indicating that the *Igf1r* knockout in the intestine had no influence on intestinal tumor formation using the AOM / DSS model.

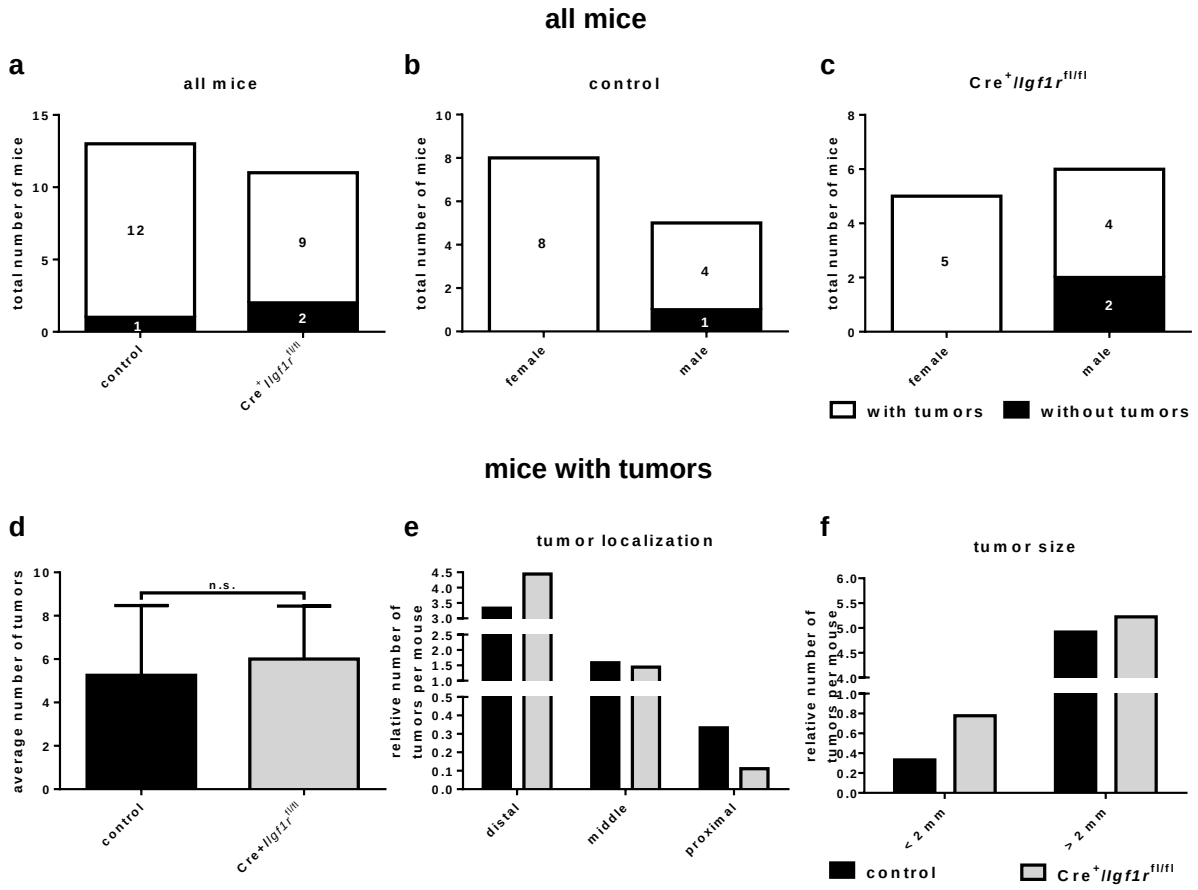

Fig. 64: Macroscopic analyses of Villin-CreERT-Igf1r mice administered to AOM / DSS to induce colonic tumor formation and inflammation.

To analyze the influence of the *Igf1r* on colonic tumor formation and progression, Cre^{+}/*Igf1r*$^{fl/fl}$ (n=11) and control (n=13) Villin-CreERT-Igf1r mice were injected with tamoxifen to induce the *Igf1r* knockout and were administered to AOM / DSS to induce colonic tumor formation and inflammation. To check for tumor formation in the colon of the mice, colonoscopy was performed regularly. Seven weeks after AOM injection, mice were sacrificed and the small intestine and colon were excised from the animals. The developed tumors were counted and measured. **(a)** Ninety-two percent of control mice developed colonic tumors, whereas only 82% of Cre^{+}/*Igf1r*$^{fl/fl}$ mice showed tumor formation. **(b)** Discrimination between the sexes showed that 100% of the female and 80% of the male control mice formed colonic tumors. **(c)** In Cre^{+}/*Igf1r*$^{fl/fl}$ mice, 100% of female and approx. 67% of male mice formed tumors in the colon. **(d)** Cre^{+}/*Igf1r*$^{fl/fl}$ mice (n=9) formed on average 6.25 tumors, whereas control mice (n=12) formed on average 5.25 tumors. **(e)** Cre^{+}/*Igf1r*$^{fl/fl}$ mice displayed an increased number of distal tumors, but a decreased number of tumors in the middle and proximal part of the colon compared to control mice. **(f)** The Cre^{+}/*Igf1r*$^{fl/fl}$ mice formed a higher number of tumors smaller than 2 mm as well as bigger than 2 mm compared to control mice.

For histopathological analyses, colonic tissues were fixed, paraffin-embedded and cut stepwise. For this purpose, the first section was taken whereas the following ten sections were discarded. This process was repeated until three tissue sections were

available. This process was done to increase the probability to detect as many tumors as possible along the axis from distal to proximal for histopathological analyses. Hematoxylin and eosin stainings were prepared and analyzed together with Dr. med. Felix Bremmer (Institute of Pathology, University Medical Center Göttingen, Germany). The developed tumors were classified in low and high grade intraepithelial neoplasia, and intramucosal and invasive carcinoma, respectively. Representative pictures of the different tumor stages were already shown in Fig. 34a (chapter 3.11). Histopathologically, the developed tumors of Villin-CreERT-Igf1r mice induced by AOM / DSS were comparable to those of Villin-TRE-IGF1R mice (*IGF1R* overexpression). As depicted in Fig. 65a, Cre$^+$/*Igf1r*$^{fl/fl}$ mice showed a decreased number of low grade intraepithelial neoplasias, an increased number of high grade intraepithelial neoplasias, whereas the number of intramucosal carcinomas was reduced compared to control mice. Neither Cre$^+$/*Igf1r*$^{fl/fl}$ nor control mice formed invasive carcinomas. In addition, the average tumor size per mouse was examined. Cre$^+$/*Igf1r*$^{fl/fl}$ mice developed tumors with an average size of 1555.94 µm^2 per mouse, while control mice revealed a 30.1% reduced average tumor size (1087.57 µm^2) (Fig. 65b).

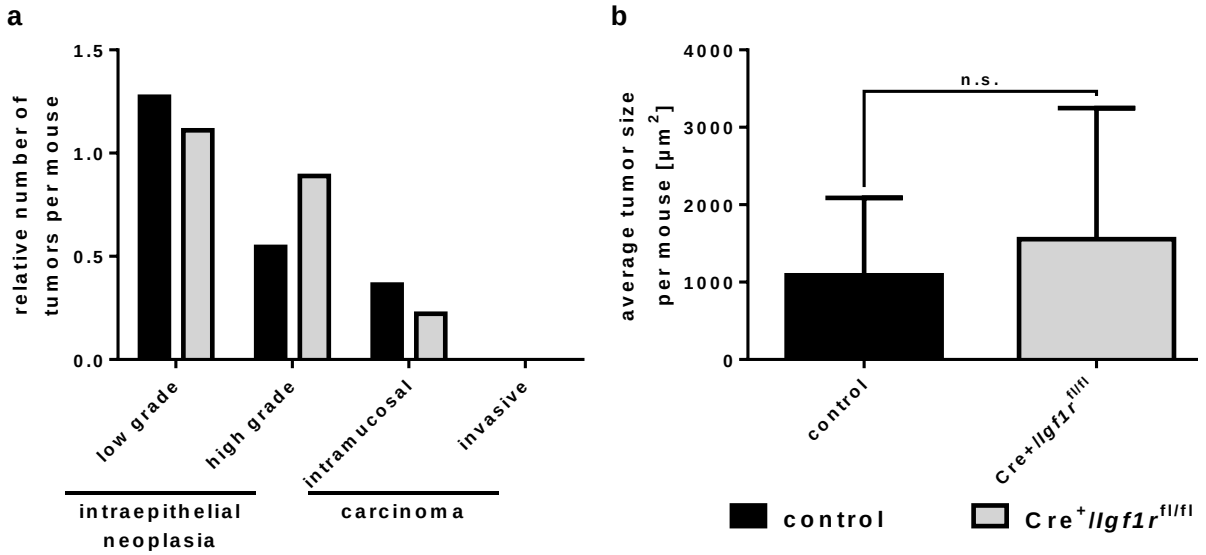

Fig. 65: Histopathological analyses of AOM / DSS-induced tumors of Cre$^+$/*Igf1r*$^{fl/fl}$ and control Villin-CreERT-Igf1r mice.

(a) Cre$^+$/*Igf1r*$^{fl/fl}$ mice (n=9) developed a decreased number of low grade intraepithelial neoplasias and intramucosal carcinomas but a higher number of high grade intraepithelial neoplasias than control mice (n=12). Neither Cre$^+$/*Igf1r*$^{fl/fl}$ mice nor control mice developed invasive carcinomas. **(b)** No significant difference in the average tumor size per mouse between Cre$^+$/*Igf1r*$^{fl/fl}$ and control mice was observed (student's *t* test).

3.25 The knockout of the *Igf1r* results in diminished downstream PI3K signaling in colonic tumors

To examine the influence of the *Igf1r* knockout on the downstream PI3K and MAPK signaling pathways, $Cre^{+}/Igf1r^{fl/fl}$, $Cre^{+}/Igf1r^{fl/+}$ and control mice were injected with tamoxifen, respectively. Additionally, the mice were administered to AOM / DSS to induce colonic tumor formation and inflammation. After tumors had developed, mice were sacrificed, tumors were excised from the colon, proteins of the tumors were extracted and western blot (Fig. 66a) and subsequent densitometrical analyses (Fig. 66b- e) were performed. IGF1Rα and IGF1Rβ expression was shown to be approx. 75% decreased in tumors of $Cre^{+}/Igf1r^{fl/fl}$ mice compared to control mice, demonstrating that *Igf1r* expression was also reduced in the developed tumors of *Igf1r* knockout mice (Fig. 66a- c). The activity of AKT (pAKT) was more than 2-fold reduced in tumors of $Cre^{+}/Igf1r^{fl/fl}$ mice compared to control mice. This result indicated that the downstream PI3K signaling pathway was diminished in tumors that developed in $Cre^{+}/Igf1r^{fl/fl}$ mice (Fig. 66a, d). Interestingly, the phosphorylation level of ERK (pERK) was highly elevated in tumors of $Cre^{+}/Igf1r^{fl/fl}$ mice compared to control mice. This data showed that the knockout of *Igf1r* did not reduce the activation of the downstream MAPK signaling pathway (Fig. 66a, e).

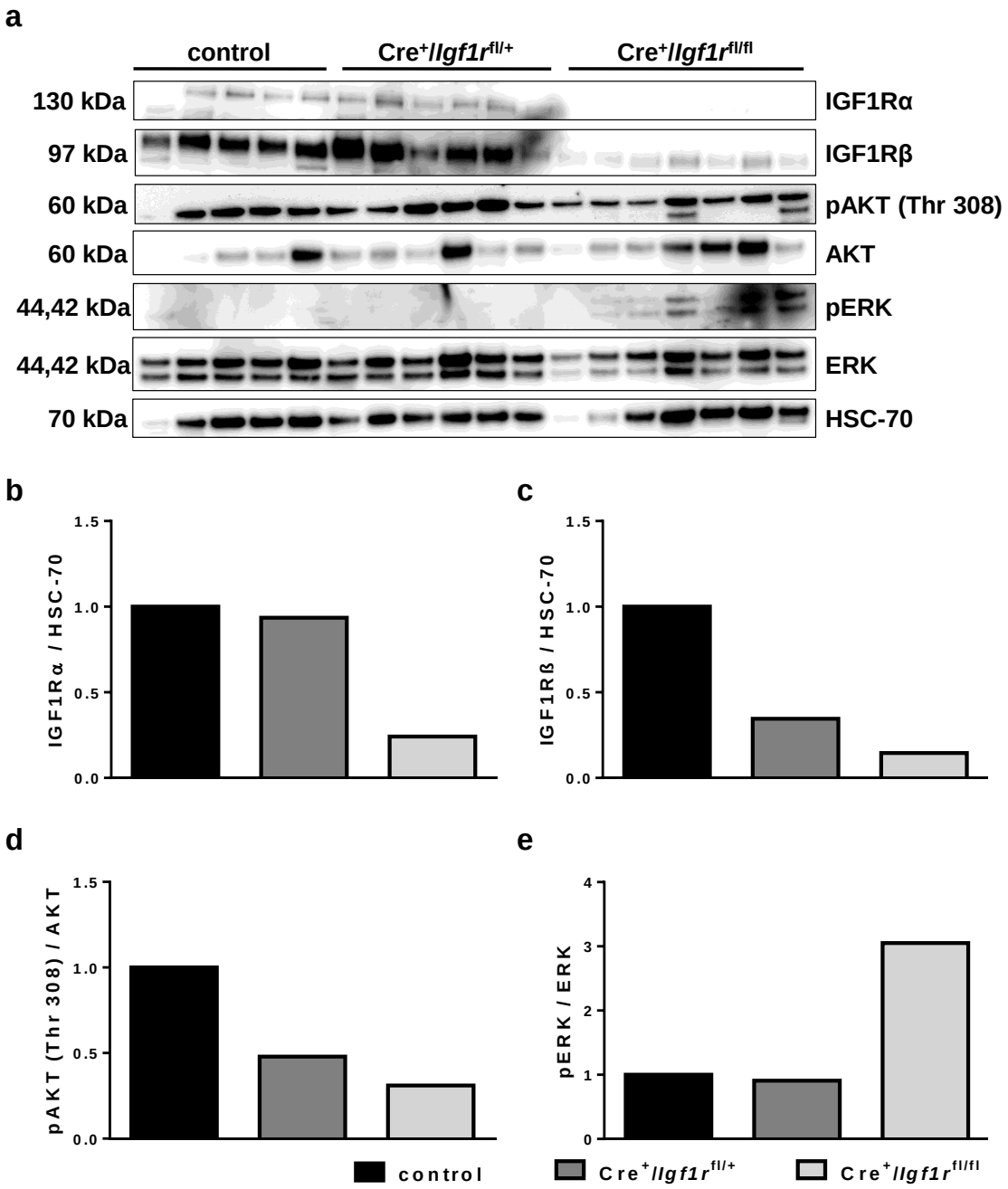

Fig. 66: Western blot and subsequent densitometrical analyses of colonic tumors of Villin-CreERT-Igf1r mice induced by AOM / DSS.

Cre^{+}/*Igf1r*$^{fl/fl}$ (n=1), Cre^{+}/*Igf1r*$^{fl/+}$ (n=5) and control (n=7) Villin-CreERT-Igf1r mice were injected with tamoxifen and additionally administered to AOM / DSS to induce colonic tumor formation and inflammation. After intestinal tumors had developed, mice were sacrificed and proteins of the tumors were extracted. **(a)** Western blot and **(b- e)** subsequent densitometrical analyses were performed. **(a- c)** The expression level of IGF1Rα and IGF1Rβ highly decreased in Cre^{+}/*Igf1r*$^{fl/fl}$ mice compared to control mice. **(a, d)** The activity of AKT (pAKT) was highly reduced in Cre^{+}/*Igf1r*$^{fl/fl}$ mice compared to control mice. **(a, e)** The phosphorylation level of ERK (pERK) was 3-fold higher in Cre^{+}/*Igf1r*$^{fl/fl}$ mice compared to control mice.

3.26 Growth inhibitory effects through simultaneous inhibition of IGF1R and EGFR in addition to combined 5-FU-based RCT *in vivo*

Recent experiments have shown that simultaneous inhibition of the IGF1R and EGFR in addition to combined RCT based on 5-fluoruracil (5-FU) results in a significant reduction of CRC cell survival *in vitro* (Seemann 2013). To investigate if similar growth inhibitory effects also occur *in vivo*, xenograft tumors of either DLD-1, CaCo-2 or SW837 cells were simultaneously treated with the small molecule kinase inhibitors AEW541 and erlotinib in addition to combined RCT.

Therefore, 7.5 x 10^5 DLD-1, 2 x 10^6 CaCo-2 or 2 x 10^6 SW837 cells were subcutaneously injected into each flank of immune-deficient 6 to 8 weeks old female nude mice (RjOrl:NMRI-*Foxn1^{nu}/Foxn1^{nu},* see chapter 2.9.2.1), respectively, depending on the proliferation rate of the cells. When the tumors have reached a volume of approx. 300 mm^3, mice were randomized into either a treatment group of AEW541 (40 mg / kg; dissolved in 25 mM L(+)-Tartaric acid (Sigma-Aldrich, Deisenhofen, Germany)), erlotinib (100 mg / kg; dissolved in 0.2% (w / v) Carboxymethylcellulose with 0.1% Tween 80), the combination of AEW541 and erlotinib or a control group. The mice were treated with combined 5-FU-based RCT (50 mg / kg, dissolved in DPBS followed by 1.8 Gy irradiation per day) in addition to inhibitor treatment. The mice in the control group received combined RCT like the treatment groups in combination with the same amount of the solvent. Importantly, the treatment scheme depended on the growth rate of the tumors. DLD-1 xenograft mice were treated with combined RCT on five consecutive days. In addition, inhibitors were administered on eight consecutive days (Fig. 67a). Unfortunately, the mice did not tolerate the treatment. Therefore, a second experiment with DLD-1 cells was performed in cooperation with Dr. rer. nat. Melanie Spitzner (Department of General, Visceral and Pediatric Surgery). Here, the mice were administered to combined RCT on the first three days of treatment as well as on the days ten and eleven. Inhibitors were applied in two cycles. The first cycle started on day one of treatment and lasted for four days, whereas the second cycle started on day seven and lasted for five days (Fig. 67b). Interestingly, the mice showed improved tolerance to the alternative treatment compared to the first treatment.

In the following CaCo-2- and SW837 xenograft experiments, the xenograft mice received combined RCT on the first three days as well as on days eleven and twelve

of treatment. Inhibitors were applied in three cycles of five consecutive days each with two days break in between (Fig. 67c, d).

Tumor volume was measured daily using a caliper. For the determination of the tumor volume, the formula “V = width^2 x length x 0.5” was used. When the tumors reached a volume of approx. 1500 mm^3, mice were sacrificed, the tumors were dissected from the mice, weighed and measured. Here, tumor volume was calculated using the formula “V = width x length x height x π / 6”.

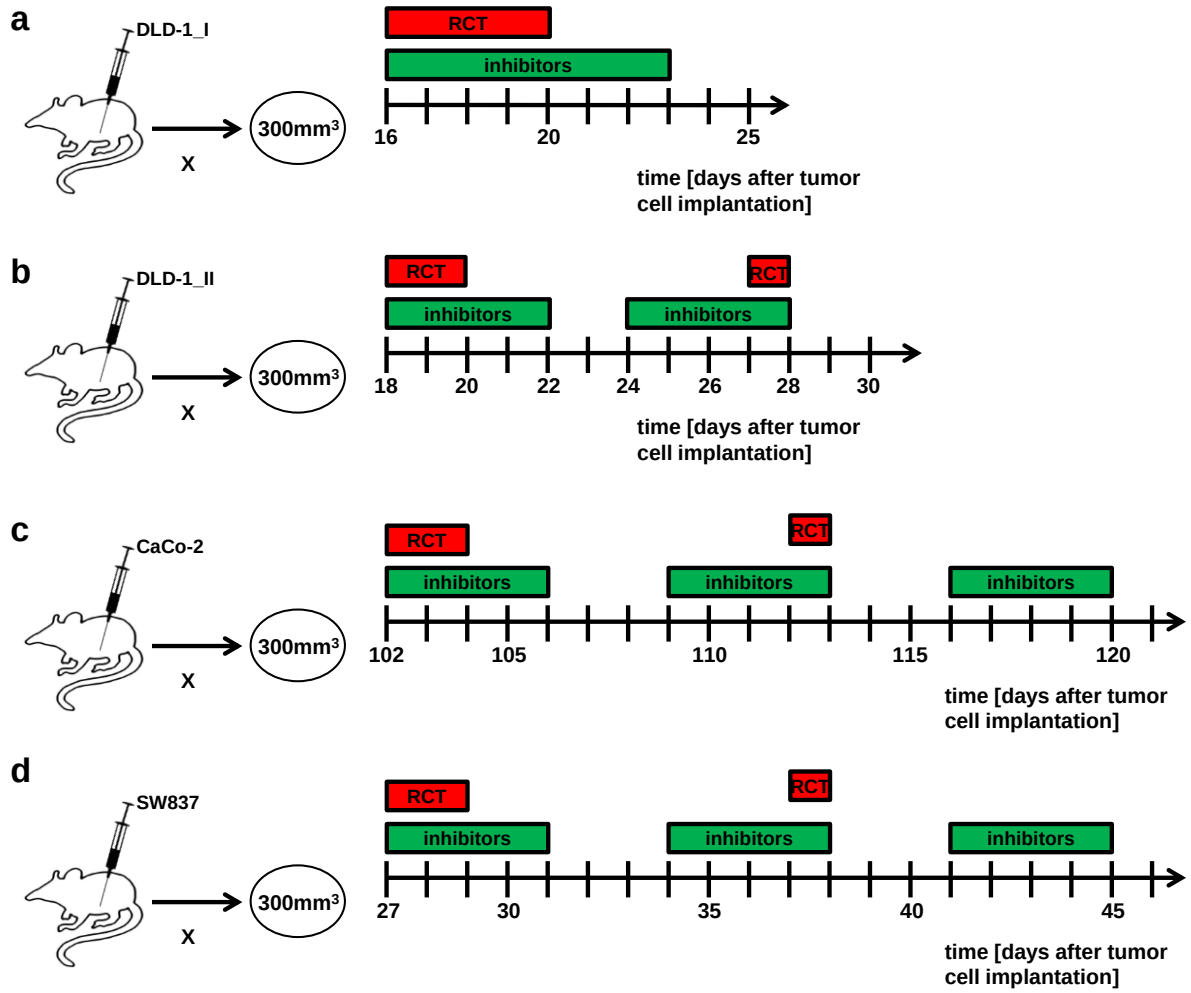

Fig. 67: Treatment schemes for the xenograft mice implanted with DLD-1, CaCo-2 or SW837 cells. For the xenograft mouse experiments, DLD-1, CaCo-2 and SW837 cells were implanted subcutaneously into immune-deficient RjOrl:NMRI-*Foxn1^{nu}/Foxn1^{nu}* mice, respectively. The therapy with the IGF1R inhibitor AEW541, with the EGFR inhibitor erlotinib, the combination of AEW541 and erlotinib or with the solvent as control in addition to combined RCT was started when the tumors reached an average tumor volume of 300 mm^3. **(a)** Mice implanted with DLD-1 cells were administered to the inhibitors on eight consecutive days in addition to RCT on five consecutive days. Unfortunately, some mice did not tolerate this treatment. For this reason, a second experiment with DLD-1 cells was performed. **(b)** Adapted treatment scheme for DLD-1 xenograft mice. Mice received inhibitor treatment in two cycles. The first cycle lasted for four days. The second cycle started at day seven of treatment and lasted for five days. Combined RCT was also administered in two cycles. The first cycle lasted for three days and the second

cycle was on days ten and eleven of treatment. **(c, d)** Mice implanted with CaCo-2 or SW837 cells were treated with three cycles of inhibitors on five consecutive days each with two days break in between in addition to RCT on the first three days and the days eleven and twelve of treatment. When the tumors reached a volume of approx. 1500 mm^3, the mice were sacrificed and the tumors were prepared.

Tumors of the DLD-1 xenografted cells grew very fast. In the first experiment, the treatment with the inhibitors in addition to combined RCT was started already 16 days after injection. Single treatment with erlotinib and simultaneous treatment with AEW541 / erlotinib in addition to combined RCT resulted in a significant reduction of the tumor volume compared to the control (Fig. 68).

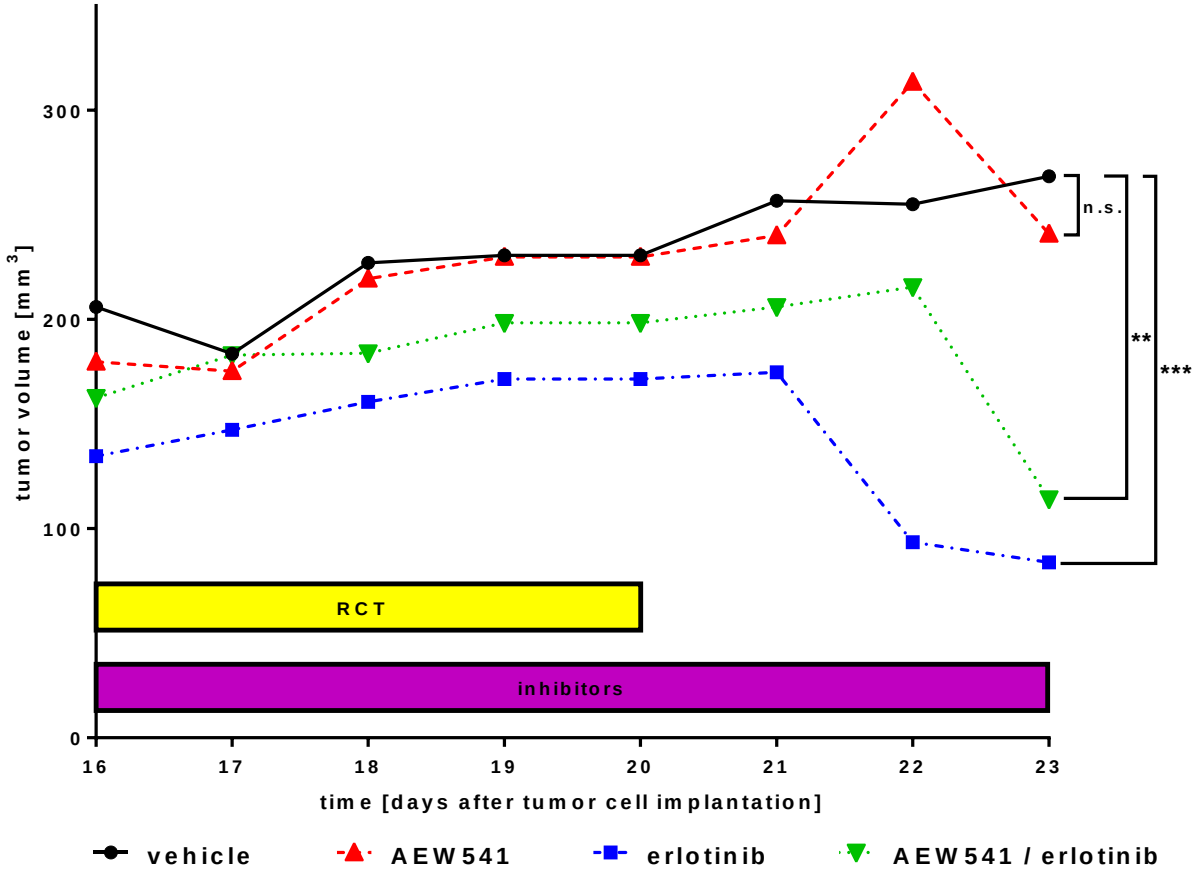

Fig. 68: Progression of the volume of the DLD-1 xenograft tumors after inhibition of the IGF1R and EGFR in addition to combined RCT (experiment I).

DLD-1 cells were subcutaneously implanted into immune-deficient nude mice. After tumors have developed, mice were administered to the IGF1R inhibitor AEW541 (n=3), the EGFR inhibitor erlotinib (n=3), the combination of both inhibitors (n=3) or the solvent as control (n=3) in addition to combined RCT. The treatment scheme is shown in Fig. 67a. Single inhibition of the EGFR by erlotinib and simultaneous inhibition of the IGF1R by AEW541 and EGFR by erlotinib resulted in a significant reduction of the tumor volume. ** $P < 0.01$, *** $P < 0.0001$ (student's *t* test).

In the second experiment with DLD-1 xenografted cells, the treatment scheme was adapted (Fig. 67b). Interestingly, single inhibition of the IGF1R as well as simultaneous inhibition of the IGF1R and EGFR in addition to combined RCT led to a significant decrease in the tumor volume compared to the control, whereas single inhibition of the EGFR showed no significant reduction in tumor volume (Fig. 69a). Noteworthy was the extreme difference in tumor volume between the inhibitor-treated and the control group at the beginning of the treatment. For this reason, the tumor volume increase was additionally determined (Fig. 69b). Interestingly, neither single nor simultaneous inhibitor treatment in addition to combined RCT resulted in a significant reduction in the increase in tumor volume.

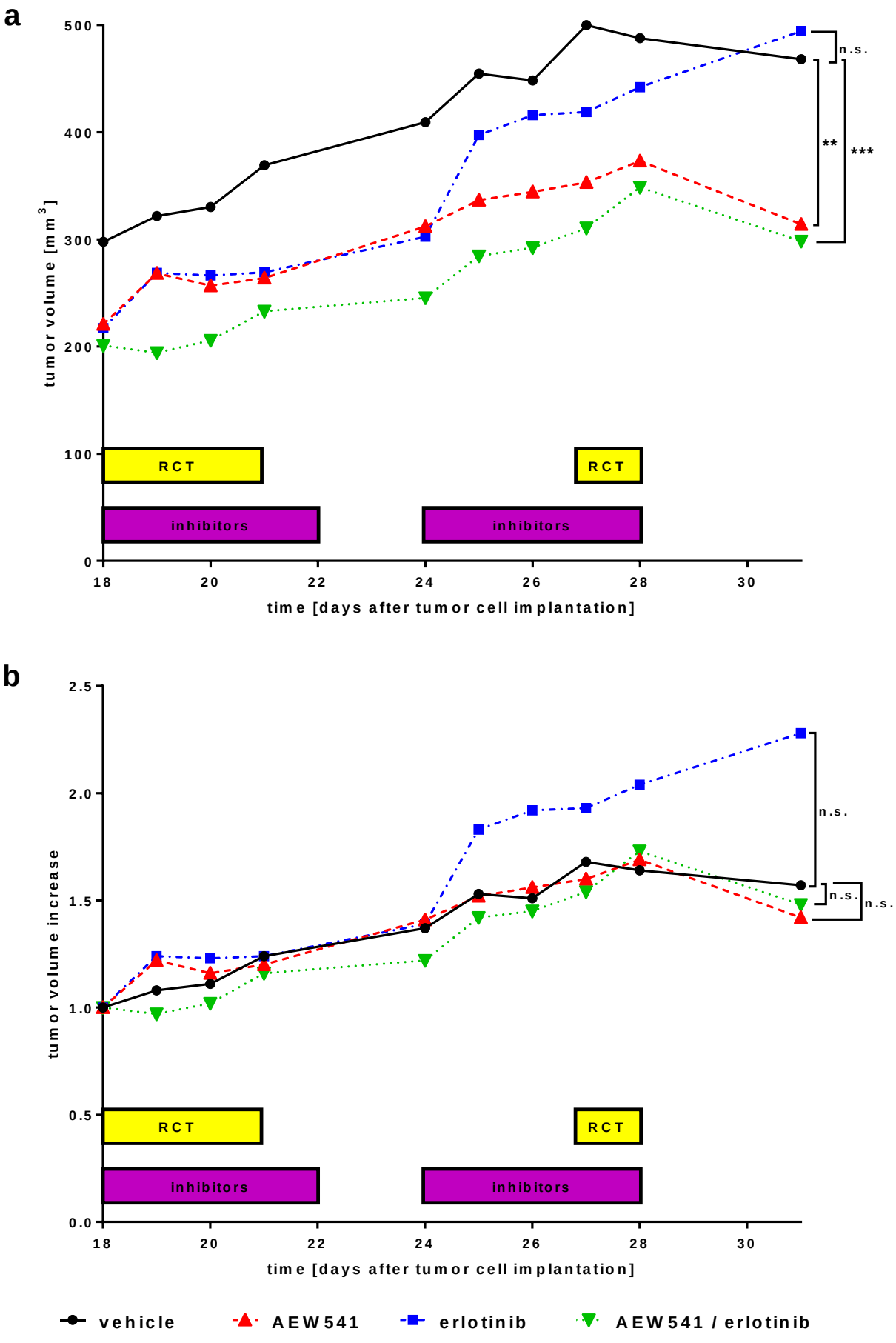
a
500
400
300
200
100
0
tumor volume [mm3]
n.s.
**
***
RCT
RCT
inhibitors
inhibitors
18
20
22
24
26
28
30
time [days after tumor cell implantation]
b
2.5
2.0
1.5
1.0
0.5
0.0
tumor volume increase
n.s.
n.s.
n.s.
RCT
RCT
inhibitors
inhibitors
18
20
22
24
26
28
30
time [days after tumor cell implantation]
vehicle
AEW541
erlotinib
AEW541 / erlotinib

Fig. 69: Progression of the volume of the DLD-1 xenograft tumors after inhibition of the IGF1R and EGFR in addition to combined RCT (experiment II).

DLD-1 cells were subcutaneously implanted into immune-deficient nude mice. After tumors have developed, mice were administered to the IGF1R inhibitor AEW541 (n=3), the EGFR inhibitor erlotinib (n=3), the combination of both inhibitors (n=4) or the solvent as control (n=4) in addition to combined RCT. The treatment scheme is shown in Fig. 67b. **(a)** Single inhibition of the IGFR and simultaneous inhibition of the IGF1R and EGFR resulted in a significant reduction of the tumor volume compared to the control. **(b)** Neither single nor simultaneous inhibition of the IGF1R and EGFR led to a significant reduction of the tumor volume increase compared to the control. ** $P < 0.01$, *** $P < 0.0001$ (student's *t* test).

Thirty-one days after DLD-1 tumor cell implantation, the mice were sacrificed, the tumors were dissected from the animals, measured and weighed (Fig. 70). Single inhibition of the IGF1R and simultaneous inhibition of the IGF1R and EGFR in addition to combined RCT resulted in a weak reduction of the tumor volume compared to the control, whereas single inhibition of the EGFR showed no difference in the tumor volume compared to the control (Fig. 70a). Regarding tumor weight, single inhibition of the IGF1R displayed a weak reduction of the tumor weight, whereas single inhibition of the EGFR led to a slight increase of the tumor weight compared to the control. The comparison of the tumor weight after simultaneous inhibition of the IGF1R and EGFR with the control showed no difference (Fig. 70b).

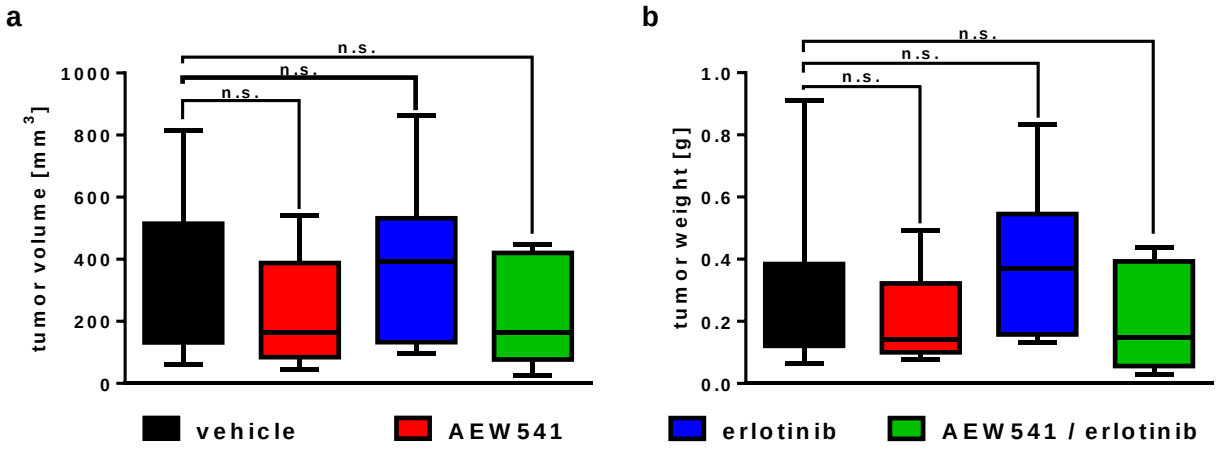

Fig. 70: Determination of the tumor volume and tumor weight of DLD-1 xenograft tumors (experiment II).

DLD-1 cells were injected into immune-deficient nude mice. Mice were treated with the small molecule kinase inhibitors AEW541 (n=3), erlotinib (n=3) or the combination of AEW541 and erlotinib (n=4) or the solvent as control (n=4) in addition to combined RCT. When the tumors reached a volume of 1500 mm^3, mice were sacrificed and the tumors were measured and weighed. **(a)** Single treatment with AEW541

as well as simultaneous treatment with AEW541 / erlotinib in addition to combined RCT resulted in a weak reduction of the tumor volume compared to the control. **(b)** Single inhibition of the IGF1R showed a weak reduction of the tumor weight, whereas single inhibition of the EGFR as well as simultaneous inhibition of the IGF1R and EGFR led to a slight increase in the tumor weight compared to the control. (student's *t* test).

Tumors of the CaCo-2 xenografted cells grew extremely slow. The treatment with inhibitors and combined RCT was started not before 102 days after tumor cell injection. Treatment with the inhibitors in addition to combined RCT resulted in a highly significant decrease in tumor volume compared to the control. Interestingly, single inhibition of either IGF1R or EGFR showed a stronger reduction of the tumor volume than simultaneous inhibition of the IGF1R and EGFR in addition to combined RCT (Fig.71a). At the beginning of the treatment with the inhibitors in addition to combined RCT the average tumor volume of the control mice differed extremely from the average tumor volume of the other treatment groups. For this reason, the increase in the tumor volume was additionally analyzed. This analysis revealed a slight elevation of tumor volume increase after single inhibition of the EGFR as well as simultaneous inhibition of the IGF1R and EGFR. Single inhibition of the IGF1R resulted in a significant reduction of tumor volume increase compared to the control (Fig. 71b).

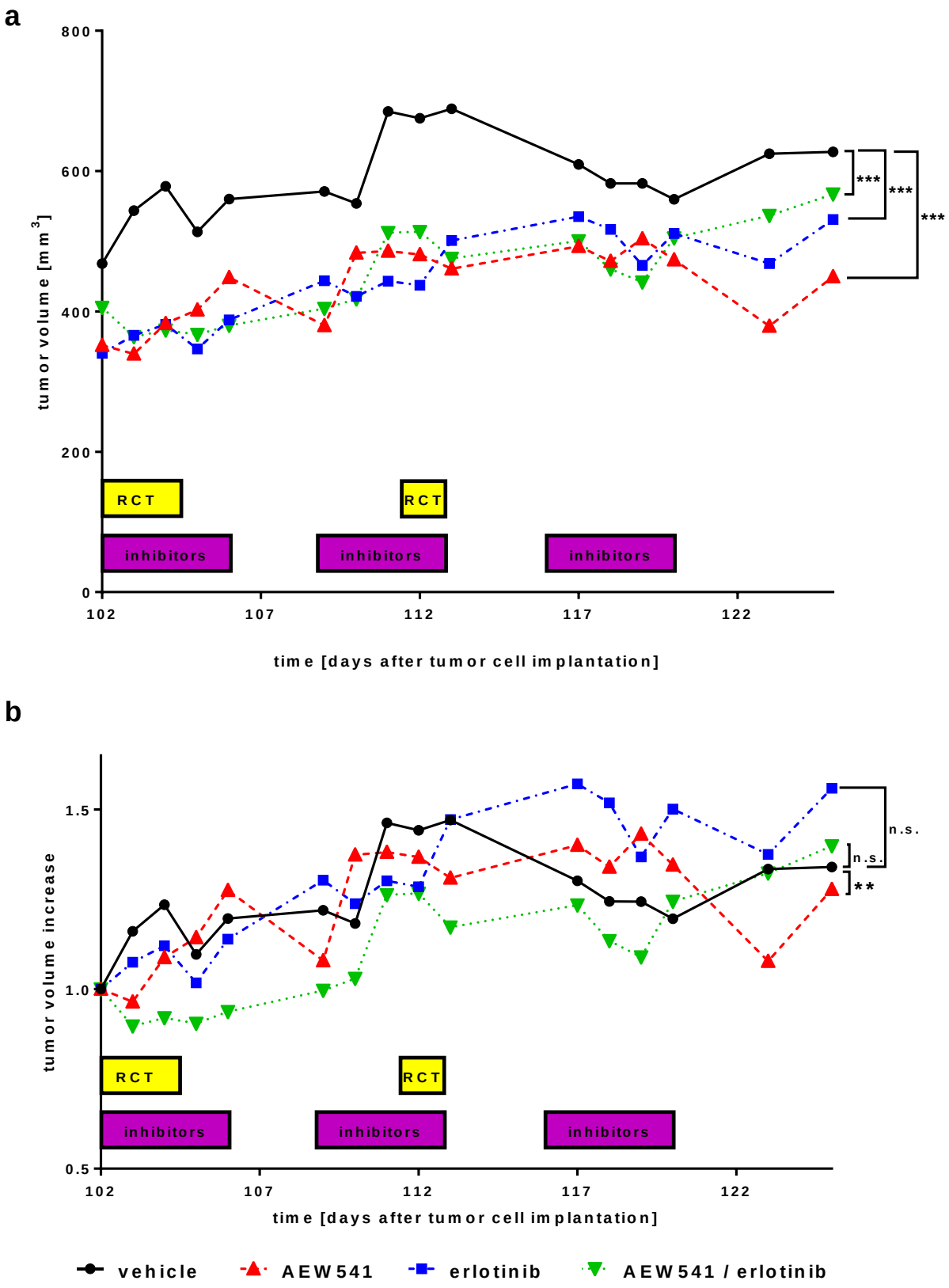

Fig. 71: Progression of the volume of the CaCo-2 xenograft tumors after inhibition of the IGF1R and EGFR in addition to combined RCT.

CaCo-2 cells were implanted into immune-deficient nude mice. After tumors have developed, mice were administered to the IGF1R inhibitor AEW541 (n=5), the EGFR inhibitor erlotinib (n=5), the combination of both inhibitors (n=6) or to the solvent as control (n=4) in addition to combined RCT. The treatment

scheme is shown in Fig. 67c. **(a)** Single inhibition of the IGF1R, the EGFR and simultaneous inhibition of the IGF1R and EGFR in addition to combined RCT resulted in a highly significant slower tumor progression compared to control mice. **(b)** Simultaneous inhibition of the IGF1R and EGFR in addition to combined RCT led to a significant reduction in tumor increase compared to the control. ** $P < 0.01$, *** $P < 0.0001$ (student's *t* test).

One hundred twenty-five days after CaCo-2 tumor cell injection, the mice were sacrificed, the tumors were excised from the animals, weighed and measured (Fig. 72). Single as well as simultaneous inhibition of the IGF1R and EGFR resulted in a decrease in tumor volume compared to the control mice (Fig. 72a). Treatment of the xenograft mice with the inhibitors in addition to combined RCT did not lead to a change in tumor weight compared to the control (Fig. 72b).

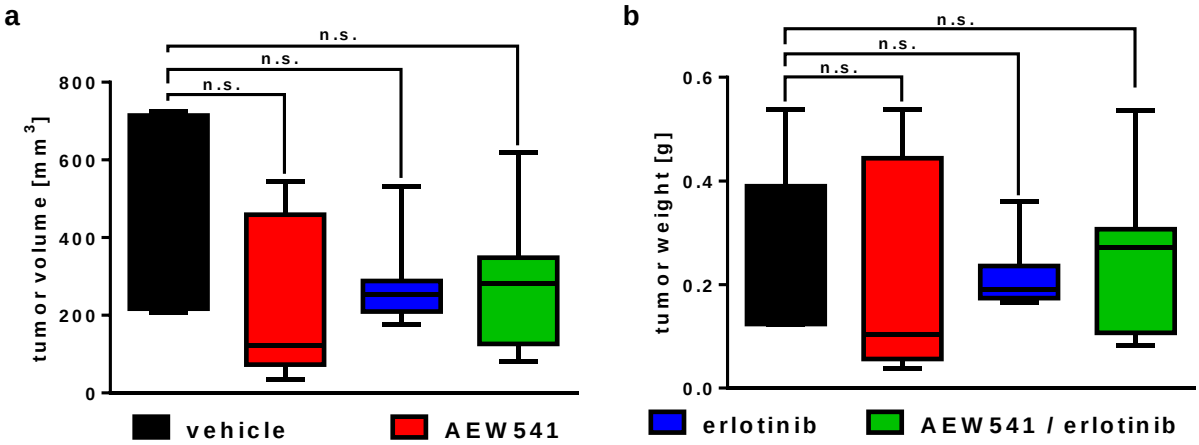

Fig. 72: Determination of the tumor volume and tumor weight of CaCo-2 xenograft tumors. CaCo-2 cells were injected into immune-deficient nude mice. Mice were treated with the inhibitor AEW541 (n=5), erlotinib (n=5), the combination of AEW541 and erlotinib (n=6) or the solvent as control (n=4) in addition to combined RCT. When the tumors reached an average volume of 1500 mm^3, mice were sacrificed, the tumors were excised from the animals and measured and weighed. **(a)** Single as well as simultaneous inhibition of the IGF1R and EGFR resulted in decreased tumor volume compared to control mice. **(b)** Treatment of the xenograft mice with the inhibitors did not lead to a reduction in tumor weight compared to the control. (student's *t* test).

For the SW837 xenograft experiment, SW837 cells were injected and the treatment was started already 27 days after injection. The xenograft tumors of the SW837 cells showed a decrease in tumor volume when treated with AEW541 in addition to combined RCT compared to control mice. Single treatment of the tumors with erlotinib

and simultaneous treatment of the tumors with AEW541 and erlotinib in addition to combined RCT revealed a significant reduction of the tumor volume (Fig. 73).

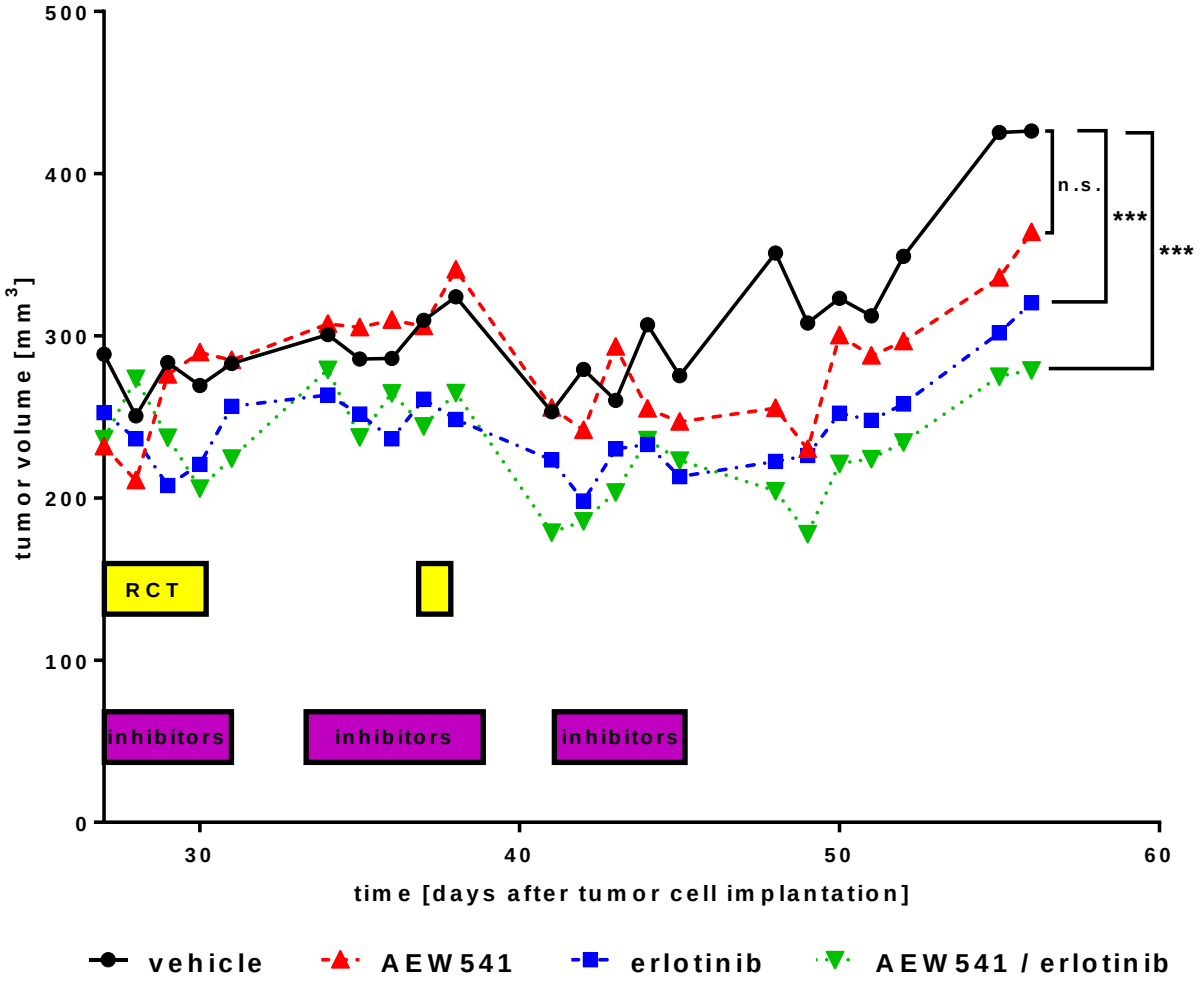

Fig. 73: Progression of the volume of the SW837 xenograft tumors after inhibition of the IGF1R and EGFR in addition to combined RCT.

Immune-deficient nude mice were implanted with the rectal cancer cell line SW837. After tumors have developed, mice were administered to the IGF1R inhibitor AEW541 (n=6), the EGFR inhibitor erlotinib (n=6), the combination of both inhibitors (n=7) or the solvent as control (n=7) in addition to combined RCT. The treatment scheme is shown in Fig. 67d. Single inhibition of the EGFR and simultaneous inhibition of the IGF1R and EGFR in addition to combined RCT resulted in a highly significant slower tumor progression compared to control mice. *** $P < 0.0001$ (student's *t* test).

On day 57, the mice were sacrificed and tumor tissues were dissected and measured. The SW837 xenograft mice treated with either AEW541 or erlotinib showed a reduction in tumor volume and weight compared to control mice. A significant reduction in tumor volume and weight could be observed in mice simultaneously treated with the combination of AEW541 and erlotinib in addition to combined RCT (Fig. 74).

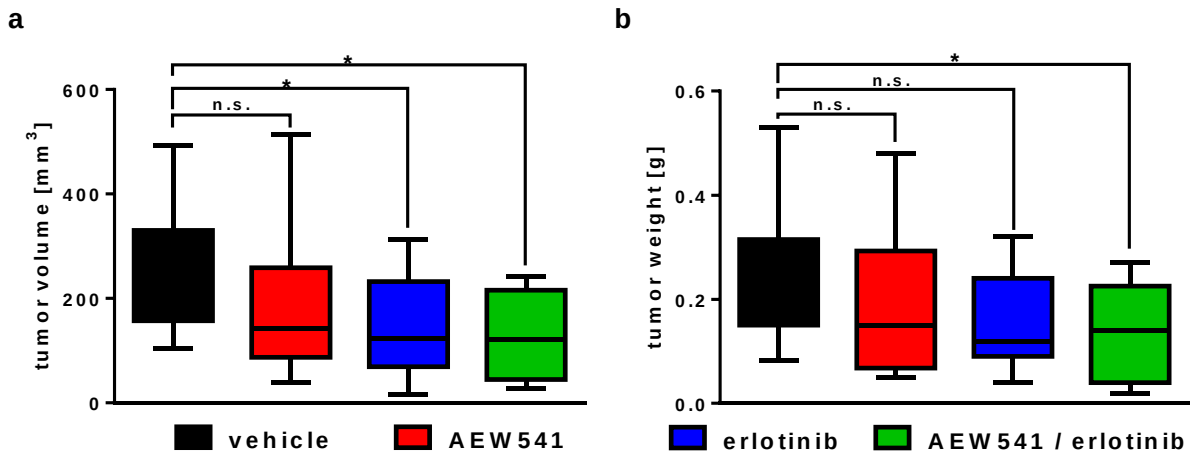

Fig. 74: Determination of the tumor volume and tumor weight of SW837 xenograft tumors. SW837 cells were implanted into immune-deficient nude mice and treated with the small molecule kinase inhibitors AEW541 (n=6), erlotinib (n=6), the combination of AEW541 / erlotinib (n=7) or the solvent as control (n=7) in addition to combined RCT. After reaching an average tumor volume of 1500 mm^3, mice were sacrificed and the tumors were measured and weighed. **(a)** Single inhibition of the EGFR as well as simultaneous inhibition of the IGF1R and EGFR resulted in a significantly reduced tumor volume compared to control mice. **(b)** Regarding tumor weight, simultaneous inhibition of the IGF1R and EGFR in addition to combined RCT led to a significant reduction compared to the control. * *P* <0.05 (student's *t* test).

3.27 Simultaneous inhibition of IGF1R and EGFR is associated with diminished downstream signaling *in vivo*

To assess whether inhibition of the IGF1R and EGFR affects the downstream PI3K and MAPK signaling pathways, western blot and subsequent densitometrical analyses with proteins of the SW837 xenograft tumors were performed (Fig. 75). Single as well as simultaneous inhibition of the IGF1R and EGFR resulted in a significant reduction of IGF1Rβ expression compared to the control, however, treatment with both inhibitors could not increase single treatment effects (Fig. 75b). The level of IGF1R activity decreased when xenograft tumors were treated with erlotinib or the combination of AEW541 and erlotinib compared to the control. Single treatment with AEW541 did not change IGF1R activity (Fig. 75c). Single treatment of the xenograft tumors with AEW541 or erlotinib led to a reduction of activated AKT (pAKT) and ERK (pERK), respectively. However, simultaneous treatment with AEW541 and erlotinib even further decreased activation of AKT (pAKT) and ERK (pERK) in comparison to single treatments (Fig. 75d, e).

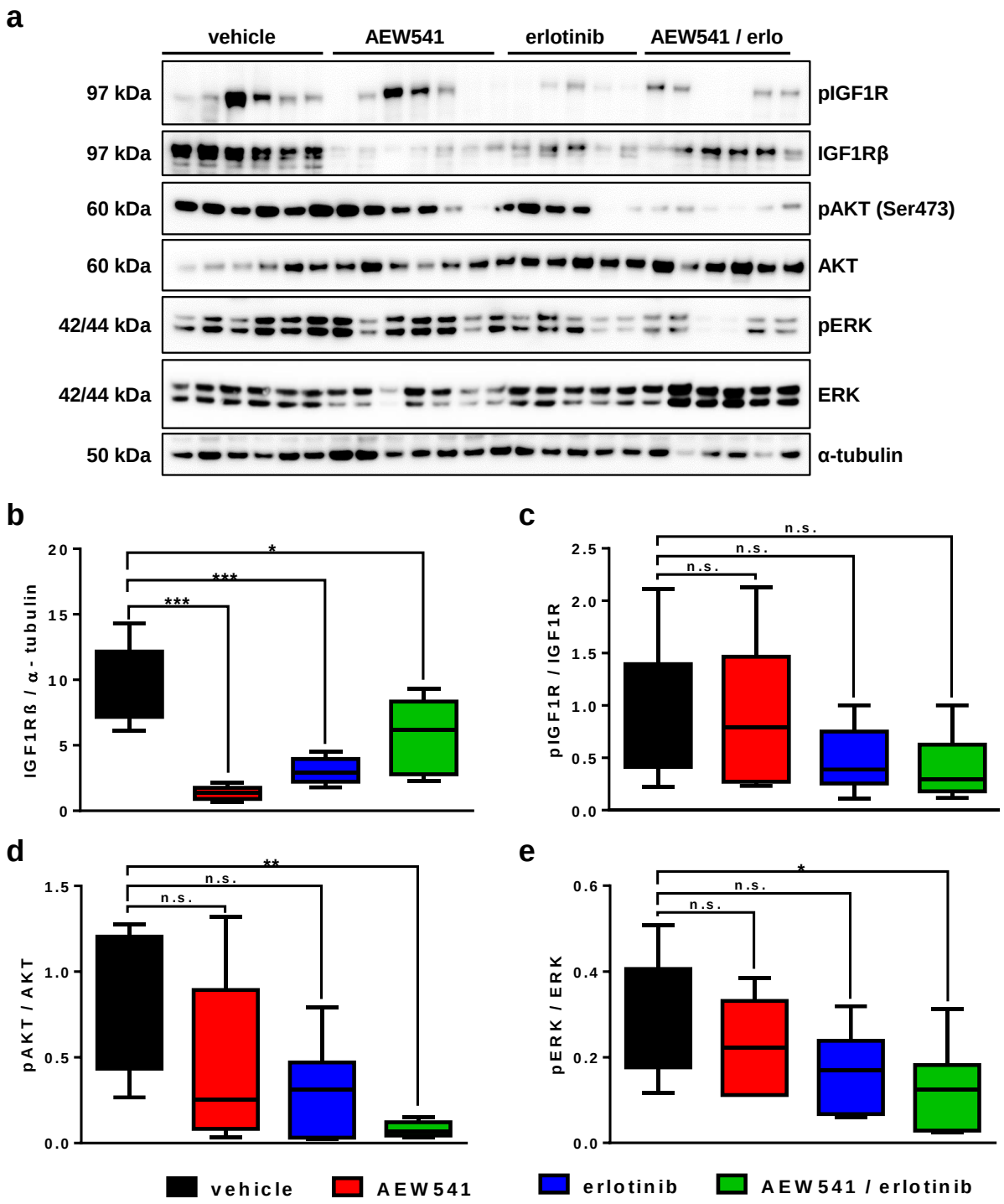

Fig. 75: Expression patterns of the IGF1R and members of the downstream PI3K and MAPK signaling pathways after treatment with the small molecule kinase inhibitors AEW541 and erlotinib in addition to combined RCT.

Immune-deficient nude mice were injected with SW837 cells and treated with the small molecule kinase inhibitors AEW541, erlotinib or the combination of AEW541 and erlotinib in addition to combined RCT. The tumors were excised from the mice, proteins were isolated from the tumors and western blot **(a)** and subsequent densitometrical analyses **(b- e)** were performed. **(a)** IGF1Rβ was highly expressed in the tumors of control animals. The phosphorylation level of AKT (pAKT) and ERK (pERK) was reduced in tumors treated with the combination of AEW541 and erlotinib. α-tubulin was used as loading control. **(b)**

The expression of IGF1Rβ decreased significantly after single inhibition of the IGF1R, the EGFR and the simultaneous inhibition of the IGF1R and EGFR. **(c)** No significant difference in the level of activated IGF1R between the different inhibitor treatments was visible. **(d, e)** A significant reduction of the activity of AKT (pAKT) and ERK (pERK), respectively, was visible after simultaneous inhibition of the IGF1R and EGFR. * P <0.05, ** P < 0.01, *** P < 0.0001 (student's t test).

4 Discussion

4.1 Summary of the results

The *insulin-like growth factor 1 receptor* (IGF1R) is a receptor tyrosine kinase (RTK) that is overexpressed in a variety of cancer entities, including colorectal cancer (CRC). In the course of the present study, the role of the IGF1R / Igf1r during intestinal development and during colonic tumor formation and progression was analyzed. For this reason, two inducible mouse models were generated. The Villin-TRE-IGF1R mouse line drives villin-guided expression of human *IGF1R* in the small intestine and colon induced by doxycycline administration. *IGF1R* overexpression and the activation of its downstream PI3K signaling pathway could be confirmed in the small intestine and colon by immunohistochemistry and western blot analysis. Immunofluorescence stainings revealed a gradient of high *IGF1R* overexpression in the villi of the small intestine and at the tip of the colonic crypts to low *IGF1R* overexpression in the crypts of the small intestine and at the bottom of the colonic crypts. Goblet cells, enteroendocrine cells, Paneth cells and proliferating cells could be excluded as cell type of IGF1R overexpression by immunofluorescence double stainings. To analyze if *IGF1R* overexpression was capable of inducing intestinal tumor formation, Villin-TRE-IGF1R mice were administered to 2 mg / ml doxycycline for 1.5 years to induce *IGF1R* overexpression. Colonoscopy was regularly performed to screen for colonic tumors, but villin-guided *IGF1R* overexpression was not sufficient to induce intestinal tumor formation. Interestingly, a possible effect of *IGF1R* overexpression on intestinal morphology and epithelial cell composition was hypothesized. *De facto*, *IGF1R* overexpression could be proven to significantly extend the average crypt depth in the small intestine. In addition, a reduced goblet and Paneth cell density and an increased number of proliferating cells were detected in IGF1R-overexpressing (IGF1R-oe) mice. These findings indicated that the IGF1R promotes epithelial cell proliferation and inhibits epithelial cell differentiation, pointing to a role of the IGF1R in normal intestine homeostasis.

Since *IGF1R* overexpression was proven to be not sufficient to induce intestinal tumor formation, it was hypothesized to promote tumor progression. To verify this hypothesis, Villin-TRE-IGF1R mice were administered to doxycycline to induce *IGF1R* overexpression and additionally treated with the mutagenic agent AOM or the

combination of AOM and the inflammatory agent DSS, respectively, to induce colonic tumor formation and inflammation. When using AOM as CRC-inducing agent, only IGF1R-oe mice developed intramucosal and even invasive carcinomas, whereas no difference was observed regarding adenoma development. Furthermore, this IGF1R-induced tumor progression was clearly shown when using AOM / DSS for CRC induction. In this mouse model, IGF1R-oe mice revealed an extremely elevated number of intramucosal carcinomas. IGF1R-oe mice even developed invasive carcinomas, whereas control mice did not. Metastases in the liver and lymph nodes of IGF1R-oe mice were not detected. In addition, the average tumor size of IGF1R-oe mice was increased by 66.2% compared to the tumor size of control mice. Moreover, western blot analysis was performed on the tumors to investigate the effect of *IGF1R* overexpression on the downstream PI3K and MAPK signaling pathways. The phosphorylation level of AKT (pAKT) was strongly elevated, whereas ERK activity was diminished in tumors which developed in IGF1R-oe mice compared to control mice, indicating that the PI3K and MAPK signaling pathways were activated and involved in the IGF1R-driven promotion of tumor progression. Taken together, these results impressively indicate that *IGF1R* overexpression promotes colonic tumor progression and influences the differentiation of the intestinal epithelium.

To study the function of murine Igf1r in the intestine and tumor development in more detail, the Villin-CreERT-Igf1r mouse line was established which expressed a cre recombinase fused with a modified ligand binding site of the human estrogen receptor and carried *Igf1r* alleles flanked by *loxP* sites. Tamoxifen administration to $Cre^{+}/Igf1r^{fl/fl}$ Villin-CreERT-Igf1r mice resulted in the deletion of exon 3 of the *Igf1r* gene specifically in the epithelium of the small intestine and colon. The *Igf1r* knockout was confirmed by PCR on genomic DNA and western blot analysis. Detailed analyses of the differentiation in the intestinal epithelium revealed an increase of goblet cells and a decrease of proliferating cells in $Cre^{+}/Igf1r^{fl/fl}$ mice compared to control mice, supporting the hypothesis that the Igf1r could function as a promoter of epithelial cell proliferation and as an inhibitor of epithelial cell differentiation. The influence of the *Igf1r* knockout on colonic tumor formation and progression was examined using both the AOM and AOM / DSS mouse models. AOM administration resulted in a moderate decrease in the number of colonic tumors in $Cre^{+}/Igf1r^{fl/fl}$ mice compared to control mice. However, AOM / DSS administration revealed opposing results with a slight increase in the colonic tumor number in $Cre^{+}/Igf1r^{fl/fl}$ mice compared to control mice. Regarding the

tumor stage, $Cre^{+}/Igf1r^{fl/fl}$ mice revealed a reduced number of colonic tumors with advanced stage compared to control mice. Western blot analysis on the colonic tumors showed a reduction of AKT activity (pAKT) but an increase in ERK activity (pERK) in $Cre^{+}/Igf1r^{fl/fl}$ mice compared to control mice, which leads to the hypothesis that tumor development in *Igf1r* knockout mice follows different driver mechanisms.

Since it is known that the IGF1R is highly upregulated in CRC, the IGF1R was predicted to be an important molecular target to treat patients with advanced CRC. *In vitro* studies, in which the IGF1R and EGFR were simultaneously inhibited in addition to a combined 5-FU-based radiochemotherapy (RCT) revealed a decrease in the survival fraction compared to single inhibition of either IGF1R, EGFR or control treatment in the CRC cell line DLD-1 and in the rectal cancer cell line SW837. In the CRC cell line CaCo-2, simultaneous inhibition of IGF1R and EGFR in addition to combined RCT even resulted in a complete loss of survival. One main aim of the present study was to analyze if these *in vitro* results can also be observed *in vivo*. To answer this question, DLD-1, CaCo-2 and SW837 cells were subcutaneously implanted into immune-deficient nude mice and resulting tumors were treated with the small molecule kinase inhibitors AEW541 (directed against the IGF1R), erlotinib (directed against the EGFR), the combination of AEW541 / erlotinib or the solvent as control in addition to combined RCT. In DLD-1 as well as in CaCo-2 xenograft mice, single or simultaneous inhibition of IGF1R and EGFR did not result in a significant reduction of tumor volume increase, tumor volume or weight. In contrast, in SW837 xenograft mice tumor progression, tumor volume and weight were significantly reduced after simultaneous treatment with AEW541 / erlotinib. Western blot analysis was performed on the SW837 tumors to investigate the effect of simultaneous inhibition of IGF1R and EGFR on the downstream PI3K and MAPK signaling pathways. AKT (pAKT) and ERK (pERK) activity were significantly reduced after simultaneous treatment with AEW541 / erlotinib. These results indicated that simultaneous inhibition of IGF1R and EGFR might be a potential treatment opportunity for advanced CRC.

4.2 Development, cellular organization and function of the intestine

The intestine is a winding muscular tube extending from the stomach to the anus. It consists of the small and large intestine. The main function of the small and large intestine is the digestion and absorption of nutrients, which is facilitated by numerous

epithelial infoldings that result in the extension of the surface area (Jaladanki and Wang 2011). The wall of the intestine is divided into four layers: mucosa, submucosa, muscularis propia and serosa. The mucosa lines the lumen of the intestine and is further divided into the epithelium, which is composed of a single-cell-layer of epithelial cells, the lamina propia, which consists of connective tissue and lymph nodes and the muscularis mucosae, which is a continuous sheet of smooth muscle cells (Bustos-Fernández 1983; Jaladanki and Wang 2011).

In human, the small intestine is a hollow tube of approx. 6 to 7 m length and a narrowing diameter from the beginning to the end. The small intestine is the longest part of the gastrointestinal tract and extends from the pyloric orifice of the stomach to the ileocecal fold. The small intestine is divided into the duodenum, the jejunum and the ileum (Drake and Gray 2010). The inner lining of the small intestine is covered with a columnar epithelium with invaginations, known as the crypts of Lieberkuhn (in the following text named crypts) and villi (Jaladanki and Wang 2011). Villi are 0.2 to 1 mm tall and 0.15 mm thick finger-like projections containing the majority of differentiated absorptive cells. The surface of the mucosa is 7- to 14-fold enlarged by the presence of the villi and crypts. The main function of the villi is the resorption of nutrients, while secretion and regeneration of cells take place in the crypts (Benninghoff *et al.* 2008).

The ontogeny of the small intestine is a process with three successive phases, containing morphogenesis and cell proliferation, cell differentiation, and cellular and functional maturation. In contrast to rodents, development of the human intestine is largely completed before birth. In human, mucosal remodeling and villus formation starts cranial and proceeds caudally beginning at 9 to 10 weeks of gestation. At first, crypts appear as solid cords of epithelial cells but form a small lumen lined by undifferentiated columnar cells by 12 weeks of gestation. Undifferentiated absorptive cells, goblet cells, and enteroendocrine cells are localized in the stratified epithelium before the villi have formed, whereas Paneth cells are observed at the base of developing crypts at weeks 11 to 12 of gestation. Enteroendocrine cells firstly appear by 12 weeks of gestation. In rodents, villus length, crypt depth, and the number of epithelial cells increase with development and finally reach maturity during the weaning period. Numerous potential extrinsic regulators of the human intestinal development have been identified, containing many growth factors and their receptors, such as EGF, IGF-2 and TGF-β (Montgomery *et al.* 1999).

The large intestine extends from the distal end of the ileum to the anus (Drake and Gray 2010). In the adult human, the large intestine is approx. 1.5 m in length (Bustos-Fernández 1983; Jaladanki and Wang 2011). The large intestine consists of the cecum, appendix, colon, rectum and the anal canal. The main functions of the large intestine are the absorption of fluids and salts from the intestinal contents, thus forming the feces (Drake and Gray 2010). In contrast to the small intestine, the epithelium of the large intestine is not covered with villi but contains tubular invaginations, the crypts (Jaladanki and Wang 2011). Due to the fact that the colon is the largest part of the large intestine (Benninghoff *et al.* 2008), the large intestine is simply called colon in the further text.

The development of the colon is very similar to that of the small intestine. It is marked by three stages of cell differentiation. At first, a primitive stratified epithelium appears at weeks 8 to 10 of gestation. At weeks 12 to 14 of gestation, this stratified epithelium is converted to a villus epithelium with developing crypts. At around 30 weeks of gestation, the remodeling of the epithelium occurs and the villi disappear, resulting in the adult-type epithelium with crypts but without villi (Montgomery *et al.* 1999).

The intestinal epithelium exhibits a remarkable constant and rapid renewal capacity on a weekly basis (Bustos-Fernández 1983; Medema and Vermeulen 2011). Crucial for the homeostasis of the intestinal epithelium are the intestinal stem cells (ISCs) that reside at the bottom of the crypts in both, the small intestine and colon (Medema and Vermeulen 2011). The undifferentiated ISCs divide and thus constantly provide new cells (Bustos-Fernández 1983). Interestingly, ISCs divide asymmetrically and thus give rise to one daughter stem cell and one progenitor cell (Jaladanki and Wang 2011). Therefore, all different intestinal cell types have their origin in one single stem cell. Several studies about the localization and identification of intestinal stem cells exist, predicting that the +4 cells (+4 cells are localized predominantly four cells above the cells of the crypt =+4 position (Sangiorgi and Capecchi 2008)) as well as the crypt base columnar cells (CBCCs) function as ISCs. Paneth cells are localized between the CBCCs in the crypts of the small intestine, and, of note, are not detected in the colon. The remainder of the crypts of the small intestine and colon largely consists of the rapidly proliferating progenitor cells, also known as transit-amplifying (TA) cells, that reside within the crypts for two to three days and divide approx. twice a day (Bustos-Fernández 1983; Sato *et al.* 2009; Medema and Vermeulen 2011). When the newly divided TA cells reach the top of the crypts, cell proliferation halts and the

TA cells rapidly differentiate into mature epithelial cells (Jaladanki and Wang 2011). The intestinal epithelial layer consists of either secretory cells, namely the mucus-secreting goblet cells, the hormone-secreting enteroendocrine cells and the antimicrobial-secreting Paneth cells, or enterocytes (Medema and Vermeulen 2011; Konsavage *et al.* 2012). Interestingly, the goblet cells, enteroendocrine cells and enterocytes migrate upward towards the intestinal lumen, whereas Paneth cells of the small intestine migrate downward towards the base of the crypt (Konsavage *et al.* 2012).

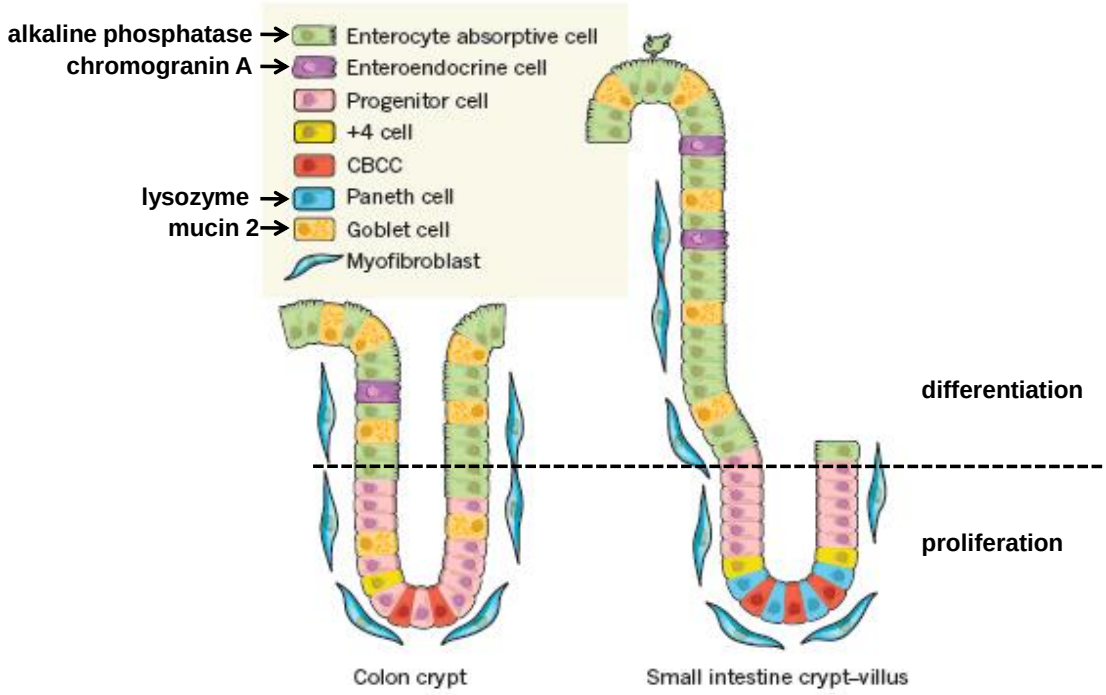

Fig. 76: Cellular organization of the colonic crypt and the small intestinal crypt and villus.
At the bottom of the intestinal crypts, pluripotent intestinal stem cells (ISCs) are localized, namely +4 cells and crypt base columnar cells (CBCCs). Additionally, at the bottom of the small intestinal crypt, Paneth cells are localized, whereas Paneth cells are not detected in the colon. ISCs divide and thus give rise to progenitor cells also known as transit-amplifying (TA) cells. TA cells divide and rapidly differentiate into goblet cells, Paneth cells, enteroendocrine cells or enterocytes when they reach the crypt-villus junction (modified after Medema and Vermeulen, 2011).

The goblet cells are localized in the small intestine and colon (Medema and Vermeulen 2011). The number of goblet cells increases caudally from the small intestine to the colon, in concordance with the rising number of microbial organisms that are present in the proximal intestine to the colon (Benninghoff *et al.* 2008; Kim and Ho 2010). In the human fetal small intestine, goblet cells appear early in development, at weeks 9 to

10 of gestation. The main function of goblet cells is the synthesis and secretion of bioactive molecules, such as secretory mucin glycoproteins like mucin 2 (*MUC2*) and epithelial membrane-bound mucins (*MUC1*, *MUC3* and *MUC17*), which are components of the mucus. The major function of intestinal goblet cells and mucin as their main secretory product is the formation of the intestinal mucus layers. The small intestine has only a monolayer of mucus, whereas the mucus of the colon is two-layered (Johansson *et al.* 2011). The intestinal mucus layers mainly consist of the gel-forming MUC2 mucin and serve as the physical and chemical barrier against endogenous and exogenous irritants, such as bacteria, toxins of bacteria or the environment, or some dietary components (Specian and Oliver 1991; Kim and Ho 2010). Nevertheless, intestinal mucus layers allow the transport of nutrients (Kim and Ho 2010). A correlation between the volume density of goblet cells and malignant transformation is not known to date. Interestingly, alterations in mucin production were observed during intestinal neoplasia. In human tumors of the small intestine, mucin secretion was found to be dramatically decreased or even absent, and histologically the mucins showed an altered pattern (Specian and Oliver 1991). Furthermore, a link between the fibroblast growth factor 10 (Fgf10) expression and the number of goblet cells was shown (Al Alam *et al.* 2015). Al Alam *et al.* (2015) proved that *Fgf10* overexpression in the murine small intestine induced goblet cell differentiation and a decrease in the number of Paneth cells, indicating that Fgf10 influences the balance between goblet and Paneth cells. FGF10 belongs to the FGF family and is the ligand for the fibroblast growth factor receptor 1 (FGFR1) and FGFR2, which are transmembrane tyrosine kinase receptors (Ahmad *et al.* 2012). To date, studies showing a correlation between the IGF1R expression and goblet cell differentiation and the maintenance of the goblet cell population are not available.

Paneth cells are specialized secretory cells in the epithelium of the small intestine. Like the other epithelial cells, Paneth cells originate from the adjacent leucine-rich-repeat-containing G protein-coupled receptor 5 (LGR5)-positive intestinal stem cells (Bevins and Salzman 2011). Paneth cells are localized at the base of the crypts and synthesize and secrete antimicrobial peptides and proteins (Elphick 2005; Clevers and Bevins 2013). In humans, the development of Paneth cells starts in the colon and small intestine at a gestational stage of 13.5 weeks. After 17 weeks of gestation, Paneth cells are mainly restricted to the small intestine and are not found in the colon anymore (Bevins and Salzman 2011). On average, each small intestinal crypt contains 5 to

12 Paneth cells. As already mentioned, in contrast to other epithelial cells, Paneth cells migrate downward from the stem cell zone to the bottom of the crypt, where they can reside for approx. 1 month (Elphick 2005; Clevers and Bevins 2013). The localization of the Paneth cells close to the Lgr5-expressing CBCCs indicate a functional interaction between these cells, and indeed it was shown that Paneth cells provide large amounts of essential niche signals to the CBCCs (Clevers and Bevins 2013). Paneth cells contain numerous cytoplasmic granules which are released into the crypt lumen upon microbial challenge (Elphick 2005; Bevins and Salzman 2011). Antimicrobials are the most prominent proteins in the granules and are able to prevent microbial invasion of the crypt (Bevins and Salzman 2011). Among several antimicrobial peptides of Paneth cells, lysozyme is an antimicrobial protein found in many human secretions, such as tears, breast milk and small intestinal secretions. Lysozyme is predominantly active against Gram positive bacteria (Elphick 2005; Bevins and Salzman 2011).

Interestingly, a link between the insulin receptor (IR) and the intestinal Paneth cell number was proven by Andres *et al.* (2015). These authors showed that during high-fat diet-induced obesity the number of Paneth cells decreased in mice that harbor an IR disruption in intestinal cells. Furthermore, they predicted that the IR expressed in the intestinal epithelium contributes to an increase in Paneth cell-derived mRNAs during high-fat diet-induced obesity (Andres *et al.* 2015). However, a link between the IGF1R, which is closely related to the IR, and Paneth cell differentiation and maintenance is not known.

Enteroendocrine cells (EECs) are the basis of the largest endocrine system in the body, the intestine. EECs secrete multiple regulatory peptide hormones which control physiological and homeostatic functions and act as sensors of nutrients in the digestive tract (Moran *et al.* 2008; Gunawardene *et al.* 2011). EECs develop from the pluripotent stem cells and are localized as single cells in the intestinal crypts and villi, interspersed by non-endocrine epithelial cells (Moran *et al.* 2008; Gunawardene *et al.* 2011). EECs express the cell surface protein Notch and prevent the differentiation of adjacent cells into EECs by lateral inhibition (Gunawardene *et al.* 2011). From the duodenum to the rectum, the highest number of EECs can be found proximally, then the number of EECs falls steadily with the lowest number in the colon and rises again within the rectum (Gunawardene *et al.* 2011). The turnover of EECs is very rapidly with a lifespan of approx. 4 to 6 days (Moran *et al.* 2008). EECs contain secretory vesicles holding

chromogranin A, which is a matrix-soluble glycoprotein that transports biogenic amines, and synaptophysin, which is a membrane glycoprotein (Gunawardene *et al.* 2011). Of importance, publications presenting data about a crosslink between EECs and the IGF1R do not exist to date.

Enterocytes are the absorptive cells in the intestinal epithelium. Enterocytes develop, similarly as the goblet, Paneth and enteroendocrine cells, from the intestinal stem cells. The enterocytes differentiate and migrate within 3 to 4 days from the crypt to the villus tip, where they are released into the lumen of the intestine. Microvilli at the apical surface of enterocytes increase the absorptive surface area of the cells (Overeem *et al.* 2016). The main function of enterocytes is the uptake of ions, water, nutrients, vitamins and the absorption of unconjugated bile salts during digestion. Furthermore, enterocytes cooperate with cells of the intestinal mucosa-associated lymphoid tissue (MALT). Together, these cells preserve a non-reactivity state toward dietary and microbial antigens. Thus, enterocytes are actively involved in the immunological tolerance to ingested proteins (Miron and Cristea 2012). Of note, a connection between the Igf-axis and enterocytes was shown in growing rats after mid small bowel resection. Treatment with ectopic Igf-1 increased the proliferation level of enterocytes and even expanded the size of the proliferative compartment in the crypt after resection (Dahly *et al.* 2003). A direct link between the IGF1R and enterocytes and regarding to CRC is not known to date.

4.3 Physiological role of the IGF1R in the intestine

Several studies have proven that the IGF1R is overexpressed in colorectal and rectal cancer biopsies (Freier *et al.* 1999; Hakam *et al.* 1999; Weber *et al.* 2002; Li 2013; Zhang *et al.* 2013; Wu *et al.* 2014). In contrast, only little is known about the role of the IGF1R in normal intestinal tissue. *In vivo*, an influence of the IGF1R and its ligands on murine embryonal growth could be shown by Baserga (1995). At birth, mouse embryos with disrupted *Igf1r* and *Igf-2* genes were smaller than their wild type littermates. Furthermore, cells derived from the knockout embryos revealed growth deficits, which could be abrogated by transfection of the cells with wild type *Igf1r* cDNA. These facts indicated that the Igf1r is important for growth (Baserga 1995). Dong *et al.* (2014) found a connection between the glucagon-like peptide-2 (GLP-2) and the Igf1r in the intestine, respectively. They showed that GLP-2 requires the Igf1r, expressed in the

intestinal epithelium, to promote intestinal growth and to modulate intestinal barrier function (Dong *et al.* 2014). In addition, the insulin receptor substrate 1 (IRS1), that is known to mediate downstream signaling (Sachdev and Yee 2007; Ekyalongo *et al.* 2013), was proven to be expressed in the colonic crypt epithelium and was predicted to play a role in CRC progression (Esposito *et al.* 2012). Astonishingly, only one publication was found in which the expression of components of the IGF-axis and therefore the expression of IGF1R in normal human colorectal tissue was examined. The researchers observed staining of the IGF1R in the colonic crypts of all 46 colonic and 43 rectal biopsies in both, the cytoplasm and cell membrane, with significantly stronger expression of IGF1R in the rectum compared to the colon (Vrieling *et al.* 2009). Of note, van Landeghem *et al.* (2015) analyzed the effect of a short-term human IGF-1 administration on ISCs during normal intestinal renewal, and crypt regeneration after injury induced by high-dose radiation. They showed that IGF-1 administration in uninjured mice stimulated mucosal growth indicated by a significant increase in crypt density as well as significant increases in crypt depth and villus height. In addition, they proved that IGF-1 administration stimulated the expansion of CBCCs, which was indicated by the significant increase in the number of CBCCs per crypt section. Interestingly, these authors further observed enriched mRNA levels of the *Igf1r* in CBCCs, indicating involvement of the Igf1r in the effects of IGF-1 on ISCs (van Landeghem *et al.* 2015). In general, it was shown that the IGF1R / Igf1r plays a crucial role in maintaining normal growth and development (Reinmuth *et al.* 2002). In the skin, an association between elevating Igf1r levels and increased cell proliferation could be proven. Lack of Igf1r expression was shown to be associated with decreased proliferation and with the facilitation of the differentiation process in primary skin keratinocytes (Sadagurski *et al.* 2006). In the mammary terminal end bud, which is the proliferative compartment within the virgin mouse mammary gland, the loss of *Igf1r* resulted in decreased proliferation (Bonnette and Hadsell 2001).

In the present study, one aim was the examination of the physiological role of the IGF1R / Igf1r in the intestine. For this purpose, an *IGF1R* overexpression (Villin-TRE-IGF1R mice) and an *Igf1r* knockout mouse model (Villin-CreERT-Igf1r mice), respectively, were established.

No data exist demonstrating morphological changes in the intestine as a consequence of an *IGF1R* overexpression or an *Igf1r* knockout. Van Landeghem *et al.* (2015) demonstrated that IGF-1 administration induced significant changes in intestinal

morphology, such as increased crypt depth and villus height, and predicted an involvement of the Igf1r. The present study shows that the small intestine and colon are intact in IGF1R-overexpressing (IGF1R-oe) (see chapter 3.8) and Igf1r-knockout ($Cre^+/Igf1r^{fl/fl}$) mice (see chapter 3.21). However, a significant increase in the average depth of the small intestinal crypts was found in IGF1R-oe mice compared to the particular control mice (see chapter 3.8). As already described, the Igf1r is known to promote cell proliferation in the skin (Sadagurski *et al.* 2006), and IGF-1 administration was shown to stimulate mucosal growth and expansion of CBCCs in the intestine (van Landeghem *et al.* 2015). Additionally, it is also known that proliferation in the intestine takes place in the crypts, whereas cell differentiation occurs in the villi of the small intestine (Medema and Vermeulen 2011). Thus, a prolonged small intestinal crypt could possibly account for an elevated level of cell proliferation. A controversial issue is the fact that no significant increase of the colonic crypt depth was observed, because proliferating ISCs are not only localized in the crypts of the small intestine, but also in the crypts of the colon. Thus, further investigations are required. Epithelial cell differentiation and proliferation was examined by the quantification of goblet cells, enteroendocrine cells, Paneth cells and proliferating cells of IGF1R-oe and $Cre^+/Igf1r^{fl/fl}$ mice. The overall results are summarized in table 1.

Table 1: Results of the quantification of the different intestinal cell types in IGF1R-overexpressing (IGF1R-oe) and *Igf1r* knockout mice ($Cre^+/Igf1r^{fl/fl}$) compared to the particular control.

↑=increased -, ↓=decreased -, →=unchanged number of the particular cell type; SI=small intestine. 4 w= quantification of proliferating cells four weeks after the *Igf1r* knockout was induced. 3 m= quantification of proliferating cells three months after the *Igf1r* knockout was induced.

Cell type	IGF1R-oe		$Cre^+/Igf1r^{fl/fl}$	
	SI	colon	SI	colon
Goblet cells	↓	↓	↑	↑
Enteroendocrine cells	→	→	→	→
Paneth cells	↓		↓	
Proliferating cells (Ki 67-positive)	↑	↓	↓	↓ 4 w ↑ 3 m

In the small intestine, IGF1R-oe mice revealed a reduction of goblet and Paneth cells, whereas the number of enteroendocrine cells did not alter after *IGF1R* overexpression. Numbers of proliferating cells increased in the crypts of the small intestine. These results support the hypothesis that the extended crypt depth in the small intestine is the consequence of increased cell proliferation promoted by the *IGF1R* overexpression. Under physiological conditions, stem cells at the base of the crypts divide to self-renew and give rise to daughter progenitor cells. The progenitor cells divide approx. six times and rapidly differentiate as they migrate along the crypt-villus axis (Jaladanki and Wang 2011; van Landeghem *et al.* 2015). However, upon *IGF1R* overexpression, the progenitor cells do not differentiate, but rather keep on proliferating promoted by the IGF1R. As a consequence, the proliferative compartment is extended, indicated by the elongated crypt depth. This hypothesis is supported by the fact, that the density of goblet cells and Paneth cells is reduced upon *IGF1R* overexpression in the small intestine, showing that differentiation is inhibited by IGF1R overexpression. Interestingly, comparable results in primary skin keratinocytes were published by Sadagurski *et al.* (2006) who proved that loss of Igf1r expression is associated with decreased proliferation and increased differentiation.

If this hypothesis of the IGF1R as a proliferation-promoting and a differentiation-inhibiting factor is true, opposing results are expected in Cre^{+}/*Igf1r*$^{fl/fl}$ mice. Indeed, Cre^{+}/*Igf1r*$^{fl/fl}$ mice revealed an increase in goblet cells as expected, but a decrease in Paneth cells. The number of proliferating cells in the small intestine was reduced. Again, the density of enteroendocrine cells did not change, indicating that the Igf1r seems to have no influence on the differentiation of this cell type. Both, the increase in the number of goblet cells and the reduction of proliferating cells in the small intestine support the hypothesis that the Igf1r promotes cell proliferation and inhibits epithelial cell differentiation in this tissue.

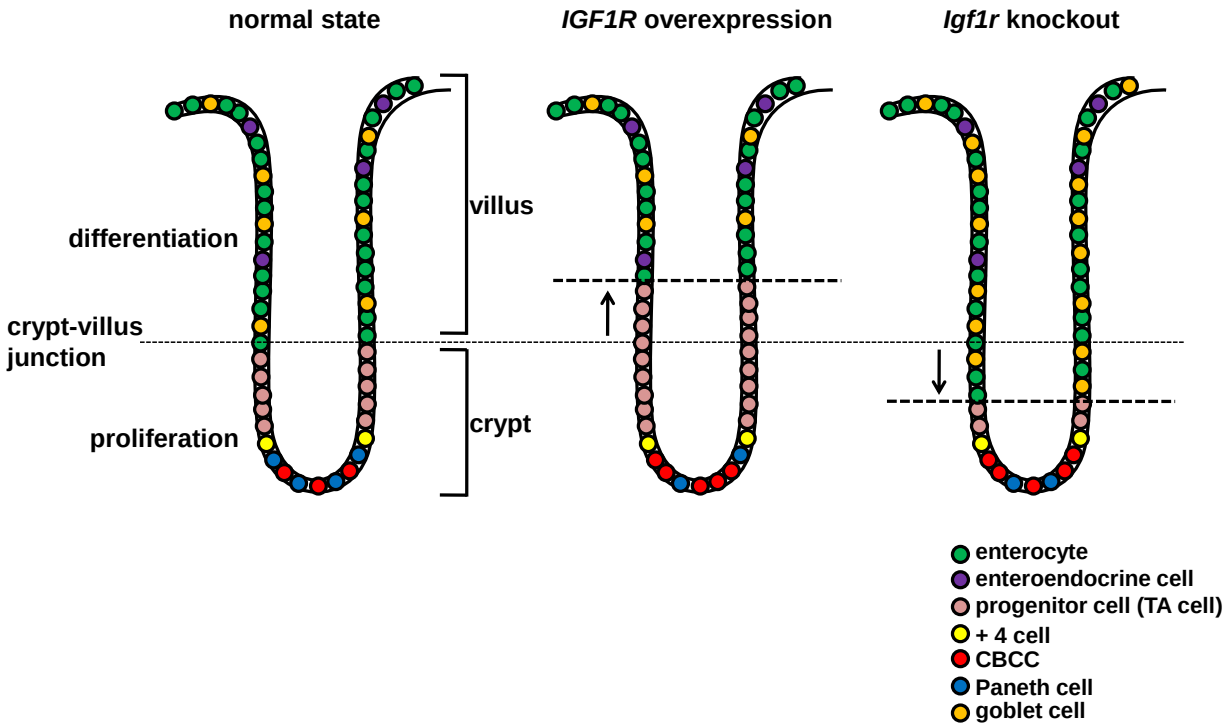

Fig. 77: Schematic representation of the influence of the *IGF1R* overexpression and the *Igf1r* knockout on epithelial cell proliferation and differentiation in the small intestine.
In the normal state, CBCCs are localized at the bottom of the crypts and Paneth cells are localized in between. +4 cells are localized above the Paneth cells on position +4. CBCCs and +4 cells divide and thus give rise to progenitor cells, also known as transit-amplifying (TA) cells. TA cells divide as they migrate upwards along the crypt-villus-axis and differentiate into goblet cells, Paneth cells, enteroendocrine cells or enterocytes when they reach the crypt-villus junction. Upon *IGF1R* overexpression, the progenitor cells keep on proliferating instead of differentiating which results in an elongated proliferative compartment and the reduction of goblet and Paneth cells. In contrast, upon *Igf1r* knockout, the number of proliferating cells decreases, whereas the density of goblet cells increases, leading to the shrinkage of the proliferative compartment (modified after Hägebarth 2005; Medema and Vermeulen 2011).

In the crypts of the colon, IGF1R-oe mice showed a decreased number of goblet cells, Paneth cells and, against expectation, also proliferating cells. The number of enteroendocrine cells did not change after *IGF1R* overexpression compared to control mice. In $Cre^{+}/Igf1r^{fl/fl}$ mice, the number of goblet cells increased, the Paneth cell number decreased and the number of enteroendocrine cells did not change compared to the cell numbers in control mice. The number of proliferating cells revealed opposing effects in the colonic crypts of $Cre^{+}/Igf1r^{fl/fl}$ mice. Four weeks after the *Igf1r* knockout was induced, the number of proliferating cells decreased, whereas it increased three months after *Igf1r* knockout induction. The fact that *IGF1R* overexpression did not

affect colonic crypt depth as well as the fact that in IGF1R-oe mice the number of proliferating cells in the colonic crypts was decreased, whereas it was increased in $Cre^{+}/Igf1r^{fl/fl}$ mice three months after *Igf1r* knockout induction seem to dispute the hypothesis of IGF1R / Igf1r being a promoter of cell proliferation and an inhibitor of cell differentiation. Of note, the *IGF1R* overexpression and the *Igf1r* knockout were also confirmed in the colon. An explanation for these observations in the colon could be the fact that villin expression was observed to be lower in the colon compared to the small intestine in both Villin-TRE-IGF1R and Villin-CreERT-Igf1r mice (see chapter 3.3, 3.5 and 3.18). Since the villin promoter guides *IGF1R* overexpression and the *Igf1r* knockout, lower villin expression in the colon could indicate that also *IGF1R* overexpression and the *Igf1r* knockout are impaired in the colon and that the villin promoter is not a suitable promoter in studies of the colon (see chapter 4.5.1). In fact, *IGF1R* overexpression in the Villin-TRE-IGF1R mouse model was shown to be more prominent in the small intestine than in the colon.

Interestingly, a concordant expression pattern of villin expression and IGF1R overexpression in Villin-TRE-IGF1R mice was not observed. As already described, villin was expressed in epithelial cells of the small intestine and colon with a gradient from high expression in the villi of the small intestine and at the tip of the colonic crypts to low villin expression in the crypts of the small intestine and at the bottom of the colonic crypts (see chapter 3.3). In contrast, IGF1R overexpression was indeed evenly distributed over the villi, but only some particular cells overexpressed IGF1R, whereas in other cells IGF1R overexpression was hardly visible (see chapter 3.4 and 3.6). Since IGF1R overexpression was guided by the villin promoter, which is expressed in all epithelial cells along the crypt-villus axis, IGF1R was also expected to be overexpressed by all epithelial cells. These observations led to the assumption that, despite the fact that the villin promoter guides IGF1R overexpression, not all epithelial cells but only a special intestinal cell type overexpressed IGF1R upon doxycycline treatment. Furthermore, endogenous Igf1r was shown to be strongly expressed at the base of the crypts with intense staining in CBCCs (van Landeghem *et al.* 2015). Consistent with these findings were Igf1r stainings of small intestinal and colonic tissue sections of control Villin-TRE-IGF1R mice in the present study which showed that endogenous Igf1r is abundantly localized at the base of the crypts in the small intestine and colon. Along the crypt-villus-axis, immunoreactivity of endogenous Igf1r was observed to decline (Fig. 78).

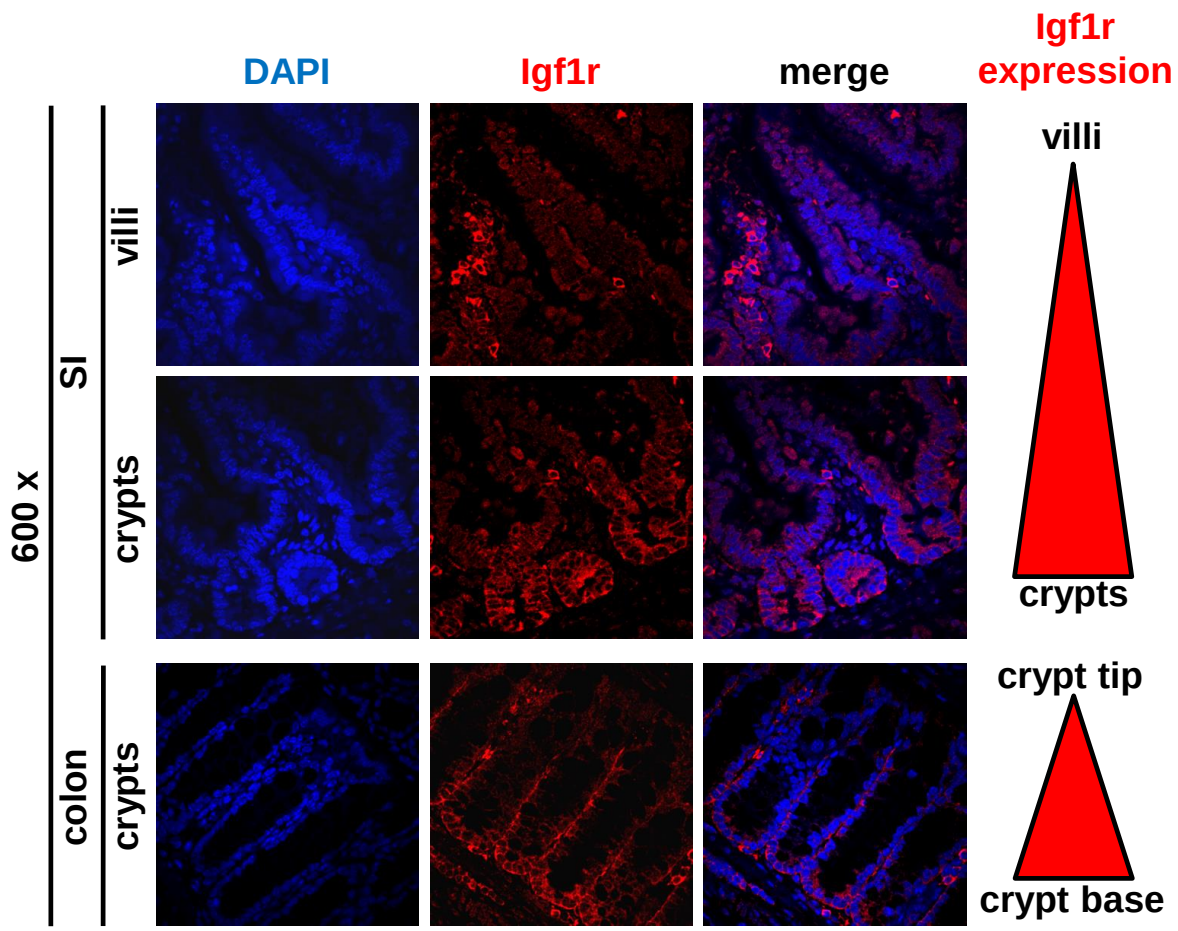

Fig. 78: Immunofluorescence stainings of endogenous Igf1r in the small intestine (SI) and colon using an antibody against murine Igf1rβ.

A gradient of low endogenous Igf1r expression (red) in the villi (SI) and at the tip of the crypts (colon) to strong expression in the crypts (SI) and at the base of the crypts (colon) is visible. DAPI visualized cell nuclei (blue).

In contrast, ectopic IGF1R induced by *IGF1R* overexpression was predominantly observed to be localized at the tip of the crypts as described in chapter 3.4, raising the suggestion that endogenous *Igf1r* and ectopic villin-guided *IGF1R* were expressed by different epithelial cell types. The identification of the cell type that endogenously and exogenously expressed IGF1R / Igf1r was part of the present study. Unfortunately, double stainings with endogenous Igf1r did not lead to evaluable results due to the fact that the antibodies specific for goblet cells, enteroendocrine cells and Paneth cells and specific for endogenous Igf1r were of the same host species. In addition, the establishment of a new purchased antibody for endogenous Igf1r did also not lead to feasible results. In contrast, double stainings with exogenous IGF1R induced by *IGF1R* overexpression could successfully be performed in IGF1R-oe Villin-TRE-IGF1R mice.

A concordant staining could not be observed for IGF1R with mucin2, CHGA or lysozyme, indicating that neither goblet cells, nor enteroendocrine cells nor Paneth cells overexpressed IGF1R in Villin-TRE-IGF1R mice (see chapter 3.6). Double staining experiments of the IGF1R and Ki 67 as a marker for proliferating cells did not precede to suitable results. Nevertheless, proliferating cells as the cell type overexpressing the IGF1R could be excluded since IGF1R expression was prevalently observed at the tips of the crypts and in the villi (see chapter 3.6), whereas proliferation is known to occur at the base of the crypts (Medema and Vermeulen 2011). In addition, enterocytes could also be excluded to be the cell type overexpressing the IGF1R, because enterocytes are known to be arranged as a monolayer (Overeem *et al.* 2016) and represent the vast majority of epithelial cells in the intestine (Ye *et al.* 1998; Gerbe *et al.* 2012), which was not comparable to the IGF1R overexpression pattern seen in the fluorescence stainings of the present study. Hence, these facts led to the question which cell type overexpressed the IGF1R. Although seven different cell types have been described in the intestinal epithelium, the three cell lineages of microfold (M) cells, cup cells and tuft cells are often not considered (Gerbe *et al.* 2012). Of note, these three cell types were also not considered in the present study and still remain as candidates of cells overexpressing the IGF1R.

Altogether, these results raised several questions:

1. Why did we observe different expression patterns for villin expression and IGF1R overexpression despite the fact that the villin promoter guides IGF1R overexpression?
2. Does the IGF1R promote cell proliferation and inhibit cell differentiation in the colon as can be seen in the small intestine?
3. Which epithelial cell type of the intestine overexpressed the IGF1R?
4. Was the villin promoter the accurate promoter for the present study?

These questions show that further experiments are needed to analyze if *IGF1R* overexpression and the *Igf1r* knockout, respectively, affect cell proliferation and epithelial cell differentiation, and to identify the epithelial cell type overexpressing the IGF1R. A detailed discussion about the villin promoter and the question if the villin promoter was the accurate promoter for the guided *IGF1R* overexpression and the *Igf1r* knockout in the murine intestine can be found in chapter 4.5.

4.4 The role of the IGF1R in carcinogenesis

Carcinogenesis is defined as tumor / cancer formation and requires the conversion of benign, hyperplastic cells to malignant cells (Holland *et al.* 2003). The hallmarks of cancer comprise eight biological features that enable the tumor to grow and metastasize, namely sustaining proliferative signaling, evading growth suppressors, activating invasion and metastasis, enabling replicative immortality, inducing angiogenesis, resisting cell death, reprogramming of energy metabolism and evading immune destruction (Hanahan and Weinberg 2000, 2011). There is strong experimental and clinical evidence that the IGF1R is involved in neoplasia (Pollak 2008). In general, the IGF1R is crucial for cell proliferation and differentiation (Zhang *et al.* 2013). *In vivo,* it could be shown that the Igf1r and its ligands control approx. 70% of murine embryonal growth. Mouse embryos with disrupted *Igf1r* and *Igf-2* genes were at birth only 30% of the size of wild type littermates. Cells derived from the *Igf1r* knockout embryos grew at a lower rate compared to cells derived from wild type mice. However, these growth deficits could be abrogated by transfection of the cells with wild type *Igf1r* cDNA, indicating that the Igf1r is important for cell growth. Even more interestingly is the fact that cells derived from the *Igf1r* knockout mice could not be transformed by the SV40 T antigen or the *ras* oncogene. However, transfection of these cells with a plasmid expressing wild type *Igf1r* cDNA abolished this transformation defect, indicating that the Igf1r is obligatory for transformation (Baserga 1995). Furthermore, Coppola *et al.* (1994) even proved that cells derived from the *Igf1r* knockout mice, which overexpress the human *EGFR*, were unable to grow and could not be transformed, and that the mitogenic and transforming potential of EGFR was restored by transfection with wild type Igf1r, indicating that also other growth factor receptors are dependent on Igf1r. In addition, a correlation between an increase in apoptosis and decreasing levels of Igf1r was observed *in vivo,* revealing the anti-apoptotic potential of the Igf1r (Resnicoff *et al.* 1995). Additionally, it could be shown that *IGF1R* overexpression in NIH 3T3 cells resulted *in vitro* in anchorage-independent growth and promoted *in vivo* tumor formation in nude mice (Kaleko *et al.* 1990). Interestingly, in humans, *IGF1R* is well known to be overexpressed in a variety of malignancies, including hepatocellular carcinoma (Höpfner *et al.* 2006), pancreatic, gastric and esophageal cancer (Shiratsuchi *et al.* 2011), breast cancer (Jones *et al.* 2007) and colorectal cancer (Garrouste *et al.* 1997; Freier *et al.* 1999; Hakam *et al.* 1999; Fürstenberger and Senn 2002; Reinmuth *et al.* 2002; Adachi *et al.* 2009;

Shiratsuchi *et al.* 2011; Li 2013; Zhang *et al.* 2013). A correlation of IGF1R expression and tumor stage (Hakam *et al.* 1999), tumor size and depth of invasion (Shiratsuchi *et al.* 2011) were proven. Adachi *et al.* (2009) observed that a dominant-negative inhibitor for IGF1R reduced the invasiveness of three gastrointestinal cancer cell lines by suppression of the matrix metalloproteinase matrilysin, which function is the proteolytic degradation of the extracellular matrix. Furthermore, studies demonstrated that the IGF1R / Igf1r also plays a role in angiogenesis and metastasis. Human colon cancer cells transfected with truncated IGF1R revealed strongly impaired induction of VEGF expression. *In vivo*, KM12L4 colon cancer cells transfected with the truncated IGF1R showed significantly reduced growth, decreased proliferation and importantly, decreased blood vessel formation and failure to form liver metastases (Reinmuth *et al.* 2002). In addition, lymphatic vessel density was found to positively correlate with the IGF1R expression level and lymphatic metastasis, indicating that the IGF1R induced lymphangiogenesis and thus promoted lymph node metastasis of CRC (Li 2013).

Of note, Carboni *et al.* (2005) demonstrated that constitutively active *IGF1R* in transgenic mice resulted in the development of salivary and mammary adenocarcinomas. They generated a novel mouse model that overexpressed a constitutively active receptor constructed by the fusion of the cytoplasmic sequence of the human *IGF1R* to the extracellular and transmembrane sequences of the human T-cell antigen CD8α under the control of the mouse mammary tumor virus (MMTV) promoter. In addition, Jones *et al.* (2007) proved that the exclusive overexpression of the *IGF1R* was even sufficient for the induction of mammary tumor formation *in vivo*. These authors generated a transgenic mouse line that contained the human *IGF1R* cDNA under a doxycycline-inducible TRE promoter and the transactivator protein rtTA2 under the control of the MMTV promoter. Induction of *IGF1R* overexpression by administration of doxycycline over the drinking water resulted in mammary epithelial hyperplasia and the formation of palpable mammary tumors (Jones *et al.* 2007).

These findings of Jones *et al.* (2007) led to the hypothesis that *IGF1R* overexpression is also sufficient to induce intestinal tumor formation. To verify this hypothesis, transgenic mice that contained the human *IGF1R* cDNA under the doxycycline-inducible TRE promoter and the transactivator protein rtTA2-M2 under the villin promoter were generated in the present study (Villin-TRE-IGF1R mice). Administration of doxycycline over the drinking water induced the overexpression of *IGF1R* in particular epithelial cells of the intestine. In contrast to the results obtained by

Jones *et al.* (2007), tumor formation in the intestine was not observed in the present study. Even after 1.5 years of continuous doxycycline administration, the IGF1R-oe mice had not developed any tumors, indicating that in contrast to mammary tumor formation, *IGF1R* overexpression seems not to be sufficient to induce intestinal tumor formation. However, in contrast to El Marjou *et al.* (2004) who proved villin-guided expression of the cre recombinase in all epithelial cells of the intestine, in the present study villin-guided IGF1R overexpression was only observed in particular epithelial cells of the intestine (see chapter 4.3). This fact could also contribute to the finding that IGF1R overexpression *per se* did not induce colonic tumor formation and raised the question if the villin promoter was the accurate promoter for the present study.
Altogether, these results indeed disproved the hypothesis of *IGF1R* overexpression being sufficient for intestinal tumor formation, but led to the suggestion that the IGF1R might promote intestinal tumor progression. To investigate the role of IGF1R / Igf1r during colonic tumor progression, the well-established AOM- and AOM / DSS-based CRC models were used.

4.4.1 Chemical induction of colonic tumor formation

Among several naturally mutant or genetically modified rodent models, which are predominantly used to study hereditary CRC and which will be discussed later (see chapter 4.5.3), inducible tumor models to study non-hereditary tumor development exist (Neufert *et al.* 2007). Azoxymethane (AOM) is a specific colon carcinogen that is used to mimic sporadic CRC (Bissahoyo 2005; Rosenberg *et al.* 2008). Of note, AOM itself is not the final carcinogenic metabolite, it is rather a pro-carcinogen that requires metabolic activation (Neufert *et al.* 2007; Rosenberg *et al.* 2008). The first step of metabolism is the conversion of AOM to methylazoxymethanol (MAM) by hydroxylation catalyzed by CYP2E1 in the liver, which is an alcohol-inducible cytochrome P-450 isoform (Sohn *et al.* 2001; Rosenberg *et al.* 2008). MAM, which is an unstable compound that spontaneously decomposes to formaldehyde and methyldiazonium, is transported to the colon *via* the bloodstream (Rosenberg *et al.* 2008). Methyldiazonium is responsible for the alkylation of guanine and thymine and thereby facilitates base mispairings, which, if not repaired, result in initiation of tumorigenesis (Sohn *et al.* 2001; Neufert *et al.* 2007). Bissahoyo (2005) performed mouse experiments to standardize AOM treatment. They revealed significant dose- and strain-dependent susceptibility to

AOM, and predicted 10 mg AOM per kg body weight as the standard dose that is maximal tolerated for tumor induction. They showed four weekly intraperitoneally treatments as the best route of administration, and did not observe any sex-dependent differences. They revealed that AOM is not only a tumor initiator, but also a tumor promoter. Interestingly, AOM-induced tumors were predominantly found in the distal colon, which is also the predominant localization in humans. Furthermore, the tumors were pathologically similar to sporadic CRC in humans (Bissahoyo 2005; Neufert *et al.* 2007). In addition, AOM-induced tumors also mirrored human CRC at the molecular level. As already described, mutations in the tumor suppressor gene *APC* occur early during colorectal tumorigenesis (see chapter 1.2.1 and Powell *et al.* 1992) and were predicted to be the initiating events in the development of CRC (Maltzman *et al.* 1997). *APC* is known to be mutated in more than 70% of sporadic cancers (Kheirelseid *et al.* 2013). Maltzman *et al.* (1997) investigated the role of Apc in murine colorectal tumors induced by AOM by immunofluorescence staining of Apc. They observed Apc staining in the small intestine and in the colon. Interestingly, Apc staining was absent in 96.7% of the analyzed adenomas and carcinomas induced by AOM, indicating that wild type Apc is lost in AOM-induced colonic tumors, which mirrors the situation in human CRCs (Maltzman *et al.* 1997).

Fifty percent of human colonic tumors that carry an intact *APC* gene reveal mutations of the *β-catenin* gene at codons 33, 41 and 45 leading to constitutive transcriptional activation (Takahashi *et al.* 2000b). Analyzing ten murine colonic tumors induced by AOM revealed that all tumors had mutations in the *β-catenin* gene at codons 33, 34, 37 and 41 (Takahashi *et al.* 2000b).

Cyclin D1 is a positive regulator of cell cycle progression. Cyclin D1 forms a complex with Cdk4 and Cdk6, which regulate the progression of the G_1 phase and the G_1 / S phase transition. Overexpression of cyclin D1 was found in human colon cancer and concurrent overexpression of cyclin D1 and Cdk4 was reported in adenomatous polyps of the human colon (Wang *et al.* 1998). Interestingly, examination of AOM-induced murine tumors revealed a significant increase in *cyclin D1* and *Cdk4* mRNA levels compared to control colonic tissue (Wang *et al.* 1998).

The *K-RAS* oncogene was also proven to play a role during the development of human CRC as described earlier (see chapter 1.2.1). In humans, mutations of *K-RAS* have been reported in 50% of CRCs (Luceri 2000). Takahashi *et al.* (2000a) investigated *K-ras* gene mutations in tumors induced by AOM in F344 rats and found that *K-ras*

gene mutations were as frequent in rat colonic carcinogenesis induced by AOM as in human CRCs.

In addition, Takahashi *et al.* (2000a) observed elevated levels of inducible nitric oxide synthase (iNOS) and cyclooxygenase (COX)-2 in rat colon adenocarcinomas induced by AOM. Interestingly, expression of *iNOS* and *COX-2* are known to be often increased in human colon tumors.

Thus, the AOM-based model is a suitable tool to analyze sporadic CRC and advantages of AOM-induced carcinogenesis are for example high potency, simple route of administration, low price and the comparability to human colonic tumors at the molecular level. However, one major disadvantage is the lack of invasiveness and the rareness of metastases (Neufert *et al.* 2007).

In addition to the AOM-based tumor model, which mimics sporadic human CRC, a colitis model based on dextran sodium sulfate (DSS) exists (Tanaka *et al.* 2003). DSS is a pro-inflammatory reagent with highly variable molecular weight that is extremely toxic to the epithelial lining of the colon, leading to severe colitis with bloody diarrhea (Neufert *et al.* 2007; Perše and Cerar 2012). Since the DSS model is known to reflect clinical and histopathological features seen in human chronic colitis (Perše and Cerar 2012), this model is particularly used to study tumor progression driven by chronic colitis, which is known to be the case in ulcerative colitis and Crohn's disease (Neufert *et al.* 2007). In rodents, DSS is given over the drinking water (Neufert *et al.* 2007). The response of mice to DSS highly varies and was predicted to be dependent on e.g. the molecular weight of DSS, DSS concentration and the duration of DSS administration, but also on the strain and the sex of the mice (Perše and Cerar 2012). Analyses of uptake and tissue distribution revealed that DSS penetrates the mucosal membrane in the intestine, and that DSS was mainly detected in the liver Kupffer cells and in macrophages in the mesenteric lymph node and colon (Kitajima *et al.* 1999). A disadvantage of this colitis model based on DSS is the fact that a long period or repeated administration of DSS is needed to induce colitis or colitis-associated CRC, and that the incidence of induced tumors is relatively low (Tanaka *et al.* 2003). Tanaka *et al.* (2003) developed a new mouse model based on the combination of AOM and DSS. This model for colitis-associated cancer consists of a single intraperitoneal administration of 10 mg AOM per kg body weight and a one-week administration of 2% DSS over the drinking water. In week 20, colonic adenocarcinomas with 100% incidence and adenomas with 38% incidence with the presence of dysplasia and

colitis with mucosal ulceration have developed. Examination of the developed tumors by immunohistochemistry and immunofluorescence stainings revealed that all of the induced colonic adenocarcinomas were positive for β-catenin, COS-2 and iNOS, but were negative for p53 (Tanaka *et al.* 2003).

4.4.2 The IGF1R promotes progression of colonic tumors induced by AOM and AOM / DSS

The present study revealed that *IGF1R* overexpression did not result in the induction of colonic tumor formation *per se*, indicating that *IGF1R* overexpression is not the initiating event for intestinal tumorigenesis. However, *IGF1R* overexpression might play a role during colonic tumor progression. For the verification of this hypothesis, *IGF1R* overexpressing (IGF1R-oe) and *Igf1r* knockout mice (Cre^{+}/$Igf1r^{fl/fl}$) were treated with AOM and AOM / DSS, respectively, to induce colonic tumor formation and inflammation. To screen for colonic tumors, colonoscopy was regularly performed. Macroscopic and histopathologic analyses were performed to examine if the IGF1R / Igf1r influences tumor growth and progression.

Four weekly repeated intraperitoneal injections in IGF1R-oe and control Villin-TRE-IGF1R mice with 10 mg AOM per kg body weight revealed colonic tumor formation within 35 weeks. Thirty-five weeks after the first AOM injection mice were sacrificed and tumor growth and progression were analyzed. The average colon length, which is used as an indicator for acute intestinal inflammation (Ito *et al.* 2006), revealed no significant differences between IGF1R-oe and control mice (see chapter 3.10), indicating that *IGF1R* overexpression did not influence the susceptibility of the mice to AOM. Remarkably, the incidence for tumor formation of IGF1R-oe mice with approx. 55% was twice the incidence of control mice with approx. 27%, indicating that *IGF1R* overexpression promotes tumor formation. Strikingly, an extreme female preference for tumor development was observed since only female IGF1R-oe and control mice showed any tumor formation. This finding was strongly contradictory to the observations of Bissahoyo (2005), who did not observe any sex-dependent responses of mice to AOM. Of note, in the present study only five control males and even only one IGF1R-oe male mouse were included. To investigate if female Villin-TRE-IGF1R mice are indeed more sensitive to AOM, further studies with a higher number of animals have to be performed. Additionally, Bissahoyo (2005) observed

strong strain-dependent responses to AOM in AKR/J, SWR/J and A/J mouse strains, and Nambiar *et al.* (2003) reported that FVB/N mice showed a remarkable susceptibility to AOM, whereas C57BL/6J mice revealed low sensitivity to AOM. Since Villin-TRE-IGF1R mice were a crossing between the C57BL/6 and the FVB mouse strains, the observed sex-dependent responses to AOM could additionally depend on the mouse strain. A prevalence of tumor occurrence in the distal part of the colon was observed in the present study, whereas no tumor formation was seen in the proximal part. These observations are consistent with reports of other researchers (Nambiar *et al.* 2003; Bissahoyo 2005; Neufert *et al.* 2007). Impressively, this finding mirrored human sporadic CRC since human tumors are predominantly localized in the distal part of the colon (Neufert *et al.* 2007). IGF1R-oe mice revealed tumors with an increase in the average tumor size of approx. 23% compared to control mice. Strikingly, in contrast to control mice, one IGF1R-oe mouse even developed an intramucosal and invasive adenocarcinoma, indicating that IGF1R promotes colonic tumor progression and even tumor cell invasion.

Furthermore, remarkable results were also obtained using the AOM / DSS model. Villin-TRE-IGF1R mice were intraperitoneally injected with 10 mg AOM per kg body weight and administered to two cycles of 2% DSS to induce colonic tumor formation and inflammation. Twelve weeks after AOM injection, several IGF1R-oe and control mice had developed tumors of a score of four to five (Becker *et al.* 2007). No difference concerning tumor initiation was observed between IGF1R-oe and control mice. The Villin-TRE-IGF1R mice revealed no sex-dependent responses to AOM / DSS, which was oppositional to the observations in AOM-only-treated Villin-TRE-IGF1R mice. Again, tumors were found to be predominantly localized in the distal part of the colon, which reflects the feature of human sporadic CRC. Histopathologically, control mice showed a reduced number of tumors with advanced stage, whereas IGF1R-oe mice developed an elevated number of intramucosal and even invasive adenocarcinomas. Additionally, tumors of IGF1R-oe mice exhibited a 66.2% increased average tumor size compared to control mice, indicating that the IGF1R influenced tumor progression. In order to analyze if IGF1R overexpression even promotes metastasis, liver tissues and lymph nodes in regional colonic fat tissue were examined for the presence of CRC cells. Metastases were not found, which was consistent with observations of other groups (Nambiar *et al.* 2003; Neufert *et al.* 2007). Remarkably, activating invasion and metastasis is one of the eight biological features of cancer cells (Hanahan and

Weinberg 2000, 2011). It could be shown that transfection of the human MDA-MB-435 metastatic breast cancer cells with a dominant negative form of the *IGF1R* inhibited cellular adhesion to laminin and collagen. *In vivo*, injection of MDA-MB-435 cells transfected with the dominant negative form of the *IGF1R* did not suppress primary tumor growth, but significantly decreased metastasis to the lungs, livers and lymph nodes, demonstrating that the IGF1R plays a crucial role in adhesion, invasion and metastasis of breast cancer (Dunn *et al.* 1998). Furthermore, injection of the human CRC cell line HCT116 overexpressing the *IGF1R* into nude mice resulted in highly invasive tumors and the development of distant metastases whereas the implantation of parental HCT116 cells did not (Sekharam *et al.* 2003). To study CRC colonization, Nguyen *et al.* (2016) performed a large-scale *in vivo* RNAi screen and identified the IGF1R as a driver of metastatic liver colonization (Nguyen *et al.* 2016). In addition, a positive correlation of IGF1R expression and the lymph node status as well as the UICC stage was shown in a study of 120 rectal cancer patients (unpublished data of the working group). Consistent with these findings are the observations of the present study. Here, only IGF1R-oe mice formed invasive carcinomas after AOM / DSS administration, whereas control mice did not, pointing to the IGF1R as being essential for CRC cells to grow in an invasive manner and clearly indicating that *IGF1R* overexpression strongly promotes colonic tumor invasiveness. Despite the fact that IGF1R-oe mice developed invasive carcinomas, metastatic cells in the liver and lymph nodes in regional colonic fat tissue examined were not detected. The fact that AOM / DSS-induced tumors are known to rarely exhibit metastases (Thaker *et al.* 2012) or the assumption that the tumors grew too fast might be the reasons for this finding. To investigate if *IGF1R* overexpression affects metastasis of CRC cells, another CRC model in which metastasis is common would be needed.

Interestingly, western blot analysis revealed that AKT (pAKT) was highly activated, whereas ERK activation (pERK) was reduced in tumors induced by AOM / DSS in IGF1R-oe mice compared to control mice. Furthermore, the activation level of the PI3K signaling pathway was elevated in tumors derived in IGF1R-oe mice compared to the intestinal epithelial cells. These facts indicated that tumor progression was mediated *via* the PI3K signaling pathway rather than the MAPK signaling pathway. Deregulated AKT is known to contribute to the development and progression of cancer. Some investigations have demonstrated that elevated AKT activity was predominantly found in high grade, late stage and metastatic breast and ovarian tumors, whereas other

researchers did not find a correlation between elevated AKT activity and tumor stage or grade (Altomare and Testa 2005). Interestingly, Itoh *et al.* (2002) performed immunohistochemical analyses on a total of 65 human colorectal carcinomas and observed a significant correlation of AKT activity with several clinicopathological parameters, such as depth of invasion, venous vessel infiltration, tumor stage and lymph node metastasis. Furthermore, the AKT phosphorylation level was found to significantly correlate with the Ki 67 growth index. These findings indicate that AKT activation is associated with the progression of colorectal carcinomas by promoting tumor cell growth (Itoh *et al.* 2002). In the present study, AKT activity was increased in AOM / DSS-induced colonic tumors derived in IGF1R-oe mice compared to control mice (see chapter 3.14), predicting that *IGF1R* overexpression and thus activation of AKT might promote colonic tumor progression. These findings were consistent with observations of Saglam *et al.* (2007) who stained 99 human invasive colorectal carcinomas, 28 tubular colorectal adenomas and 18 samples of normal colonic mucosa with a monoclonal antibody against phospho-AKT. They found AKT activity predominantly in the invasive carcinomas, whereas 78% of normal colonic mucosa was pAKT negative, demonstrating increasing activation of AKT during CRC progression (Saglam *et al.* 2007). In the present study, western blot analysis was only performed on a small number of tumors and tumors examined were not discriminated regarding their stage. To clearly prove a correlation of AKT activity and colonic tumor progression, western blot analysis should be repeated with a higher number of tumor samples. Furthermore, the tumors should be discriminated regarding their stage to compare AKT activity between colorectal adenomas and carcinomas. Additionally, immunohistochemical stainings of low and high grade intraepithelial neoplasias and intramucosal and invasive carcinomas with an antibody against pAKT would also contribute to the clarification if increased AKT activity due to *IGF1R* overexpression is associated with CRC progression.

Analyses of the tumors induced by AOM / DSS and also by AOM at the molecular level are lacking in the present study and should be performed in order to investigate the influence of IGF1R on e.g. the *K-ras* and *β-catenin* mutation status.

Interestingly, AOM was shown to be a potent tumor promoter in addition to its role as a tumor initiator (Bissahoyo 2005). For this reason one could claim that not IGF1R but rather AOM is responsible for the tumor growth promoting effects observed in IGF1R-oe mice after AOM and AOM / DSS administration. Since not only

IGF1R-oe mice, but also control mice were treated with AOM and AOM / DSS in the present study, the increasing tumor size and the presence of even intramucosal and invasive adenocarcinomas in IGF1R-oe mice can be referred to *IGF1R* overexpression and not to AOM treatment. Furthermore, Nanda *et al.* (2016) reported recently that doxycycline enhanced the efficacy of DMH (metabolic precursor of AOM and MAM) in tumor progression, indicated by stimulated progression of colonic tumor growth from adenomas to adenocarcinomas. This finding could argue against the results of the present study since *IGF1R* overexpression in Villin-TRE-IGF1R mice was induced by continuous administration of doxycycline over the drinking water. Importantly, in this experiment not only the IGF1R-oe mice but also the control mice were administered to doxycycline. The control group consisted of mice that carried only the Villin-rtTA2-M2 transgene, but not the TRE-IGF1R transgene and thus were impotent for the induction of *IGF1R* overexpression by doxycycline administration. Thus, the tumor growth promoting effects observed were the effect of *IGF1R* overexpression rather than the effect of doxycycline treatment.

In order to prove the hypothesis that the Igf1r is essential in intestinal tumor development, Villin-CreERT-Igf1r mice were treated with both, AOM and AOM / DSS, to induce colonic tumor formation and inflammation, respectively. In the AOM-only setting, the time points of tumor formation strongly differed between individual mice regardless of their *Igf1r* status. There was no difference in tumor initiation between $Cre^{+}/Igf1r^{fl/fl}$, $Cre^{+}/Igf1r^{fl/+}$ and control mice, indicating that the Igf1r is not essential for tumor development as seen in cell culture models (Reinmuth *et al.* 2002; Sachdev *et al.* 2004). Since only a small number of mice was used for the AOM-only setting and no difference in tumor initiation was observed between $Cre^{+}/Igf1r^{fl/fl}$, $Cre^{+}/Igf1r^{fl/+}$ and control mice, the AOM-based experiment was not continued.

Treatment of Villin-CreERT-Igf1r mice with AOM / DSS resulted in the development of tumors within seven weeks after AOM injection, pointing to a strong susceptibility of C57BL/6 to AOM / DSS. Interestingly, C57BL/6 mice are known to be less sensitive to AOM (Nambiar *et al.* 2003; Neufert *et al.* 2007), whereas these mice are relatively susceptible to DSS (Suzuki *et al.* 2006). This shows that the AOM / DSS model even enables tumor growth in mouse strains that possess lower sensitivity to AOM (Neufert *et al.* 2007). Measurement of the colon length as an indicator for acute intestinal inflammation revealed no significant differences between $Cre^{+}/Igf1r^{fl/fl}$ and control mice (see chapter 3.24), indicating that the Igf1r rather than inflammation is responsible for

the observed differences between Cre$^+$/*Igf1r*$^{fl/fl}$ and control mice. As in the AOM-only setting, the AOM / DSS-based setting exhibited no hint that *Igf1r* expression in the intestine is essential for the development of tumors, i.e., both Cre$^+$/*Igf1r*$^{fl/fl}$ and control mice developed tumors to a high extent (81% vs. 92%). A slight preference for tumor development was observed in female mice (100% (in both Cre$^+$/*Igf1r*$^{fl/fl}$ and control mice) vs. 80% (male control mice) and 67% (male Cre$^+$/*Igf1r*$^{fl/fl}$ mice)). Cre$^+$/*Igf1r*$^{fl/fl}$ and control mice revealed only a slight difference in the number of developed tumors, but histopathological analyses showed that Cre$^+$/*Igf1r*$^{fl/fl}$ mice developed an elevated number of high grade intraepithelial neoplasias and a reduced number of intramucosal and invasive adenocarcinomas compared to control mice. These findings support the prediction of IGF1R / Igf1r being a strong promoter of colonic tumor invasiveness based on the results of the histopathological analyses of tumors derived in Villin-TRE-IGF1R mice administered to AOM / DSS. The fact that no significant difference in tumor initiation between Cre$^+$/*Igf1r*$^{fl/fl}$ and control mice was observed, but Cre$^+$/*Igf1r*$^{fl/fl}$ mice developed a decreased number of intramucosal carcinomas compared to control mice supports the hypothesis that the IGF1R / Igf1r promotes colonic tumor progression rather than tumor formation.

In addition, tumors of Cre$^+$/*Igf1r*$^{fl/fl}$ mice revealed decreased phosphorylation levels of AKT (pAKT) and thus diminished signaling *via* the PI3K signaling pathway compared to control mice. Instead, the activation level of ERK was elevated in Cre$^+$/*Igf1r*$^{fl/fl}$ mice, indicating that signaling was mediated *via* the MAPK signaling pathway. Again, these findings fit to the elevated levels of activated AKT in tumors derived in Villin-TRE-IGF1R mice after AOM / DSS administration compared to normal intestinal epithelial cells, and led to the suggestion that tumor progression promoted by *IGF1R* overexpression is mediated *via* the PI3K signaling pathway in tumors derived in Villin-TRE-IGF1R mice administered to AOM / DSS. In mice harboring the *Igf1r* knockout, signaling *via* the downstream PI3K pathway is diminished indicated by reduced AKT activation (pAKT) and thus results in inhibited progression of the colonic tumors, indicated by the reduced number of intramucosal carcinomas. Controversial is the fact that ERK activation (pERK) was highly elevated in colonic tumors derived in Cre$^+$/*Igf1r*$^{fl/fl}$ mice compared to control mice since MAPK signaling is known to be activated by RTKs and to play an important role in the progression of CRC (Fang and Richardson 2005). Since the *Igf1r* was not available in Cre$^+$/*Igf1r*$^{fl/fl}$ mice to activate the ERK cascade, and the number of intramucosal carcinomas was reduced in

Cre^{+}/*Igf1r*$^{fl/fl}$ mice compared to control mice, the result of the western blot and subsequent densitometrical analyses of ERK phosphorylation should be analyzed in more detail. It is known, that the IGF1R is not capable of activating MAPK signaling itself, instead it was shown that an active EGFR is essential in CRC cells (Kaulfuß *et al.* 2009). To clearly investigate the role of MAPK signaling in colonic tumor progression, western blot analysis with antibodies against phosphorylated ERK (pERK) and total ERK (ERK) should be performed with a high number of colonic tumors of different stages.

Again, the molecular analysis of the mutation status of e.g. *Apc* and *K-ras* is lacking in the present study. Analysis of the *K-ras* mutation status of the colonic tumors derived after AOM / DSS administration could also contribute to the clarification if MAPK signaling is involved in CRC progression since it is known that constitutively active *K-RAS* due to single nucleotide point mutations result in the activation of downstream pro-proliferative pathways (Tan and Du 2012).

In summary, the present study revealed that the IGF1R / Igf1r plays no crucial role during colonic tumor formation, and *IGF1R* overexpression is not sufficient for the induction of colonic tumor development. Instead, results of the *IGF1R* overexpression and the *Igf1r* knockout experiments of the present study impressively show that the IGF1R / Igf1r strongly promotes colonic tumor progression and that tumor progression is mediated *via* the PI3K signaling pathway.

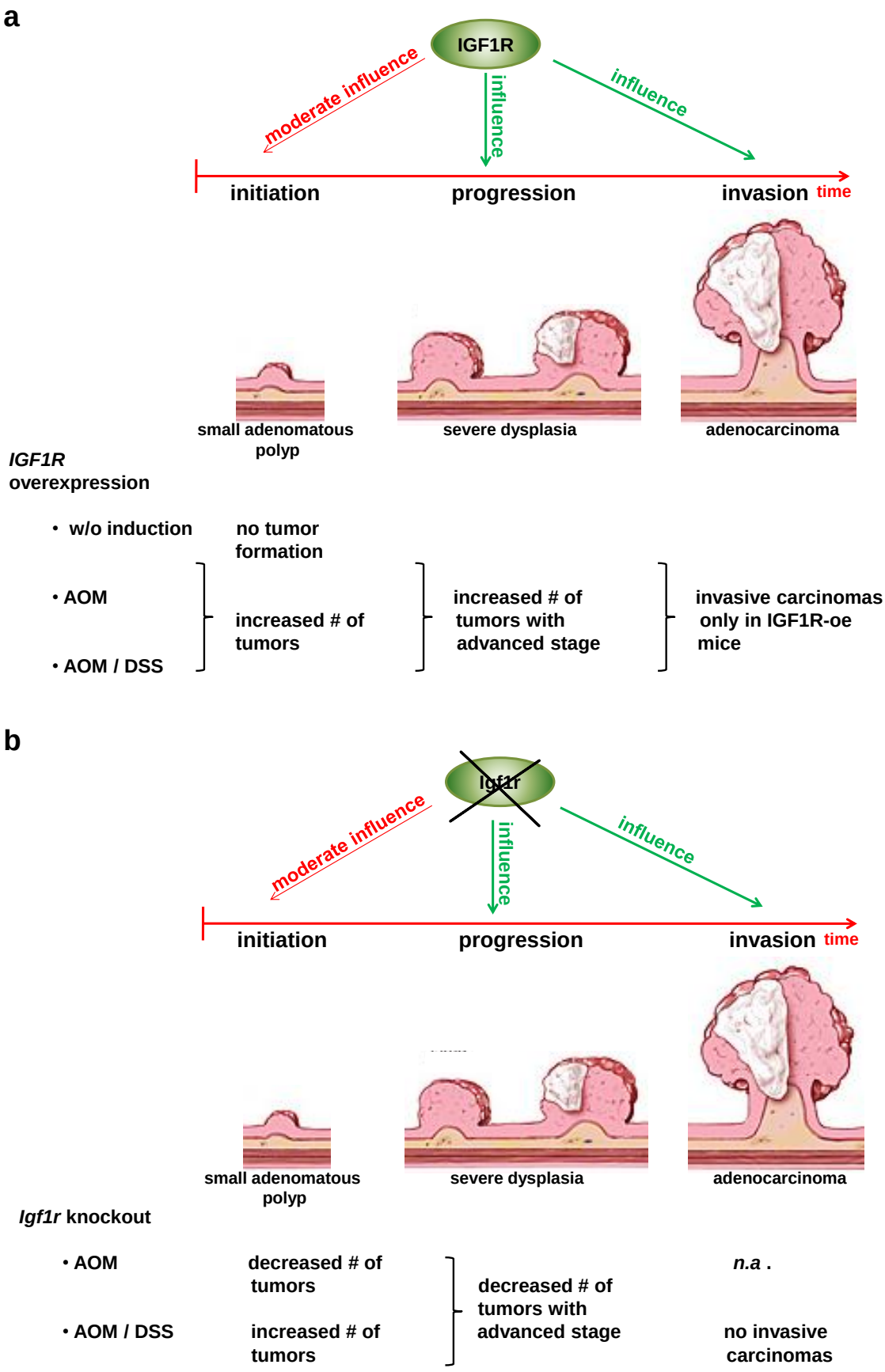

Fig. 79: Schematic overview of the influence of *IGF1R* overexpression and *Igf1r* knockout in the intestine alone or after AOM and AOM / DSS administration, respectively, on colonic tumor formation, progression and invasion compared to the particular control.

(a) *IGF1R* overexpression in the intestine alone did not induce tumor formation. *IGF1R* overexpression in the intestine after AOM and AOM / DSS administration, respectively, resulted in an increased number of tumors, demonstrating moderate influence of the IGF1R on colonic tumor initiation, an increased number of tumors with advanced stage, indicating an influence of the IGF1R on tumor progression, and in the development of invasive carcinomas, pointing to influence of the IGF1R on tumor invasion. **(b)** The *Igf1r* knockout in the intestine after AOM administration resulted in a decreased number of tumors, whereas it led to an increased number of tumors after AOM / DSS administration, indicating that the Igf1r might have a moderate influence on tumor initiation. The *Igf1r* knockout in the intestine after AOM and AOM / DSS administration, respectively, led to a decreased number of tumors with advanced stage, clearly demonstrating a role of the Igf1r on tumor progression. The effect of the *Igf1r* knockout on tumor invasion was not analyzed in the AOM-only setting, whereas no invasive carcinomas were detected in tumors derived in mice after AOM / DSS administration, indicating that the Igf1r has influence on colonic tumor invasion. #= number. *n.a.*= not analyzed. Modified after Johns Hopkins Medicine Gastroenterology & Hepatology.

4.4.3 Why does *IGF1R* overexpression in colorectal epithelial cells not induce tumor development? A comparison with the literature

Baserga (1995) proved that the Igf1r is obligatory for the transformation by the SV40 T antigen or the *ras* oncogene *in vitro*. *In vivo*, Carboni *et al.* (2005) demonstrated that constitutively activated *IGF1R* specifically in the mammary and salivary glands of transgenic mice resulted in the development of salivary and mammary adenomas and adenocarcinomas. Since Jones *et al.* (2007) showed that *IGF1R* overexpression is sufficient for the induction of mammary tumor formation *in vivo*, we expected that *IGF1R* overexpression is also sufficient to induce intestinal tumor formation *in vivo*. Against our expectation, *IGF1R* overexpression in the mouse intestine *per se* did not result in intestinal tumor development in the present study. These findings lead to the following questions:

1. Why was *IGF1R* overexpression sufficient to induce mammary tumor formation, but was not sufficient for the induction of intestinal tumor development?

2. Does the expression pattern of the two different promoters that guide *IGF1R* overexpression in the mammary gland and intestine, respectively, play a role for the successful / failed induction of tumor formation?

These questions point to the necessity of a comparison of the mouse mammary tumor virus (MMTV) promoter that directed the constitutively activated *IGF1R* expression and *IGF1R* overexpression in the mammary glands in the studies of Carboni *et al.* (2005) and Jones *et al.* (2007), respectively, and the villin promoter that controlled intestine-specific *IGF1R* overexpression in the present study.

The MMTV promoter was shown to drive transgene expression throughout the epithelium of the mammary gland (Albanese *et al.* 2000). MMTV-guided transgene expression was additionally detected in the salivary gland (Albanese *et al.* 2000), the seminal vesicle and thymus (Gunther *et al.* 2002), but not in the liver, heart, spleen, kidney, ureter, ovary or uterus (Albanese *et al.* 2000). However, the expression level of the transgene in the salivary gland, seminal vesicle and thymus were very low, confirming that MMTV-driven transgene expression was mammary gland specific (Albanese *et al.* 2000; Gunther *et al.* 2002). In addition, Gunther *et al.* (2002) proved MMTV-guided transgene expression in all stages of postnatal mammary gland development, including puberty, pregnancy, lactation and postlactational involution (Gunther *et al.* 2002).

The MMTV is an oncoRNAvirus and belongs to the *Retroviridae* family. Once activated, MMTV causes breast tumors. The predominant replication site of MMTV are the alveolar epithelial cells of the mammary gland (Taneja *et al.* 2009). These alveolar epithelial cells are functionally differentiated secretory luminal cells which form a single layer in the alveolar structures (Gajewska *et al.* 2013).

Comparing the activity of the MMTV promoter with the activity of the villin promoter reveals that both promoters are more or less tissue-specific. The MMTV promoter predominantly drives transgene expression in the mammary gland, only weak MMTV promoter-directed transgene expression was detected in the salivary gland, seminal vesicle and thymus (Albanese *et al.* 2000; Gunther *et al.* 2002). The villin promoter is mainly intestine-specific, it drives transgene expression in the small intestine and colon. However, villin-guided expression was also observed in the kidney (El Marjou *et al.* 2004; Roth *et al.* 2009). Interestingly, both promoters guide transgene expression in epithelial cells (Albanese *et al.* 2000). The MMTV promoter drives transgene expression in mammary epithelial cells, whereas the villin promoter targets intestinal epithelial cells (El Marjou *et al.* 2004; Roth *et al.* 2009). In addition, these epithelial cells are secretory cells in the mammary epithelium, namely luminal epithelial cells, and in the intestinal epithelium, namely goblet cells, enteroendocrine cells and Paneth

cells. Remarkably, villin was proven to also be active in the progenitor cells, leading to villin-guided transgene expression for more than 60 days despite the rapid renewal of the intestine (El Marjou *et al.* 2004). Interestingly, MMTV was also predicted to infect stem cells in the mammary gland (Callahan and Smith 2008), indicating that the MMTV promoter also drives transgene expression in mammary gland stem cells.

Taken together, this comparison of the MMTV promoter with the villin promoter indicated that both promoters share particular features. The only difference was their tissue-specificity. Thus, the villin promoter seemed not to be the reason for the fact that villin-guided *IGF1R* overexpression was not sufficient to induce intestinal tumor formation. This finding led again to the question why *IGF1R* overexpression induced mammary but not intestinal tumor formation. Therefore, we hypothesized that the downstream PI3K and MAPK signaling pathways, which mediate the cell to proliferate, were not activated although the *IGF1R* was overexpressed in intestinal epithelial cells. For this reason, in the present study, the expression level of IGF1R as well as of activated and total AKT and ERK, respectively, were examined in IGF1R-oe and control Villin-TRE-IGF1R mice which were additionally injected with IGF-1. *De facto*, serum IGF-1 concentration was found to be significantly higher in CRC patients compared to healthy controls. Interestingly, serum IGF-1 and mucosal *IGF1R* mRNA levels were shown to significantly correlate in CRC patients (Zhang *et al.* 2013). *In vitro,* Li (2013) demonstrated that IGF-1 promoted migration and invasion of the human CRC cell line LoVo. Furthermore, they showed that daily administration of IGF-1 to LoVo cell xenograft mice resulted in significantly higher lymphangiogenesis (Li 2013). In the present study, IGF1R-oe and control Villin-TRE-IGF1R mice were administered to doxycycline to induce *IGF1R* overexpression in the intestinal epithelium. In addition, Villin-TRE-IGF1R mice were intravenously injected with 4.8 µg human IGF-1 (GroPep, Thebarton, Australia). Afterwards, proteins of small intestinal and colonic epithelial cells were extracted and western blot analysis was performed (Fig. 80).

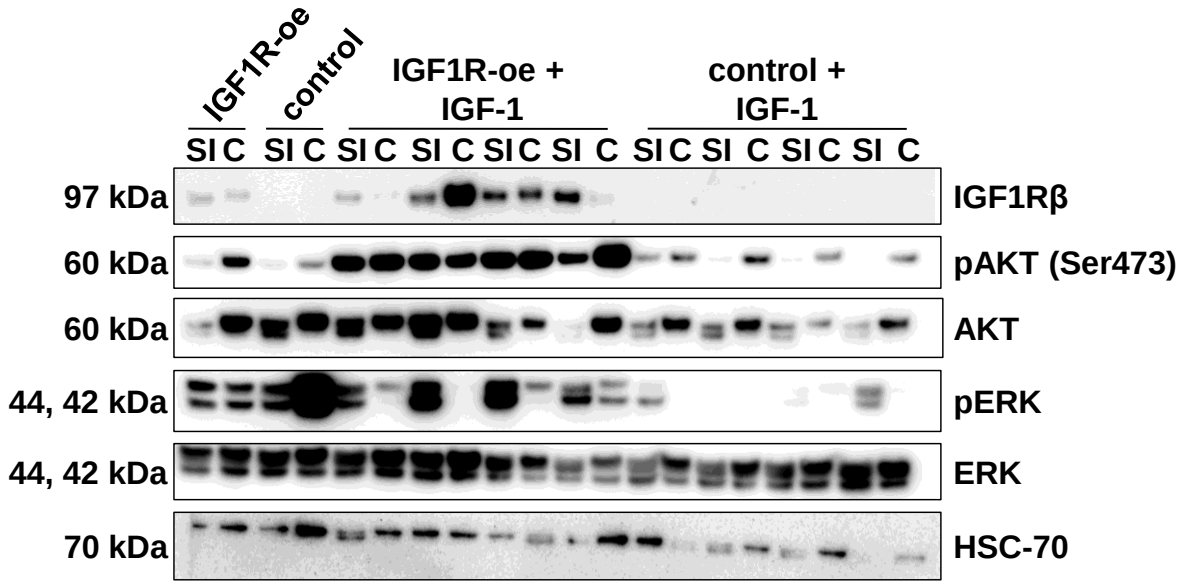

Fig. 80: Western blot analysis of epithelial cells of the small intestine and colon of Villin-TRE-IGF1R mice injected with IGF-1.

IGF1R-oe (n=4) and control (n=4) Villin-TRE-IGF1R mice were administered to doxycycline and intravenously injected with IGF-1. Immediately after IGF-1 injection, mice were sacrificed, the small intestine (SI) and colon (C) were excised from the animals and proteins were extracted from the epithelial cells. Western blot analysis was performed. IGF1R-oe mice injected with IGF-1 revealed high IGF1Rβ expression compared to control mice injected with IGF-1 as well as IGF1R-oe and control mice which were not injected with IGF-1. The AKT phosphorylation level (pAKT) is highly increased in IGF1R-oe mice injected with IGF-1. Activation of ERK (pERK) is strong in control and IGF1R-oe mice as well as in the small intestinal epithelial cells of IGF1R-oe mice injected with IGF-1. HSC-70 was used as loading control.

Interestingly, high IGF1Rβ expression was detected in IGF1R-oe mice which were injected with IGF-1, whereas control and IGF1R-oe mice not injected with IGF-1 as well as control mice injected with IGF-1 showed low or even no IGF1Rβ expression. Furthermore, AKT was highly activated (pAKT) in IGF1R-oe mice injected with IGF-1, whereas the other treatment groups revealed low phosphorylation levels of AKT. In fact, *IGF1R* overexpression was confirmed in epithelial cells of the small intestine and colon by immunohistochemical (see chapter 3.4) and immunofluorescence staining (see chapter 3.6) as well as western blot analysis (see chapter 3.5), but not only overexpression but rather activation of the IGF1R is needed for activation of the downstream signaling pathways. The finding that AKT was only highly phosphorylated in IGF1R-oe mice injected with IGF-1 could indicate that IGF1R-oe mice indeed overexpress the *IGF1R,* but that the activation of downstream PI3K signaling can be

further enhanced with elevated IGF-1-levels. Furthermore, this result could be the reason for the fact that *IGF1R* overexpression in the intestinal epithelium of IGF1R-oe mice did not result in the development of intestinal tumors. Interestingly, in the mammary glands overexpression of the *IGF1R* alone was sufficient to induce mammary tumor formation (Jones *et al.* 2007), indicating that in the mammary gland high levels of endogenous Igf, which is able to activate the overexpressed IGF1R, might be present. For this reason, analysis of the endogenous Igf-level in the intestine would be of high interest. Of note, Jones *et al.* (2007) used transgenic mice with a FVB background, whereas in the present study *IGF1R* overexpression was induced in mice with a mixed FVB and C57BL/6 background. This leads to the suggestion that the different mouse strains might display strain-dependent Igf-levels, which can influence the activity of the IGF1R.

Controversial is the finding that the phosphorylation level of ERK (pERK) is high in small intestinal and colonic epithelial cells of control and IGF1R-oe mice which were not injected with IGF-1 as well as in small intestinal epithelial cells of IGF1R-oe mice injected with IGF-1 (Fig. 80). The fact that ERK activation is low in colonic epithelial cells of IGF1R-oe mice injected with IGF-1 might also explain why *IGF1R* overexpression *per se* did not induce colonic tumor formation.

Taken together, it would be of high interest to analyze if *IGF-1* overexpression in addition to *IGF1R* overexpression in the intestine would induce colonic tumor formation. Therefore, a tri-transgenic mouse line or the continuous injection of the ligand IGF-1 is needed.

4.5 Mouse models of CRC – which model to choose?

One main aim of the present study was to analyze which role the IGF1R / Igf1r plays during the development and maintenance of the intestine, colonic tumor formation and progression *in vivo*. In order to answer these questions, a suitable mouse model had to be chosen.

4.5.1 Directing the *IGF1R* overexpression and the *Igf1r* knockout to the intestinal epithelium

In order to investigate the role of the IGF1R during intestinal development and maintenance as well as during intestinal tumor formation and progression *in vivo,* we wanted to specifically overexpress the human *IGF1R* and to knockout endogenous *Igf1r*, respectively, in the murine intestinal epithelium. For this purpose a suitable promoter had to be selected. To date, several promoters that guide transgene expression in the intestine are known. In the following chapter the different established mouse lines in which transgene expression is under the control of an intestine-specific promoter will be discussed:

Pinto *et al.* (1999) reported that a 9 kb regulatory region of the mouse *villin* gene is sufficient to direct high and tissue-specific transgene expression in epithelial cells along the crypt-villus axis in the small intestine and colon. Additionally, this region was found to maintain a gradient of transgene expression from the crypts to the tips of the villi that is precisely similar to that exhibited by the murine *villin* gene (Pinto *et al.* 1999). Madison (2002) generated a 12.4 kb variant of the regulatory region of the *villin* gene that was proven to drive high expression of two reporter genes within the entire intestinal epithelium. Both the 9 kb and the 12.4 kb promoter variants have been successfully used to generate several intestine-specific transgenic mouse models (Roth *et al.* 2009). El Marjou *et al.* (2004) generated a mouse expressing the tamoxifen-dependent cre recombinase under the 9 kb villin promoter construct and thus provided an inducible model for the tissue- and time-specific cre recombinase-mediated recombination in the intestinal epithelium. Interestingly, the recombined locus lasted, despite rapid and continuous intestinal renewal, for 60 days after tamoxifen administration, indicating that epithelial progenitor cells have been targeted (El Marjou *et al.* 2004). Roth *et al.* (2009) generated a transgenic doxycycline-inducible mouse model that expresses the rtTA2-M2 under the control of the 12.4 kb villin promoter, and proved transgene expression throughout the entire intestine from the pyloric area to the distal colon and rectum. Furthermore, expression was observed in all epithelial cells of the small intestine and colon, with decreased levels in the crypts of the small intestine and the lower half of colonic crypts, respectively (Roth *et al.* 2009). The advantage of the villin promoter is due to the fact that transgene expression is restricted to epithelial cells throughout the intestine. Only a small amount of villin expression was found in the proximal tubules of the kidney. However, the big disadvantage of the villin

promoter is the finding that transgene expression is not limited to epithelial cells of the colon, but was also observed in epithelial cells of the small intestine and in the kidney. For this reason several attempts have been performed to generate a model with a more limited expression pattern (Johnson and Fleet 2013):

Saam and Gordon (1999) generated a mouse model that expresses the rtTA under the control of transcriptional regulatory elements from the fatty acid-binding protein gene (*Fabp*) as well as the cre recombinase under the control of *tet* operator sequences. This mouse model allowed the induction of the recombination only in the intestine in the presence of doxycycline. Upon doxycycline administration, recombination occurred in the small intestinal, cecal and colonic epithelium. The recombined locus was shown to persist for at least 60 days after doxycycline withdrawal, indicating that recombination has occurred in the intestinal epithelial progenitor cells (Saam and Gordon 1999).

Means *et al.* (2008) generated the so called *K19*^{CreERT} mouse in which the tamoxifen-dependent CreER^{T} was knocked into the endogenous cytokeratin 19 locus. *K19* is known to be highly expressed in the ducts of the adult pancreas and of the liver. The *K19*^{CreERT} mouse revealed recombination in epithelial cells of pancreatic and hepatic ducts, the stomach and the intestine (Means *et al.* 2008).

Barker *et al.* (2007) generated a tamoxifen-inducible mouse in which expression of the lacZ reporter was under the control of Lgr5-expressing cells. Therefore, they integrated the enhanced green fluorescent protein (EGFP)-IRES-creERT2 cassette into the first exon of the *Lgr5* gene. Subsequently, they crossed the EGFP-IRES-creERT2 knock-in allele with the cre-activatable Rosa26-lacZ reporter strain. Thus, by injecting tamoxifen the CreER^{T2} fusion protein was activated in Lgr5-expressing cells. They found lacZ expression at the typical CBCC position, indicating that Lgr5-positive cells are the small intestinal and colonic stem cells (Barker *et al.* 2007). However, *Lgr5* was further found to be expressed in e.g. hair follicle and mammary glands and is therefore a more general marker of adult stem cells rather than an intestine-specific stem cell marker (Barker *et al.* 2007; Johnson and Fleet 2013).

Hinoi *et al.* (2007) generated a mouse that drives cre recombinase expression under the CDX2P-NLS promoter and that carries a *loxP*-modified *Apc* allele. The human *CDX2* homeobox gene is known to be expressed in epithelial cells throughout the adult small intestine and colon. They found that mice carrying the

CDX2P-NLS Cre recombinase transgene and a floxed *Apc* allele develop colorectal adenomas and even carcinomas in approx. 15 to 20% of mice. Unfortunately, they observed β-gal reporter expression in the tail bud and caudal part of the neural tube in *CDX2P-NLS Cre* recombinase transgenic embryos, whereas transgene expression was limited to distal small intestine, cecum, colon and rectum in adult mice. Furthermore, they also found tumor development in the small intestine and predicted that the small intestinal tumor burden inhibits the development and progression of colorectal tumors in the mouse (Hinoi *et al.* 2007).

Xue *et al.* (2010) generated a transgenic mouse in which cre recombinase expression is restricted to epithelial cells of the colon. Therefore, a 10.6 kb colon-specific promoter and a 2.5 kb erythroid / colon enhancer fragment of the mouse carbonic anhydrase 1 (*mCA1*) gene, which is conserved between mouse and human, were used to drive cre recombinase expression (*CAC*). They found transgene expression limited to epithelial cells of the colon. Afterwards, the *CAC* mice were crossed with APC^{580S} mice (see chapter 4.5.3), which carry *loxP* sites flanking the introns 13 and 14 of the *Apc* gene, to generate heterozygous ($CAC;APC^{580S/+}$) and homozygous ($CAC;APC^{580S/580S}$) *Apc* knockout mice, and observed adenomas predominantly in the distal part of the colon. However, carcinomas were not detected in this mouse model (Xue *et al.* 2010).

In the present study, the villin promoter was chosen to drive intestinal-specific *IGF1R* overexpression and the *Igf1*r knockout, respectively. As previously described, several intestine-specific promoters are known, leading to the question if the villin promoter is the accurate promoter to drive transgene expression in the present study.

The main advantage of the villin promoter is the fact that it is known to drive stable and homogeneous expression of transgenes in all epithelial cells of the small intestine and colon along the crypt-villus axis (El Marjou *et al.* 2004). However, this advantage could be interpreted at the same time as a disadvantage since tumor development occurs predominantly in the distal colon and rectum in human sporadic CRC and familial adenomatous polyposis (FAP). In addition, the villin promoter was found to be active in the putative undifferentiated stem cell compartment of the intestinal epithelium (El Marjou *et al.* 2004; Roth *et al.* 2009). This fact is a big advantage of the villin promoter, because it was shown that villin-guided transgene expression thus lasted for more than 60 days (El Marjou *et al.* 2004) despite the remarkable constant and rapid renewal capacity of intestinal epithelial cells (Bustos-Fernández 1983; Medema and

Vermeulen 2011). If transgene expression is directed by a promoter that is only active in differentiating epithelial cells in the intestine, the recombination efficacy could become too low due to the loss of differentiating epithelial cells during intestinal renewal (El Marjou *et al.* 2004). A general disadvantage of the villin promoter is the fact that it also drives transgene expression in the proximal tubules of the kidney (Roth *et al.* 2009), indicating that the villin promoter is not intestine-specific. In addition, villin-guided transgene expression was observed to be stronger in the differentiated cells compared to cells of the crypts in the small intestine and cells of the lower half of the crypts in the colon (El Marjou *et al.* 2004; Roth *et al.* 2009). Regarding the present study, this finding is a big disadvantage of the villin promoter since endogenous Igf1r reveals an opposing expression pattern with high expression in the crypts of the small intestine and at the bottom of the crypts of the colon and low expression in the villi of the small intestine and at the tip of the crypts of the colon (see chapter 4.3). These opposing expression gradients of villin and endogenous Igf1r lead to the assumption that the *Igf1r* knockout may be impaired in the crypts because villin expression is low (for detailed discussion see chapter 4.5.2). Furthermore, also *IGF1R* overexpression is suggested to be not optimal, because villin-guided ectopic IGF1R is predominantly expressed in the villi of the small intestine and at the tip of the colonic crypts (see chapter 3.6), whereas endogenous Igf1r is mainly expressed in the crypts of the small intestine and at the bottom of the colonic crypts (see chapter 4.3). Thus, villin-guided ectopic IGF1R expression reveals a different localization compared to endogenous Igf1r expression, which might have influenced the results of the present study.

Comparison of the villin promoter with the other described promoters shows that also the other promoters exhibit advantages and disadvantages. The main advantages and disadvantages of the different promoters are summarized in table 2. The advantage of the Fabp promoter is that it also targets the progenitor cells of the intestine, leading to recombination that lasts for more than 60 days, which was also shown for the villin promoter. The disadvantage of the Fabp promoter is that it drives transgene expression in the small intestine, cecum and colon (Saam and Gordon 1999). Transgene expression under control of the CDX2P-NLS promoter is found in epithelial cells throughout the adult small intestine and colon, which is also true for the villin promoter. Interestingly, *CDX2P-NLS Cre* (CPC) mice and Villin-Cre mice were crossed with mice carrying *loxP*-modified *Apc* alleles ($Apc^{loxP/loxP}$) and tumor development was compared

between these two mouse lines. *CPC;Apc* mice developed 5 to 8 tumors per mouse in the colon and 3 tumors per mouse in the small intestine, whereas *Vilin-Cre;Apc* mice revealed formation of approx. 36 tumors per mouse, but of which the vast majority developed in the small intestine (Hinoi *et al.* 2007). On the one hand, this comparison shows that the CDX2P-NLS promoter seems to be the better choice, because the majority of tumors developed in the colon. On the other hand, the villin promoter appears to be the superior choice, because the incidence of tumor formation is much higher than under the control of the CDX2P-NLS promoter. The Lgr5 promoter drives transgene expression in the Lgr5-positive CBC stem cells. However, Lgr5 is also expressed in hair follicle and mammary glands, and thus, Lgr5 is more a general marker of adult stem cells rather than an intestine-specific stem cell marker (Barker *et al.* 2007). Transgene expression under the control of the mCA1 promoter was found to be limited to epithelial cells of the colon (Xue *et al.* 2010) which is a big advantage over the villin promoter. Furthermore, mCA1-guided β-galactosidase expression was found to reach from the crypt base to the luminal surface (Xue *et al.* 2010) which is more consistent with the expression pattern of endogenous Igf1r than villin expression. This comparison leads to the suggestion that the mCA1 promoter could be a better choice to drive transgene expression than the villin promoter in the present study. Of note, a mouse model that expresses a reverse tetracycline transactivator under the control of the mCA1 promoter does not exist to date. Thus, for the present study a mouse for the mCA1-guided overexpression of the *IGF1R* had to be generated first.

Table 2: Summary of the advantages and disadvantages of the different intestine-specific promoters.

Promoter	Advantage	Disadvantage	Reference
Villin	villin-guided transgene expression in all epithelial cells of the intestine is also active in progenitor cells	villin-guided transgene expression in small intestine, colon and kidney reduced expression levels in crypts of the small intestine and in lower half of colonic crypts	El Marjou *et al.* 2004 Roth *et al.* 2009

	mouse with villin-guided rtTA2-M2 transgene expression available mouse with villin-guided CreER^{T2} transgene expression available		
Fabp	is active in progenitor cells	Fabp-guided transgene expression in small intestine, cecum and colon	Saam and Gordon 1999
Lgr5	is active in CBCCs	Lgr5-guided transgene expression also in hair follicle and mammary glands	Barker *et al.* 2007
CDX2P-NLS	CDX2P-NLS-guided transgene expression in epithelial cells in adult small intestine and colon	CDX2P-NLS-guided transgene expression also in tail bud and caudal part of neural tube in embryos CDX2P-NLS-guided transgene expression also in small intestine, cecum, colon and rectum in adults	Hinoi *et al.* 2007
mCA1	mCA1-guided transgene expression limited to epithelial cells of the colon	mouse with mCA1-guided rtTA2 transgene expression not available	Xue *et al.* 2010

Taken together, the promoters described above exhibit advantages and disadvantages over the villin promoter. In regard to choose the right promoter the work of Janssen *et al.* (2002) was of high interest. They generated a transgenic mouse line expressing K-ras^{V12G}, which is the most frequent point mutation in human tumors, under the control of the 9 kb murine villin promoter variant. At nine months of age more than 80% of the transgenic mice had developed tubuloglandular adenomas and malignant

adenocarcinomas predominantly in the small intestine (90%), but also in the colon (7%) (Janssen *et al.* 2002). However, Cheung *et al.* (2010) generated a mouse line with a cre-regulable null allele of the *Apc* gene and crossed these *Apc*$^{fle1-15}$ mice to Villin-Cre transgenic mice. At approx. 4 months of age, the *Apc*$^{+/fle1-15}$; *Villin-Cre* mice developed several adenomas in their small intestines and colons. However, carcinomas were not detected (Cheung *et al.* 2010). These examples in which transgene expression guided by the villin promoter induced intestinal tumor formation further indicate that the villin promoter was a suitable promoter for the present study. Since the Villin-rtTA2-M2 mouse line expressing the reverse tetracycline transactivator and the Villin-CreER^{T2} mouse line expressing the cre recombinase under the control of the villin promoter, respectively, were available, we decided to utilize these mouse lines for the present study to generate the *IGF1R* overexpressing and *Igf1r* knockout mice.

4.5.2 Different expression patterns of endogenous Igf1r and villin

In the present study, the villin promoter was used to direct the overexpression of the human *IGF1R* and the knockout of the endogenous *Igf1r*, respectively. Villin is a cytoskeletal protein localized in the intestinal and kidney brush border of epithelial cells, contributing in the absorption process (Ferrary *et al.* 1999; Pinto *et al.* 1999; Madison 2002). During mouse embryogenesis, villin was first detected in endodermal cells at day 6 in the early post implantation stage (Maunoury *et al.* 1988). Villin expression is upregulated during remodeling of the intestinal epithelium and the formation of the villi. Once the intestinal crypts have been established, villin is expressed along the crypt-villus axis with higher expression at the tips of the villi than in the crypts (Braunstein *et al.* 2002; Madison 2002). Furthermore, epithelial cells of all four lineages express villin (Braunstein *et al.* 2002). In the human, villin expression was studied during embryonic development using a cell extract prepared from the intestinal tube of an 8-week-old human fetus. At 8 weeks, villin expression was already detected, and in a 16-week-old fetus, villin expression was observed in the small intestine and colon, demonstrating the early expression of villin during embryonic development (Robine *et al.* 1985). In the adult rat intestine, villin expression was found in epithelial cells, but not in the underlying mucosa. In addition, mature enterocytes at the tips of the villi revealed a 10-fold higher amount of villin expression than immature crypt cells (Robine *et al.*

1985). Nevertheless, villin is also expressed in stem cells and proliferative cells localized in the intestinal crypts (Pinto *et al.* 1999).

The crypt-villus gradient of villin expression is of high interest regarding the *Igf1r* knockout experiments of the present study. Here, the knockout of endogenous *Igf1r* was directed to the intestinal epithelium by using the villin promoter. As already described in chapter 4.3, staining of endogenous Igf1r using an antibody against the Igf1rβ revealed an opposing gradient with decreasing Igf1r expression from the intestinal crypts to the villi in the small intestine and from the bottom to the top of the colonic crypts, respectively, compared to that of villin expression. The existence of these opposing expression gradients supports the idea that in the present study the villin-guided knockout of endogenous *Igf1r* in epithelial cells of the intestine might be impaired. In the intestinal crypts strong endogenous Igf1r expression was observed, whereas weak villin expression was found, which guides the *Igf1r* knockout by controlling the amount of expressed cre recombinase. These observations lead to the assumption that a low amount of cre recombinase in the intestinal crypts is not able to delete exon 3 of the highly expressed *Igf1r* gene. This hypothesis would further explain why the knockout of the endogenous *Igf1r* in the present study did not significantly influence the number of the different cell types in the intestinal crypts, whereas differences were observed in the small intestine (see chapter 3.22). In addition, a difference in the number of tumors derived in control and $Cre^{+}/Igf1r^{fl/fl}$ Villin-CreERT-Igf1r mice was also not visible in the present study (see chapter 3.23 and 3.24), supporting the hypothesis that the *Igf1r* knockout could be impaired. For the analysis if the *Igf1r* knockout is in fact extenuated, staining of small intestinal and colonic tissue sections of control and $Cre^{+}/Igf1r^{fl/fl}$ Villin-CreERT-Igf1r mice for endogenous Igf1r should be performed. Unfortunately, staining of intestinal tissue sections using an antibody against endogenous Igf1rβ did not reveal valuable results in the present study.

In conclusion, the opposing expression patterns of endogenous Igf1r and villin point to the assumption that the villin promoter is not suitable to induce a sufficient *Igf1r* knockout in the intestinal epithelium. Since the villin promoter was primarily used for the overexpression of human *IGF1R* in the present study, it was also chosen for the *Igf1r* knockout experiment. However, several intestine-specific promoters are known (see 4.5.1). The *Lgr5-EGFP-IRES-creERT2* mouse was demonstrated to drive transgene expression in *Lgr5*-expressing CBCCs (Barker *et al.* 2007), which are

localized at the bottom of the intestinal crypts (see chapter 4.2 and Medema and Vermeulen 2011). Using the *Lgr5-EGFP-IRES-creERT2* mouse, the *Igf1r* knockout would be guided to the intestinal crypts where high *Igfr* expression was observed. In order to prove if the *Igf1r* knockout in the intestinal epithelium indeed has no significant influence on epithelial cell proliferation and differentiation as well as on colonic tumor formation, the *Igf1r* knockout experiments of the present study should be repeated with the *Lgr5-EGFP-IRES-creERT2* mouse.

4.5.3 Combining IGF1R models with well characterized models of CRC to study IGF1R-induced tumor progression

The present study displayed that *IGF1R* overexpression *per se* is not sufficient to induce CRC development. Instead, we hypothesized that the IGF1R / Igf1r is involved in tumor progression. To analyze this hypothesis in detail, we had to cross our IGF1R mouse models (Villin-TRE-IGF1R and Villin-CreERT-Igf1r mouse models) either with a mouse model that develops CRC or to use a chemically induced CRC mouse model. A detailed literature search revealed several genetic as well as chemically induced CRC mouse models. In the next section the advantages and disadvantages of these mouse models are described and the choice for the AOM / DSS model is explained.
The *APC* tumor suppressor gene is known to be mutated in more than 70% of sporadic CRCs (Kheirelseid *et al.* 2013). The majority of mutations in *APC* result in a truncated protein (Chung 2000; HGMD® Professional 2016.1). Patients with familial adenomatous polyposis (FAP) are carriers of a germline mutation in one *APC* allele and develop large numbers of adenomas in their colon and rectum (Heyer *et al.* 1999; Karim and Huso 2013). The so called multiple intestinal neoplasia (*Min*) mouse was the first mouse that contained a mutation in the *Apc* gene. The mutation was identified to be a nonsense mutation resulting in a truncated protein of 850 amino acids. The Apc^{Min} homozygous mice are embryonically lethal, whereas Apc^{Min} heterozygotes are born normally, but show a reduced lifespan of approx. 150 days. Apc^{Min} heterozygous mice can develop more than 100 adenomas in the small intestine (Heyer *et al.* 1999), which is similar regarding the number of adenomas in FAP patients (Karim and Huso 2013). A disadvantage of the Apc^{Min} mouse is the fact that the adenomas are localized in the small intestine, whereas FAP patients develop adenomas in the colon and rectum.

In recent years, many mouse models which carry specific *Apc* mutations leading to a truncated protein were generated, such as the *Apc1638N* (Fodde *et al.* 1994), $Apc^{\Delta 716}$ (Oshima *et al.* 1995), Apc^{580S} (Shibata *et al.* 1997), *Apc1638T* (Smits *et al.* 1999), $Apc^{\Delta 474}$ (Sasai *et al.* 2000), Apc^{1322T} (Pollard *et al.* 2009), $Apc^{\Delta 14/+}$ (Colnot *et al.* 2004) and the $Apc^{\Delta 15}$ mouse (Robanus-Maandag *et al.* 2010). Almost all mouse models revealed a predominant or even absolute induction of tumor formation in the small intestine, such as the Apc^{Min}, Apc^{1638N}, $Apc^{\Delta 716}$ and Apc^{1322T} mice. Since sporadic CRC and FAP are characterized by tumor formation mainly in the colon and rectum, these models are not suitable to mimic the human features of CRC. Another disadvantage is the fact that homozygous mice of some mouse models were not viable which was described for Apc^{Min}, Apc^{1638N}, $Apc^{\Delta 716}$ and $Apc^{\Delta 14}$ mice. To circumvent this homozygous lethality, inducible knockout models were established, such as the Apc^{580} mouse, which seems to be a good choice since homozygous Apc^{580} mice developed adenomas in the colorectum within 4 weeks. However, all tumors were histopathologically diagnosed as carcinomas (Shibata *et al.* 1997).

Hereditary nonpolyposis colorectal cancer (HNPCC) is an autosomal dominant inherited form of CRC. HNPCC shows high penetrance and an early onset of tumorigenesis. Patients suffering from HNPCC often develop extracolonic cancers, such as gastric, endometrial, ovarian and renal cancers (Heyer *et al.* 1999; Fearon 2011). The characteristic feature of HNPCC is the small number or even the absence of polyps (Bosman 2010). Genes mutated in HNPCC patients are found to be involved in DNA repair, such as *MLH1* and *MSH2* (Haggar and Boushey 2009). Several mouse models for HNPCC exist, such as the *Msh2*-deficient mice, that are known to develop gastrointestinal and skin tumors, and *Msh6*-deficient mice, that develop invasive B and T cell lymphomas and tumors in the gastrointestinal tract (Heyer *et al.* 1999). Since the major aim of the present study was the investigation of the role of the IGF1R / Igf1r in sporadic CRC, these mouse models are not discussed in detail.

Besides genetically modified mice, also chemically induced CRC models exist, including models based on AOM and DSS, which were already discussed in chapter 4.4.1. In addition to these agents, other carcinogens that induce colonic tumors are available. Dimethylhydrazine (DMH) is a metabolic precursor of MAM and was frequently used in the past to induce colonic tumors in rodents which also mirror many of the pathological features seen in human sporadic CRC (Rosenberg *et al.* 2008). However, more recently, AOM is used, because it shows enhanced potency and

greater stability in dosing solution compared to DMH (Neufert *et al.* 2007; Rosenberg *et al.* 2008).

Heterocyclic amines (HCAs), such as 2-amino-3-methylimidazo-[4,5-*f*]quinoline (IQ) (Kleman *et al.* 1993) produced from food pyrolysis and 2-amino-1-methyl-6-phenylimidazo[4,5-*b*]pyridine (PhIP) produced during the cooking of meat and fish, are highly mutagenic and tumorigenic agents that cause cancer induction in the colon, mammary gland and prostate of rodents. Unfortunately, tumor incidence was reported to be very low and tumors were predominantly localized in the small intestine, only few tumors were found in the colon (Rosenberg *et al.* 2008).

Dimethylaminoborane (DMAB) is an aromatic amine with carcinogenic potential. It was described to induce multiple colon tumors in F344 rats upon 20 weekly subcutaneous injections with 50 mg DMAB per kg body weight. Interestingly, DMAB-induced tumors were benign adenomas as well as malignant adenocarcinomas. The disadvantages of the DMAB-based model is on the one hand, that multiple DMAB injections are necessary to induce colonic tumors, and on the other hand that also several extracolonic tumors are induced by DMAB, such as adenocarcinomas of mammary glands, sarcomas of the salivary gland and squamous cell carcinomas of the ear duct and skin (Rosenberg *et al.* 2008).

N-methyl-N-nitro-N-nitrosoguanidine (MNNG) and N-methyl-N-nitrosourea (MNU) are direct-acting carcinogens that do not need metabolic activation (Rosenberg *et al.* 2008). Rats and mice which have been orally administered to MNNG and MNU show a high incidence of neoplasias in the stomach, small intestine, colon, kidney, skin, lung and thymus. When administered *via* the rectum, MNU induces a high incidence of colonic tumors, but also thymic lymphomas (Johnson and Fleet 2013). Intrarectal administration of MNNG in F344 rats induced colonic tumors with an incidence of 100%. Forty-three percent of the induced tumors were adenocarcinomas, whereas 57% were adenomas. Although selectively colorectal tumors were induced by MNNG and MNU when administered intrarectally, the big disadvantage of this model is the fact that intrarectal instillation is a highly challenging form of administration and requires good technical skills (Rosenberg *et al.* 2008).

Taken together, many of the described models, either based on genetic modifications or induced by genotoxic agents, possess one disadvantage: the development of tumors predominantly in the small intestine. Since patients with sporadic CRC develop tumors in the colon and rectum, the AOM- and AOM / DSS-based CRC models,

respectively, are suitable models to mimic the patient's situation. In addition, the short period of colonic tumor development (mice treated with AOM / DSS developed tumors in as little as 7 to 10 weeks (see chapter 3.11, 3.24 and Thaker *et al.* 2012), the high incidence of tumor development (see chapter 3.11, 3.15 and 3.24), the fact that AOM- and DSS- administration does not require professional skills (compare with intrarectal instillation of MNNG) and the fact that the AOM- and AOM / DSS- induced colonic tumors histologically resemble human CRC (see chapter 3.10, 3.11 and Thaker *et al.* 2012) are further advantages of the AOM- and AOM / DSS-based CRC models. For this reason, the AOM- and AOM / DSS-based CRC models were chosen for analyzing the IGF1R-induced colonic tumor development and progression in the present study.

4.6 Current treatment of CRC

The present study proved that the IGF1R / Igf1r plays a crucial role during colonic tumor progression. This finding indicates that targeting and thereby inhibiting IGF1R signaling could improve the treatment and outcome of CRC patients. *De facto*, targeted therapy against the IGF1R and also other RTKs, such as the EGFR, PDGFR and VEGFR are used in the clinics for e.g. the treatment of lung cancer, head and neck cancer and advanced CRC (Huether *et al.* 2006; Wheeler *et al.* 2008; Lin and Bivona 2012; Tang *et al.* 2013; Suda *et al.* 2014; Seow *et al.* 2016) (see table 3).

In the clinical setting, treatment of patients with CRC depends on tumor stage. Furthermore, for treatment, colon cancer is distinguished from rectal cancer (American Cancer Society; National Cancer Institute). The current standard treatment options according to the stage of the tumor are summarized in table 3.

Table 3: The current standard treatment options according to the stage for colon and rectal cancer (after American Cancer Society; National Cancer Institute).

		Current standard treatment options	
Tumor stage	**Characteristics of stage**	**Colon cancer**	**Rectal cancer**
0	cancer has not grown beyond the inner lining of the colon	surgery	surgery
I	cancer has grown into the layers of the colon wall, but has not spread outside the colon wall	surgery	surgery
II	cancer has grown through the colon wall and have possibly affected nearby tissue, but has not spread to the neighboring lymph nodes	surgery + adjuvant chemotherapy (CT)	neoadjuvant radiochemotherapy (RCT) + surgery
III	cancer has spread to nearby lymph nodes, but has not yet spread to other parts of the body	surgery + adjuvant CT	neoadjuvant RCT + surgery
IV	cancer has spread from the colon to distant organs and tissues, such as the liver, lungs and distant lymph nodes	surgery + adjuvant CT + **targeted therapy**	neoadjuvant RCT + surgery + **targeted therapy**

4.6.1 RTK-targeted therapy as treatment option for advanced CRC

As depicted in table 3, targeted therapy is an applied treatment option for patients with advanced CRC. The major targets in these therapy strategies for advanced CRC are the EGFR and VEGFR. The current biologic agents used for targeted therapy of advanced CRC are monoclonal antibodies, such as cetuximab and panitumumab against the EGFR as well as bevacizumab against the VEGFA, and small molecule

kinase inhibitors, such as regorafenib inhibiting VEGFR1 to VEGFR3 (Seow *et al.* 2016). In 2006, panitumumab was approved as a single agent therapy, whereas cetuximab was approved in 2012 in combination with the chemotherapeutics 5-FU, leucovorin and irinotecan (FOLFIRI) for the treatment of metastatic CRC (Haraldsdottir and Bekaii-Saab 2013). However, new therapeutic agents and drug combinations that target other RTKs and signaling pathways, such as the IGF1R, PDGFR, MET, MEK, PI3K, Wnt, Notch and Hedgehog were developed (Seow *et al.* 2016) and are now under clinical investigation.

One main obstacle of targeted therapies is the development of resistance to the treatment. *De novo* resistance to EGFR inhibitors is often observed (Wheeler *et al.* 2008; Lin and Bivona 2012). Bertotti *et al.* (2015) performed complete exome sequence and copy number analyses of 129 patient-derived CRC tumorgrafts and targeted genomic analyses of 55 patient CRCs and analyzed the response of the tumors to anti-EGFR antibody blockade. The authors detected mutations for example in *ERBB2*, *EGFR* and *FGFR1* and predicted these mutations as potential mechanisms of primary resistance to the anti-EGFR therapy (Bertotti *et al.* 2015). Lurje and Lenz (2009) suggested that the activation of alternative RTKs and the downstream signaling pathways, by which EGFR inhibition is circumvented, are potential mechanisms of resistance to EGFR-targeted therapy (Lurje and Lenz 2009). In lung cancer cells with wild type EGFR, Suda *et al.* (2014) proved that the IGF1R caused acquired resistance to erlotinib (small molecule kinase inhibitor of the EGFR) and predicted the IGF1R as an important target to circumvent or overcome erlotinib resistance (Suda *et al.* 2014). In CRC, resistance to EGFR inhibitors was also associated with IGF1R signaling (Buck *et al.* 2008; Kaulfuß *et al.* 2009; Yang *et al.* 2011). For this reason, Kaulfuß *et al.* (2009) and Seemann (2013) targeted both RTKs and showed that simultaneous silencing of IGF1R and EGFR by siRNA or the small molecule kinase inhibitors AEW541 (directed against the IGF1R) and erlotinib (directed against the EGFR) with or without combined RCT in CRC cells resulted in the reduction of cell proliferation and the induction of apoptosis (Kaulfuß *et al.* 2009; Seemann 2013).

4.6.2 Combination of IGF1R- and EGFR-targeted therapy in addition to combined 5-FU-based RCT as treatment option of CRC

In the present study, the effect of simultaneous inhibition of IGF1R and EGFR in addition to combined RCT on tumor growth was analyzed *in vivo*. Therefore, the CRC cell lines DLD-1 and CaCo-2 and the rectal cancer cell line SW837 were subcutaneously implanted in immune-deficient nude mice. After establishment of the tumors, mice were treated with AEW541, erlotinib, the combination of AEW541 / erlotinib or the solvent as control. In addition to inhibitor treatment, mice were administered to combined 5-FU-based RCT similar to the human treatment settings of neoadjuvant RCT (Spitzner *et al.* 2010).

In the DLD-1 (see Fig. 68, Fig. 69a, b and Fig. 70a, b) and CaCo-2 xenograft mouse models (see Fig. 71a, b and Fig. 72a, b), single and even simultaneous inhibition of IGF1R and EGFR in addition to combined RCT did not result in a significant reduction of tumor progression, tumor volume and weight compared to control treatment. Interestingly, in contrast to the DLD-1 and CaCo-2 xenograft mice, SW837 xenograft mice simultaneously treated with AEW541 / erlotinib in addition to combined RCT revealed a significant decrease in tumor growth, tumor volume and weight compared to control mice (see Fig. 73 and Fig. 74a, b). These *in vivo* data indicate that the DLD-1, CaCo-2 and SW837 xenograft mice exhibited a differential sensitivity to the inhibitor treatment in addition to the combined RCT. Furthermore, only the results of the SW837 xenograft experiment reflected the *in vitro* data of the colony formation experiments of Seemann (2013). Seemann (2013) demonstrated that simultaneous inhibition of the IGF1R and EGFR in addition to combined RCT resulted in a significant reduction of cell survival in DLD-1 and SW837 cells. The inhibitor treatment in addition to combined RCT even led to a complete loss of survival in CaCo-2 cells (Seemann 2013), which could not be observed *in vivo* (see chapter 3.26). These findings lead to the following questions:

1. Why did the three cell lines (DLD-1, CaCo-2 and SW837) respond differentially to inhibitor treatment in addition to combined RCT *in vivo*?
2. Why did the results of the DLD-1 and CaCo-2 xenograft experiments not mirror the *in vitro* data of Seemann (2013)?

Regarding question 1, the fact that the DLD-1 and CaCo-2 cell lines are CRC cell lines, whereas SW837 cells are rectal cancer cells (see chapter 2.9.1) could be of high

importance since only the SW837 xenograft mice revealed a significant reduction of tumor progression after simultaneous treatment with AEW541 / erlotinib in addition to combined RCT (see Fig. 73). As shown in table 3, the current standard treatment for metastatic colon cancer consists of surgery in addition to **adjuvant CT** and targeted therapy, whereas in the case of advanced rectal cancer the standard treatment is surgery plus **neoadjuvant RCT** plus targeted therapy (American Cancer Society; National Cancer Institute). In the present study, **neoadjuvant RCT** in addition to targeted therapy was applied to the SW837 xenograft mice, but also to the DLD-1 and CaCo-2 xenograft mice, although DLD-1 and CaCo-2 cells are colorectal cancer cell lines. The effect of neoadjuvant therapy on survival and surgical benefits in colon cancer is still controversial (Huang *et al.* 2014). Jakobsen *et al.* (2015) studied the effect of neoadjuvant chemotherapy (NCT) in 77 patients with resectable colon cancer and demonstrated that NCT in colon cancer is feasible. Nevertheless, they also discussed the limitations of their study, including that it was a phase II trial not allowing any conclusion about the importance of NCT. Furthermore, the authors argued that the observation time was too short for allowing any conclusion regarding the long-term recurrence rate (Jakobsen *et al.* 2015). Karoui *et al.* (2015) showed that approx. 70% of colon cancers responded to NCT displayed by using the tumor regression grade (Karoui *et al.* 2015). In the FOxTROT (Fluoropyrimidine Oxaliplatin and Targeted Receptor Pre-Operative Therapy) trial 150 high risk stage II and stage III patients were treated with preoperative plus postoperative adjuvant CT *vs.* postoperative CT. Significant tumor downstaging and greater regression were shown for the preoperative group compared to the postoperative group, indicating that preoperative CT in locally advanced resectable primary colon cancer was feasible (Zhou *et al.* 2013). However, analysis of six randomized controlled trials in which the efficacy of NCT was compared with that of surgery alone showed that NCT did not contribute to significant survival benefits for CRC and that NCT did not outweigh surgery alone regarding survival and surgical benefits (Huang *et al.* 2014). In contrast, preoperative radiotherapy with or without chemotherapy followed by total mesorectal excision surgery is currently the standard treatment option for locally advanced rectal cancer (Hav *et al.* 2015). It could be shown that neoadjuvant RCT reduced the rates of local recurrence, led to reliable tumor downstaging and improved survival (Ferrari and Fichera 2015). In addition, neoadjuvant RCT displayed higher reduction rates of local recurrence than postoperative treatment (Sauer *et al.* 2004).

Since the efficacy of NCT in colon cancer is still discussed controversially, it could possibly explain why the DLD-1 and CaCo-2 xenograft mice showed less or even no response to the inhibitor treatment in addition to combined RCT which was applied in a neoadjuvant manner. The fact that neoadjuvant RCT is currently applied to rectal cancer patients in the clinics might explain that in contrast to the DLD-1 and CaCo-2 xenograft mice the SW837 xenograft mice displayed a significant response rate to the applied treatment in the present study.

Seemann (2013) proved that the three cell lines DLD-1, CaCo-2 and SW837 revealed differential responses to simultaneous inhibition of IGF1R and EGFR in addition to combined RCT *in vitro*. DLD-1 cells showed a decreased survival fraction after simultaneous treatment with AEW541 / erlotinib in addition to combined RCT. SW837 cells revealed an even stronger reduction of the survival fraction and CaCo-2 cells showed a complete loss of survival after inhibitor treatment in addition to combined RCT (Seemann 2013). *In vivo*, single and simultaneous inhibition of IGF1R and EGFR in addition to combined RCT did not result in significantly decreased tumor progression compared to control treatment in DLD-1 xenograft mice (see Fig. 68 and Fig. 69a, b). In the present study, the DLD-1 xenograft experiment was the first xenograft experiment performed. Since many DLD-1 xenograft mice did not tolerate the treatment and died already before the treatment was completed as a consequence of the combined RCT, the treatment settings were adapted in cooperation with Dr. Melanie Spitzner (Department of General, Visceral and Pediatric Surgery) (see chapter 3.26). Furthermore, DLD-1 cells exhibit a high proliferation rate. In the present study, DLD-1 tumors grew rapidly so that treatment was already started 16 to 18 days after DLD-1 cell implantation, and mice were already sacrificed 31 days after CRC cell implantation (see Fig. 68 and Fig. 69a, b). These facts could indicate that the tumors were growing rapidly and therefore sufficient treatment to inhibit tumor progression was not successful. In addition, DLD-1 cells are known to harbor a point mutation in the *K-RAS* gene, namely G13D (Ahmed *et al.* 2013), leading to a constitutively active protein (Shaib *et al.* 2013). *K-RAS* is a proto-oncogene in the MAPK pathway downstream of the EGFR promoting cell growth (Ahmed *et al.* 2013). Interestingly, it was shown that the *K-RAS* mutation status predicts the response rate to EGFR-targeted therapy (Haraldsdottir and Bekaii-Saab 2013) and that an activating mutation in codon 12 of the *K-RAS* gene is a predominate mechanism of resistance to EGFR inhibitors in CRC patients (Shaib *et al.* 2013). Regarding the DLD-1 xenograft

experiment this would indicate that inhibition of the EGFR with erlotinib upstream of K-RAS did not inhibit MAPK signaling, because K-RAS was constitutively active due to the G13D mutation. Furthermore, DLD-1 cells additionally harbor an activating mutation in the *PI3KCA* gene (Seemann 2013), leading to the suggestion that inhibition of the IGF1R and EGFR by the small molecule kinase inhibitors does also not inhibit downstream signaling *via* the PI3K signaling pathway. These facts might explain why the DLD-1 xenograft mice did not benefit from the IGF1R- and EGFR-targeted treatment.

In contrast to DLD-1 cells, CaCo-2 cells are wild type for *K-RAS* (Ahmed *et al.* 2013), indicating that the *K-RAS* mutation status is not the reason for the finding that CaCo-2 xenograft mice did not respond to the treatment applied. Interestingly, Spitzner *et al.* (2010) demonstrated that CaCo-2 cells exhibit intermediate sensitivity to RCT *in vitro* (Spitzner *et al.* 2010). This observation leads to the suggestion that the CaCo-2 xenograft mice highly responded to the combined RCT and therefore additional inhibition of the IGF1R and EGFR did not improve the outcome. This hypothesis is supported by the observation that the tumor volume decreased immediately after RCT was completed in the mouse model (see Fig. 71).

SW837 cells were shown to exhibit low sensitivity to RCT (Spitzner *et al.* 2010), indicating that inhibitor treatment against the IGF1R and EGFR contributed to the benefits of the combined RCT. Furthermore, as already discussed, SW837 are rectal cancer cells and thus SW837 xenograft mice received, by applying inhibitors against the IGF1R and EGFR in addition to combined RCT, the treatment setting which is currently used in the clinics for advanced rectal cancer. These facts could explain why the SW837 xenograft mice showed significant response rates toward the treatment setting. Of note, SW837 cells are also known to harbor a *K-RAS* mutation (Spitzner *et al.* 2010). Again, this fact would point to the suggestion that, as in DLD-1 cells, inhibition of the EGFR is useless since the downstream MAPK signaling pathway is constitutively activated due to the activating *K-RAS* mutation.

In conclusion, inhibition of the IGF1R and EGFR in addition to combined RCT led to a significant decrease in tumor progression only in SW837 xenograft mice. In contrast, a significant reduction of tumor growth could not be observed in the DLD-1 and CaCo-2 xenograft experiments. The underlying causes for the different response rates remain unknown. Assumptions to explain the differential responding comprise the *K-RAS* mutation status, the differential sensitivity to combined RCT and the treatment

setting. In addition, these facts indicate that xenograft experiments might not be suitable models to investigate the effect of IGF1R- and EGFR-targeted inhibition. The present study impressively displayed that the IGF1R / Igf1r predominantly plays a role during colonic tumor progression rather than colonic tumor formation (see chapter 4.4.2). In the xenograft mouse model the effect of treatment on tumor cell proliferation was analyzed rather than the effect on tumor progression and invasion, demonstrating that other models are needed. For example, IGF1R-oe Villin-TRE-IGF1R mice administered to AOM / DSS to induce colonic tumor formation could be used in a future experiment. These mice overexpress the *IGF1R* in epithelial cells of the intestine and develop colonic tumors, thus mimicking the situation of CRC patients. Using this mouse model, the effect of IGF1R- and EGFR-targeted therapy in addition to combined RCT could be examined. Furthermore, this mouse model can be used to analyze also other novel treatment strategies in CRC (see chapter 4.7).

4.7 Perspectives

In the present study, the receptor tyrosine kinase IGF1R was proven to play an important role during the development of the intestine and during colonic tumor progression.

The *IGF1R* was overexpressed, under the control of the villin promoter, in epithelial cells of the small intestine and colon of IGF1R-overexpressing mice. Strikingly, the ectopic, villin-guided expression pattern of IGF1R overexpression did not resemble the endogenous Igf1r expression pattern. In addition, staining for ectopic, villin-guided IGF1R overexpression indicated that only a particular epithelial cell type overexpressed IGF1R in the small intestine and colon. Double stainings proved that neither goblet cells, nor Paneth cells, nor enteroendocrine cells overexpressed IGF1R. CBCCs and transit-amplifying cells could also be excluded. To date, analyses did not include microfold cells (M cells), cup cells and tuft cells, indicating that these epithelial cell types are still potential candidates for being the cell type overexpressing the *IGF1R* in the Villin-TRE-IGF1R mouse model. To finally identify the epithelial cell type overexpressing the *IGF1R*, further double staining experiments with markers specific for M cells, such as glycoprotein 2 (GP2) (Kobayashi *et al.* 2013), cup cells, such as vimentin (Ramirez and Gebert 2003), and tuft cells, such as the combination of

microtubule-linked protein kinase Dclk1 and cytokeratin 18 (CK-18) (Gerbe *et al.* 2012), in combination with an antibody against human IGF1R should be performed.

Nevertheless, the present study proved that *IGF1R* overexpression led to a significant extension of the average crypt depth in the small intestine. Furthermore, *IGF1R* overexpression was shown to promote epithelial cell proliferation and to inhibit epithelial cell differentiation in four weeks and three months old and adult IGF1R-oe mice. These facts indicated that *IGF1R* overexpression influences the development of the murine intestine. In fact, it is known that in contrast to humans, development of the murine intestine is not completed before birth (Montgomery *et al.* 1999), but it was also proven that particular stages of intestinal development occur during murine embryogenesis (Gregorieff and Clevers 2005). Specification of definitive endodermal cells occurs at E6.0 during gastrulation. At E8.5, the endodermal tube is initiated to form by folding of the endodermal lining. The primitive gut tube is patterned along the anterior-posterior axis at 9.5 to E14.5. At E14.5, villus formation and differentiation into either goblet cells, enteroendocrine cell, Paneth cells or enterocytes is initiated (Gregorieff and Clevers 2005). These facts indicate that important developmental stages of the murine intestine occur already before birth. Since the influence of *IGF1R* overexpression on intestinal development was only investigated postnatally, the effect of *IGF1R* overexpression on intestinal development should be further analyzed in embryonic mice. Therefore, *IGF1R* overexpression should be already induced in pregnant mice by doxycycline administration. For the detailed analysis if *IGF1R* overexpression influences a particular stage of intestinal development, *IGF1R* overexpression should be induced at the different development stages mentioned above. Similar to this plan, the *Igf1r* knockout should also be induced in small intestinal and colonic epithelial cells of embryonic mice by tamoxifen injection to analyze if the Igf1r is sufficient for “normal” intestinal development. Again, the *Igf1r* knockout should also be induced at the different embryonic stages mentioned above to examine if *Igf1r* expression is necessary for a particular stage of “normal” intestinal development.

Against our expectation, the present study revealed that villin-directed *IGF1R* overexpression *per se* did not induce colonic tumor formation. In chapter 4.5.1 some issues were discussed that the villin promoter might not be a suitable promoter to direct *IGF1R* expression to intestinal epithelium, i.e., differences in the expression pattern of endogenous Igf1r and villin. Furthermore, a comparison of the studies of Bennecke *et*

al. (2010) and Feng *et al.* (2011) revealed that the intestinal expression of oncogenic *K-ras*^{G12D} under the control of different promoters in mice lead to different results. Bennecke *et al.* (2010) reported that expression of *K-ras*^{G12D} under the control of the villin promoter resulted in the upregulation of p16i^{nk4a}. In contrast, Feng *et al.* (2011) observed that expression of *K-ras*^{G12D} under the control of the CDX2P9.5 promoter did not significantly increase the p16^{ink4a} protein expression. For these reasons, *IGF1R* overexpression should again be induced in the small intestine and colon, but under the control of another promoter to verify that *IGF1R* overexpression is indeed not sufficient to induce colonic tumor formation. Possible promoters were already discussed (see chapter 4.5.1). The mCA1 promoter appeared to be an excellent promoter candidate for the present study (Xue *et al.* 2010), but to date a mouse model that drives rtTA2-M2 expression under the control of the mCA1 promoter is not available. Thus, a mouse line driving mCA1-guided rtTA2-M2 expression has to be generated first. Interestingly, Dow *et al.* (2014) generated a mouse line that guided cre-dependent, robust expression of rtTA3 and thus provided tissue-restricted and consistent induction of TRE-controlled *mKate2* and *TG-Ren.713* transgenes. Strong and uniform transgene expression was detected in the small intestine along the crypt-villus axis (Dow *et al.* 2014). Crossing this mouse strain with the Lgr5-EGFP-IRES-creERT2 knock-in mouse (Barker *et al.* 2007) (see 4.5.1) and the TRE-IGF1R mouse line (Jones *et al.* 2007), that was already used in the present study, would result in *IGF1R* overexpression specifically in the crypts of the small intestine and at the bottom of the colonic crypts, because Lgr5^{+} CBCCs are known to be localized at the bottom of the crypts (Medema and Vermeulen 2011). *IGF1R* overexpression induced by doxycycline administration in the progeny mice of this crossing (CAGs-rtTA3/Lgr5-EGFP-IRES-creERT2/TRE-IGF1R mice) would lead to a superior resemblance of the endogenous *Igf1r* expression pattern than the villin-guided *IGF1R* overexpression. Since the TRE-IGF1R mouse was already established for the present study and the other two mouse lines are available to purchase, the long term experiment should be repeated using the CAGs-rtTA3/Lgr5-EGFP-IRES-creERT2/TRE-IGF1R mouse to examine if *IGF1R* overexpression *per se* induces colonic tumor formation when the *IGF1R* is exclusively expressed at the bottom of the crypts of the small intestine and colon.

Remarkably, the present study proved that *IGF1R* overexpression promotes colonic tumor progression, demonstrated by a higher number of tumors of advanced stage derived in IGF1R-oe mice compared to control Villin-TRE-IGF1R mice. In addition,

IGF1R-oe even developed invasive carcinomas, whereas control mice did not (see chapter 3.10, 3.11 and 3.15). These results are of high interest since the *IGF1R* is known to be frequently overexpressed in CRC patients (Hakam *et al.* 1999; Reinmuth *et al.* 2002; Wu *et al.* 2014). These facts lead to the suggestion that tumors with *IGF1R* overexpression of CRC patients reveal enhanced tumor progression. *De facto*, strong IGF1R positivity was shown to correlate with higher-stage tumors, predicting a role of IGF1R expression during the transition of colorectal adenoma to carcinoma (Hakam *et al.* 1999). Thus, inhibition of IGF1R and thereby inhibition of the downstream signaling pathway would theoretically prevent tumor progression in CRC patients. Several biologic agents that inhibit the IGF1R are known, such as the monoclonal antibodies dalotuzumab, cixutumumab and AMG479 (Seow *et al.* 2016) and the small molecule kinase inhibitor AEW541 that was already used in the present study. To examine the effect of these inhibitors *in vivo*, also in combination with e.g. inhibitors targeting EGFR or in combination with chemotherapeutics, such as irinotecan or 5-FU and irradiation, IGF1R-overexpressing Villin-TRE-IGF1R mice administered to AOM / DSS to induce colonic tumor formation could be used. In addition, inhibition of the IGF1R in IGF1R-overexpressing Villin-TRE-IGF1R mice treated with AOM / DSS could finally prove that *IGF1R* overexpression promotes tumor progression since IGF1R inhibition should reduce tumor progression, indicated by a lower number of tumors with increasing stage compared to IGF1R-overexpressing mice. Furthermore, IGF1R- and EGFR-targeted inhibitor treatment in addition to combined RCT that was applied to the xenograft mice in the present study could also be administered to IGF1R-overexpressing Villin-TRE-IGF1R mice treated with AOM / DSS.

To date, molecular analyses of the tumors regarding their mutation status, e.g. *K-Ras, β-catenin, Apc* and *p53*, are lacking in the present study. These analyses would possibly explain the advanced progression of tumors derived in IGF1R-overexpressing mice compared to control mice. In addition, these molecular analyses would also be of high interest when treating IGF1R-overexpressing Villin-TRE-IGF1R mice with colonic tumors induced by AOM / DSS with IGF1R- and EGFR-targeted inhibitor treatment in addition to combined RCT as previously proposed since an activating *K-ras* mutation would influence the benefit of IGF1R- and EGFR-targeted therapy as described in chapter 4.6.2. Furthermore, in the present study the analysis of PI3K and MAPK signaling was only performed on a small number of tumors. In addition, tumors were

not discriminated regarding their stage. This discrimination of the tumors regarding their stage would further contribute to the clarification if *IGF1R* overexpression promotes tumor progression.

Taken together, *IGF1R* overexpression was shown to influence intestinal development by promoting epithelial cell proliferation and inhibiting epithelial cell differentiation in the murine intestine. In addition, *IGF1R* overexpression was proven to promote colonic tumor formation. The *Igf1r* knockout was shown to moderately influence colonic tumor initiation and to inhibit colonic tumor progression. Thus, the IGF1R turned out to possibly be an important molecular target in CRC treatment.

5 Summary

It is well known that the *IGF1R* is overexpressed in several tumor entities, such as ovarian-, prostate-, endometrial-, gastric- and colorectal cancer (Hewish *et al.* 2009). Several studies examining the expression of the IGF1R in human colorectal cancer biopsies exist, confirming a strong correlation of high IGF1R expression with an increased tumor stage (Freier *et al.* 1999; Hakam *et al.* 1999; Weber *et al.* 2002). Additionally, *IGF1R* overexpression was found to induce the formation of mammary tumors in transgenic mice (Carboni *et al.* 2005; Jones *et al.* 2007). Interestingly, studies analyzing if the IGF1R / Igf1r plays a role during epithelial cell differentiation and proliferation in the intestine and furthermore analyzing the function of the IGF1R / Igf1r during the development and progression of intestinal tumors were not available to date. Therefore, one mouse line used as a model for the inducible overexpression of human *IGF1R* in the intestine, called Villin-TRE-IGF1R, and another mouse line used as a model for the inducible knockout of *Igf1r* in the intestine, called Villin-CreERT-Igf1r, were established in the present study. Overexpression of *IGF1R* in the small intestine and colon of IGF1R-overexpressing Villin-TRE-IGF1R mice (IGF1R-oe) upon doxycycline administration could be confirmed by immunohistochemical staining and western blot analysis. Multiple immunofluorescence stainings using an antibody specific for human IGF1R in combination with an antibody against one specific epithelial cell type of the intestine, i.e., goblet cells (mucin 2), enteroendocrine cells (Chromogranin A) and Paneth cells (lysozyme), were performed to identify the cell type overexpressing the IGF1R. Interestingly, a concordant staining of IGF1R with one of these cell types could not be observed, showing that neither goblet cells nor enteroendocrine cells nor Paneth cells overexpress the IGF1R. Although IGF1R is not overexpressed by these cells, it influences the differentiation process of these cells in the intestine. This observation is the result of the quantification of the number of goblet cells, enteroendocrine cells, Paneth cells and proliferating cells in IGF1R-oe mice compared to control mice at three different time points. The number of goblet cells and Paneth cells decreased in IGF1R-oe mice compared to control mice, whereas the number of proliferating cells increased in IGF1R-oe mice, showing that *IGF1R* overexpression in the intestine led to a reduction of differentiation and an elevation of proliferation. The number of enteroendocrine cells did not alter after *IGF1R* overexpression. Sustained proliferation is a hallmark of cancer (Hanahan and

Weinberg 2011). For this reason it was of high interest to analyze if *IGF1R* overexpression in the intestine *per se* induces intestinal tumor formation in IGF1R-oe Villin-TRE-IGF1R mice. Therefore, *IGF1R* overexpression was induced in IGF1R-oe mice by administration of doxycycline. Colonoscopy was regularly performed to screen for colonic tumor formation. Since the mice had not developed intestinal tumors after 1.5 years, mice were sacrificed. Macroscopic and histopathological analyses confirmed that *IGF1R* overexpression *per se* did not result in intestinal tumor formation. This result led to the hypothesis that *IGF1R* overexpression rather influences intestinal tumor progression. To test this hypothesis, colonic tumor formation was induced in IGF1R-oe and control Villin-TRE-IGF1R mice by the mutagenic agent azoxymethane (AOM) or the combination of AOM and the inflammatory agent dextran sulfate sodium (DSS). Interestingly, after AOM treatment, IGF1R-oe mice revealed an increased number of intraepithelial neoplasias compared to control mice and even developed an intramucosal as well as an invasive carcinoma. The average tumor sizes showed an increase of 22.5% in IGF1R-oe mice compared to control mice. Even more remarkable results could be observed after AOM / DSS administration in IGF1R-oe mice. Here, histopathological analyses revealed an elevated number of intraepithelial neoplasias of increased stage in IGF1R-oe mice compared to control mice. In contrast to control mice, IGF1R-oe mice developed a high number of intramucosal carcinomas and even invasive carcinomas. The average tumor sizes showed an increase of 66.2% in IGF1R-oe mice compared to control mice. Western blot analysis of the downstream PI3K and MAPK signaling pathways revealed elevated activation levels in the tumors of IGF1R-oe mice. Taken together, these results support the hypothesis that the IGF1R promotes intestinal tumor progression.

Additionally, the influence of the endogenous *Igf1r* during the development of the intestine and during colonic tumor formation and progression was also analyzed using the *Igf1r* knockout mouse line Villin-CreERT-Igf1r. The knockout of *Igf1r* in the murine intestine was confirmed by PCR on genomic DNA extracted from small intestinal and colonic tissue samples and by western blot analysis. Morphological examination of the villi and crypts in the small intestine and colon using hematoxylin and eosin stainings indicated that the *Igf1r* knockout had no influence on intestinal morphology. Although the *Igf1r* knockout did not alter the morphology of the villi and crypts, the *Igf1r* may play a role during epithelial cell proliferation and differentiation in the intestine. To verify this hypothesis, the different epithelial cell types in Villin-CreERT-Igf1r mice were quantified

as described above. The number of goblet cells showed indeed an increase, whereas the number of Paneth cells decreased in Cre^{+}/*Igf1r*$^{fl/fl}$ mice compared to control mice. Interestingly, the number of proliferating cells was reduced in Cre^{+}/*Igf1r*$^{fl/fl}$ mice, supporting the hypothesis that *Igf1r* influences the differentiation and proliferation processes in the intestine. Furthermore, experiments in which colonic tumor formation and inflammation was induced by AOM / DSS indicated that the *Igf1r* knockout moderately influenced colonic tumor formation. Regarding tumor progression, Cre^{+}/*Igf1r*$^{fl/fl}$ mice showed a decreased number of tumors with advanced stage compared to control mice, indicating that the *Igf1r* knockout influenced colonic tumor progression. Western blot analysis of the downstream PI3K and MAPK signaling pathways in the colonic tumors revealed a reduced activation level of AKT (pAKT) in Cre^{+}/*Igf1r*$^{fl/fl}$ mice compared to control mice, but phosphorylation of ERK (pERK) was increased in Cre^{+}/*Igf1r*$^{fl/fl}$ mice compared to control mice. These data showed that the downstream MAPK signaling pathway was activated in colonic tumors.

In summary, the *IGF1R* overexpression experiments and the *Igf1r* knockout experiments of the present study display an important role of the IGF1R / Igf1r in colonic tumor progression. These results lead to the suggestion, that the IGF1R could be an important molecular target to treat patients with CRC. It is well known that the overexpression of the *IGF1R* is associated with an aggressive phenotype, tumor progression and poor prognosis in ovarian-, prostate-, endometrial- and colorectal cancer (Hewish *et al.* 2009). In addition, in non-small lung cancer patients, IGF1R overexpression has been implicated with resistance to erlotinib, a small molecule kinase inhibitor of the epidermal growth factor receptor (EGFR) (Lin and Bivona 2012). Interestingly, the EGFR was also found to be overexpressed in up to 80% of colorectal cancer patients (Spano 2005b). For this reason, a potential strategy to improve the patient's outcome could be the inhibition of the IGF1R combined with the inhibition of the EGFR. Kaulfuß *et al.* (2009) proved that simultaneous inhibition of the IGF1R by the small molecule kinase inhibitor AEW541, and EGFR by erlotinib leads to a reduction of proliferation and an increase in apoptosis induction in colorectal cancer cells. To confirm these *in vitro* results of Kaulfuß *et al.* (2009) *in vivo*, immune-deficient nude mice that were subcutaneously implanted with the colorectal cancer cells DLD-1 and CaCo-2 and the rectal cancer cell line SW837 were treated with the inhibitors in addition to combined 5-FU-based RCT. Single as well as simultaneous treatment of DLD-1 and CaCo-2 xenograft mice with AEW541 / erlotinib in addition to combined

RCT did not result in a significant decrease in tumor progression as well as tumor volume and weight compared to control mice. In contrast, SW837 xenograft mice showed a significant reduction of tumor growth, tumor volume and weight after simultaneous treatment with the inhibitors compared to control mice. Additionally, western blot analysis of the downstream PI3K and MAPK signaling pathways revealed diminished activation after simultaneous inhibition of the IGF1R and EGFR in the SW837 tumors. These *in vivo* results thus supported the hypothesis that the simultaneous inhibition of the IGF1R and EGFR is a potential strategy in CRC treatment.

In conclusion, the results of the present study display a pivotal role of the IGF1R in CRC. The data indicate that *IGF1R* overexpression reduces epithelial cell differentiation and promotes proliferation. In fact, the results show that *IGF1R* overexpression is not sufficient to induce colonic tumor formation, but indicate that *IGF1R* overexpression promotes intestinal tumor progression. These findings can be used to investigate new therapeutic strategies, in which tumor progression is prevented by the inhibition of the IGF1R. In this context, the Villin-TRE-IGF1R mouse line can be used to examine the effect of IGF1R inhibiting agents after colonic tumor induction by AOM or AOM / DSS administration

6 Bibliography

Adachi, Y., Li, R., Yamamoto, H., Min, Y., Piao, W., Wang, Y., Imsumran, A., Li, H., Arimura, Y., Lee, C.-T., Imai, K., Carbone, D. P. & Shinomura, Y. 2009: Insulin-like growth factor-I receptor blockade reduces the invasiveness of gastrointestinal cancers via blocking production of matrilysin. *Carcinogenesis 30*, 1305–1313.

Ahmad, I., Iwata, T. & Leung, H. Y. 2012: Mechanisms of FGFR-mediated carcinogenesis. *Biochimica et Biophysica Acta (BBA) - Molecular Cell Research 1823*, 850–860.

Ahmed, D., Eide, P. W., Eilertsen, I. A., Danielsen, S. A., Eknaes, M., Hektoen, M., Lind, G. E. & Lothe, R. A. 2013: Epigenetic and genetic features of 24 colon cancer cell lines. *Oncogenesis 2*, e71.

Al Alam, D., Danopoulos, S., Schall, K., Sala, F. G., Almohazey, D., Fernandez, G. E., Georgia, S., Frey, M. R., Ford, H. R., Grikscheit, T. & Bellusci, S. 2015: Fibroblast growth factor 10 alters the balance between goblet and Paneth cells in the adult mouse small intestine. *American Journal of Physiology - Gastrointestinal and Liver Physiology 308*, G678-G690.

Albanese, C., Reutens, A. T., Bouzahzah, B., Fu, M., D'Amico, M., Link, T., Nicholson, R., Depinho, R. A. & Pestell, R. G. 2000: Sustained mammary gland-directed, ponasterone A-inducible expression in transgenic mice. *FASEB journal official publication of the Federation of American Societies for Experimental Biology 14*, 877–884.

Altomare, D. A. & Testa, J. R. 2005: Perturbations of the AKT signaling pathway in human cancer. *Oncogene 24*, 7455–7464.

American Cancer Society: Treatment of colon cancer, by stage. Available at: http://www.cancer.org/cancer/colonandrectumcancer/detailedguide/colorectal-cancer-treating-by-stage-colon.

Andres, S. F., Santoro, M. A., Mah, A. T., Keku, J. A., Bortvedt, A. E., Blue, R. E. & Lund, P. K. 2015: Deletion of intestinal epithelial insulin receptor attenuates high-fat diet-induced elevations in cholesterol and stem, enteroendocrine, and Paneth cell mRNAs. *American Journal of Physiology - Gastrointestinal and Liver Physiology 308*, G100-G111.

Barker, N., van Es, J. H., Kuipers, J., Kujala, P., van den Born, M., Cozijnsen, M., Haegebarth, A., Korving, J., Begthel, H., Peters, P. J. & Clevers, H. 2007: Identification of stem cells in small intestine and colon by marker gene Lgr5. *Nature 449*, 1003–1007.

Baserga, R. 1995: The insulin-like growth factor I receptor: a key to tumor growth? *Cancer Research 55*, 249–252.

Becker, C., Fantini, M. C. & Neurath, M. F. 2007: High resolution colonoscopy in live mice. *Nature Protocols 1*, 2900–2904.

Bedi, A., Pasricha, P. J., Akhtar, A. J., Barber, J. P., Bedi, G. C., Giardiello, F. M., Zehnbauer, B. A., Hamilton, S. R. & Jones, R. J. 1995: Inhibition of apoptosis during development of colorectal cancer. *Cancer Research 55*, 1811–1816.

Bennecke, M., Kriegl, L., Bajbouj, M., Retzlaff, K., Robine, S., Jung, A., Arkan, M. C., Kirchner, T. & Greten, F. R. 2010: Ink4a/Arf and oncogene-induced senescence prevent tumor progression during alternative colorectal tumorigenesis. *Cancer cell 18*, 135–146.

Benninghoff, A., Drenckhahn, D. & Benninghoff-Drenckhahn (eds.) 2008: *Zellen- und Gewebelehre, Entwicklungslehre, Skelett- und Muskelsystem, Atemsystem, Verdauungssystem, Harn- und Genitalsystem ; [Online-Zugang + interaktive Extras www.studentconsult.de].* Anatomie, makroskopische Anatomie, Histologie, Embryologie, Zellbiologie / Benninghoff; Drenckhahn ; Bd. 1. 956 pp. Elsevier Urban & Fischer, München.

Bertotti, A., Papp, E., Jones, S., Adleff, V., Anagnostou, V., Lupo, B., Sausen, M., Phallen, J., Hruban, C. A., Tokheim, C., Niknafs, N., Nesselbush, M., Lytle, K., Sassi, F., Cottino, F., Migliardi, G., Zanella, E. R., Ribero, D., Russolillo, N., Mellano, A., Muratore, A., Paraluppi, G., Salizzoni, M., Marsoni, S., Kragh, M., Lantto, J., Cassingena, A., Li, Q. K., Karchin, R., Scharpf, R., Sartore-Bianchi, A., Siena, S., Diaz, L. A., JR, Trusolino, L. & Velculescu, V. E. 2015: The genomic landscape of response to EGFR blockade in colorectal cancer. *Nature 526*, 263–267.

Bevins, C. L. & Salzman, N. H. 2011: Paneth cells, antimicrobial peptides and maintenance of intestinal homeostasis. *Nature Reviews Microbiology 9*, 356–368.

Bissahoyo, A. 2005: Azoxymethane Is a Genetic Background-Dependent Colorectal Tumor Initiator and Promoter in Mice: Effects of Dose, Route, and Diet. *Toxicological Sciences 88*, 340–345.

Bonnette, S. G. & Hadsell, D. L. 2001: Targeted disruption of the IGF-I receptor gene decreases cellular proliferation in mammary terminal end buds. *Endocrinology 142*, 4937–4945.

Bos, J. L. 1989: ras oncogenes in human cancer: a review. *Cancer Research 49*, 4682–4689.

Bosman, F. T. (ed.) 2010: *WHO classification of tumours of the digestive system: [reflects the views of a working group that convened for an editorial and consensus conference at the International Agency for Research on Cancer (IARC), Lyon, December 10 - 12, 2009 ; third volume of the 4th edition of the WHO series on histological and genetic typing of human tumours].* World Health Organization classification of tumours, 3 (der 4. ed.). 417 pp. IARC, Lyon.

Bradford, M. M. 1976: A rapid and sensitive method for the quantitation of microgram quantities of protein utilizing the principle of protein-dye binding. *Analytical Biochemistry 72*, 248–254.

Braunstein, E. M., Qiao, X. T., Madison, B., Pinson, K., Dunbar, L. & Gumucio, D. L. 2002: Villin: A marker for development of the epithelial pyloric border. *Developmental Dynamics 224*, 90–102.

Buck, E., Eyzaguirre, A., Rosenfeld-Franklin, M., Thomson, S., Mulvihill, M., Barr, S., Brown, E., O'Connor, M., Yao, Y., Pachter, J., Miglarese, M., Epstein, D., Iwata, K. K., Haley, J. D., Gibson, N. W. & Ji, Q.-S. 2008: Feedback mechanisms promote cooperativity for small molecule inhibitors of epidermal and insulin-like growth factor receptors. *Cancer Research 68*, 8322–8332.

Bustos-Fernández, L. (ed.) (1983): *Colon: Structure and function.* Topics in gastroenterology. 308 pp. Plenum Med. Book Co, New York.

Callahan, R. & Smith, G. H. 2008: Common integration sites for MMTV in viral induced mouse mammary tumors. *Journal of mammary gland biology and neoplasia 13*, 309–321.

Carboni, J. M., Lee, A. V., Hadsell, D. L., Rowley, B. R., Lee, F. Y., Bol, D. K., Camuso, A. E., Gottardis, M., Greer, A. F., Ho, C. P., Hurlburt, W., Li, A., Saulnier, M., Velaparthi, U., Wang, C., Wen, M.-L., Westhouse, R. A., Wittman, M., Zimmermann, K., Rupnow, B. A. & Wong, T. W. 2005: Tumor development by transgenic expression of a constitutively active insulin-like growth factor I receptor. *Cancer Research 65*, 3781–3787.

Cheung, A. F., Am Carter, Kostova, K. K., Woodruff, J. F., Crowley, D., Bronson, R. T., Haigis, K. M. & Jacks, T. 2010: Complete deletion of Apc results in severe polyposis in mice. *Oncogene 29*, 1857–1864.

Cho, K. R. & Vogelstein, B. 1992: Genetic alterations in the adenoma--carcinoma sequence. *Cancer 70*, 1727–1731.

Christensen, J. G., Schreck, R. E., Chan, E., Wang, X., Yang, C., Liu, L., Cui, J., Sun, L., Wei, J., Cherrington, J. M. & Mendel, D. B. 2001: High levels of HER-2 expression alter the ability of epidermal growth factor receptor (EGFR) family tyrosine kinase inhibitors to inhibit EGFR phosphorylation in vivo. *Clinical cancer research an official journal of the American Association for Cancer Research 7*, 4230–4238.

Chung, D. C. 2000: The genetic basis of colorectal cancer: insights into critical pathways of tumorigenesis. *Gastroenterology 119*, 854–865.

Clevers, H. C. & Bevins, C. L. 2013: Paneth Cells: Maestros of the Small Intestinal Crypts. *Annual Review of Physiology 75*, 289–311.

Colnot, S., Niwa-Kawakita, M., Hamard, G., Godard, C., Le Plenier, S., Houbron, C., Romagnolo, B., Berrebi, D., Giovannini, M. & Perret, C. 2004: Colorectal cancers in a new mouse model of familial adenomatous polyposis: Influence of genetic and environmental modifiers. *Laboratory Investigation 84*, 1619–1630.

Coppola, D., Ferber, A., Miura, M., Sell, C., D'Ambrosio, C., Rubin, R. & Baserga, R. 1994: A functional insulin-like growth factor I receptor is required for the mitogenic and transforming activities of the epidermal growth factor receptor. *Molecular and Cellular Biology 14*, 4588–4595.

Dahly, E. M., Guo, Z. & Ney, D. M. 2003: IGF-I augments resection-induced mucosal hyperplasia by altering enterocyte kinetics. *American journal of physiology. Regulatory, integrative and comparative physiology 285*, R800-8.

Dietrich, P., Dragatsis, I., Xuan, S., Zeitlin, S. & Efstratiadis, A. 2000: Conditional mutagenesis in mice with heat shock promoter-driven cre transgenes. *Mammalian genome official journal of the International Mammalian Genome Society 11*, 196–205.

Dong, C. X., Zhao, W., Solomon, C., Rowland, K. J., Ackerley, C., Robine, S., Holzenberger, M., Gonska, T. & Brubaker, P. L. 2014: The Intestinal Epithelial Insulin-Like Growth Factor-1 Receptor Links Glucagon-Like Peptide-2 Action to Gut Barrier Function. *Endocrinology 155*, 370–379.

Dow, L. E., Nasr, Z., Saborowski, M., Ebbesen, S. H., Manchado, E., Tasdemir, N., Lee, T., Pelletier, J. & Lowe, S. W. 2014: Conditional reverse tet-transactivator mouse strains for the efficient induction of TRE-regulated transgenes in mice. *PLoS ONE 9*, e95236.

Drake, R. L. & Gray, H. 2010: *Gray's anatomy for students: [studentconsult …]*. 1103 pp. Elsevier Churchill Livingstone, Philadelphia.

Dunn, S. E., Ehrlich, M., Sharp, N. J., Reiss, K., Solomon, G., Hawkins, R., Baserga, R. & Barrett, J. C. 1998: A dominant negative mutant of the insulin-like growth factor-I receptor inhibits the adhesion, invasion, and metastasis of breast cancer. *Cancer Research 58*, 3353–3361.

Ekyalongo, R. C., Mukohara, T., Kataoka, Y., Funakoshi, Y., Tomioka, H., Kiyota, N., Fujiwara, Y. & Minami, H. 2013: Mechanisms of acquired resistance to insulin-like growth factor 1 receptor inhibitor in MCF-7 breast cancer cell line. *Investigational New Drugs 31*, 293–303.

El Marjou, F., Janssen, K.-P., Hung-Junn Chang, B., Li, M., Hindie, V., Chan, L., Louvard, D., Chambon, P., Metzger, D. & Robine, S. 2004: Tissue-specific and inducible Cre-mediated recombination in the gut epithelium. *genesis 39*, 186–193.

Elphick, D. A. 2005: Paneth cells: Their role in innate immunity and inflammatory disease. *Gut 54*, 1802–1809.

Esposito, D. L., Aru, F., Lattanzio, R., Morgano, A., Abbondanza, M., Malekzadeh, R., Bishehsari, F., Valanzano, R., Russo, A., Piantelli, M., Moschetta, A., Lotti, L. V., Mariani-Costantini, R. & Cheriyath, V. 2012: The Insulin Receptor Substrate 1 (Irs1) in Intestinal Epithelial Differentiation and in Colorectal Cancer. *PLoS ONE 7*, e36190.

Fang, J. Y. & Richardson, B. C. 2005: The MAPK signalling pathways and colorectal cancer. *The Lancet. Oncology 6*, 322–327.

Fearon, E. R. 2011: Molecular Genetics of Colorectal Cancer. *Annual Review of Pathology: Mechanisms of Disease 6*, 479–507.

Fearon, E. R. & Vogelstein, B. 1990: A genetic model for colorectal tumorigenesis. *Cell 61*, 759–767.

Feil, R., Brocard, J., Mascrez, B., LeMeur, M., Metzger, D. & Chambon, P. 1996: Ligand-activated site-specific recombination in mice. *Proceedings of the National Academy of Sciences of the United States of America 93*, 10887–10890.

Feng, Y., Bommer, G. T., Zhao, J., Green, M., Sands, E., Zhai, Y., Brown, K., Burberry, A., Cho, K. R. & Fearon, E. R. 2011: Mutant KRAS promotes hyperplasia and alters differentiation in the colon epithelium but does not expand the presumptive stem cell pool. *Gastroenterology 141*, 1003-1013.e1-10.

Ferrari, L. & Fichera, A. 2015: Neoadjuvant chemoradiation therapy and pathological complete response in rectal cancer. *Gastroenterology report 3*, 277–288.

Ferrary, E., Cohen-Tannoudji, M., Pehau-Arnaudet, G., Lapillonne, A., Athman, R., Ruiz, T., Boulouha, L., El Marjou, F., Doye, A., Fontaine, J. J., Antony, C., Babinet, C., Louvard, D., Jaisser, F. & Robine, S. 1999: In vivo, villin is required for Ca(2+)-dependent F-actin disruption in intestinal brush borders. *The Journal of cell biology 146*, 819–830.

Fodde, R., Edelmann, W., Yang, K., van Leeuwen, C., Carlson, C., Renault, B., Breukel, C., Alt, E., Lipkin, M. & Khan, P. M. 1994: A targeted chain-termination mutation in the mouse Apc gene results in multiple intestinal tumors. *Proceedings of the National Academy of Sciences of the United States of America 91*, 8969–8973.

Forrester, K., Almoguera, C., Han, K., Grizzle, W. E. & Perucho, M. 1987: Detection of high incidence of K-ras oncogenes during human colon tumorigenesis. *Nature 327*, 298–303.

Freier, S., Weiss, O., Eran, M., Flyvbjerg, A., Dahan, R., Nephesh, I., Safra, T., Shiloni, E. & Raz, I. 1999: Expression of the insulin-like growth factors and their receptors in adenocarcinoma of the colon. *Gut 44*, 704–708.

Fürstenberger, G. & Senn, H.-J. 2002: Insulin-like growth factors and cancer. *The Lancet. Oncology 3*, 298–302.

Gajewska, M., Zielniok, K. & Motyl, T. 2013: Autophagy in Development and Remodeling of Mammary Gland. *In* Bailly, Y. (ed.): *Autophagy - A Double-Edged Sword - Cell Survival or Death?* InTech.

Garrouste, F. L., Remacle-Bonnet, M. M., Lehmann, M. M., Marvaldi, J. L. & Pommier, G. J. 1997: Up-regulation of insulin/insulin-like growth factor-I hybrid receptors during differentiation of HT29-D4 human colonic carcinoma cells. *Endocrinology 138*, 2021–2032.

Gerbe, F., Legraverend, C. & Jay, P. 2012: The intestinal epithelium tuft cells: Specification and function. *Cellular and Molecular Life Sciences 69*, 2907–2917.

Gershoni, J. M. & Palade, G. E. 1982: Electrophoretic transfer of proteins from sodium dodecyl sulfate-polyacrylamide gels to a positively charged membrane filter. *Analytical Biochemistry 124*, 396–405.

Gershoni, J. M. & Palade, G. E. 1983: Protein blotting: principles and applications. *Analytical Biochemistry 131*, 1–15.

Ghadimi, B. M., Sackett, D. L., Difilippantonio, M. J., Schröck, E., Neumann, T., Jauho, A., Auer, G. & Ried, T. 2000: Centrosome amplification and instability occurs exclusively in aneuploid, but not in diploid colorectal cancer cell lines, and correlates with numerical chromosomal aberrations. *Genes, chromosomes & cancer 27*, 183–190.

Gregorieff, A. & Clevers, H. 2005: Wnt signaling in the intestinal epithelium: from endoderm to cancer. *Genes & development 19*, 877–890.

Grünwald, V. & Hidalgo, M. 2003: Developing inhibitors of the epidermal growth factor receptor for cancer treatment. *Journal of the National Cancer Institute 95*, 851–867.

Gryfe, R., Swallow, C., Bapat, B., Redston, M., Gallinger, S. & Couture, J. 1997: Molecular biology of colorectal cancer. *Current problems in cancer 21*, 233–300.

Gunawardene, A. R., Corfe, B. M. & Staton, C. A. 2011: Classification and functions of enteroendocrine cells of the lower gastrointestinal tract. *International Journal of Experimental Pathology 92*, 219–231.

Gunther, E. J., Belka, G. K., Wertheim, G. B. W., Wang, J., Hartman, J. L., Boxer, R. B. & Chodosh, L. A. 2002: A novel doxycycline-inducible system for the transgenic analysis of mammary gland biology. *FASEB journal official publication of the Federation of American Societies for Experimental Biology 16*, 283–292.

Gustavsson, B., Carlsson, G., Machover, D., Petrelli, N., Roth, A., Schmoll, H.-J., Tveit, K.-M. & Gibson, F. 2015: A Review of the Evolution of Systemic Chemotherapy in the Management of Colorectal Cancer. *Clinical Colorectal Cancer 14*, 1–10.

Hagan, S., Orr, M. C. M. & Doyle, B. 2013: Targeted therapies in colorectal cancer—an integrative view by PPPM. *EPMA Journal 4*, 3.

Hägebarth, A. 2005: *Brk tyrosine kinase signalling in the gastrointestinal tract*.

Haggar, F. & Boushey, R. 2009: Colorectal Cancer Epidemiology: Incidence, Mortality, Survival, and Risk Factors. *Clinics in Colon and Rectal Surgery 22*, 191–197.

Hakam, A., Yeatman, T. J., Lu, L., Mora, L., Marcet, G., Nicosia, S. V., Karl, R. C. & Coppola, D. 1999: Expression of insulin-like growth factor-1 receptor in human colorectal cancer. *Human Pathology 30*, 1128–1133.

Hanahan, D. & Weinberg, R. A. 2000: The Hallmarks of Cancer. *Cell 100*, 57–70.

Hanahan, D. & Weinberg, R. A. 2011: Hallmarks of Cancer: The Next Generation. *Cell 144*, 646–674.

Haraldsdottir, S. & Bekaii-Saab, T. 2013: Integrating anti-EGFR therapies in metastatic colorectal cancer. *Journal of gastrointestinal oncology 4*, 285–298.

Hav, M., Libbrecht, L., Ferdinande, L., Geboes, K., Pattyn, P. & Cuvelier, C. A. 2015: Pathologic Assessment of Rectal Carcinoma after Neoadjuvant Radio(chemo)therapy: Prognostic Implications. *BioMed research international 2015*, 574540.

Hess, K. R., Varadhachary, G. R., Taylor, S. H., Wei, W., Raber, M. N., Lenzi, R. & Abbruzzese, J. L. 2006: Metastatic patterns in adenocarcinoma. *Cancer 106*, 1624–1633.

Hewish, M., Chau, I. & Cunningham, D. 2009: Insulin-like growth factor 1 receptor targeted therapeutics: novel compounds and novel treatment strategies for cancer medicine. *Recent patents on anti-cancer drug discovery 4*, 54–72.

Heyer, J., Yang, K., Lipkin, M., Edelmann, W. & Kucherlapati, R. 1999: Mouse models for colorectal cancer. *Oncogene 18*, 5325–5333.

Hinoi, T., Akyol, A., Theisen, B. K., Ferguson, D. O., Greenson, J. K., Williams, B. O., Cho, K. R. & Fearon, E. R. 2007: Mouse model of colonic adenoma-carcinoma progression based on somatic Apc inactivation. *Cancer Research 67*, 9721–9730.

Holland, J. F., Frei, E. & Kufe, D. W. 2003: *Cancer medicine*. Decker, Hamilton, Ont.

Höpfner, M., Huether, A., Sutter, A. P., Baradari, V., Schuppan, D. & Scherübl, H. 2006: Blockade of IGF-1 receptor tyrosine kinase has antineoplastic effects in hepatocellular carcinoma cells. *Biochemical Pharmacology 71*, 1435–1448.

Huang, L., Li, T.-J., Zhang, J.-W., Liu, S., Fu, B.-S. & Liu, W. 2014: Neoadjuvant chemotherapy followed by surgery versus surgery alone for colorectal cancer: meta-analysis of randomized controlled trials. *Medicine 93*, e231.

Huether, A., Hopfner, M., Sutter, A. P., Baradari, V., Schuppan, D. & Scherubl, H. 2006: Signaling pathways involved in the inhibition of epidermal growth factor receptor by erlotinib in hepatocellular cancer. *World journal of gastroenterology 12*, 5160–5167.

Ito, R., Shin-Ya, M., Kishida, T., Urano, A., Takada, R., Sakagami, J., Imanishi, J., Kita, M., Ueda, Y., Iwakura, Y., Kataoka, K., Okanoue, T. & Mazda, O. 2006: Interferon-gamma is causatively involved in experimental inflammatory bowel disease in mice. *Clinical and Experimental Immunology 146*, 330–338.

Itoh, N., Semba, S., Ito, M., Takeda, H., Kawata, S. & Yamakawa, M. 2002: Phosphorylation of Akt/PKB is required for suppression of cancer cell apoptosis and tumor progression in human colorectal carcinoma. *Cancer 94*, 3127–3134.

Jakobsen, A., Andersen, F., Fischer, A., Jensen, L. H., Jorgensen, J. C. R., Larsen, O., Lindebjerg, J., Ploen, J., Rafaelsen, S. R. & Vilandt, J. 2015: Neoadjuvant chemotherapy in locally advanced colon cancer. A phase II trial. *Acta oncologica (Stockholm, Sweden) 54*, 1747–1753.

Jaladanki, R. N. & Wang, J.-Y. 2011: Regulation of Gastrointestinal Mucosal Growth. *Colloquium Series on Integrated Systems Physiology: From Molecule to Function 3*, 1–114.

Janku, F., Stewart, D. J. & Kurzrock, R. 2010: Targeted therapy in non-small-cell lung cancer—is it becoming a reality? *Nature Reviews Clinical Oncology 7*, 401–414.

Janssen, K. P., el-Marjou, F., Pinto, D., Sastre, X., Rouillard, D., Fouquet, C., Soussi, T., Louvard, D. & Robine, S. 2002: Targeted expression of oncogenic K-ras in intestinal epithelium causes spontaneous tumorigenesis in mice. *Gastroenterology 123*, 492–504.

Johansson, M. E. V., Ambort, D., Pelaseyed, T., Schütte, A., Gustafsson, J. K., Ermund, A., Subramani, D. B., Holmén-Larsson, J. M., Thomsson, K. A., Bergström, J. H., van der Post, S., Rodriguez-Piñeiro, A. M., Sjövall, H., Bäckström, M. & Hansson, G. C. 2011: Composition and functional role of the mucus layers in the intestine. *Cellular and Molecular Life Sciences 68*, 3635–3641.

Johnson, R. L. & Fleet, J. C. 2013: Animal models of colorectal cancer. *Cancer and Metastasis Reviews 32*, 39–61.

Jones, R. A., Campbell, C. I., Gunther, E. J., Chodosh, L. A., Petrik, J. J., Khokha, R. & Moorehead, R. A. 2007: Transgenic overexpression of IGF-IR disrupts mammary ductal morphogenesis and induces tumor formation. *Oncogene 26*, 1636–1644.

Kaleko, M., Rutter, W. J. & Miller, A. D. 1990: Overexpression of the human insulinlike growth factor I receptor promotes ligand-dependent neoplastic transformation. *Molecular and Cellular Biology 10*, 464–473.

Karim, B. O. & Huso, D. L. 2013: Mouse models for colorectal cancer. *American journal of cancer research 3*, 240–250.

Karoui, M., Rullier, A., Luciani, A., Bonnetain, F., Auriault, M.-L., Sarran, A., Monges, G., Trillaud, H., Le Malicot, K., Leroy, K., Sobhani, I., Bardier, A., Moreau, M., Brindel, I., Seitz, J. F. & Taieb, J. 2015: Neoadjuvant FOLFOX 4 versus FOLFOX 4 with Cetuximab versus immediate surgery for high-risk stage II and III colon cancers: a multicentre randomised controlled phase II trial--the PRODIGE 22--ECKINOXE trial. *BMC cancer 15*, 511.

Kaulfuß, S., Burfeind, P., Gaedcke, J. & Scharf, J.-G. 2009: Dual silencing of insulin-like growth factor-I receptor and epidermal growth factor receptor in colorectal cancer cells is associated with decreased proliferation and enhanced apoptosis. *Molecular cancer therapeutics 8*, 821–833.

Kheirelseid, E. A. H., Miller, N. & Kerin, M. J. 2013: Molecular biology of colorectal cancer: Review of the literature. *American Journal of Molecular Biology 03*, 72–80.

Kim, Y. S. & Ho, S. B. 2010: Intestinal Goblet Cells and Mucins in Health and Disease: Recent Insights and Progress. *Current Gastroenterology Reports 12*, 319–330.

Kitajima, S., Takuma, S. & Morimoto, M. 1999: Tissue distribution of dextran sulfate sodium (DSS) in the acute phase of murine DSS-induced colitis. *The Journal of veterinary medical science / the Japanese Society of Veterinary Science 61*, 67–70.

Kleman, M. I., Overvik, E., Porsch-Hallstrom, I., Blanck, A. & Gustafsson, J. A. 1993: The heterocyclic amines IQ and MeIQx show no promotive effect in a short-term in vivo liver carcinogenesis assay. *Carcinogenesis 14*, 2123–2125.

Kobayashi, A., Donaldson, D. S., Erridge, C., Kanaya, T., Williams, I. R., Ohno, H., Mahajan, A. & Mabbott, N. A. 2013: The functional maturation of M cells is dramatically reduced in the Peyer's patches of aged mice. *Mucosal immunology 6*, 1027–1037.

Konsavage, W. M., Jin, G. & Yochum, G. S. 2012: The Myc 3' Wnt-Responsive Element Regulates Homeostasis and Regeneration in the Mouse Intestinal Tract. *Molecular and Cellular Biology 32*, 3891–3902.

Krimpenfort, P., Song, J.-Y., Proost, N., Zevenhoven, J., Jonkers, J. & Berns, A. 2012: Deleted in colorectal carcinoma suppresses metastasis in p53-deficient mammary tumours. *Nature 482*, 538–541.

Kuhry, E., Schwenk, W., Gaupset, R., Romild, U. & Bonjer, J. 2008: Long-term outcome of laparoscopic surgery for colorectal cancer: A cochrane systematic review of randomised controlled trials. *Cancer Treatment Reviews 34*, 498–504.

Laemmli, U. K. 1970: Cleavage of Structural Proteins during the Assembly of the Head of Bacteriophage T4. *Nature 227*, 680–685.

Lemmon, M. A. & Schlessinger, J. 2010: Cell Signaling by Receptor Tyrosine Kinases. *Cell 141*, 1117–1134.

Levin, B., Lieberman, D. A., McFarland, B., Smith, R. A., Brooks, D., Andrews, K. S., Dash, C., Giardiello, F. M., Glick, S., Levin, T. R., Pickhardt, P., Rex, D. K., Thorson, A. & Winawer, S. J. 2008: Screening and Surveillance for the Early Detection of Colorectal Cancer and Adenomatous Polyps, 2008: A Joint Guideline from the American Cancer Society, the US Multi-Society Task Force on Colorectal Cancer, and the American College of Radiology. *CA: A Cancer Journal for Clinicians 58*, 130–160.

Li, Z.-J. 2013: Insulin-like growth factor-1 induces lymphangiogenesis and facilitates lymphatic metastasis in colorectal cancer. *World Journal of Gastroenterology 19*, 7788.

Lin, L. & Bivona, T. G. 2012: Mechanisms of Resistance to Epidermal Growth Factor Receptor Inhibitors and Novel Therapeutic Strategies to Overcome Resistance in NSCLC Patients. *Chemotherapy Research and Practice 2012*, 1–9.

Luceri, C. 2000: Detection of somatic DNA alterations in azoxymethane-induced F344 rat colon tumors by random amplified polymorphic DNA analysis. *Carcinogenesis 21*, 1753–1756.

Lurje, G. & Lenz, H.-J. 2009: EGFR Signaling and Drug Discovery. *Oncology 77*, 400–410.

Madison, B. B. 2002: cis Elements of the Villin Gene Control Expression in Restricted Domains of the Vertical (Crypt) and Horizontal (Duodenum, Cecum) Axes of the Intestine. *Journal of Biological Chemistry 277*, 33275–33283.

Maltzman, T., Whittington, J., Driggers, L., Stephens, J. & Ahnen, D. 1997: AOM-induced mouse colon tumors do not express full-length APC protein. *Carcinogenesis 18*, 2435–2439.

Malumbres, M. & Barbacid, M. 2003: RAS oncogenes: the first 30 years. *Nature reviews. Cancer 3*, 459–465.

Mamiatis, T., Fritsch, E. F., Sambrook, J. & Engel, J. 1985: Molecular cloning-A laboratory manual. New York: Cold Spring Harbor Laboratory. 1982, 545 S., 42 $. *Acta Biotechnologica 5*, 104.

Martel, C. de, Ferlay, J., Franceschi, S., Vignat, J., Bray, F., Forman, D. & Plummer, M. 2012: Global burden of cancers attributable to infections in 2008: A review and synthetic analysis. *The Lancet Oncology 13*, 607–615.

Maunoury, R., Robine, S., Pringault, E., Huet, C., Guenet, J. L., Gaillard, J. A. & Louvard, D. 1988: Villin expression in the visceral endoderm and in the gut anlage during early mouse embryogenesis. *The EMBO journal 7*, 3321–3329.

McCarthy, K., Pearson, K., Fulton, R. & Hewitt, J. 1996: Pre-operative chemoradiation for non-metastatic locally advanced rectal cancer. *In* McCarthy, K. (ed.): *Cochrane Database of Systematic Reviews*. John Wiley & Sons, Ltd, Chichester, UK.

Means, A. L., Xu, Y., Zhao, A., Ray, K. C. & Gu, G. 2008: A CK19(CreERT) knockin mouse line allows for conditional DNA recombination in epithelial cells in multiple endodermal organs. *Genesis (New York, N.Y. 2000) 46*, 318–323.

Medema, J. P. & Vermeulen, L. 2011: Microenvironmental regulation of stem cells in intestinal homeostasis and cancer. *Nature 474*, 318–326.

Miron, N. & Cristea, V. 2012: Enterocytes: Active cells in tolerance to food and microbial antigens in the gut. *Clinical & Experimental Immunology 167*, 405–412.

Montagut, C., Dalmases, A., Bellosillo, B., Crespo, M., Pairet, S., Iglesias, M., Salido, M., Gallen, M., Marsters, S., Tsai, S. P., Minoche, A., Somasekar, S., Serrano, S., Himmelbauer, H., Bellmunt, J., Rovira, A., Settleman, J., Bosch, F. & Albanell, J. 2012: Identification of a mutation in the extracellular domain of the Epidermal Growth Factor Receptor conferring cetuximab resistance in colorectal cancer. *Nature Medicine 18*, 221–223.

Montgomery, R. K., Mulberg, A. E. & Grand, R. J. 1999: Development of the human gastrointestinal tract: twenty years of progress. *Gastroenterology 116*, 702–731.

Moran, G. W., Leslie, F. C., Levison, S. E., Worthington J. & McLaughlin, J. T. 2008: Enteroendocrine cells: Neglected players in gastrointestinal disorders? *Therapeutic Advances in Gastroenterology 1*, 51–60.

Muzny, D. M., Bainbridge, M. N., Chang, K., Dinh, H. H., Drummond, J. A., Fowler, G., Kovar, C. L., Lewis, L. R., Morgan, M. B., Newsham, I. F., Reid, J. G., Santibanez, J., Shinbrot, E., Trevino, L. R., Wu, Y.-Q., Wang, M., Gunaratne, P., Donehower, L. A., Creighton, C. J., Wheeler, D. A., Gibbs, R. A., Lawrence, M. S., Voet, D., Jing, R., Cibulskis, K., Sivachenko, A., Stojanov, P., McKenna, A., Lander, E. S., Gabriel, S., Getz, G., Ding, L., Fulton, R. S., Koboldt, D. C., Wylie, T., Walker, J., Dooling, D. J., Fulton, L., Delehaunty, K. D., Fronick, C. C., Demeter, R., Mardis, E. R., Wilson, R. K., Chu, A., Chun, H.-J. E., Mungall, A. J., Pleasance, E., Gordon Robertson, A., Stoll, D., Balasundaram, M., Birol, I., Butterfield, Y. S. N., Chuah, E., Coope, R. J. N., Dhalla, N., Guin, R., Hirst, C., Hirst, M., Holt, R. A., Lee, D., Li, H. I., Mayo, M., Moore, R. A., Schein, J. E., Slobodan, J. R., Tam, A., Thiessen, N., Varhol, R., Zeng, T., Zhao, Y., Jones, S. J. M., Marra, M. A., Bass, A. J., Ramos, A. H., Saksena, G., Cherniack, A. D., Schumacher, S. E., Tabak, B., Carter, S. L., Pho, N. H., Nguyen, H., Onofrio, R. C., Crenshaw, A., Ardlie, K., Beroukhim, R., Winckler, W., Meyerson, M., Protopopov, A., Zhang, J., Hadjipanayis, A., Lee, E., Xi, R., Yang, L., Ren, X., Zhang, H., Sathiamoorthy, N., Shukla, S., Chen, P.-C., Haseley, P., Xiao, Y., Lee, S., Seidman, J., Chin, L., Park, P. J., Kucherlapati, R.,

Todd Auman, J., Hoadley, K. A., Du, Y., Wilkerson, M. D., Shi, Y., Liquori, C., Meng, S., Li, L., Turman, Y. J., Topal, M. D., Tan, D., Waring, S., Buda, E., Walsh, J., Jones, C. D., Mieczkowski, P. A., Singh, D., Wu, J., Gulabani, A., Dolina, P., Bodenheimer, T., Hoyle, A. P., Simons, J. V., Soloway, M., Mose, L. E., Jefferys, S. R., Balu, S., O'Connor, B. D., Prins, J. F., Chiang, D. Y., Neil Hayes, D., Perou, C. M., Hinoue, T., Weisenberger, D. J., Maglinte, D. T., Pan, F., Berman, B. P., Van Den Berg, David J., Shen, H., Triche Jr, T., Baylin, S. B., Laird, P. W., Noble, M., Voet, D., Gehlenborg, N., DiCara, D., Wu, C.-J., Yingchun Liu, S., Zhou, L., Lin, P., Park, R. W., Nazaire, M.-D., Robinson, J., Thorvaldsdottir, H., Mesirov, J., Thorsson, V., Reynolds, S. M., Bernard, B., Kreisberg, R., Lin, J., Iype, L., Bressler, R., Erkkilä, T., Gundapuneni, M., Liu, Y., Norberg, A., Robinson, T., Yang, D., Zhang, W., Shmulevich, I., Ronde, J. J. de, Schultz, N., Cerami, E., Ciriello, G., Goldberg, A. P., Gross, B., Jacobsen, A., Gao, J., Kaczkowski, B., Sinha, R., Arman Aksoy, B., Antipin, Y., Reva, B., Shen, R., Taylor, B. S., Chan, T. A., Ladanyi, M., Sander, C., Akbani, R., Zhang, N., Broom, B. M., Casasent, T., Unruh, A., Wakefield, C., Hamilton, S. R., Craig Cason, R., Baggerly, K. A., Weinstein, J. N., Haussler, D., Benz, C. C., Stuart, J. M., Benz, S. C., Zachary Sanborn, J., Vaske, C. J., Zhu, J., Szeto, C., Scott, G. K., Yau, C., Ng, S., Goldstein, T., Ellrott, K., Collisson, E., Cozen, A. E., Zerbino, D., Wilks, C., Craft, B., Spellman, P., Penny, R., Shelton, T., Hatfield, M., Morris, S., Yena, P., Shelton, C., Sherman, M., Paulauskis, J., Gastier-Foster, J. M., Bowen, J., Ramirez, N. C., Black, A., Pyatt, R., Wise, L., White, P., Bertagnolli, M., Brown, J., Chu, G. C., Czerwinski, C., Denstman, F., Dhir, R., Dörner, A., Fuchs, C. S., Guillem, J. G., Iacocca, M., Juhl, H., Kaufman, A., Kohl III, B., van Le, X., Mariano, M. C., Medina, E. N., Meyers, M., Nash, G. M., Paty, P. B., Petrelli, N., Rabeno, B., Richards, W. G., Solit, D., Swanson, P., Temple, L., Tepper, J. E., Thorp, R., Vakiani, E., Weiser, M. R., Willis, J. E., Witkin, G., Zeng, Z., Zinner, M. J., Zornig, C., Jensen, M. A., Sfeir, R., Kahn, A. B., Chu, A. L., Kothiyal, P., Wang, Z., Snyder, E. E., Pontius, J., Pihl, T. D., Ayala, B., Backus, M., Walton, J., Whitmore, J., Baboud, J., Berton, D. L., Nicholls, M. C., Srinivasan, D., Raman, R., Girshik, S., Kigonya, P. A., Alonso, S., Sanbhadti, R. N., Barletta, S. P., Greene, J. M., Pot, D. A., Mills Shaw, K. R., Dillon, L. A. L., Buetow, K., Davidsen, T., Demchok, J. A., Eley, G., Ferguson, M., Fielding, P., Schaefer, C., Sheth, M., Yang, L., Guyer, M. S., Ozenberger, B. A., Palchik, J. D., Peterson, J., Sofia, H. J. & Thomson., E. 2012: Comprehensive molecular characterization of human colon and rectal cancer. *Nature 487*, 330–337.

Nambiar, P. R., Girnun, G., Lillo, N. A., Guda, K., Whiteley, H. E. & Rosenberg, D. W. 2003: Preliminary analysis of azoxymethane induced colon tumors in inbred mice commonly used as transgenic/knockout progenitors. *International journal of oncology 22*, 145–150.

Nanda, N., Dhawan, D. K., Bhatia, A., Mahmood, A., Mahmood, S. & Sethi, G. 2016: Doxycycline Promotes Carcinogenesis & Metastasis via Chronic Inflammatory Pathway: An In Vivo Approach. *PLOS ONE 11*, e0151539.

National Cancer Institute: Colon Cancer Treatment–Patient Version (PDQ®). Available at: http://www.cancer.gov/types/colorectal/patient/colon-treatment-pdq#link/_163_toc.

Neufert, C., Becker, C. & Neurath, M. F. 2007: An inducible mouse model of colon carcinogenesis for the analysis of sporadic and inflammation-driven tumor progression. *Nature Protocols 2*, 1998–2004.

Nguyen, A., Loo, J. M., Mital, R., Weinberg, E. M., Man, F. Y., Zeng, Z., Paty, P. B., Saltz, L., Janjigian, Y. Y., Stanchina, E. de & Tavazoie, S. F. 2016: PKLR promotes colorectal cancer liver colonization through induction of glutathione synthesis. *The Journal of clinical investigation 126*, 681–694.

Ohue, M., Tomita, N., Monden, T., Fujita, M., Fukunaga, M., Takami, K., Yana, I., Ohnishi, T., Enomoto, T. & Inoue, M. 1994: A frequent alteration of p53 gene in carcinoma in adenoma of colon. *Cancer Research 54*, 4798–4804.

Oshima, M., Oshima, H., Kitagawa, K., Kobayashi, M., Itakura, C. & Taketo, M. 1995: Loss of Apc heterozygosity and abnormal tissue building in nascent intestinal polyps in mice carrying a truncated Apc gene. *Proceedings of the National Academy of Sciences of the United States of America 92*, 4482–4486.

Overeem, A. W., Posovszky, C., Rings, E. H. M. M., Giepmans, B. N. G. & van IJzendoorn, S. C. D. 2016: The role of enterocyte defects in the pathogenesis of congenital diarrheal disorders. *Disease Models & Mechanisms 9*, 1–12.

Perše, M. & Cerar, A. 2012: Dextran Sodium Sulphate Colitis Mouse Model: Traps and Tricks. *Journal of Biomedicine and Biotechnology 2012*, 1–13.

Petersen, S. H., Harling, H., Kirkeby, L. T., Wille-Jørgensen, P. & Mocellin, S. 1996: Postoperative adjuvant chemotherapy in rectal cancer operated for cure. *In* Petersen, S. H. (ed.): *Cochrane Database of Systematic Reviews*. John Wiley & Sons, Ltd, Chichester, UK.

Pillai, R. N. & Ramalingam, S. S. 2013: Inhibition of insulin-like growth factor receptor: end of a targeted therapy? *Translational lung cancer research 2*, 14–22.

Pinto, D., Robine, S., Jaisser, F., El Marjou, F. E. & Louvard, D. 1999: Regulatory sequences of the mouse villin gene that efficiently drive transgenic expression in immature and differentiated epithelial cells of small and large intestines. *The Journal of biological chemistry 274*, 6476–6482.

Pollak, M. 2008: Insulin and insulin-like growth factor signalling in neoplasia. *Nature Reviews Cancer 8*, 915–928.

Pollard, P., Deheragoda, M., Segditsas, S., Lewis, A., Rowan, A., Howarth, K., Willis, L., Nye, E., McCart, A., Mandir, N., Silver, A., Goodlad, R., Stamp, G., Cockman, M., East, P., Spencer–Dene, B., Poulsom, R., Wright, N. & Tomlinson, I. 2009: The Apc1322T Mouse Develops Severe Polyposis Associated With Submaximal Nuclear β-Catenin Expression. *Gastroenterology 136*, 2204-2213.e13.

Powell, S. M., Zilz, N., Beazer-Barclay, Y., Bryan, T. M., Hamilton, S. R., Thibodeau, S. N., Vogelstein, B. & Kinzler, K. W. 1992: APC mutations occur early during colorectal tumorigenesis. *Nature 359*, 235–237.

Qiao, X. T., Ziel, J. W., McKimpson, W., Madison, B. B., Todisco, A., Merchant, J. L., Samuelson, L. C. & Gumucio, D. L. 2007: Prospective identification of a multilineage progenitor in murine stomach epithelium. *Gastroenterology 133*, 1989–1998.

Ramirez, C. & Gebert, A. 2003: Vimentin-positive Cells in the Epithelium of Rabbit Ileal Villi Represent Cup Cells but not M-cells. *Journal of Histochemistry & Cytochemistry 51*, 1533–1544.

Reinmuth, N., Fan, F., Liu, W., Parikh, A. A., Stoeltzing, O., Jung, Y. D., Bucana, C. D., Radinsky, R., Gallick, G. E. & Ellis, L. M. 2002: Impact of Insulin-Like Growth Factor Receptor-I Function on Angiogenesis, Growth, and Metastasis of Colon Cancer. *Laboratory Investigation 82*, 1377–1389.

Resnicoff, M., Burgaud, J. L., Rotman, H. L., Abraham, D. & Baserga, R. 1995: Correlation between apoptosis, tumorigenesis, and levels of insulin-like growth factor I receptors. *Cancer Research 55*, 3739–3741.

Robanus-Maandag, E. C., Koelink, P. J., Breukel, C., Salvatori, D. C. F., Jagmohan-Changur, S. C., Bosch, C. A. J., Verspaget, H. W., Devilee, P., Fodde, R. & Smits, R. 2010: A new conditional Apc-mutant mouse model for colorectal cancer. *Carcinogenesis 31*, 946–952.

Robine, S., Huet, C., Moll, R., Sahuquillo-Merino, C., Coudrier, E., Zweibaum, A. & Louvard, D. 1985: Can villin be used to identify malignant and undifferentiated normal digestive epithelial cells? *Proceedings of the National Academy of Sciences of the United States of America 82*, 8488–8492.

Rosenberg, D. W., Giardina, C. & Tanaka, T. 2008: Mouse models for the study of colon carcinogenesis. *Carcinogenesis 30*, 183–196.

Roth, S., Franken, P., van Veelen, W., Blonden, L., Raghoebir, L., Beverloo, B., van Drunen, E., Kuipers, E. J., Rottier, R., Fodde, R. & Smits, R. 2009: Generation of a tightly regulated doxycycline-inducible model for studying mouse intestinal biology. *genesis 47*, 7–13.

Saam, J. R. & Gordon, J. I. 1999: Inducible gene knockouts in the small intestinal and colonic epithelium. *The Journal of biological chemistry 274*, 38071–38082.

Sachdev, D., Hartell, J. S., Lee, A. V., Zhang, X. & Yee, D. 2004: A dominant negative type I insulin-like growth factor receptor inhibits metastasis of human cancer cells. *The Journal of biological chemistry 279*, 5017–5024.

Sachdev, D. & Yee, D. 2007: Disrupting insulin-like growth factor signaling as a potential cancer therapy. *Molecular cancer therapeutics 6*, 1–12.

Sadagurski, M., Yakar, S., Weingarten, G., Holzenberger, M., Rhodes, C. J., Breitkreutz, D., LeRoith, D. & Wertheimer, E. 2006: Insulin-Like Growth Factor 1 Receptor Signaling Regulates Skin Development and Inhibits Skin Keratinocyte Differentiation. *Molecular and Cellular Biology 26*, 2675–2687.

Saglam, O., Garrett, C. R., Boulware, D., Sayegh, Z., Shibata, D., Malafa, M., Yeatman, T., Cheng, J. Q., Sebti, S. & Coppola, D. 2007: Activation of the serine/threonine protein kinase AKT during the progression of colorectal neoplasia. *Clinical Colorectal Cancer 6*, 652–656.

Saiki, R. K., Scharf, S., Faloona, F., Mullis, K. B., Horn, G. T., Erlich, H. A. & Arnheim, N. 1985: Enzymatic amplification of beta-globin genomic sequences and restriction site analysis for diagnosis of sickle cell anemia. *Science (New York, N.Y.) 230*, 1350–1354.

Sangiorgi, E. & Capecchi, M. R. 2008: Bmi1 is expressed in vivo in intestinal stem cells. *Nature Genetics 40*, 915–920.

Sasai, H., Masaki, M. & Wakitani, K. 2000: Suppression of polypogenesis in a new mouse strain with a truncated Apc(Delta474) by a novel COX-2 inhibitor, JTE-522. *Carcinogenesis 21*, 953–958.

Sato, T., Vries, R. G., Snippert, H. J., van de Wetering, M., Barker, N., Stange, D. E., van Es, J. H., Abo, A., Kujala, P., Peters, P. J. & Clevers, H. 2009: Single Lgr5 stem cells build crypt–villus structures in vitro without a mesenchymal niche. *Nature 459*, 262–265.

Sauer, R., Becker, H., Hohenberger, W., Rodel, C., Wittekind, C., Fietkau, R., Martus, P., Tschmelitsch, J., Hager, E., Hess, C. F., Karstens, J.-H., Liersch, T., Schmidberger, H. & Raab, R. 2004: Preoperative versus postoperative chemoradiotherapy for rectal cancer. *The New England journal of medicine 351*, 1731–1740.

Seemann, H. 2013: Die Rolle der IGF-Achse in Kombination mit anderen Wachstumsfaktor-Signalwegen bei der Resistenz oder dem Ansprechen von kolorektalen Karzinomen auf eine Radiochemotherapie. *Dissertation*.

Sekharam, M., Zhao, H., Sun, M., Fang, Q., Zhang, Q., Yuan, Z., Dan, H. C., Boulware, D., Cheng, J. Q. & Coppola, D. 2003: Insulin-like growth factor 1 receptor enhances invasion and induces resistance to apoptosis of colon cancer cells through the Akt/Bcl-x(L) pathway. *Cancer Research 63*, 7708–7716.

Seow, H. F., Yip, W. K. & Fifis, T. 2016: Advances in targeted and immunobased therapies for colorectal cancer in the genomic era. *OncoTargets and therapy 9*, 1899–1920.

Shaib, W., Mahajan, R. & El-Rayes, B. 2013: Markers of resistance to anti-EGFR therapy in colorectal cancer. *Journal of gastrointestinal oncology 4*, 308–318.

Shaukat, A., Arain, M., Anway, R., Manaktala, S., Pohlman, L. & Thyagarajan, B. 2012: Is KRAS Mutation Associated with Interval Colorectal Cancers? *Digestive Diseases and Sciences 57*, 913–917.

Shibata, H., Toyama, K., Shioya, H., Ito, M., Hirota, M., Hasegawa, S., Matsumoto, H., Takano, H., Akiyama, T., Toyoshima, K., Kanamaru, R., Kanegae, Y., Saito, I., Nakamura, Y., Shiba, K. & Noda, T. 1997: Rapid colorectal adenoma formation initiated by conditional targeting of the Apc gene. *Science (New York, N.Y.) 278*, 120–123.

Shinya, H. & Wolff, W. I. 1979: Morphology, anatomic distribution and cancer potential of colonic polyps. *Annals of surgery 190*, 679–683.

Shiratsuchi, I., Akagi, Y., Kawahara, A., Kinugasa, T., Romeo, K., Yoshida, T., Ryu, Y., Gotanda, Y., Kage, M. & Shirouzu, K. 2011: Expression of IGF-1 and IGF-1R and their relation to clinicopathological factors in colorectal cancer. *Anticancer research 31*, 2541–2545.

Smits, R., Kielman, M. F., Breukel, C., Zurcher, C., Neufeld, K., Jagmohan-Changur, S., Hofland, N., van Dijk, J., White, R., Edelmann, W., Kucherlapati, R., Khan, P. M. & Fodde, R. 1999: Apc1638T: a mouse model delineating critical domains of the adenomatous polyposis coli protein involved in tumorigenesis and development. *Genes & development 13*, 1309–1321.

Sohn, O. S., Fiala, E. S., Requeijo, S. P., Weisburger, J. H. & Gonzalez, F. J. 2001: Differential effects of CYP2E1 status on the metabolic activation of the colon carcinogens azoxymethane and methylazoxymethanol. *Cancer Research 61*, 8435–8440.

Somasundaram, K. 2000: Tumor suppressor p53: regulation and function. *Frontiers in bioscience a journal and virtual library 5*, D424-37.

Spano, J. P. 2005a: Epidermal growth factor receptor signaling in colorectal cancer: Preclinical data and therapeutic perspectives. *Annals of Oncology 16*, 189–194.

Spano, J. P. 2005b: Impact of EGFR expression on colorectal cancer patient prognosis and survival. *Annals of Oncology 16*, 102–108.

Specian, R. D. & Oliver, M. G. 1991: Functional biology of intestinal goblet cells. *The American journal of physiology 260*, C183-93.

Spitzner, M., Emons, G., Kramer, F., Gaedcke, J., Rave-Fränk, M., Scharf, J.-G., Burfeind, P., Becker, H., Beissbarth, T., Ghadimi, B. M., Ried, T. & Grade, M. 2010: A gene expression signature for chemoradiosensitivity of colorectal cancer cells. *International journal of radiation oncology, biology, physics 78*, 1184–1192.

Suda, K., Mizuuchi, H., Sato, K., Takemoto, T., Iwasaki, T. & Mitsudomi, T. 2014: The insulin-like growth factor 1 receptor causes acquired resistance to erlotinib in lung cancer cells with the wild-type epidermal growth factor receptor. *International Journal of Cancer 135*, 1002–1006.

Suzuki, R., Kohno, H., Sugie, S., Nakagama, H. & Tanaka, T. 2006: Strain differences in the susceptibility to azoxymethane and dextran sodium sulfate-induced colon carcinogenesis in mice. *Carcinogenesis 27*, 162–169.

Tabernero, J., Salazar, R., Casado, E., Martinelli, E., Gómez, P. & Baselga, J. 2004: Targeted therapy in advanced colon cancer: the role of new therapies. *Annals of oncology official journal of the European Society for Medical Oncology / ESMO 15 Suppl 4*, iv55-62.

Takahashi, M., Mutoh, M., Kawamori, T., Sugimura, T. & Wakabayashi, K. 2000a: Altered expression of beta-catenin, inducible nitric oxide synthase and cyclooxygenase-2 in azoxymethane-induced rat colon carcinogenesis. *Carcinogenesis 21*, 1319–1327.

Takahashi, M., Nakatsugi, S., Sugimura, T. & Wakabayashi, K. 2000b: Frequent mutations of the beta-catenin gene in mouse colon tumors induced by azoxymethane. *Carcinogenesis 21*, 1117–1120.

Takayama, T., Miyanishi, K., Hayashi, T., Sato, Y. & Niitsu, Y. 2006: Colorectal cancer: Genetics of development and metastasis. *Journal of Gastroenterology 41*, 185–192.

Tan, C. & Du, X. 2012: KRAS mutation testing in metastatic colorectal cancer. *World journal of gastroenterology 18*, 5171–5180.

Tanaka, T., Kohno, H., Suzuki, R., Yamada, Y., Sugie, S. & Mori, H. 2003: A novel inflammation-related mouse colon carcinogenesis model induced by azoxymethane and dextran sodium sulfate. *Cancer Science 94*, 965–973.

Taneja, P., Frazier, D. P., Kendig, R. D., Maglic, D., Sugiyama, T., Kai, F., Taneja, N. K. & Inoue, K. 2009: MMTV mouse models and the diagnostic values of MMTV-like sequences in human breast cancer. *Expert review of molecular diagnostics 9*, 423–440.

Tang, J., Salama, R., Gadgeel, S. M., Sarkar, F. H. & Ahmad, A. 2013: Erlotinib Resistance in Lung Cancer: Current Progress and Future Perspectives. *Frontiers in Pharmacology 4*.

Thaker, A. I., Shaker, A., Rao, M. S. & Ciorba, M. A. 2012: Modeling Colitis-Associated Cancer with Azoxymethane (AOM) and Dextran Sulfate Sodium (DSS). *Journal of Visualized Experiments*.

Tomasetti, C., Marchionni, L., Nowak, M. A., Parmigiani, G. & Vogelstein, B. 2015: Only three driver gene mutations are required for the development of lung and colorectal cancers. *Proceedings of the National Academy of Sciences 112*, 118–123.

Tsao, J. & Shibata, D. 1994: Further evidence that one of the earliest alterations in colorectal carcinogenesis involves APC. *The American journal of pathology 145*, 531–534.

van Landeghem, L., Santoro, M. A., Mah, A. T., Krebs, A. E., Dehmer, J. J., McNaughton, K. K., Helmrath, M. A., Magness, S. T. & Lund, P. K. 2015: IGF1 stimulates crypt expansion via differential activation of 2 intestinal stem cell populations. *The FASEB Journal 29*, 2828–2842.

Vogelstein, B., Fearon, E. R., Hamilton, S. R., Kern, S. E., Preisinger, A. C., Leppert, M., Nakamura, Y., White, R., Smits, A. M. & Bos, J. L. 1988: Genetic alterations during colorectal-tumor development. *The New England journal of medicine 319*, 525–532.

Vrieling, A., Voskuil, D. W., Bosma, A., Majoor, D. M., van Doorn, J., Cats, A., Depla, A. C., Timmer, R., Witteman, B. J., Wesseling, J., Kampman, E. & Van't Veer, L. J. 2009: Expression of insulin-like growth factor system components in colorectal tissue and its relation with serum IGF levels. *Growth Hormone & IGF Research 19*, 126–135.

Wang, Q. S., Papanikolaou, A., Sabourin, C. L. & Rosenberg, D. W. 1998: Altered expression of cyclin D1 and cyclin-dependent kinase 4 in azoxymethane-induced mouse colon tumorigenesis. *Carcinogenesis 19*, 2001–2006.

Weber, M. M., Fottner, C., Liu, S. B., Jung, M. C., Engelhardt, D. & Baretton, G. B. 2002: Overexpression of the insulin-like growth factor I receptor in human colon carcinomas. *Cancer 95*, 2086–2095.

Wheeler, D. L., Huang, S., Kruser, T. J., Nechrebecki, M. M., Armstrong, E. A., Benavente, S., Gondi, V., Hsu, K.-T. & Harari, P. M. 2008: Mechanisms of acquired resistance to cetuximab: role of HER (ErbB) family members. *Oncogene 27*, 3944–3956.

Wu, X.-Y., Wu, Z.-F., Cao, Q.-H., Chen, C., Chen, Z.-W., Xu, Z., Li, W.-S., Liu, F.-K., Yao, X.-Q. & Li, G. 2014: Insulin-like growth factor receptor-1 overexpression is associated with poor response of rectal cancers to radiotherapy. *World Journal of Gastroenterology 20*, 16268.

Xuan, S., Kitamura, T., Nakae, J., Politi, K., Kido, Y., Fisher, P. E., Morroni, M., Cinti, S., White, M. F., Herrera, P. L., Accili, D. & Efstratiadis, A. 2002: Defective insulin secretion in pancreatic β cells lacking type 1 IGF receptor. *Journal of Clinical Investigation 110*, 1011–1019.

Xue, Y., Johnson, R., Desmet, M., Snyder, P. W. & Fleet, J. C. 2010: Generation of a transgenic mouse for colorectal cancer research with intestinal cre expression limited to the large intestine. *Molecular cancer research MCR 8*, 1095–1104.

Yang, L., Li, J., Ran, L., Pan, F., Zhao, X., Ding, Z., Chen, Y., Peng, Q. & Liang, H. 2011: Phosphorylated insulin-like growth factor 1 receptor is implicated in resistance to the cytostatic effect of gefitinib in colorectal cancer cells. *Journal of gastrointestinal surgery official journal of the Society for Surgery of the Alimentary Tract 15*, 942–957.

Yano, S., Kondo, K., Yamaguchi, M., Richmond, G., Hutchison, M., Wakeling, A., Averbuch, S. & Wadsworth, P. 2003: Distribution and function of EGFR in human tissue and the effect of EGFR tyrosine kinase inhibition. *Anticancer research 23*, 3639–3650.

Ye, F., Chevrier, A. M., Langlois, D., Cuber, J. C., Saez, J. M., Chayvialle, J. A. & Abello, J. 1998: Insulin-like growth factor I receptors are expressed by the enteroendocrine cell line STC-1: relationship with proliferation and cholecystokinin expression. *Hormone research 50*, 183–189.

Zhang, G., Li, X., Zhang, L., Zhao, L., Jiang, J., Wang, J. & Wei, L. 2010: The expression and role of hybrid insulin/insulin-like growth factor receptor type 1 in endometrial carcinoma cells. *Cancer Genetics and Cytogenetics 200*, 140–148.

Zhang, R., Xu, G.-L., Li, Y., He, L.-J., Chen, L.-M., Wang, G.-B., Lin, S.-Y., Luo, G.-Y., Gao, X.-Y. & Shan, H.-B. 2013: The role of insulin-like growth factor 1 and its receptor in the formation and development of colorectal carcinoma. *Journal of International Medical Research 41*, 1228–1235.

Zhou, Z., Nimeiri, H. S. & Benson, A. B. 3. 2013: Preoperative chemotherapy for locally advanced resectable colon cancer - a new treatment paradigm in colon cancer? *Annals of translational medicine 1*, 11.

Acknowledgements

In the course of my PhD thesis many people have contributed to its success. For this reason, I want to thank all those who supported me during the time of my promotion.

I would like to express my gratitude to Prof. Dr. Peter Burfeind for being my referee and supervisor, for the critical but rather helpful and friendly discussions and suggestions and for proofreading my thesis.

I would like to extend my gratitude to Dr. Silke Kaulfuß for being my supervisor, for her patient support and encouragement, her great advice, her confidence and for proofreading my manuscripts.

I sincerely thank Prof. Dr. Matthias Dobbelstein and Prof. Dr. Ralf Dressel for being my thesis committee members.

I am very thankful to Dr. Felix Bremmer for his invaluable support regarding the histopathological analyses of the tumors. Special thanks to Valerie for embedding and cutting all tissue samples.

I would like to thank Dr. Ramona Schulz for giving me the opportunity to use the colonoscopy device.

I sincerely thank Margret Rave-Fränk for giving me the opportunity to use the irradiation device.

I am thankful to all members of the animal houses in the Institute of Human Genetics and at the European Neuroscience Institute Göttingen and especially to Lea for doing a great job in taking care of “my” mice.

Special thanks to my current and former lab colleagues Amanda, Anna, Britta, Claudia, Daniel, Daria, Henning, Jasmin, Julia, Kristin, Laura, Lisa, Rovena, Sascha and Tashina for the cheerful and friendly atmosphere in- but also outside the lab, for their patient help and advice and for the serious but also joking conversations. I had a great time with you.

Thanks Lisa and Rovena for your great support regarding hours and hours of colonoscopy and sacrificing “my” mice. Your presence made time go by very quickly.

I would like to thank all my colleagues from the institute for being friendly and helpful.

Special thanks to my friends, family and Daniel... ♥